FINAL REPORT
U.S. Department of Energy

Advanced Experimental Analysis of Controls on Microbial Fe(III) Oxide Reduction

Principle Investigator: Eric E. Roden
Institution: The University of Alabama
Collaborators: Matilde M. Urrutia
Institution: The University of Alabama

Project Number: 55164
Grant Number: DE-FG07-96ER62321
Grant Project Officers: Paul Bayer
Project Duration: September 16, 1996 to March 16, 2001

Table of Contents

	Pages
Executive Summary	3-5
Research Background and Objectives	6
Methods and Results	6-12
Relevance, Impact, and Technology Transfer	12-14
Project Productivity	14-15
Personnel Supported	15
Publications	15-16
Interactions	16-17
Transitions	17
Patents	17
Future Work	18
Literature Cited	18-22
Appendix 1: Reprints of published papers	
Appendix 2: Numerical simulation of U(VI) reductive immobilization in Fe(III) oxide-reducing subsurface sediments	
Appendix 3: One-dimensional simulation of U(VI) reactive transport in a hypothetical Fe(III) oxide-reducing column reactor	

Executive Summary

Microbial reduction of Fe(III) oxides and associated dissimilatory metal-reducing bacterial activities have numerous consequences for the transport and fate of heavy metals, radionuclides, organic contaminants, and organic/metal cocontaminants in subsurface environments on DOE lands. These processes have the potential to fundamentally alter the behavior of virtually all metal-radionuclide contaminant species in anaerobic Fe(III) oxide-bearing subsurface environments, e.g. through their influence on aqueous geochemical conditions (e.g. pH, alkalinity), surface-chemical properties (e.g. sorption site density and reactivity), mineral formation/destruction reactions (e.g. Fe(III) oxide dissolution, Fe(II)- and other reduced metal-bearing mineral formation), and surface-catalyzed redox reactions. Despite the potential importance of such processes to metal-radionuclide fate and transport, quantitative models of microbial Fe(III) oxide reduction and its influence on contaminant transformations in the subsurface have not yet been developed due to lack of basic information on how physical, chemical and microbiological components interact to control rates of dissimilatory metal-reducing bacterial (DMRB) growth and activity in subsurface systems. To date, laboratory studies of the controls on microbial Fe(III) oxide reduction have been conducted almost exclusively in batch culture systems. In contrast, the subsurface represents an open system in which removal of reaction end-products (e.g. Fe(II)) can occur. Recent assessments of subsurface Fe(III) oxide reduction and associated contaminant (e.g. metal/radionuclide/chelator cocontaminants) transformations have emphasized the need for development of new experimental approaches that allow for the study of Fe(III) oxide reduction under long-term growth conditions in hydrologically open systems.

The objectives of this research project were to refine existing models of microbiological and geochemical controls on Fe(III) oxide reduction, using laboratory reactor systems which mimic to varying degrees the physical and chemical conditions of the subsurface. Novel experimental methods for studying the kinetics of microbial Fe(III) oxide reduction and measuring growth rates of Fe(III) oxide-reducing bacteria in open reactor systems have been developed. These studies indicate that advective removal of Fe(II) can significantly stimulate bacterial reduction of synthetic and natural Fe(III) oxide reduction phases and DMRB growth. The mechanism for this stimulation is related to the inhibitory impact of sorbed and/or surface-precipitated Fe(II) on oxide reduction activity, which is reduced as a result of advective Fe(II)

removal. The sustained Fe(III) oxide reduction activity which occurs in hydrologically open reactors is associated with sustained DMRB cell growth. In flow-through column experiments, such growth resulted in the production and export of a quantity of cell biomass more than 100-fold in excess of the biomass initially added during column inoculation. In contrast, estimates cell growth in batch reactors suggested that only small (≤ 2-fold) increases cell biomass were likely to have occurred. Overall, our findings indicate that removal of biogenic Fe(II) via aqueous-phase transport in hydrologically open reaction systems can significantly decrease the passivating influence of surface-bound Fe(II) on oxide reduction activity, thereby allowing for a dramatic increase in the extent of crystalline Fe(III) oxide reduction and associated DMRB cell growth. These findings have important implications for fate and transport of metal-radionuclide contaminants whose behavior is closely linked to Fe biogeochemistry in subsurface environments. In addition, *the* production and export of large quantities of pelagic (i.e. unattached, at least temporarily) DMRB cells during growth coupled to solid-phase Fe(III) oxide reduction has important implications for the transport of DMRB in subsurface sediments. One of the major mechanisms for such transport is the production of mobile daughter cells, and our results suggest that DMRB growth under conditions of aqueous phase flux could lead to enhanced mobility of DMRB in the subsurface. Our findings indicate that the coupling between stimulation of oxide reduction activity through advective Fe(II) removal and cell growth-promoted transport is likely to be an important consideration in terms of the spatial and temporal scales on which subsurface bioremediation strategies involving DMRB may be effectively implemented.

The new methodologies developed in this project are applicable to bench-scale studies of subsurface contaminant transformations directly coupled to or influenced by microbial Fe(III) oxide reduction. Such studies represent an important knowledge-gathering step required to bridge the gap between fundamental research and implementation of *in situ* treatment strategies for metal-radionuclide contaminant remediation. As an example, the renewal award for this project (Project Number 73914, "Reductive immobilization of uranium(VI) in Fe(III)-oxide reducing subsurface sediments: Analysis of coupled microbial-geochemical processes in experimental reactive transport systems; E.E. Roden (University of Alabama), PI/PD; M.M. Urrutia (University of Alabama), M.O. Barnett (Auburn University) and C.R. Lange (Auburn

University), Co-PIs) will examine the potential utility of *in situ* "redox barriers" for remediation of subsurface uranium contamination at site such as Hanford, ORNL, and SRS.

Our studies have also provided information useful for development of mathematical models of subsurface Fe(III) oxide reduction and DMRB growth, and the influence of Fe(III) oxide reduction on metal-radionuclide contaminant fate and transport. This information has been incorporated into a general simulation model of coupled Fe(III) oxide/uranium(VI) reduction, and into a provisional 1-dimensional model of uranium(VI) reactive transport in Fe(III)-reducing subsurface sediments. Through collaboration with other DOE-funded investigators, these models will be expanded and refined for use in simulation of the bench-scale reactor studies to be conducted in the renewal project. In addition, the suite of coupled microbial-geochemical processes incorporated in the models has been proposed as the basis for a field-scale reactive transport simulation study of the impact of subsurface chemical-microbiological heterogeneity on the effectiveness of *in situ* reactive barriers for radionuclide contaminant immobilization (proposal submitted to the DOE-NABIR Program, Biogeochemical Dynamics Element, February 2001, C.J. Murray, PI/PD; T.D. Scheibe, E.E. Roden, P.R. Jaffe, S.S. Hubbard, Co-PIs).

Research Background and Objectives

The transport and fate of trace metals and metal-radionuclide contaminants in subsurface environments is controlled by coupled physical, chemical and microbiological processes (Hunter et al., 1998; Salvage and Yeh, 1998; Tebes-Stevens et al., 1998). Microbial metabolism can cause both dissolution and precipitation of inorganic mineral phases, primarily through redox reactions associated with organic matter oxidation (Lovley and Chapelle, 1995). Such microbially-catalyzed redox reactions have the potential to strongly influence the fate of metals and radionuclides in the subsurface (Davis et al., 1993; Fish, 1993). Microbial Fe(III) oxide reduction is a dominant microbial redox process in many anaerobic subsurface environments (Lovley, 1991). This process has the potential to fundamentally alter the behavior of virtually all metal-radionuclide contaminant species in anaerobic Fe(III) oxide-bearing subsurface environments, e.g. through its influence on aqueous geochemical conditions (e.g. pH, alkalinity), surface-chemical properties (e.g. sorption site density and reactivity), mineral formation/destruction reactions (e.g. Fe(III) oxide dissolution, Fe(II)- and other reduced metal-bearing mineral formation), and surface-catalyzed redox reactions (e.g. reduction of Cr(VI) to Cr(III) and Tc(VI) to Tc(V)) (Lovley, 1991, 1993; Nealson and Saffarini, 1994; Lovley, 1995; Fredrickson and Gorby, 1996; Lloyd and Macaskie, 2000; Lovley, 2000). Microbial Fe(III) oxide reduction is a complex process involving the interaction between dissimilatory metal-reducing bacterial (DMRB) cells, endogenous solid-phase Fe(III) oxide minerals, aqueous-phase components (organic and inorganic ligands), and a variety of secondary mineral phases which can form as a result of enzymatic reduction activity. As a result of this complexity, detailed quantitative models of microbial Fe(III) oxide reduction and the influence of this process on contaminant transformations have not been developed due to the lack of basic information on how physical, chemical and microbiological components interact to control rates of DMRB growth and activity in subsurface systems. To date, laboratory studies of the controls on microbial Fe(III) oxide reduction have been conducted almost exclusively in batch cultures. In contrast, the subsurface represents an open system in which removal of reaction end-products (e.g. Fe(II)) can occur. Recent assessments of subsurface Fe(III) oxide reduction and associated contaminant (e.g. metal/chelator co-contaminants) transformations (Zachara et al., 1995; Zachara, 1996) have emphasized the need for development of new experimental approaches that allow for the study of Fe(III) oxide reduction under long-term growth conditions in hydrologically open systems.

The objectives of this research project were to refine existing models of microbiological and geochemical controls on Fe(III) oxide reduction, using laboratory reactor systems which mimic the physical and chemical conditions of the subsurface. We sought to develop novel experimental methods for studying the kinetics of microbial Fe(III) oxide reduction and measuring growth rates of Fe(III) oxide-reducing bacteria that could be applied to studies of subsurface contaminant transformations directly coupled to or influenced by microbial Fe(III) oxide reduction. In addition, we anticipated that our experimental research would be useful for development of mathematical models of subsurface Fe(III)-reducing bacterial growth and Fe(III) oxide reduction, and the influence of Fe(III) oxide reduction on aqueous/solid-phase biogeochemistry and metal-radionuclide contaminant fate and transport.

Methods and Results

The summary given below of major research findings generated by the project is organized around papers which have been published in the peer-reviewed scientific journals. We have thus far published 4 manuscript from support provided by the award, have two additional papers submitted for publication, and anticipate submission of one or two more manuscripts within the next 6 months. Copies of the published papers are included as appendices to this report, and should be consulted for detailed description of the experimental methodology and data analysis/interpretation.

In accordance with the stated objectives of the project, our research has focused on experimental studies of the microbiological and geochemical controls on bacterial Fe(III) oxide reduction, with an emphasis on crystalline Fe(III) oxide phases. Although amorphous Fe(III) oxides have traditionally been considered to be the major Fe(III) oxide phases subject to microbial reduction in anaerobic soils and sediments (Lovley, 1991), several recent publications from our own (Roden and Zachara, 1996) and our DOE colleagues laboratories (Zachara et al., 1998; Zachara et al., 1999; Zachara et al., 2001) indicate that crystalline Fe(III) oxide are in fact subject to substantial microbial reduction. Microbial reduction of crystalline Fe(III) oxides has important considerations toward subsurface metal-radionuclide contaminant biogeochemistry, since crystalline Fe(III) oxide are often far more abundant than amorphous Fe(III) oxides in soils and sediments (Cornell and Schwertmann, 1996). The latter are typically present as coatings on larger mineral grains, including crystalline Fe(III) oxides (Swartz et al., 1997). Production of Fe(II), liberation of sorbed/precipitated contaminant metals and radionuclides, and promotion of DMRB growth coupled to crystalline Fe(III) oxide reduction are issues of immediate concern to DOE subsurface metal-radionuclide contaminant research.

The first paper (Urrutia et al., 1998) describes work that was in progress at the time the award was made, and which was brought to completion (including several additional experiments) during the course of this project. This foundational paper clearly established that association of Fe(II) with Fe(III) oxide as well as Fe(III)-reducing bacteria exerts a major influence on the rate and extent of bacterial Fe(III) oxide reduction. It also indicated that aqueous chemical components present during bacterial Fe(III) oxide reduction can have a substantial influence on the long-term extent of oxide reduction. These findings supported the speculations presented in a previous paper (Roden and Zachara, 1996) regarding the controls on Fe(III) oxide reduction.

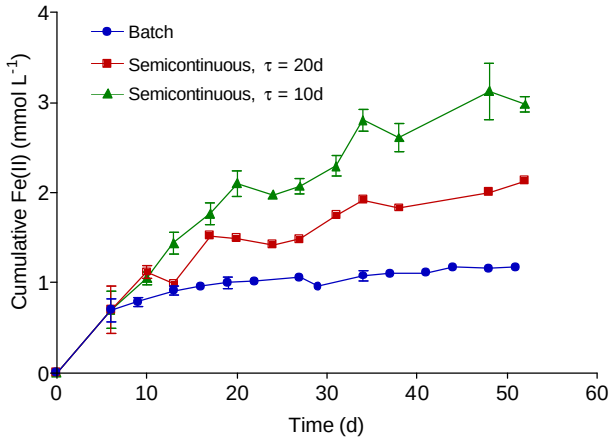


Fig. 1. Influence of advective Fe(II) removal on cumulative reduction of synthetic goethite by *S. alga* strain BrY in semicontinuous vs. batch culture systems. τ refers to the aqueous-phase residence time in the semicontinuous cultures.

The Roden and Urrutia (1999) paper established for the first time that advective removal of Fe(II) can significantly stimulate bacterial reduction of synthetic and natural Fe(III) oxide reduction phases and DMRB growth (see Fig. 1). The mechanism for this

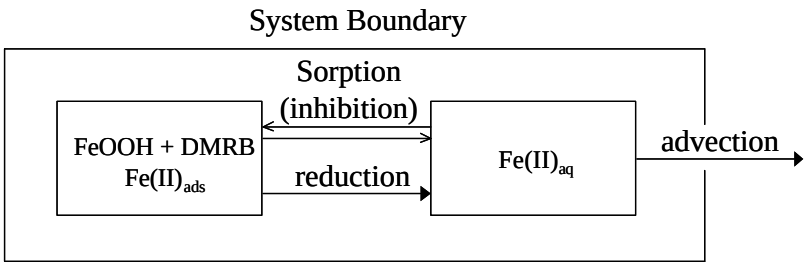


Fig. 2. Conceptual model of the influence of advective Fe(II) removal on microbial Fe(III) oxide reduction

stimulation is related to the inhibitory impact of sorbed and/or surface-precipitated Fe(II) on oxide reduction activity, which is reduced as a result of advective Fe(II) removal (illustrated in Fig. 2). The experimental approach developed for in these studies - semicontinuous culturing – provides a simple but reliable and easily replicable means of examining Fe(III) oxide reduction and associated geochemical processes in open reactor systems. Residence times of 5-20 days can be easily achieved by altering the ratio of medium replacement to total reactor volume. Another significant accomplishment of this paper was the development of a simulation modeling approach for depicting the regulation of Fe(III) oxide reduction activity by sorption of Fe(II) to oxide/DMRB cell surfaces, taking into account the kinetics of bacterial Fe(III) oxide reduction as a function of the abundance of reactive Fe(III) oxide surface sites, and the dynamic balance between Fe(II) sorption to such surface sites and its removal from the reactor via aqueous phase flushing. The simulation model presented in the paper did a reasonable job of capturing the contrasting behavior of the batch vs. semicontinuous culture systems. This represents an important step forward in the development of mechanistic models of Fe(III) oxide reduction and DMRB growth in subsurface sediments.

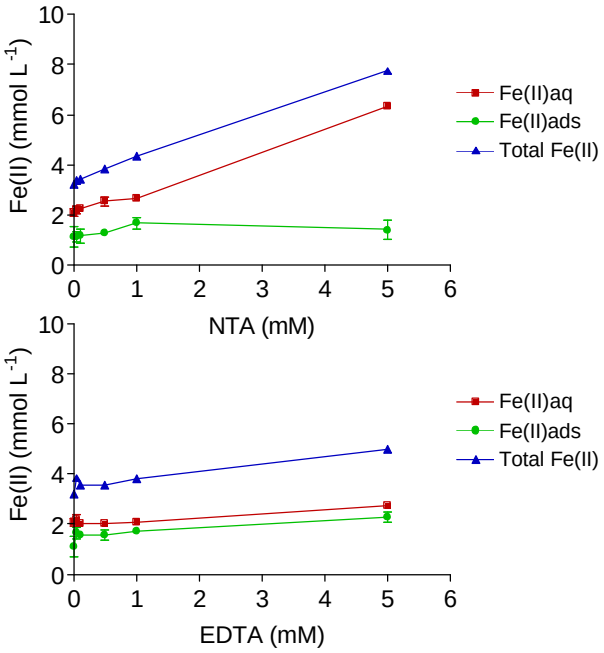


Fig. 3. Influence of NTA and EDTA on long-term extent (30-d incubation) of synthetic goethite reduction by *S. alga* strain BrY in batch culture.

Urrutia et al. (1999) further explored the issue of how aqueous and solid-phase compounds which can complex Fe(II) may influence bacterial crystalline Fe(III) oxide reduction activity. Specifically, we tested the hypothesis that synthetic chelators such as EDTA and NTA would enhance the long-term reducibility of a model crystalline Fe(III) oxide (goethite), by complexing Fe(II) and thereby delaying/retarding its association with oxide/DMRB surfaces. In addition, we examined the hypothesis that the presence of solid-phase compounds, such as aluminum oxide and layered silicate minerals (which may both be present in substantial abundance in subsoils and subsurface sediments) which have the capacity to complex Fe(II) would stimulate bacterial reduction of goethite. In general, our experimental hypotheses were supported: the presence of NTA led to a stimulation of the long-term extent of goethite reduction in direct proportion to its concentration in the culture medium (Fig. 3); and both aluminum oxide and layered silicates (sequestered in

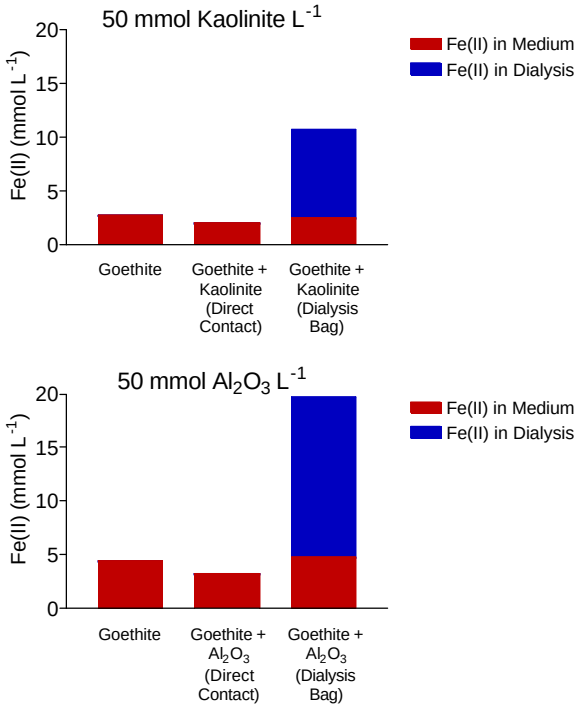


Fig. 4. Influence of solid-phase Fe(II) sinks on long-term (30-d incubation) extent of synthetic goethite by *S. alga* strain BrY in batch culture.

dialysis tubing) were able to act as Fe(II) sinks which dramatically increased (2-10 fold) the extent of oxide reduction (Fig. 4). However, we found that EDTA did not substantially stimulate goethite reduction, which was surprising given the fact that the Fe(II)-EDTA complex is even strong than the Fe(II)-NTA complex. The reason for this result appears to be that Fe(II)-EDTA complexes readily adsorb to Fe(III) oxide/DMRB cell surfaces. The contrasting behavior of the NTA vs. EDTA systems was captured in a series of aqueous speciation-surface complexation model simulations conducted with MINTEQA2 (Allison et al., 1991), which showed in a theoretical way how the presence of NTA, but not EDTA, would be expected to reduce the ratio of aqueous:sorbed Fe(II) for a specified total Fe(II) concentration. These simulations were all based on independently measured isotherms for sorption of Fe(II) alone and Fe(II)-NTA/Fe(II)-EDTA complexes to a mixture of synthetic goethite and DMRB cells. To our knowledge, this work represents the first application of established aqueous/surface complexation modeling techniques to the controls on bacterial Fe(III) oxide reduction. The findings reported in this paper suggest that the in some situations, the presence of organic ligands in groundwaters which can complex Fe(II) could significantly impact the long-term extent of crystalline Fe(III) oxide reduction, not by causing dissolution/solubilization of the oxide phases, but rather by complexing Fe(II) producing during bacterial Fe(III) oxide reduction. In addition, it is likely that binding of Fe(II) by aluminosilicate minerals in soils and sediments is likely to play an important (but as yet unquantified) role in regulating Fe(III) oxide reduction. With regard to this latter point, it is interesting to note that in the Roden and Urrutia (1999) paper, we found that medium replacement in the semicontinuous cultures did not stimulate the reduction of natural Fe(III) oxide-bearing subsoils as strongly as it stimulated synthetic (pure phase) crystalline Fe(III) oxide reduction, and attributed this effect to the presence of various auxiliary solid-phases with the capacity to bind Fe(II), the presence of which decreased the relative importance of aqueous phase flushing as a regulator of Fe(III) oxide reduction activity. Finally, this paper played an important role in developing our knowledge and facility with aqueous speciation-surface complexation modeling, which led ultimately to our ability to incorporate such modeling into dynamic (time-dependent) simulations of bacterial Fe(III) oxide reduction in flow-through reactor systems (see below).

Our most recent paper (Roden et al., 2000) examined the long-term capacity for crystalline Fe(III) oxide (synthetic goethite-coated sand) in column reactors in comparison with batch cultures. Based on our previous findings, we hypothesized that the potential might exist for more-or-less complete reductive dissolution of crystalline oxide in flow-through column

reactors in which continuous removal of Fe(II) end-products could be achieved. In order to examine this hypothesis over a reasonable period of time, a relatively short (ca. 6 hr) aqueous phase residence time was established in the columns. As hypothesized, sustained reductive dissolution of the crystalline oxide was observed over a 6-month incubation period, resulting in the export of aqueous Fe(II) equal to 95 ± 4 % of the original Fe(III) oxide content of the columns (Fig. 5). The near-complete removal of Fe from the columns was evidence by extensive bleaching of color from the columns (Fig. 6), and verified by wet chemical analysis of the column contents at the end of the experiment. In contrast to the column reactors, Fe(II) production quickly reached an asymptote in the batch cultures (Fig. 5), and only ca. 13% of the Fe(III) oxide content was reduced. These results showed for the first time that microbial reduction activity has the potential to cause quantitative reductive dissolution of crystalline Fe(III) oxides in the situation where advective aqueous phase flow leads to removal of Fe(II) end products. These findings provide an explanation for the virtually complete removal of crystalline Fe(III) oxide minerals in landfill leachate-contaminated aquifer sediments reported by Heron et al. (1995).

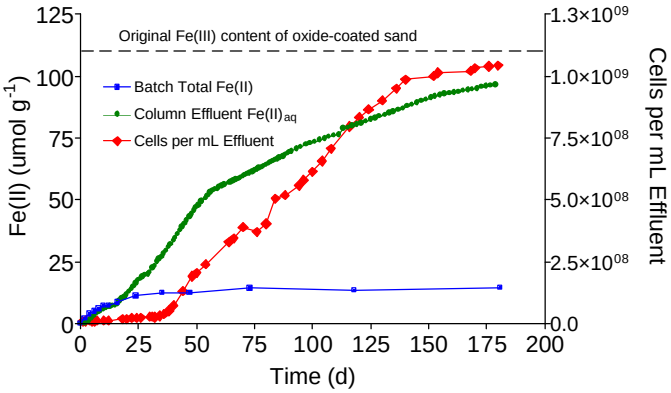


Fig. 5. Reduction of synthetic goethite-coated sand in continuous-flow column vs. batch reactors.



Fig. 6. Photo of Fe(III) oxide reduction column reactor after 6-month incubation (left) vs. inoculated and uninoculated batch reactors (near right and far right, respectively). Note bleaching of color from sand in the column reactor.

Another important finding presented in this paper is that the sustained Fe(III) oxide reduction activity which occurred in the column reactors was associated with associated with continual DMRB cell growth, which resulted in the production and export of a quantity of cells from the column reactors more than 100-fold in excess of the biomass added during column inoculation. In contrast, indirect estimates of potential cell growth, based on the quantity of Fe(III) reduced, suggested that only an approximate doubling of initial cell biomass was likely to have occurred in the batch reactors. Overall, our results indicate that removal of biogenic Fe(II) via aqueous-phase transport in the column reactors decreased the passivating influence of surface-bound Fe(II) on oxide reduction activity, thereby allowing for a dramatic increase in the extent of crystalline Fe(III) oxide reduction and associated DMRB cell growth. The production and export of large quantities of pelagic (i.e. unattached, at least temporarily) DMRB cells during growth coupled to solid-phase Fe(III) oxide reduction has important implications for the transport of DMRB in subsurface sediments. One of the major mechanisms for such transport is the production of mobile daughter cells (Kjelleberg et

al., 1982), and our results suggest that DMRB growth under conditions of aqueous phase flux could enhance the mobility of DMRB in the subsurface. Our findings lead us to speculate that the coupling between stimulation of oxide reduction activity through advective Fe(II) removal and cell growth-promoted transport is likely to be an important consideration in terms of the spatial and temporal scales on which subsurface bioremediation strategies involving DMRB may be effectively implemented.

The final pieces of published work to be generated by the project will deal with (1) studies of DMRB (*Shewanella and Geobacter*) biomass production and growth rate during reduction of soluble Fe(III) and solid-phase Fe(III) oxides (Roden and Urrutia, 2001a). This paper will include an analysis of the potential utility of ^{3}H-thymidine and ^{3}H-leucine incorporation (into cellular DNA and protein, respectively) assays for estimation of instantaneous DMRB growth rates during growth on soluble and solid-phase Fe(III). Additional comments on this line of research are provided in the Project Productivity section below; (2) a review/synthesis paper on the impact of biogenic Fe(II) on the rate and extent of crystalline Fe(III) oxide reduction (Roden and Urrutia, 2001b). This paper will present new experiments examining the influence of advective Fe(II) removal (semicontinuous culturing) on synthetic goethite reduction by *G. metallireducens*, as well as a comparison of the inhibitory influence of Fe(II) on crystalline Fe(III) oxide reduction by *G. metallireducens* vs. *S. alga*; and (3) contribution of experimental data and theoretical interpretations to a review/synthesis paper by Danish colleagues (O. Larsen and D. Postma) on the influence of Fe(III) oxide heterogeneity on the kinetics of bacterial Fe(III) oxide reduction (Larsen et al., 2001). Our contributions to this paper include a new set of experiments examining initial rates of enzymatic vs. abiotic (ascorbate, pH 3) oxide reduction as a function of oxide surface area and thermodynamic stability across a broad range of synthetic Fe(III) oxide phases, as well as a careful evaluation of the impact of Fe(III) oxide heterogeneity on changes in the apparent reactivity of synthetic and natural Fe(III) oxides toward biotic vs. abiotic reduction in long-term experiments. Copies (PDF files) of these papers will be uploaded to the EMSP web site once they are published.

Funding from this research project has helped to support several ancillary projects in the PI/PD's laboratory dealing with microbial Fe cycling and biogeochemical Fe transformations relevant to the behavior of metal/radionuclide contaminants in subsurface sediments, namely (1) a detailed evaluation of the kinetics of bacterial amorphous Fe(III) oxide reduction in Fe-rich wetland sediments (Roden and Wetzel, 2001). This study has significant implications for modeling bacterial reduction of highly reactive amorphous Fe(III) oxide phases which typically serve to cement together much more abundant crystalline Fe(III) oxide phases in subsurface sediments (Swartz et al., 1997); (2) an experimental evaluation of the potential for immobilization of strontium during carbonate mineral formation coupled to microbial reduction of synthetic amorphous and crystalline Fe(III) oxides (Keith, 2001; Roden et al., 2001). This study (funded through a subcontract to The University of Alabama from EMSP Project Number 54790, F.G. Ferris, PI/PD) demonstrated for the first time that divalent metal cations can undergo coprecipitation (immobilization) with biogenic siderite ($FeCO_3$) formed under Fe(III) oxide-reducing conditions. Stimulation of such processes, together with other bacterially-driven carbonate mineral precipitation reactions (e.g. (Warren et al., 2001)), may represent a viable *in situ* metal-radionuclide (e.g. ^{90}Sr) immobilization strategy in carbonate-rich subsurface environments; (3) studies of bacterially-catalyzed Fe(II) oxidation at circumneutral pH by

lithoautotrophic bacteria (Roden and Sobolev, 2001; Sobolev and Roden, 2001). The results of these studies have important implications for the cycling of Fe in redox interfacial environments, in which the potential exists for rapid microscale cycling of Fe between DMRB and lithotrophic Fe(II)-oxidizing bacteria. Considering the fundamental influence which Fe geochemistry exerts on the behavior of trace and contaminant metals and radionuclides in the environment, the microscale dynamics of Fe redox cycling is likely to be a critical factor governing the fate and transport of such species in redox-heterogeneous subsurface environments.

Relevance, Impact, and Technology Transfer

Our studies on the microbiological and geochemical controls on microbial Fe(III) oxide reduction are of immediate relevance to the management of subsurface metal-radionuclide contamination on DOE lands. At the most basic level, acquisition of a better understanding of the controls on Fe(III) oxide reduction is important for predicting the potential impact of this process on the transport and fate of heavy metals, radionuclides, organic contaminants, and organic-metal cocontaminants in subsurface environments on DOE lands where conditions conducive to Fe(III) oxide reduction are present. More importantly, such an understanding is required for design of remediation technologies which take advantage of the activities of DMRB (outlined below). Enhanced conceptual understanding as well as quantitative information for use in parameterization are required for effective numerical simulations of metal-radionuclide reactive transport in engineered as well as unmanipulated Fe(III) oxide-reducing subsurface environments. Development of such predictive tools is critical for evaluation of future risks and costs associated with subsurface metal-radionuclide contaminant remediation. To date, detailed quantitative (predictive) models of microbial Fe(III) oxide reduction and its influence on contaminant transformations have not been developed due to the lack of basic information on how physical, chemical and microbiological components interact to control rates of DMRB and activity in subsurface systems. Using laboratory reactor systems which mimic the physical and chemical conditions of the subsurface, this research project has produced a wealth of experimental data that has refined existing models of microbiological and geochemical controls on Fe(III) oxide reduction. These findings have been used to develop a provisional framework for mechanistic simulation of Fe(III) oxide reduction and DMRB growth in subsurface environments.

The above basic research activities represent a critical step in knowledge development required to implement *in situ* metal/radionuclide contaminant remediation technologies involving DMRB. Three major *in situ* remediation concepts (illustrated in Fig. 7) are relevant in this regard, all of which rely on manipulation of redox and aqueous/solid-phase geochemical conditions driven by DMRB activity: (1) Fe(III) oxide reductive dissolution to mobilize metal-radionuclide contaminants (e.g. divalent cations, arsenate) in order to facilitate pump-and-treat remediation strategies. Zachara et al. (2001) have recently conducted laboratory studies demonstrating this concept. (2) immobilization of metal-radionuclide contaminants (e.g. divalent cations such as $^{90}Sr^{2+}$) via coprecipitation with carbonate minerals formed during microbial Fe(III) oxide reduction. We have recently demonstrated this concept in laboratory studies of both amorphous (Roden et al., 2001) and crystalline Keith (2001) oxide reduction. (3) reductive immobilization of redox-sensitive metal-radionuclide contaminants such as uranium(VI) through the activity of DMRB. The latter process is an example of an "*in situ* redox barrier" strategy (Perel'man, 1986; Deutsch, 1997), and is the focus of our renewal project

(Project Number 73914, "Reductive immobilization of uranium(VI) in Fe(III)-oxide reducing subsurface sediments: Analysis of coupled microbial-geochemical processes in experimental reactive transport systems"). This strategy stands to benefit substantially from the utilization of a large supply of endogenous electron acceptor in the form of Fe(III) oxides in subsurface sediments to build biomass of dissimilatory metal-reducing bacteria (DMRB), which can subsequently immobilize uranium (as well as other redox-sensitive metal-radionuclide contaminants) migrating into the engineered treatment zone (redox barrier) through reduction of soluble uranium(VI) species to insoluble uranium(IV) minerals such as uraninite ($UO_2(s)$) .

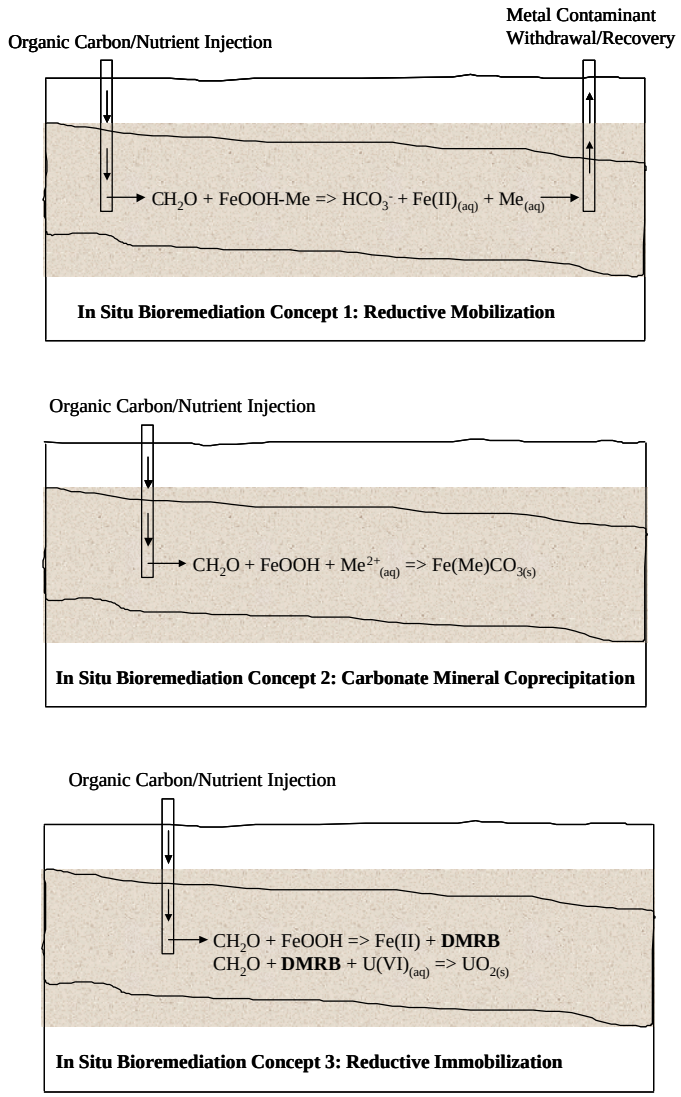


Fig. 7. Three potential *in situ* bioremediation technologies involving DMRB activity. Modified from Deutsch (1997), Fig. 8-11.

Finally, our studies have provided information useful for development of mathematical models of subsurface Fe(III) oxide reduction and DMRB growth, and the influence of Fe(III) oxide reduction on metal-radionuclide fate and transport. This information has been incorporated into a general simulation model of coupled Fe(III) oxide/uranium(VI) reduction (Appendix 2), and into a provisional 1-dimensional model of uranium(VI) reactive transport in Fe(III)-reducing subsurface sediments (Appendix 3). These models will be expanded and refined for use in simulation of the bench-scale reactor studies to be conducted in the renewal project. In addition, the suite of coupled microbial-geochemical processes incorporated in the model has been proposed as the basis for a field-scale reactive transport simulation study of the impact of subsurface chemical-microbiological heterogeneity of the effectiveness of *in situ* reactive barriers for radionuclide contaminant immobilization (proposal submitted to the DOE-NABIR Program, Biogeochemical Dynamics Element, February 2001, C.J. Murray, PI; T.D. Scheibe, E.E. Roden, P.R. Jaffe, S.S. Hubbard, Co-PIs).

As discussed in the Transitions section, we anticipate that within the next few years it will be appropriate for DOE-funded research groups to initiate collaborative pilot field-scale *in*

situ remediation experiments involving one or more of the remediation strategies outline in Fig. 7, e.g. at the NABIR Field Research Center at ORNL, the Savannah River Site, or (in the case of uranium remediation) at an UMTRA site. The support our group has received from the 96-10 award and other DOE projects has brought us into the mainstream of research on microbial metal reduction and subsurface biogeochemistry. We anticipate long-term participation in the development and assessment of *in situ* treatment technologies for subsurface metal-radionuclide contaminant clean-up.

Project Productivity

We have accomplished all but two of the major experimental research goals of the project. The two unresolved problems involve the interrelated issues of how to quantify the biomass and growth rates of DMRB in subsurface media. We discovered after substantial investment of time and funds that measurements of protein content were biased (high) by the accumulation of high levels surface-bound Fe(II) during the latter stages of solid-phase Fe(III) oxide reduction, which interfered with the sensitive bicinchoninic acid assay procedure used to detect the relatively low concentrations of bacterial protein in our experimental culture systems. This artifact leads to substantial overestimation of protein content during growth with solid-phase Fe(III), as judged by the relationship between measured protein vs. Fe(II) content of amorphous Fe(III) oxide and synthetic goethite growth cultures compared to that observed during growth with soluble Fe(III), in which interference by Fe(II) is not a major factor. We are currently optimizing a procedure for estimating DMRB biomass based on a technique designed to measure soil bacterial biomass based through determination of ATP content (Eiland, 1983). This technique will be used to track DMRB biomass during experiments on coupled Fe(III) oxide/uranium(VI) reduction in the renewal project.

The other problem we encountered surrounds the development of a radiotracer technique such as ^{3}H-thymidine or ^{3}H-leucine incorporation (Findlay, 1993; Kirchman, 1993) for measurement of instantaneous DMRB growth rates in Fe(III) oxide-reducing systems. The goal of developing such a technique was to be able to relate changes in rates of DMRB growth to changes in aqueous/solid-phase geochemical conditions which are known to influence Fe(III) oxide reduction activity. Unfortunately, we discovered that, at least for the 4 organisms tested, DMRB (like other anaerobic respiratory bacteria; (Gilmour et al., 1990)) do not possess specific thymidine uptake systems, so that even during rapid growth on soluble Fe(III), rates of ^{3}H-thymidine incorporation into cellular DNA are too low for accurate estimation of instantaneous biomass production rate. With regard to the potential use of ^{3}H-leucine incorporation into cellular protein as a means for estimating DMRB biomass production rates, the results are more promising but definitive studies are not yet available. One potential liability of this approach in terms of applicability to natural sediments with complex natural microflora is that not all of the DMRB tested possess rapid leucine uptake systems. For example, examination of rates of ^{3}H-leucine uptake as a function of cold (unlabeled) leucine concentration indicated that *Geobacter metallireducens*, unlike *Shewanella alga* strain BrY and *Shewanella putrefaciens* strain CN32, does not have the ability to rapidly take up ^{3}H-leucine. While it appears that *G. sulfurreducens* does possess a ^{3}H-leucine uptake system, there is no guarantee that the major groups of DMRB present in natural Fe(III) oxide-reducing sediments will be able to effectively take up ^{3}H-leucine. Recent research suggests that organisms within the *Geobacteraceae* lineage (Lonergan et al.,

1996) are likely to be the dominant DMRB in most subsurface sedimentary environments (Rooney-Varga et al., 1999; Lovley, 2000; Snoeyenbos-West et al., 2000). The fact that *G. metallireducens* does not possess a specific leucine uptake system casts doubt on the applicability of this technique for determination of DMRB growth rates in complex natural DMRB communities. However, the ability of *G. sulfurreducens* to rapidly take up and incorporate ^{3}H-leucine into cellular protein suggests that, once optimized (e.g. through determination of the amount of cold leucine addition required to depress *de novo* leucine biosynthesis, together with determination of the incubation time required to accurately quantify the protein biosynthesis rate), this technique may provide fruitful insight into patterns of DMRB biomass production during the coupled Fe(III)/uranium(VI) reduction experiments to be conducted in the renewal project using *G. sulfurreducens* as a model organism.

Personnel Supported

1. Eric E. Roden, Project PI/PD: 3 months summer salary
2. Matilde M. Urrutia, Project Co-PI: 36 calendar months salary
3. Michael J. Leonardo, Postdoc: collaborative scientific association through EMSP Project 54790 (F.G. Ferris, University of Toronto, PI/PD; E.E. Roden, University of Alabama, Co-PI); current position: Assistant Professor, Biology Department, Elizabethtown College, Elizabethtown, PA
4. Trisha May, Graduate Student (doctoral): 16 calendar months salary + 3 semesters tuition; terminated graduate program December 1998.

Publications

A. Peer-reviewed journals (PDF files appended):

Urrutia, M.M., E.E. Roden, J.K. Fredrickson, and J.M. Zachara. 1998. Microbial and surface chemistry controls on reduction of synthetic Fe(III) oxide minerals by the dissimilatory iron-reducing bacterium *Shewanella alga. Geomicrobiol. J.* 15:269-291.

Roden, E.E. and M.M. Urrutia. 1999. Ferrous iron removal stimulates microbial iron(III) oxide reduction in semicontinuous cultures. *Environ. Sci. Technol.* 33:1847-1853.

Urrutia, M.M., E.E. Roden, and J.M. Zachara. 1999. Influence of aqueous and solid-phase Fe(II) complexants on microbial reduction of crystalline Fe(III) oxides. *Environ. Sci. Technol.* 33:4022-4028.

Roden, E.E., M.M. Urrutia, and C.J. Mann. 2000. Bacterial reductive dissolution of crystalline Fe(III) oxide in continuous-flow column reactors. *Appl. Environ. Microbiol.* 66:1062-1065.

Sobolev, D., and E.E. Roden. 2001. Suboxic deposition of ferric iron by bacteria in opposing gradients of Fe(II) and oxygen at circumneutral pH. *Appl. Environ. Microbiol.* 67:1328-1334.

B. Submitted for publication

Roden, E.E. and M.M. Urrutia. 2001. Influence of Fe(II) surface complexation on bacterial reduction of crystalline Fe(III) oxides. *Geomicrobiol. J.* Submitted for publication. (Contribution to special issue devoted to process-oriented studies of microbial Fe(III) oxide reduction in subsurface environments; E.E. Roden and Y.A. Gorby, guest editors).

Laresen, O, D. Postma, and E.E. Roden. 2001. Influence of Fe(III) oxide heterogeneity on bacterial Fe(III) oxide reduction. *Geomicrobiol. J.* Submitted for publication. (Contribution to special issue devoted to process-oriented studies of microbial Fe(III) oxide reduction in subsurface environments; E.E. Roden and Y.A. Gorby, guest editors).

Roden, E.E. and R.G. Wetzel. 2001. Kinetics of microbial Fe(III) oxide reduction in freshwater wetland sediments. *Limnol. Oceanogr.* Submitted for publication.

Interactions

A. Invited presentations at national/international scientific meetings

Roden, E.E. 2000. Kinetics of microbial Fe(III) oxide reduction in freshwater wetland sediments. American Society of Limnology and Oceanography Aquatic Sciences Meeting.

Roden, E.E. 1999. Microbial and geochemical controls on bacterial Fe(III) oxide reduction: links between surface chemistry and microbial physiology. Gordon Conference on Applied and Environmental Microbiology.

Roden, E.E. 1997. Geochemical and microbiological controls on bacterial iron oxide reduction. Geological Society of America Southeastern Region Annual Meeting.

Roden, E.E. M.M. Urrutia, and J.M. Zachara. 1996. Surface area and microbiological controls on Fe(III) oxide reduction. American Chemical Society, Industrial and Environmental Chemistry Division Special Session on Emerging Technologies in Hazardous Waste Management.

B. Scientific conference presentations

May, T.M. and E.E. Roden. 1998. ^{3}H-Leucine incorporation by Fe(III)-reducing bacteria. American Society for Microbiology Annual Meeting.

Roden, E.E. and M.M. Urrutia. 1998. Microbial Fe(III) oxide reduction in open experimental systems. American Society for Microbiology Annual Meeting.

May, T.M. and E.E. Roden. 1998. Models of the activity and growth of Fe(III)-reducing bacteria. Annual Water Resources Conference of the American Water Resources Association.

Roden, E.E. and M.M. Urrutia. 1997. Microbial Fe(III) oxide reduction in aquatic sediments: new insights into control and significance in biogeochemical fluxes. International Symposium on Environmental Biogeochemistry.

Urrutia, M.M. and E.E. Roden. 1997. Growth parameters of Fe(III)-reducing bacteria on soluble and solid-phase Fe(III) oxides. American Society for Microbiology Annual Meeting.

C. Invited seminar engagements

"Mineral breathing microbes: bacterial Fe(III) oxide reduction in ancient and modern sedimentary environments". Summer Research Colloquium Program, Dauphin Island Sea Lab, June 2000.

"Microbial and geochemical controls on bacterial Fe(III) oxide reduction: links between surface chemistry and microbial physiology". University of Odense, Denmark, Danish Earth Sciences Center, June 2000.

"Microbial and geochemical controls on bacterial Fe(III) oxide reduction: links between surface chemistry and microbial physiology". University of Idaho, Department of Microbiology and Molecular Biology, April 2000.

"Microbial and geochemical controls on dissimilatory Fe(III) oxide reduction", University of Wyoming, Department of Geosciences, April 1998.

D. Collaborations

Y.A. Gorby, Pacific Northwest National Laboratory
F.G. Ferris, University of Toronto
James K. Fredrickson, Pacific Northwest National Laboratory
Derek R. Lovley, University of Massachusetts
John M. Zachara, Pacific Northwest National Laboratory

Transitions

We anticipate that after one (possibly two) more funding cycle of basic research by ourselves and other DOE-supported research groups (e.g. other EMSP-funded researchers and investigators in the NABIR program) working on the mechanisms and controls of microbial metal-radionuclide contaminant transformations, it will be appropriate for several research groups to initiate collaborative pilot field-scale *in situ* remediation experiments, e.g. at the NABIR Field Research Center, Savannah River Site, or (in the case of uranium remediation) at an UMTRA site. The published research findings generated by this project as well as the renewal grant will by that time be well-disseminated in the open literature, and will help to provide basic scientific information required for design of these experiments, including numerical simulation of coupled microbial-geochemical reactions that are likely to govern the effectiveness of *in situ* metal-radionuclide remediation technologies.

Patents

None

Future Work

The focus of our renewal project is on the third *in situ* metal-contaminant remediation technology discussed in the section on Relevance, Impact, and Technology Transfer. This line of research represents a logical extension of our EMSP 96-10 award. The purpose of our original request for funding to conduct basic research on microbial Fe(III) oxide reduction was to develop experimental techniques and a knowledge base that could be used for future studies of metal-radionuclide transformations which are either directly coupled to or strongly influenced by microbial Fe(III) oxide reduction. Having made substantial progress toward this goal, we are prepared to pursue bench-scale experimental research related to metal-radionuclide remediation involving the activities of Fe(III) oxide-reducing bacteria. Such studies represent an important step in the development of an *in situ* uranium(VI) reductive immobilization strategy, because although the basic processes underlying this treatment technology are well-proven (Lovley et al., 1991; Lovley and Phillips, 1992a, b; Fredrickson et al., 2000), several fundamental scientific questions need to be addressed in order to understand how effectively the treatment process would function under conditions relevant to those *in situ*. These questions revolve around the dynamic interactions between hydrologic flux and coupled microbial-geochemical processes which are likely to occur within an *in situ* redox barrier environment (see discussion of these issues in Appendix 2). In addition to examining important scientific questions related to *in situ* uranium bioremediation, during the course the our experimental (and modeling) studies of coupled Fe(III) oxide/uranium(VI) reduction, we will build on our database of information on the dynamic controls on Fe(III) oxide reduction in subsurface media. Such information will be useful for development of more detailed mechanistic models of bacterial Fe(III) oxide reduction and associated metal-radionuclide biogeochemistry in subsurface sediments.

Literature Cited

Allison, J.D., D.S. Brown, and K.J. Novo-Gradac. 1991. MINTEQA2/PRODEFA2, A geochemical assessment model for environmental systems: version 3.0 user's manual. U.S. Environmental Protection Agency.

Cornell, R.M., and U. Schwertmann. 1996. The Iron Oixides, VCH.

Davis, J.A., D.B. Kent, B.A. Rea, A.S. Maest, and S.P. Garabedian. 1993. Influence of redox environment and aqueous speciation on metal transport in groundwater, pp. 223-273. *In* Metals in groundwater, Allen, H.E., E.M. Perdue, and D.S. Brown [eds], Lewis Publishers.

Deutsch, W.J. 1997. Groundwater geochemistry: Fundamentals and applications to contamination, Lewis Publishers.

Eiland, F. 1983. A simple method for quantitative determination of ATP in soil. Soil Biol. Biochem. 15:665-670.

Findlay, S. 1993. Thymidine incorporation into DNA as an estimate of sediment bacterial production, pp. 505-508. *In* Aquatic microbial ecology, Kemp, P.F., B.F. Sherr, E.B. Sherr, and J.J. Cole [eds], Lewis Publishers.

Fish, W. 1993. Sub-surface redox chemistry: a comparison of equillibrium and reaction-based approaches, pp. 73-101. *In* Metals in groundwater, Allen, H.E., E.M. Perdue, and D.S. Brown [eds], Lewis Publishers.

Fredrickson, J.K., and Y.A. Gorby. 1996. Environmental processes mediated by iron-reducing bacteria. Curr. Opin. Biotechnol. 7:287-294.

Fredrickson, J.K., J.M. Zachara, D.W. Kennedy, M.C. Duff, Y.A. Gorby, S.W. Li, and K.M. Krupka. 2000. Reduction of U(VI) in goethite (α-FeOOH) suspensions by a dissimilatory metal-reducing bacterium. Geochim. Cosmochim. Acta 64:3085-3098.

Gilmour, C.C., M.E. Leavitt, and M.P. Shiaris. 1990. Evidence against incorporation of exogenous thymidine by sulfate-reducing bacteria. Limnol. Oceanogr. 35:1401-1409.

Heron, G., and T.H. Christensen. 1995. Impact of sediment-bound iron on redox buffering in a landfill leachate polluted aquifer (Vejen, Denmark). Environ. Sci. Technol. 29:187-192.

Hunter, K.S., Y. Wang, and P. VanCappellen. 1998. Kinetic modeling of microbially-driven redox chemistry of subsurface environments: coupling transport, microbial metabolism and geochemistry. J. Hydrol. 209:53-80.

Keith, V.K. 2001. Immobilization of aqueous strontium during bacterial reduction of synthetic Fe(III) oxides. M.S. Thesis, Department of Biological Sciences, The University of Alabama, Tuscaloosa, AL.

Kirchman, D.L. 1993. Leucine incorporation as a measure of biomass production by heterotrophic bacteria, pp. 509-512. *In* Aquatic microbial ecology, Kemp, P.F., B.F. Sherr, E.B. Sherr, and J.J. Cole [eds], Lewis Publishers.

Kjelleberg, S., B.A. Humphrey, and K.C. Marshall. 1982. Effect of interfaces on small, starved marine bacteria. Appl. Environ. Microbiol. 43:1166-1172.

Larsen, O., D. Postma, and E.E. Roden. 2001. Influence of Fe(III) oxide heterogeneity on bacterial Fe(III) oxide reduction. Geomicrobiol. J. Submitted for publication.

Lloyd, J.R., and L.E. Macaskie. 2000. Bioremediation of radionuclide-containing wastewaters, pp. 277-327. *In* Environmental metal-microbe interactions, Lovley, D.R. [ed], ASM Press.

Lonergan, D.J., H.L. Jenter, J.D. Coates, E.J.P. Phillips, T.M. Schmidt, and D.R. Lovley. 1996. Phylogenetic analysis of dissimilatory Fe(III)-reducing bacteria. J. Bacteriol. 178:2402-2408.

Lovley, D.R. 1991. Dissimilatory Fe(III) and Mn(IV) reduction. Microbiol. Rev. 55:259-287.

Lovley, D.R. 1993. Dissimilatory metal reduction. Annu. Rev. Microbiol. 47:263-290.

Lovley, D.R. 1995. Microbial reduction of iron, manganese, and other metals, pp. 175-231. *In* Advances in Agronomy, Vol 54, Sparks, D.L. [ed], Academic Press Inc.

Lovley, D.R. 2000. Fe(III) and Mn(IV) reduction, pp. 3-30. *In* Environmental metal-microbe interactions, Lovley, D.R. [ed], ASM Press.

Lovley, D.R., and E.J.P. Phillips. 1992a. Reduction of uranium by *Desulfovibrio desulfuricans*. Appl. Environ. Microbiol. 58:850-856.

Lovley, D.R., and E.J.P. Phillips. 1992b. Bioremediation of uranium contamination with enzymatic uranium reduction. Environ. Sci. Technol. 26:2228-2234.

Lovley, D.R., and F.H. Chapelle. 1995. Deep subsurface microbial processes. Rev. Geophys. 33:365-381.

Lovley, D.R., E.J.P. Phillips, Y.A. Gorby, and E.R. Landa. 1991. Microbial reduction of uranium. Nature 350:413-416.

Nealson, K.H., and D. Saffarini. 1994. Iron and manganese in anaerobic respiration: Environmental significance, physiology, and regulation. Annu. Rev. Microbiol. 48:311-343.

Perel'man, A. 1986. Geochemical barriers: theory and practical applications. Appl. Geochem. 1:669-680.

Roden, E.E., and J.M. Zachara. 1996. Microbial reduction of crystalline iron(III) oxides: Influence of oxide surface area and potential for cell growth. Environ. Sci. Technol. 30:1618-1628.

Roden, E.E., and M.M. Urrutia. 1999. Ferrous iron removal promotes microbial reduction of crystalline iron(III) oxides. Environ. Sci. Technol. 33:1847-1853.

Roden, E.E., and R.G. Wetzel. 2001. Kinetics of microbial Fe(III) oxide reduction in freshwater wetland sediments. Limnol. Oceanogr. Submitted for publication.

Roden, E.E., and M.M. Urrutia. 2001a. Growth rates and biomass production of dissimilatory Fe(III)-reducing bacteria (*Shewanella* and *Geobacter*) with soluble and solid-phase Fe(III). Manuscript in preparation.

Roden, E.E., and M.M. Urrutia. 2001b. Influence of Fe(II) surface complexation on bacterial reduction of crystalline Fe(III) oxides. Geomicrobiol. J. Submitted for publication.

Roden, E.E., and D. Sobolev. 2001. Biogeochemistry of iron in sedimentary environments: evidence for rapid microscale cycling of at redox interfaces, In preparation for Biogeochemical cycling of iron in natural environments, Coates, J.D. [ed], Kluwer.

Roden, E.E., M.M. Urrutia, and C.J. Mann. 2000. Bacterial reductive dissolution of crystalline Fe(III) oxide in continuous-flow column reactors. Appl. Environ. Microbiol. 66:1062-1065.

Roden, E.E., M.R. Leonardo, and F.G. Ferris. 2001. Immobilization of strontium during iron biomineralization coupled to dissimilatory hydrous ferric oxide reduction. Geochim. Cosmochim. Acta Submitted for publication.

Rooney-Varga, J.N., R.T. Anderson, J.L. Fraga, D. Ringelberg, and D.R. Lovley. 1999. Microbial communities associated with anaerobic benzene degradation in a petroleum-contaminated aquifer. Appl. Environ. Microbiol. 65:3056-3063.

Salvage, K.M., and G.T. Yeh. 1998. Development and application of a numerical model of kinetic and equilibrium microbiological and geochemical reactions (BIOKEMOD). J. Hydrol. 209:27-52.

Snoeyenbos-West, O.L., K.P. Nevin, R.T. Anderson, and D.R. Lovley. 2000. Enrichment of *Geobacter* species in response to stimulation of Fe(III) reduction in sandy aquifer sediments. Microb. Ecol. 39:153-167.

Sobolev, D., and E.E. Roden. 2001. Suboxic deposition of ferric iron by bacteria in opposing gradients of Fe(II) and oxygen at circumneutral pH. Appl. Environ. Microbiol. 67:1328-1334.

Swartz, C.H., A.L. Ulery, and P.M. Gschwend. 1997. An AEM-TEM study of nanometer-scale mineral associations in an aquifer sand: Implications for colloid mobilization. Geochim. Cosmochim. Acta 61:707 - 718.

Tebes-Stevens, C., A.J. Valocchi, J.M. VanBriesen, and B.E. Rittman. 1998. Multicomponent transport with coupled geochemical and microbiological reactions: model description and example simulations. J. Hydrol. 209:8-26.

Urrutia, M.M., E.E. Roden, and J.M. Zachara. 1999. Influence of aqueous and solid-phase Fe(II) complexants on microbial reduction of crystalline Fe(III) oxides. Environ. Sci. Technol. 33:4022-4028.

Urrutia, M.M., E.E. Roden, J.K. Fredrickson, and J.M. Zachara. 1998. Microbial and geochemical controls on synthetic Fe(III) oxide reduction by *Shewanella alga* strain BrY. Geomicrobiol. J. 15:269-291.

Warren, L.A., P.A. Maurice, N. Parmar, and F.G. Ferris. 2001. Microbially mediated calcium carbonate precipitation: implications for interpreting calcite precipitation and for solid phase capture of inorganic contaminants. Geomicrobiol. J. 18:93-115.

Zachara, J.M. 1996. Subsurface biogeochemistry of organically complexed radionuclides. DOE Subsurface Science Program, Co-Contaminant Subprogram Meeting. Gaithersburg, MD.

Zachara, J.M., R.W. Smith, and F.J. Wobber. 1995. Five-Year plan of basic research. U.S. DOE, Subsurface Science Program, Co-Contaminant Chemistry Subprogram.

Zachara, J.M., S.C. Smith, and J.K. Fredrickson. 1999. The effect of biogenic Fe(II) on the stability and sorption of Co(II)EDTA^{2-} to goethite and a subsurface sediment. Geochim. Cosmochim. Acta 64:1345-1362.

Zachara, J.M., J.K. Fredrickson, S.C. Smith, and P.L. Gassman. 2001. Solubilization of Fe(III) oxide-bound trace metals by a dissimilatory Fe(III) reducing bacterium. Geochim. Cosmochim. Acta 65:75-93.

Zachara, J.M., J.K. Fredrickson, S.W. Li, D.W. Kennedy, S.C. Smith, and P.L. Gassman. 1998. Bacterial reduction of crystalline Fe(III) oxides in single phase suspensions and subsurface materials. Amer. Mineral. 83:1426-1443.

Appendix 1: Reprints of Published Papers

Microbial and Surface Chemistry Controls on Reduction of Synthetic Fe(III) Oxide Minerals by the Dissimilatory Iron-Reducing Bacterium *Shewanella alga*

M. M. URRUTIA
E. E. RODEN

Department of Biological Sciences
The University of Alabama
Box 870206
Tuscaloosa, Alabama, USA

J. K. FREDRICKSON
J. M. ZACHARA

Battelle Pacific Northwest Laboratory
P.O. Box 999
Richland, Washington, USA

The role of Fe(II) biosorption and the effect of medium components on the rate and long-term extent of Fe(III) oxide reduction (FeRed) by a dissimilatory Fe(III)-reducing bacterium (Shewanella alga *strain BrY) were examined in batch culture experiments. Introduction of fresh* S. alga *cells into month-old cultures in which Fe(III) reduction had ceased resulted in further reduction of synthetic amorphous Fe(III) oxide, hematite, and two forms of goethite (Gt). Fresh* S. alga *cells were also able to reduce a substantial amount of synthetic Gt that had been partly or completely saturated with sorbed Fe(II). Cells that had been precoated with Fe(II) showed a reduced rate and capacity for FeRed. These results indicated that biosorption of Fe(II) had a major impact on FeRed.* S. alga *cells were shown to have an Fe(II) sorption capacity of ~0.1 mmol g^{-1}, compared with ~0.25 mmol g^{-1} determined for the synthetic Gt. Sorption experiments with component mixtures indicated that direct interaction between cells and oxide resulted in increased Fe(II)-binding capacity of the mixed system, possibly through production of exopolymeric materials by the cells. Medium constituents that affected Fe(II) speciation were shown to have a significant indirect influence on the extent of oxide reduction. Malate, which formed soluble complexes with Fe(II), promoted the extent of oxide reduction. In contrast, high (mM) PO_4^{3-} concentrations favored surface/bulk precipitation processes which reduced the extent of oxide reduction. Collectively, our results indicate that Fe(II) sorption by oxide and cell surfaces, together with Fe(II) complexation by or precipitation with medium components, all influence the rate and extent of FeRed. Furthermore, saturation of sorption sites with Fe(II) does not appear to limit the ability of* S. alga *to reduce Fe(III) oxides, especially if conditions favor growth.*

Keywords Fe(III) oxide reduction, Fe(III) biosorption, surface saturation, Fe(II) complexation

Received 9 January 1998; accepted 12 May 1998.

This research was supported by the Subsurface Science Program, Office of Health and Environmental Research, U.S. Department of Energy (DOE). Pacific Northwest National Laboratory is operated for DOE by Battelle Memorial Institute under contract DE-AC06-76RLO 1830.

Address correspondence to Dr. Matilde M. Urrutia, Department of Biological Sciences, The University of Alabama, Box 870206, Tuscaloosa, AL 35487-0206, USA. E-mail: murrutia@biology.as.ua.edu

Geomicrobiology, 15:269–291, 1998
Copyright © 1998 Taylor & Francis
0149-0451/98 $12.00 + .00

Fe(III) oxide reduction results primarily from the enzymatic activity of respiratory Fe(III)-reducing bacteria (FeRB) in nonsulfidogenic, anoxic sedimentary environments (Lovley 1991; Lovley et al. 1991). FeRB can play an important role in natural degradation of organic carbon in such environments (Lovley and Phillips 1986b; Lovley and Phillips 1988; Myers and Myers 1994; Nealson and Myers 1992; Roden and Wetzel 1996) and in the oxidation of aromatic hydrocarbon contaminants (Lovley et al. 1989; Lovley et al. 1995; Lovley and Lonergan 1990; Lovley et al. 1994). Fe(III) oxide reduction may also have important indirect influences on the persistence and mobility of metal/organic contaminants in anaerobic soils and sediments. In some cases, metal oxide reduction may cause mobilization of adsorbed metals and radionuclides (Chapelle 1993; Jenne 1977; Landa et al. 1991; Lovley 1991). In other cases, production of bicarbonate during metabolism of organic matter coupled to Fe(III) respiration may lead to precipitation of carbonate minerals that can immobilize radionuclides and other metals (Lanstrom and Tullborg 1995; Pedersen and Karlsson 1995), or the metals may be reduced directly by the FeRB to an insoluble form (Fendorf and Li 1996; Lovley 1995; Makos and Hrncir 1995; Zachara et al. 1995).

Considering the broad influence that microbial Fe(III) oxide reduction can have on the biogeochemistry of both pristine and contaminated soils and sediments, understanding the mechanisms that control this process is critical for predicting its influence on natural and contaminant metal/organic transformations. Previous laboratory studies have shown that direct contact between metal oxide-reducing bacterial cells and mineral surfaces is required for reduction to occur (Arnold et al. 1988; Caccavo et al. 1992; Tugel et al. 1986), that particle size and surface area have an important influence on the rate and extent of solid-phase Fe(III) reduction (Arnold et al. 1988; Fisher and Pfanneberg 1984; Lovley and Phillips 1986a; Lovley and Phillips 1987; Roden and Zachara 1996), and that soluble Fe(III) species are more readily reduced (Arnold et al. 1986; Lovley 1991). Although poorly crystalline, high-surface-area Fe(III) oxides are the most susceptible to reduction by FeRB (Arnold et al. 1988; Roden and Zachara 1996; Tugel et al. 1986), lower-surface-area crystalline oxides such as goethite and hematite are often more abundant in soils and sediments (Schwertmann and Taylor 1989).

A thorough understanding of microbial Fe(III) oxide reduction in well-defined experimental systems is a prerequisite for understanding this complex process in the field. Although the above-mentioned studies have established important parameters controlling the rate and extent of bacterial Fe(III) oxide reduction, the geochemical and microbiological interactions that govern this process are complex and not fully defined. Recent results suggested that saturation of Fe(III) oxide surfaces with adsorbed Fe(II) controls the long-term extent of microbial Fe(III) oxide reduction in batch experiments (Roden and Zachara 1996). However, this study did not consider the possibility that Fe(II) biosorption by FeRB might affect cell viability and the rate and extent of Fe(III) oxide reduction.

The purpose of the present study was to investigate the influence of Fe(II) speciation (biosorption, aqueous complexation, ferrous phosphate precipitation) on microbial Fe(III) oxide reduction. The study included different Fe(III) oxides, but emphasis was placed in α-FeOOH (goethite) because of its ubiquitous presence in soils and sediments (Schwertmann and Taylor 1989).

Materials and Methods

Organism and Culture Conditions

The dissimilatory Fe(III)- and Mn(IV)-reducing bacterium *Shewanella alga* strain BrY (Rosselló-Mora et al. 1994) was used for all experiments. *S. alga* is a gram-negative, facultative anaerobe, able to use H_2 as electron donor and both amorphous (Caccavo et al. 1992)

and crystalline (Roden and Zachara 1996) Fe(III) oxyhydroxides as electron acceptors. *S. alga* was grown anaerobically in a modified basal culture medium (Lovley and Phillips 1988) at circumneutral pH with H_2 as electron donor, 30 mM malate as a source of carbon, and 50 or 100 mmol L^{-1} synthetic Fe(III) oxyhydroxides as electron acceptors. In some experiments (indicated below), the amount of P (added as K_2HPO_4) in the medium was reduced to 0.04 mM, whereas the basal medium contained 4.4 mM. Standard anaerobic techniques were used for all procedures as described by Lovley and Phillips (1987).

The following method of cell preparation and inoculation was used in all following experiments. *S. alga* was grown aerobically to late-exponential phase in Tryptic Soy Broth (TSB). Previous studies have demonstrated that TSB-grown cells actively reduce Fe(III) upon introduction into anaerobic medium (Roden and Zachara 1996). Cells were harvested by centrifugation (7500*g*, 15 min) and washed once with 10 mM Pipes buffer [piperazine-*N*,*N*′-bis(2-ethanesulfonic acid), dipotassium salt; Sigma] at pH 6.8–7.0 and resuspended to $\sim 10^8$ cells mL^{-1} [$\sim$4.5 g cells (dry weight) L^{-1}]. Washed cells were sparged with O_2-free N_2 under sterile conditions, and 0.5 mL of the cells was used to inoculate 10 mL of the anaerobic medium in pressure tubes (Bellco, Bellefonte, PA) after the addition of 10 mL of hydrogen gas. Culture tubes were incubated on their side, without shaking, in the dark at 31°C.

Synthesis of Fe(III) Oxyhydroxides

Hydrous ferric oxide (HFO) and hematite (Hm) were synthesized from $Fe(NO_3)_3$ (Schwertmann and Cornell 1991) and medium-surface-area goethite (55 m^2 g^{-1}) (MSA-Gt1) from $FeCl_3$ (Atkinson et al. 1968). A high-surface-area goethite (HSA-Gt) was also synthesized via $FeCl_2$ oxidation (Goodman and Lewis 1981). A second medium-surface-area goethite (MSA-Gt2) was synthesized by a similar procedure (incubated at 60°C for 10 days instead of 3 days as previously), and extracted with 0.25 M $NH_2OH \cdot HCl$ (hydroxylamine hydrochloride) in 0.25 M HCl five times to remove poorly crystalline Fe(III) oxide impurities. Subsequently, the mineral was washed three times with 0.1 M $NaClO_4$ and then dialyzed against deionized water to remove excess salt. Its surface area was 50 m^2 g^{-1}. All other minerals were washed free of electrolytes by centrifugation. HFO was maintained as a slurry, whereas MSA-Gt1, MSA-Gt2, HSA-Gt, and Hm were freeze-dried and passed through a 100-μm (150-mesh) sieve. Henceforth, we use Gt to refer to the mineral goethite in general terms.

Reinoculation Experiments

Fe(III)-reducing cultures that had come to the completion of a reduction cycle (reduction had ceased) were reinoculated with washed, TSB-grown *S. alga* cells by the procedure described above (0.5 mL of a suspension of 10^8 cells mL^{-1} per 10 mL of medium). In the initial experiment with 100 mmol L^{-1} MSA-Gt1 or Hm, cells were added and Fe(III) reduction was measured during two additional reinoculations. In a second experiment (with 50 mmol L^{-1} MSA-Gt1 and HSA-Gt), fresh anaerobic medium or H_2 (or both) were added with the second reinoculation. In this case, fresh medium additions were made inside an anaerobic chamber after aseptically removing the spent medium.

Fe(II) Sorption Isotherms

MSA-Gt1, *S. alga* cells, and mixtures of both were titrated with ferrous iron to determine their Fe(II) sorption capacity. For Gt, 0.2-mL aliquots of filter-sterilized anaerobic $FeCl_2$ stock solutions were added to triplicate 15-mL portions of sterile 50 mmol L^{-1} (4.5 g L^{-1}) Gt suspensions in either 10 mM Pipes buffer or whole medium (i.e., with 30 mM malate

and 0.04 mM PO_4^{3-}) at pH 6.9. Fe(II) concentrations added to the MSA-Gt1 suspensions were 0.043, 0.096, 0.22, 0.42, 0.64, 0.97, 1.19, 2.62, 5.04, and 6.47 mM. Samples were equilibrated for 18 h with shaking at 50 rpm, after which dissolved Fe(II) concentrations [$Fe(II)_{aq}$] were determined as described below. The sorbed Fe(II) was calculated as the difference between added Fe(II) and $Fe(II)_{aq}$.

The Fe(II) adsorption capacity of *S. alga* cells was determined by the same procedure with a thick suspension of cells [6.67 g (dry weight) of cells L^{-1}, 1.2 mg of protein mL^{-1}]. Anaerobic cell suspension (3 ml) was injected into duplicate tubes with 10 mL of sterile, anaerobic 10 mM Pipes buffer, pH 6.9. $FeCl_2$ stock solutions (0.1 mL) were added anaerobically to obtain Fe(II) concentrations of 0.012, 0.024, 0.055, 0.126, 0.241, 0.368, 0.555, 0.681, 1.505, and 2.880 mM. Samples were equilibrated and processed as indicated above.

For the mixed (Gt plus cells) titration, 3 mL of a washed cell suspension (dry weight and biomass as in the previous paragraph) was injected into 10 mL of sterile 50 mmol L^{-1} MSA-Gt1 suspension in 10 mM Pipes buffer, pH 6.9. Cells and Gt were incubated for 30 min with shaking at 50 rpm prior to addition of Fe(II). Aliquots (0.2 mL) of Fe(II) stock solutions were then added to give final Fe(II) concentrations of 0.05, 0.11, 0.25, 0.48, 0.73, 1.10, 1.35, 2.99, 5.73, and 7.35 mM. Samples were incubated and analyzed as explained above. This mixed isotherm was repeated twice at different times with the same procedure.

A third mixed isotherm was conducted in which direct contact between Gt and cells was prevented by placing them inside separate dialysis membranes. Suspensions of MSA-Gt in 1 mL of 10 mM Pipes were prepared so that addition to 50 mL of buffer would result in a Gt concentration of 50 mmol L^{-1}. These 1-mL suspensions were autoclaved and transferred into sterile dialysis bags (Spectra/Por 1.1 Biotech, sterile, 8000 molecular weight cutoff) when cool. The bags were then aseptically introduced into 50 mL of sterile 10 mM Pipes (pH 6.9) and degassed with O_2-free N_2 gas. Cells (1 mL) were also transferred into dialysis bags and added to the flasks containing the Pipes buffer and the Gt inside the dialysis tubing under N_2 flow using aseptic techniques. The flasks were then degassed for an extra 30 min and sealed, and 0.2 mL of Fe(II) solution was added. Controls with empty dialysis bags were set up in the same way to assess the amount of Fe(II) that bound to the membranes. The flasks were incubated at room temperature for 18 h with shaking at 50 rpm. At that time, the $Fe(II)_{aq}$ concentration was determined, and the flasks were taken into an anaerobic chamber. Gt-containing and cell-containing bags were allowed to drain inside the anaerobic chamber and then were placed into separate, preweighed vials containing 10 mL of 0.5 M HCl. The dialysis bag controls were also digested in 0.5 M HCl. Sorbed Fe(II) was calculated as the difference between the HCl-extractable Fe(II) and the $Fe(II)_{aq}$ for each sorbent.

Experiments with Fe(II)-Coated Cells

Washed, TSB-grown *S. alga* cells were incubated anaerobically in the presence of 1 mM Fe(II) (as ferrous ammonium sulfate) for 1 h to allow binding of Fe(II) by bacterial surfaces. The cells were then centrifuged (10,000*g*, 10 min) and washed once in 10 mM Pipes to eliminate aqueous and loosely bound Fe(II). Supernatants from the incubation and washes were analyzed for Fe(II) to determine the amount of Fe(II) that remained sorbed to the cells after washes. The Fe(II)-treated cells (FeIIBrY) were resuspended to their original volume in 10 mM anaerobic Pipes and used as inoculum for Fe(III) reduction experiments with 40 mmol L^{-1} HFO, and 50 mmol L^{-1} each of MSA-Gt1 and HSA-Gt in full basal medium (4.4 mM P) in comparison with washed, untreated cells from the same TSB culture. Fe(II)-treated and untreated cells were plated in tryptic-soy agar plates right after inoculation of Fe-reducing cultures; we found no differences in the number of colony-forming units for both types of cells.

Reduction of Fe(II)-Coated MSA-Gt

Triplicate samples of 50 mmol L^{-1} MSA-Gt1 in 10 mM Pipes at pH 6.9 that had various amounts of adsorbed Fe(II) (see procedure for Fe(II) sorption isotherms) were inoculated with washed TSB-grown *S. alga* cells after addition of H_2, and incubated at 31°C without any nutrient source (nongrowth conditions), in the dark and without shaking, and also in growth medium with 0.04 mM P. Duplicate tubes were sacrificed and 0.5 M HCl-extractable Fe(II) was determined at $t = 0$, 1, 2, and 30 days. Fe(III) reduction by *S. alga* was calculated as the difference between Fe(II) at the time of sampling and that before inoculation ($t = 0$).

Influence of Medium Composition

The effect of medium composition on the rate and amount of MSA-Gt2 (50 mmol L^{-1}) reduction by *S. alga* was studied in a series of experiments with progressively more-complex matrix:

1. H_2 + 10 mM Pipes (henceforth referred to as Pipes), nongrowth;
2. H_2 + 10 mM Pipes + 30 mM Malate (Pipes + Malate), nongrowth;
3. H_2 + 10 mM Pipes + 30 mM malate + growth-medium components (vitamins, minerals, and NH_4) + low P (0.04 mM KH_2PO_4) (Pipes + Malate + 0.04 mM P medium);
4. H_2 + 10 mM Pipes + 30 mM malate + medium components + full P (4.4 mM KH_2PO_4) (Pipes + Malate + 4.4 mM P medium);
5. H_2 + 10 mM Pipes + 30 mM lactate (Pipes + Lactate), nongrowth;
6. Same as (3) but with 30 mM lactate instead of malate (Pipes + Lactate + 0.04 mM P medium);
7. Same as (4) but with 30 mM lactate instead of malate (Pipes + Lactate + 4.4 mM P medium).

Soluble and 0.5 M HCl-extractable Fe(II) and soluble PO_4^{3-} concentrations were followed over time and pH was determined at the final sampling as indicated below.

Effect of Malate Concentration

The influence of malate concentration on the total amount of 50 mmol L^{-1} MSA-Gt2 and HFO reduction by *S. alga* was assessed by using 0.04 mM P medium and 30, 7.8, 3, and 0.3 mM Na-malate.

Analytical Techniques

Fe(III) oxide reduction was determined by extracting the oxide suspensions with 0.5 M HCl for 2 h and analyzing the Fe(II) content of the extracts with ferrozine (Lovley and Phillips 1986b). Soluble Fe(II) (Fe_{aq}) was determined by filtering the suspension through a 0.22-μm Poretics nylon syringe filter directly into ferrozine and immediately reading the absorbance at 562 nm. Total Fe in the oxides was determined by dissolving the solids in concentrated HCl and analyzing the Fe(III) content of a diluted extract by reduction with 0.25 M hydroxylamine hydrochloride in ferrozine. Soluble PO_4^{3-} was determined colorimetrically (Murphy and Riley 1962), and the pH of the medium was measured with a Corning semimicro combination pH electrode and an Orion pH meter inside N_2/H_2 anaerobic chamber (Coy products).

TABLE 1 Freundlich parameters (K_F and n), apparent sorption maxima, and log K values for the sorption of Fe(II) to *S. alga* cells, to MSA-Gt1 in either Pipes (Pipes1, Pipes2) or 0.04 mM P media (Medium), or to a mixture of MSA-Gt1 and *S. alga* in Pipes buffer (Mixed-1) corresponding to the data on Figure 4A; in all cases, pH was 6.9

Material	K_F, mol kg^{-1}	n	r^2	Adsorp. max[a] mmol Fe(II) g^{-1}	Log K[b]
S. alga	1.02	0.444	0.924	0.10	−2.25
MSA-Gt Pipes1	0.57	0.203	0.758	0.25	n.d.
MSA-Gt Pipes2	0.57	0.158	0.858	0.22	−1.74
MSA-Gt Medium	1.68	0.336	0.965	0.25	n.d.
Mixed-1	19.88	0.562	0.985	0.45	−0.49

[a]Approximate values obtained from direct titration plots, in mmol Fe(II) g^{-1} dry weight of material.
[b]K = activity Freundlich adsorption constant, in mol L^{-1}.
n.d. = not determined.

Fe(II) Speciation and Sorption Modeling

MINTEQA2 (Allison et al. 1991) was used to model the adsorption isotherms for MSA-Gt1, *S. alga*, and mixed systems, and to evaluate aqueous speciation and the potential for ferrous phosphate precipitation. The Fe(II) sorption data conformed to the Freundlich isotherm [see *Results* section on Fe(II) sorption capacity]. Therefore, the activity Freundlich adsorption model from MINTEQA2 was used to fit binding parameters to the observed data. The corrected activity Freundlich adsorption constant was obtained by refitting the isotherms plotted according to M Fe(II)-sorbed (y-axis) and M $(Fe^{2+})_{aq}$ (x-axis), where $(Fe^{2+})_{aq}$ is the computed aqueous phase activity. A log K value of 3.48 (25°C, I = 0) was used for Fe(II)-malate complexes (Smith et al. 1993). In those systems where P was present, vivianite precipitation was considered (log K = 36.00). The values of the activity Freundlich adsorption constant and n obtained for the empirical (Gt + BrY) mixed system (Table 1) were used in MINTEQA2, assuming that the system could be approximated by the equilibrium condition. The observed HCl-extractable Fe(II) concentrations from each reduction experiment shown later in Figure 7 were introduced as total Fe(II) concentrations in the model with a sweep option. The effect of malate concentration on Fe(II) speciation was also evaluated separately by calculating Fe(II) speciation at several malate concentrations (introduced as a sweep) for a system in which total Fe(II) concentration was 1.6 mM, which was the lowest final Fe(II) concentration achieved through reduction in the experiments that studied the effect of malate (see *Influence of Medium Composition*, below).

Results

Reinoculation Experiments

Reinoculation of MSA-Gt1 that had already undergone a complete reduction cycle (i.e., had been reduced by *S. alga* for 30 days or longer) resulted in further reduction, from 6% of total Fe after one reduction cycle to 10% after reinoculation with fresh cells (Figure 1A). For Hm, reduction increased from 0.27% to 1.28% after the first reinoculation and to 2.14% after a second reinoculation (Figure 1B). In a second experiment, there was an increase in MSA-Gt1 reduction from 8% to 15–18% after two reinoculations (Figure 2A), whereas

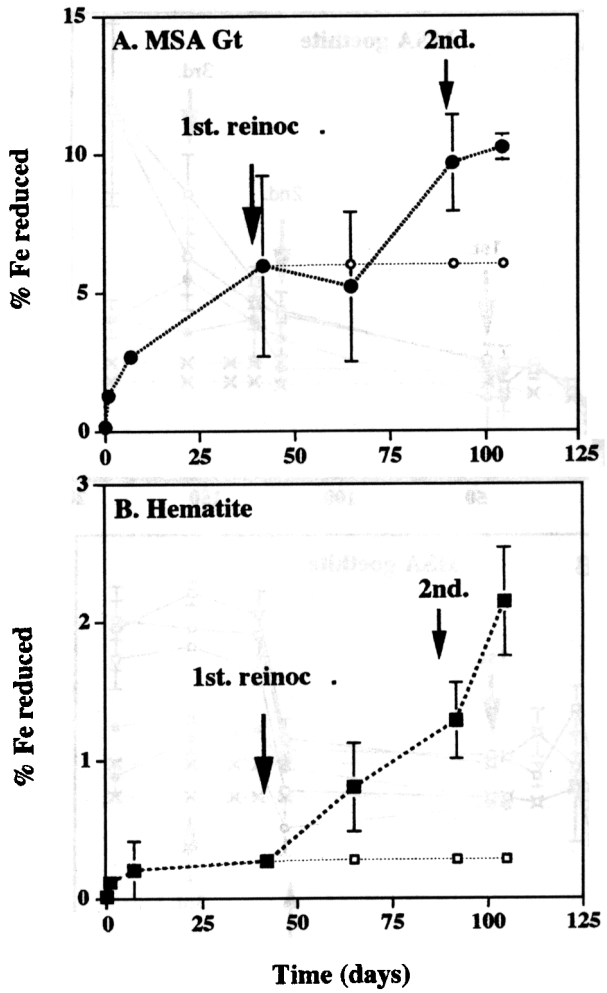


FIGURE 1 Goethite (A) and hematite (B), (100 mmol L^{-1} suspensions), reduction before and after two reinoculations (indicated by the arrows: 1st. reinoc = first reinoculation; 2nd. = second reinoculation). Closed symbols represent reinoculated samples; open symbols, nonreinoculated controls. Error bars represent standard deviation of the mean (n = 3); when not apparent, error bars are smaller than the corresponding symbol, except in the nonreinoculation controls, for which results from only one sample are presented.

reinoculation with fresh cells alone did not promote further reduction of HSA-Gt (Figure 2B, first reinoculation). However, when complete medium was added along with a second reinoculation, a further 20% reduction of HSA-Gt was obtained (Figure 2B). Addition of H_2 alone to the HSA-Gt cultures with the second reinoculation produced a 5–10% increase in Fe(III) reduction (Figure 2B). No further reduction was observed after ~30 days in the nonreinoculated controls (open symbols in Figure 1, crosses in Figure 2).

Fe(II) Sorption Capacity of Oxides and Cells

The adsorption of Fe(II) on MSA-Gt1 and *S. alga* followed Freundlich isotherms (Figures 3 and 4). *S. alga* cells showed an Fe(II) sorption capacity of 0.1 mmol Fe(II) g^{-1} dry cell

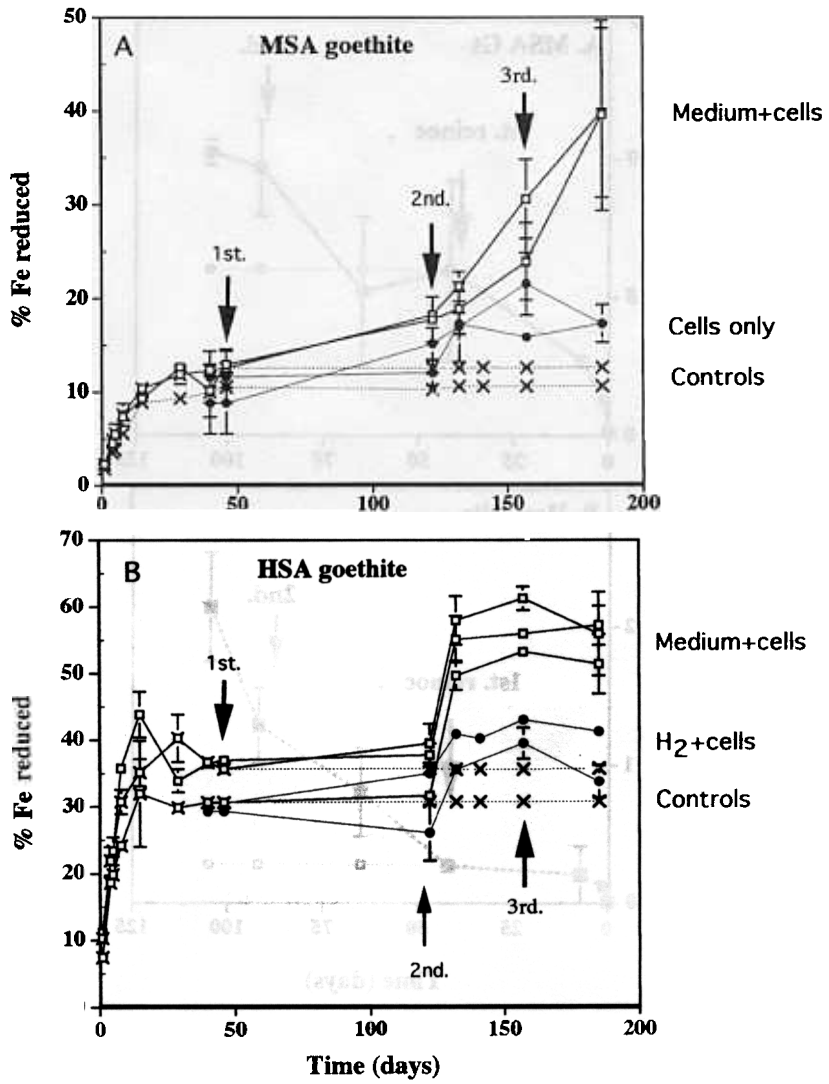
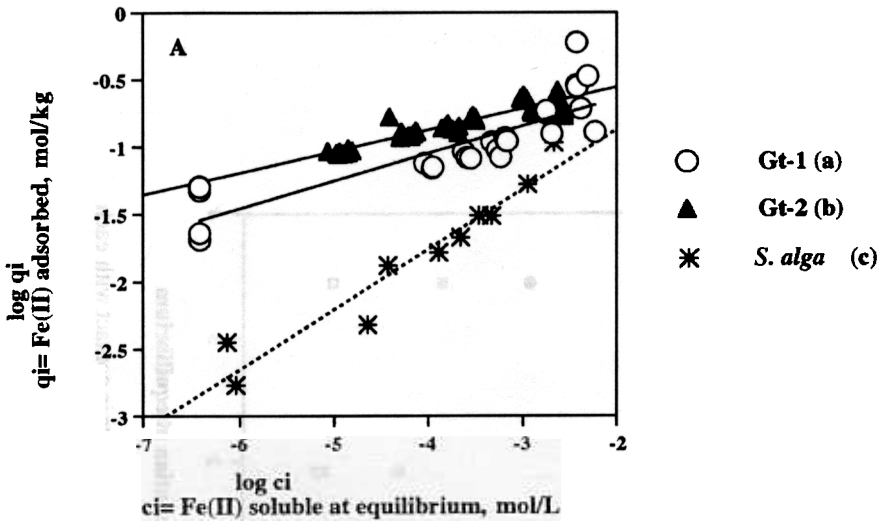


FIGURE 2 Reduction of MSA-Gt (A) and HSA-Gt (B), (50 mmol L^{-1} suspensions), by *S. alga* before and after three reinoculations. 1st., 2nd., and 3rd. represent the time points at which the first, second, and third reinoculations took place. The first reinoculation consisted of fresh cells only. Treatments at the time of the second reinoculation included: "Medium + cells" (open squares), which indicates additions of basal medium and H_2 with the second reinoculation; "H_2 + cells" (filled circles in B), which indicates addition of H_2 only with the second reinoculation; "Cells only" (filled circles in A), which indicates addition of fresh cells only. Nonreinoculated controls, which received no additions, are represented by crosses. Common symbols represent different, replicated trials using the same treatment. Error bars represent standard deviation of the mean (n = 3); when not apparent, error bars are smaller than the corresponding symbol, except in the nonreinoculated controls, for which results from only one sample are presented.



(a) $y = 0.203x - 0.241$ $r^2 = 0.758$ (b) $y = 0.158x - 0.246$ $r^2 = 0.858$

(c) $y = 0.444x + 0.009$ $r^2 = 0.924$

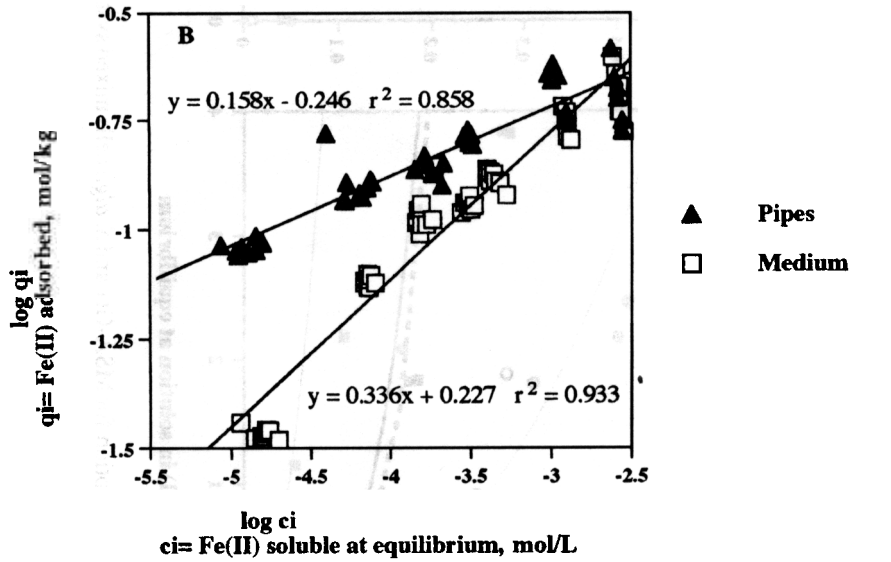


FIGURE 3 Freundlich isotherms for the sorption of Fe(II) on *S. alga* cells and MSA-Gt1 in pH 6.9, 10 mM Pipes buffer (A) and on MSA-Gt1 in pH 6.9 Pipes buffer or 0.04 mM P medium with malate (B).

weight, and the MSA-Gt1 sorption was 0.2–0.25 mmol Fe(II) g^{-1} (Figure 4A). The sorption of Fe(II) to Gt was affected if growth medium instead of Pipes buffer was used for the sorption experiments, particularly at low Fe(II) loadings (Figure 3B), but in both cases the maximum Fe(II) sorption capacity was approximately the same.

When cells and Gt were present together in direct contact (mixed isotherm), Fe(II) sorption again followed a Freundlich isotherm, and was greater than observed for the individual components (Figure 4A, Mixed-1, and Table 1) with a maximum of ~0.4 mmol

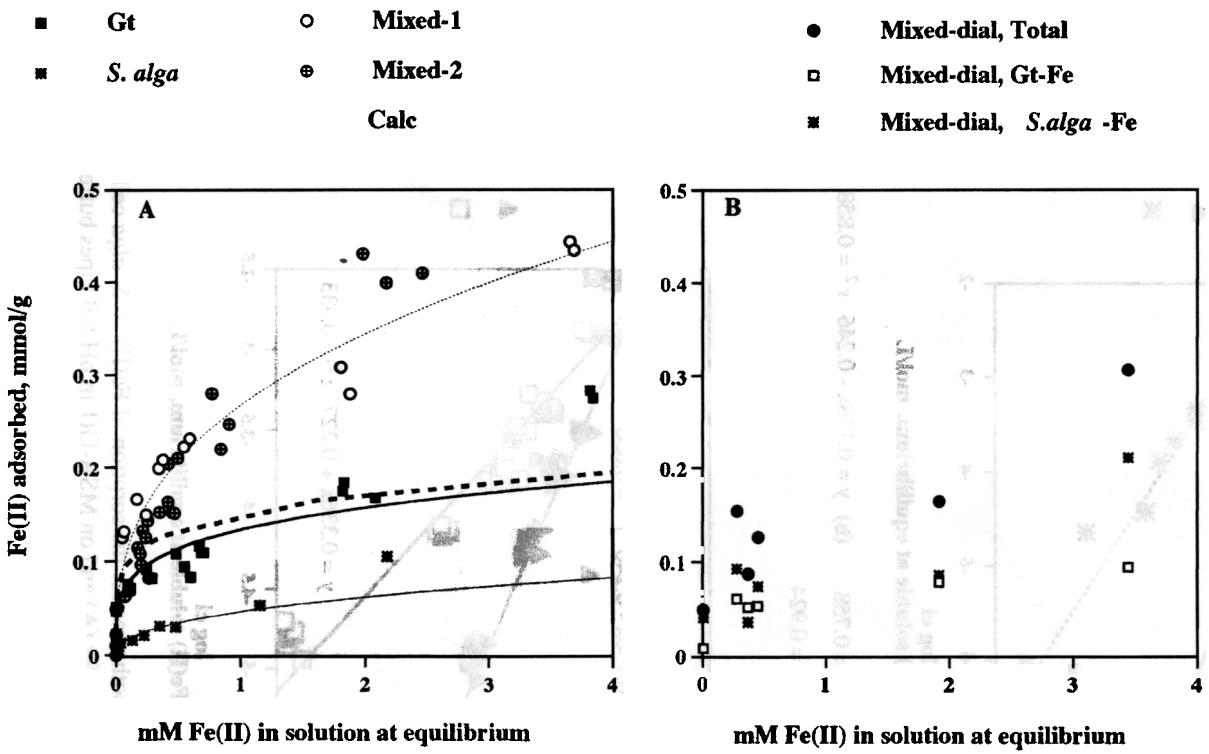


FIGURE 4 Fe(II) sorption for MSA-Gt1 and *S. alga* cells mixed systems. (A) Both constituents in contact with each other in comparison with the isotherms for the individual components, goethite (MSA-Gt1) and *S. alga* cells (BrY); Mixed-1 and Mixed-2 refer to two separate determinations of sorption by the mixed system; Calc represents the mixed adsorption isotherm calculated from the individual Gt and *S. alga* isotherms and solid lines represent Freundlich equations fitted to *S. alga*, MSA-Gt1, and mixed systems sorption data (see Table 1). (B) Constituents separeted by dialysis bags (Mixed-dial, Total) including the amounts sorbed to Gt (Mixed-dial, Gt-Fe) and to *S. alga* (Mixed-dial, *S. alga*-Fe) separately.

Fe(II) g^{-1} (dry weight Gt + cells). This result was corroborated in a second experiment (Figure 4A, Mixed-2). When direct contact between oxide and cells was prevented by placing cells and oxides inside separate dialysis bags, the overall Fe(II)-binding capacity was lower than observed in the full-contact mixed system (Figure 4B, filled circles). Quantification of Fe(II) adsorbed by *S. alga* and Gt showed that sorption (per mass unit) to both phases was approximately equivalent (Figure 4B).

The mixed isotherm was simulated with MINTEQA2, on the basis of the individually measured isotherms in Figure 3. The calculation involved two independent adsorption sites (on Gt and *S. alga*), each described by the appropiate activity Freundlich relationship (Table 1). The predicted mixed isotherm (Figure 4A, dotted line) resembled that of Gt (Figure 4A, squares and continuous line) and markedly underestimated the amount of Fe(II) sorbed in the experimental system (Figure 4A, empty and crossed circles). Therefore, the activity Freundlich adsorption model from MINTEQA2 was used to fit binding parameters to the observed data in the mixed (Gt + BrY) system (see *Materials and Methods* for methodology) that more accurately characterize Fe(II) sorption processes during the reduction experiments (Table 1).

Experiments with Fe(II)-Coated Cells

Reduction of MSA-Gt, HSA-Gt, and HFO by Fe(II)-treated cells (Figure 5A and B, filled symbols) was slower than reduction by untreated cells (Figure 5A and B, open symbols). Fe-treated cells had 0.023 mmol Fe(II) g^{-1} dry weight, which corresponded to 23% of their measured maximum binding capacity as determined in earlier sorption experiments. The initial rates (0–48 h) of Fe(III) oxide reduction by Fe(II)-coated cells were comparable with those exhibited by uncoated cells after ~10 days of incubation (Figure 5C–E). The long-term extent of MSA-Gt1 reduction by Fe(II)-coated cells was substantially less than by uncoated cells (6% after 40 days vs 10% in the controls) (Figure 5A), whereas similar amounts of HSA-Gt and HFO were reduced in the long term.

Reduction of Fe(II)-Coated MSA-Gt

MSA-Gt1 (in either Pipes buffer alone or Pipes-buffered, 4.4 mM P growth medium) was loaded with different concentrations of Fe(II) and inoculated with fresh *S. alga* cells. The initial (0–24 h) MSA-Gt1 reduction by *S. alga* in growth medium decreased with increasing amounts of presorbed Fe(II); there was little reduction of Fe(II)-loaded MSA-Gt1 in the (nongrowth) Pipes buffer (Figure 6A). However, after 30 days, the cultures generally showed similar amounts of Fe(III) reduction, regardless of the amount of presorbed Fe(II) (Figure 6B), except for the Gt samples with $\geq$~0.2 mmol g^{-1} presorbed Fe(II) in nongrowth medium. The total amount of Fe(II) produced in the different cultures in growth medium (0.7–0.9 mmol Fe(II) g^{-1} Gt, equivalent to 10–13% of total Fe in this Gt) well exceeded the maximum Fe(II) adsorption capacity of the mineral [~0.25 mmol Fe(II) g^{-1}], as well as the Fe(II) sorption capacity of the mixed system [~0.4 mmol Fe(II) g^{-1}].

Influence of Medium Composition

The influence of various medium components was studied in a series of experiments with progressively more-complex medium composition. Fe(III) reduction in medium containing H_2 and malate as the energy and C sources, respectively, was compared with that in medium containing lactate as a combined energy/C source. Fe(III) reduction was also compared in medium containing two concentrations of phosphate, and all treatments were compared with

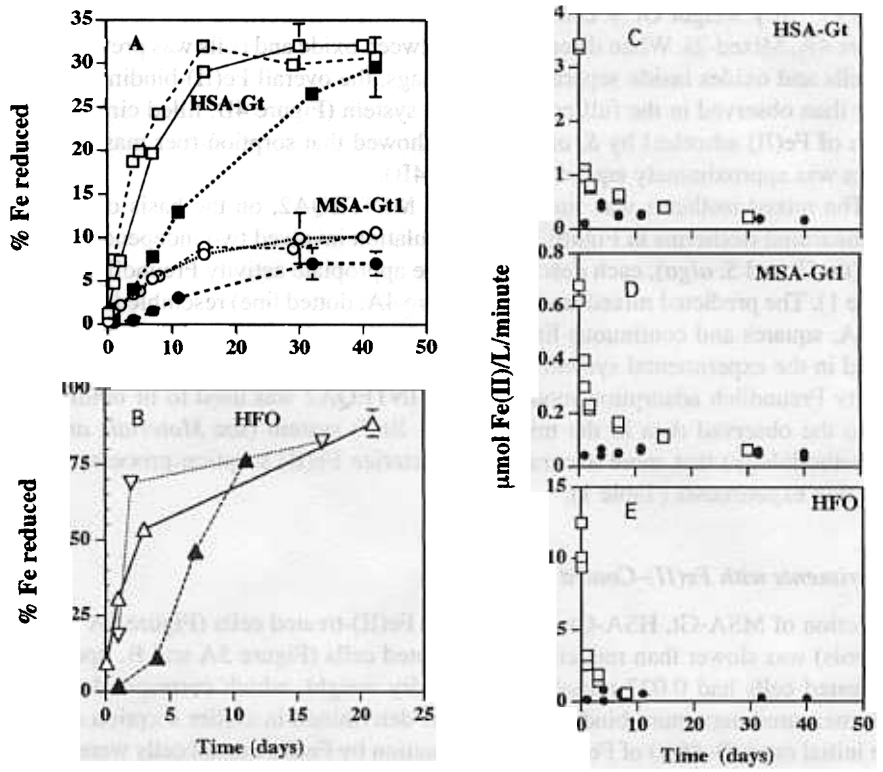


FIGURE 5 Fe(III) reduction by Fe(II)-coated cells from HSA-Gt(A), MSA-Gt1 (A), and HFO (B) in 4.4 mM P medium. Open symbols represent reduction by untreated *S. alga* (of which there are always two replicates), and filled symbols represent reduction by FeIIBrY. Panels C–E show the rates of Fe(III) reduction by *S. alga* (open symbols) vs FeIIBrY (filled circles) for HSA-Gt (C), MSA-Gt1 (D), and HFO (E) in μM Fe(II) min^{-1}. Error bars represent standard deviation of the mean (n = 3); when not apparent, error bars are smaller than the corresponding symbol.

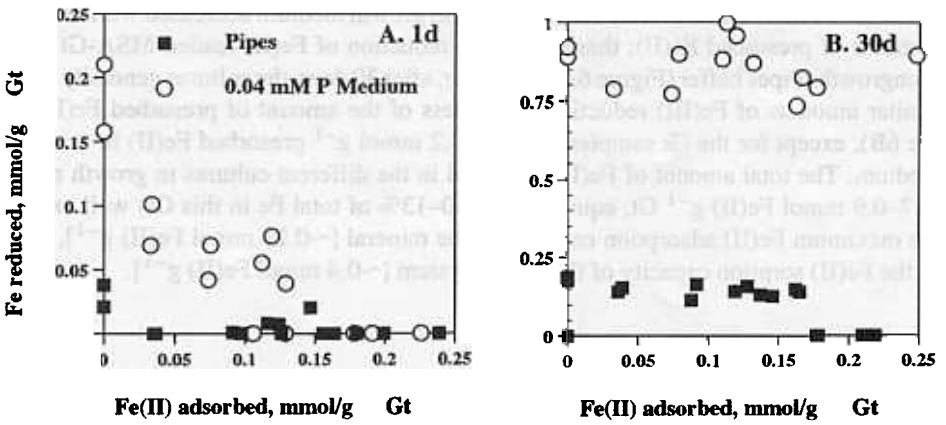


FIGURE 6 Reduction of MSA-Gt1 with preadsorbed Fe(II) by *S. alga* in Pipes or in 0.04 mM P medium (see text) at 1 day (A) or 30 days (B). Data points are from individual culture tubes.

a control containing only H_2 and Pipes buffer (nongrowth conditions). Results showed that the composition of the medium significantly influenced the extent of MSA-Gt1 reduction by *S. alga* and the distribution of Fe(II) between the aqueous and solid phases (Figure 7). In nongrowth controls (Pipes buffer + H_2 only) (Figure 7A), a maximum of 0.4 mM Fe(II) was reduced, most of which (0.35 mM) was sorbed to the oxide and cells. All other treatments showed greater extents of MSA-Gt2 reduction than Pipes + H_2 alone.

The presence of malate resulted in a greater extent of Gt reduction than did medium containing lactate (Figure 7: B vs C, D vs E), except in the high-P medium (see next paragraph). The increase in total Fe(III) reduced in the presence of malate was always associated with higher concentrations of soluble Fe(II). For instance, under nongrowth conditions, the final extent of Gt reduction was ~0.7 mM Fe(II) (1.4% Fe reduced) with lactate (Figure 7C) and 1.8 mM (3.7% reduced) with malate (Figure 7B), of which ~0.3 mM was present as $Fe(II)_{aq}$ in lactate medium in contrast to 1 mM $Fe(II)_{aq}$ in the presence of malate. A similar trend was observed in medium with 0.04 mM P (Figure 7D and E). In all cases there was an excess of electron donor (H_2 or lactate) in the medium. In another experiment (also in 0.04 mM P medium), the final extent of MSA-Gt2 reduction increased with increasing malate concentrations (Figure 8A), even though initial rates of reduction were faster with decreasing malate. Similar results were obtained in parallel experiments with HFO, although in this case the extent of HFO reduction was essentially the same for all malate concentrations after 14 days of incubation (Figure 8B) because of transformation to magnetite.

Phosphate concentration also affected the extent of MSA-Gt2 reduction by *S. alga*, as well as the distribution of evolved Fe(II) between the aqueous and solid phases. Accumulation of $Fe(II)_{aq}$ was suppressed in medium containing 4.4 mM P (Figure 7F and G). There were relatively few differences in Fe(II) speciation or the overall reduction of Gt between malate and lactate media at this P concentration, suggesting that 4.4 mM P overrode the influence of malate shown before. Determination of soluble P prior to inoculation showed that most (99.75%) of the phosphate in 0.04 mM P medium was adsorbed to Gt. In contrast, most of the phosphate in 4.4 mM P medium remained in solution before inoculation; however, it decreased rapidly as Fe(III) reduction produced 2–3 mM Fe(II) during the first 2 weeks of incubation (data not shown). The ratios of sorbed Fe(II) to P lost from solution ("sorbed"-P) at each sampling time in medium with malate and 4.4 mM P ranged from 1.8 to 1.3, comparable with the ratio of 1.5 expected for vivianite.

Geochemical speciation modeling was performed with the program MINTEQA2. The sorption behavior of Fe(II) in these experiments was defined by using the experimentally determined isotherms for the mixed (Gt + BrY) system defined above (Table 1). The model was used to calculate aqueous and solid-phase (adsorbed and precipitated) Fe(II) concentrations from the measured total Fe(II) concentrations. These calculations suggested important influences attributable to phosphate and malate. Aqueous speciation and saturation index calculations indicated that saturation with respect to vivianite was reached at $Fe(II)_{aq}$ concentrations $>\sim 10$ μM in the 4.4 mM PO_4^{3-} medium, assuming there was little P assimilation by cells. Thus, conditions were favorable for vivianite formation (as a surface or discrete phase) soon after initiation of Fe(III) reduction. Model calculations estimated that cultures were saturated with respect to vivianite after ~30% of the Fe(II) sorption sites were occupied with Fe(II). They also estimated that malate complexation of Fe(II) could have accounted for as much as 90% of the soluble Fe(II) (data not shown), assuming there was minor assimilation of malate by the bacteria. Speciation calculations for the experiment with variable malate concentrations (assuming that microbial assimilation of malate was minor) (Figure 8) showed that the computed fraction of Fe(II)-malate complexes [at a fixed Fe(II) concentration] rose at the expense of sorbed Fe(II) as the malate concentration was increased (data not shown).

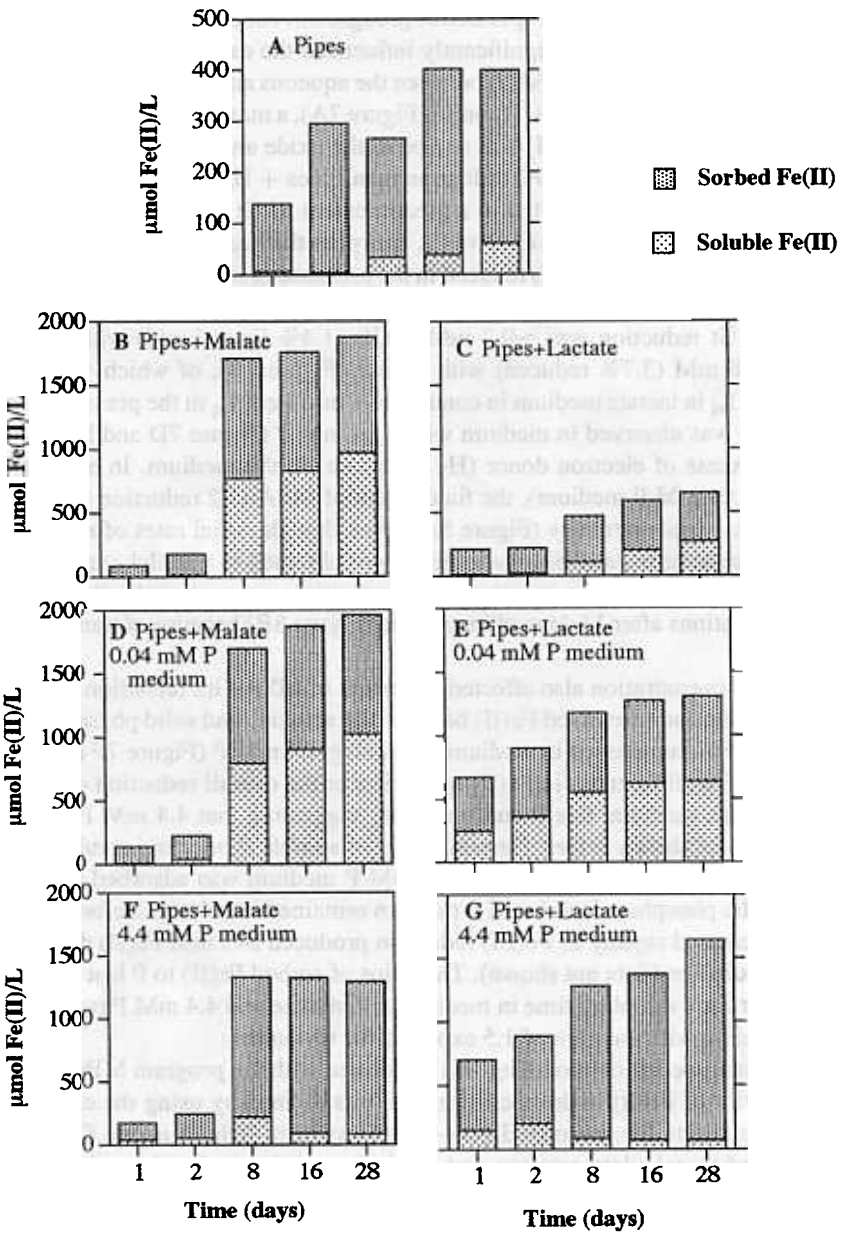


FIGURE 7 Fe(II) speciation during reduction of Gt by *S. alga* under growth and nongrowth conditions in the experiments to test the influence of medium composition. Treatments are (A) Pipes = H_2 + Pipes, pH 6.8; (B) Pipes + Malate = H_2 + Pipes + 30 mM malate, pH 6.8; (C) Pipes + Lactate = H_2 + Pipes + 30 mM lactate, pH 6.8; (D) Pipes + Malate + 0.04 mM P medium = H_2 + full medium with 30 mM malate and 0.04 mM PO_4^{3-} at pH 6.8; (E) Pipes + Lactate + 0.04 mM P Medium = H_2 + full medium with 30 mM lactate and 0.04 mM PO_4^{3-} at pH 6.8; (F) Pipes + Malate + 4.4 mM P medium = H_2 + full medium with 30 mM malate and 4.4 mM PO_4^{3-} buffered with Pipes at pH 6.8; (G) Pipes + Lactate + 4.4 mM P medium = H_2 + full medium with 30 mM lactate and 4.4 mM PO_4^{3-}, pH 6.8. For clarity, only mean values are included in the figure, but in all cases variation coefficients were <10%.

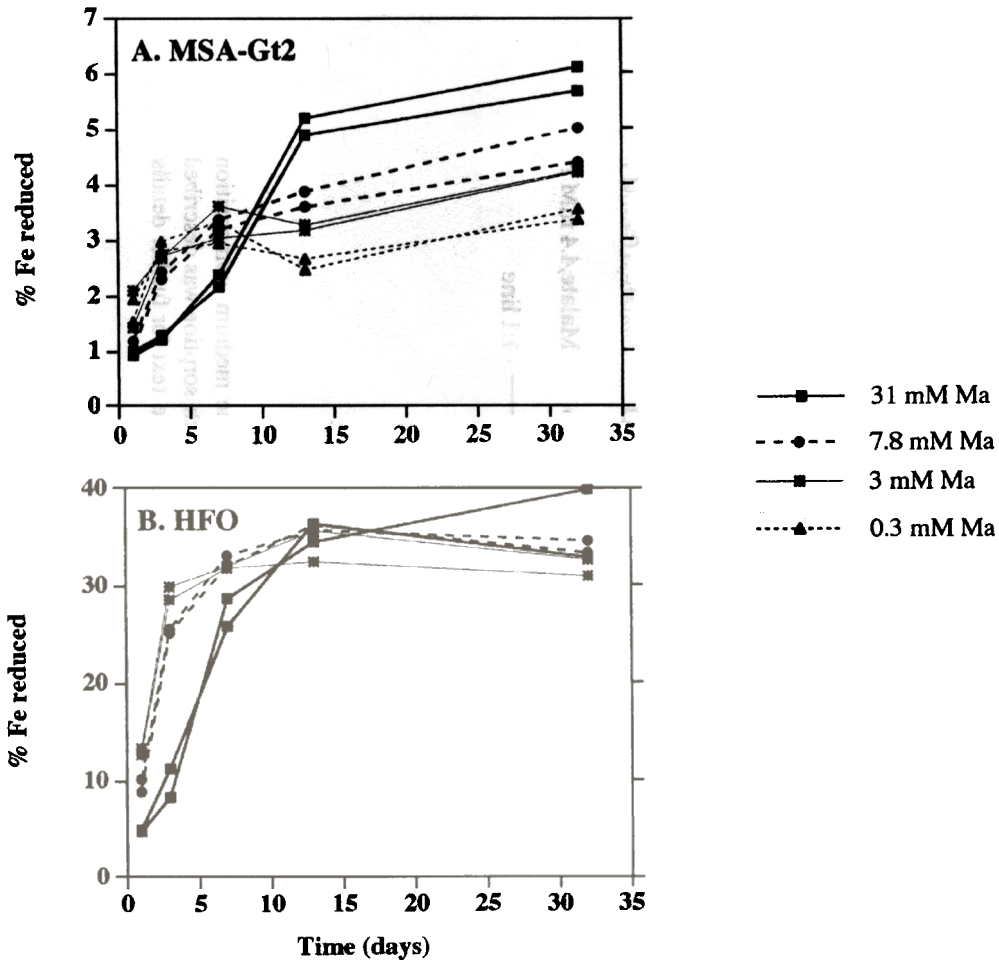


FIGURE 8 Effect of malate concentration on Fe(III) oxide reduction by *S. alga*: (A) for MSA-Gt2 goethite; (B) for hydrous ferric oxide (HFO). Data points are from individual culture tubes.

The model calculations accurately reproduced the observed Fe(II) speciation in the samples in Pipes buffer (nongrowth conditions) (Figure 9, filled circles) and the cultures with 4.4 mM P (Figure 9, filled triangles) by accounting for aqueous complexation, sorption to cells, and oxide and precipitation processes. However, sorption in the presence of malate (nongrowth conditions) or in 0.04 mM P growth medium was markedly underestimated (Figure 9, open symbols).

Discussion

Fe(II) Sorption by S. alga *Cells*

S. alga cells had a maximum Fe(II) sorption capacity of ~0.1 mmol g^{-1} dry weight of cells (Figures 3 and 4). This value is comparable with the metal sorption capacity of other bacterial cell surfaces and associated extracellular polymers reported in the literature, which range from 0.17 to 0.25 mmol g^{-1}, depending on metal, bacterium, and pH (Urrutia 1997).

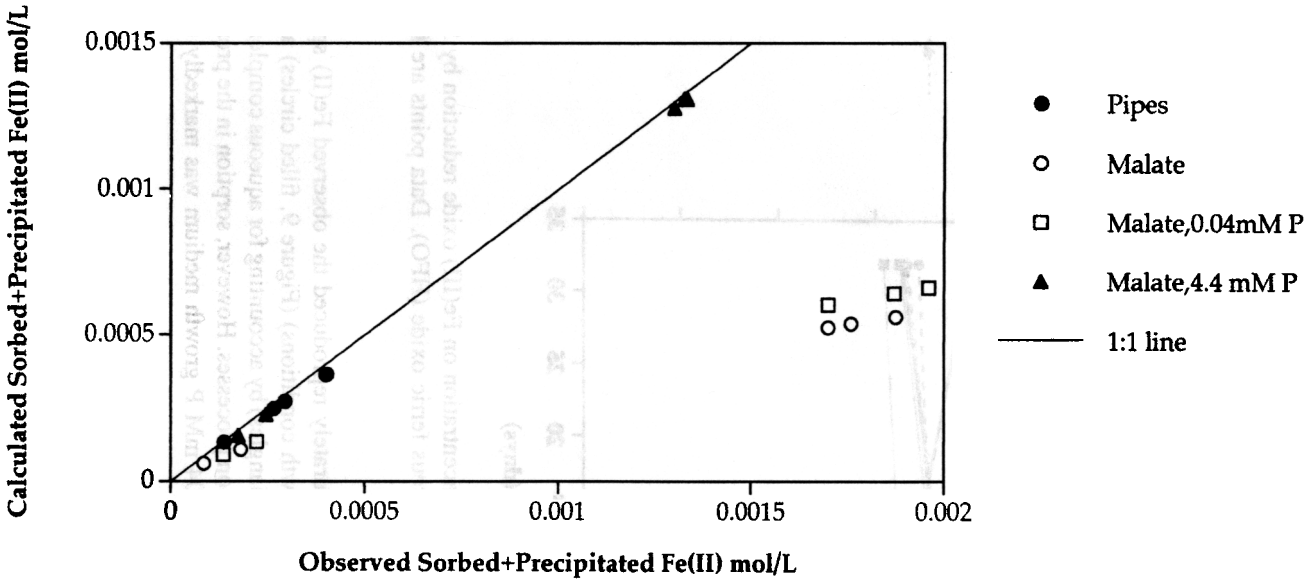


FIGURE 9 Plot of observed vs calculated sorbed + precipitated Fe(II) for all treatments in the medium composition experiments from Figure 7. Calculated values were obtained with the program MINTEQA2, in which sorption was described by the activity-based mixed isotherm parameters from Table 1, allowing vivianite precipitation (see text for further details on procedure). Sample nomenclature as in Figure 7. The 1:1 line is shown as reference.

It is also within a factor of two of that measured for Gt, 0.20–0.25 mmol g^{-1} (Figures 3 and 4).

Quantification of the Fe(II) sorption capacity of mixtures of cells and oxide showed a synergistic effect on Fe(II) sorption caused by interaction between cells and Gt. Thus, the Fe(II) sorption maximum of the mixture was greater than the additive capacity of cells and Gt measured independently (Figure 4A and Table 1). The model calculated mixed isotherm (Figure 4A, dotted line) resembled that of Gt, the strongest individual sorbent. The poor agreement between the model results and the experimental data (Figure 4A) indicated that unexpected interactions in the combined system enhanced Fe(II) sorption. This synergistic effect, presumably a biological effect, was further evidenced when contact between *S. alga* and Gt was prevented by using dialysis bags (Figure 4B). The overall amount of sorbed Fe(II) in this instance [calculated by adding Fe(II) sorbed by Gt to Fe(II) sorbed by *S. alga* in mmol g^{-1}] was lower than when cells and oxides were allowed to interact (Figure 4B circles vs 4A circles). These results show that direct contact between oxide and cells is accompanied by an enhanced capacity for Fe(II) sorption.

The production of exopolysaccharidic (EPS) material by *S. alga* cells may have promoted this effect, since EPS production by *S. alga* is stimulated in presence of Fe(III) (Urrutia, unpublished results). EPS is an extracellular component associated with the bacterial cell wall that has a high capacity for binding metal cations, including Fe(III) (Beveridge 1984; Beveridge 1986; Corzo et al. 1994; Ferris et al. 1989; Ikeda et al. 1982) and Fe(II) (McLean et al. 1992). Although Fe(II) sorption experiments with the cells were conducted under nongrowth conditions (Pipes buffer only), the allocation of endogenous cell carbon/energy reserves to production of EPS when in contact with the Fe(III) oxide may have occurred over the 18-h equilibration period. Further work is needed to identify the specific mechanism(s) involved in the synergistic effect on Fe(II) sorption observed.

To our knowledge, this is the first study to quantify metal sorption by mixtures of metabolically active bacterial cells and minerals and to demonstrate that interaction between such cells and minerals can lead to an enhancement in metal sorption capacity. These findings may have implications not only for the fate of Fe(II) but also for the fate of metals associated with the Fe(III) oxides that may be liberated during bacterial oxide reduction.

Influence of Fe(II) Biosorption on Fe(III) Oxide Reduction

Fe(III) oxide reduction in batch cultures typically ceased after 15–30 days of incubation, here refered to as one "reduction cycle." Previous studies with HFO- and Gt-reducing cultures showed that cell numbers (Lovley and Phillips 1988; Roden and Zachara 1996) and protein content (Urrutia and Roden, in preparation) paralleled Fe(II) production and then decreased with cell death/lysis occurring after 30–35 days. These results suggested that a decline in cell viability was at least partly responsible for cessation of Fe(III) oxide reduction in our batch culture experiments.

Bacterial cells with sorbed Fe(II) reduced MSA-Gt1, HSA-Gt, or HFO more slowly than did untreated cells (Figure 5, C–E), and reduced less Fe(III) overall (Figure 5A and B), even though the Fe(II) adsorption density was only 23% of the maximum capacity. Rates of oxide reduction by Fe(II)-coated cells were equivalent to those obtained for uncoated cells at the later stages of incubation (Figure 5, C–E); i.e., cells with sorbed Fe(II) behaved like cells from old Fe oxide cultures (in the later stages of the reduction cycle). These results suggest that biosorption of Fe(II) decreases cell viability or activity, and limits the extent of Fe(III) oxide reduction in batch culture systems.

Saturation of Fe(III) oxide surfaces with Fe(II) has been suggested as a dominant factor involved in the cessation of Fe(III) oxide reduction by FeRB in batch cultures (Roden and

Zachara 1996). However, we observed further reduction of Gt and Hm upon reinoculation of Fe(III) oxide cultures with fresh *S. alga* cells after completion of one reduction cycle (Figures 1 and 2). Plausible explanations for these results are that (1) reducible Fe(III)-surface sites were still available in the cultures but the existing cells were unable to access them, possibly because of sorption of Fe(II) to cell surfaces or occlusion by Fe(II) precipitates; (2) Fe(II) exchanged from the oxide onto the clean bacterial surfaces, thereby exposing additional oxide surface sites for further microbial reduction. Our results argue in favor of the first possibility. First, if we assume that Fe(II) can exchange between the Fe(II)-saturated Gt and the cells, only 2% of the Fe(II) would be removed from the oxide surface by the fresh cells, given the mass of inoculum used in the reduction experiments. Therefore, if surface exchange of Fe(II) were the only process involved in stimulating further reduction of Gt, only an additional 0.04% of Fe(III) (for a 50 mmol L^{-1} Gt concentration) would have been reduced after reinoculation. This quantity is considerably less than the 2–20% increase observed in the reinoculation experiments. Second, other experiments directly demonstrated that biosorption of Fe(II) limited the extent of Fe(III) oxide reduction, as discussed in the previous paragraph. Third, the experiments with Fe(II)-coated MSA-Gt1 showed that fresh *S. alga* cells are capable of reducing Fe(II)-saturated Gt (Figure 6B), although the initial rates of reduction by *S. alga* decreased with increasing amounts of sorbed Fe(II) (Figure 6A). These findings indicate that fresh *S. alga* cells were able to access Fe(III) metal ion centers on the Fe(II)-saturated Gt surface. In other words, the Fe(II)-saturation of Gt surfaces does not eliminate electron transfer from *S. alga* cells to the oxide surface.

Influence of Medium Composition on Fe(III) Oxide Reduction

Two main components of our growth medium may have affected the extent of Fe(III) oxide reduction by altering the fate of evolved Fe(II) (i.e., dissolved vs solid-phase partitioning): malate, the carbon source for growth of *S. alga* with H_2 as electron donor, which has the potential to complex Fe(II); and PO_4^{3-}, an essential nutrient for growth, which is present at millimolar concentrations in the medium used to culture FeRB (Lovley and Phillips 1988; Caccavo et al. 1991; Roden and Zachara 1996), and which may precipitate with evolved Fe(II). The formation of Fe(II) phosphates (i.e., vivianite, $Fe_3(PO_4)_2 \cdot 8H_2O$) becomes thermodynamically feasible under the conditions of our experiments as Fe(II) concentration increases (see below), and these may veneer oxide or cell surfaces as surface precipitates. Fe(III) reduction was enhanced during reinoculation experiments when medium was included along with cells (Figure 2). This stimulation was greater than what we could account for by an additional supply of electron donor, because H_2 + complete medium promoted Fe(III) reduction more than did H_2 alone. Medium addition may have stimulated biosynthesis of new cell materials and enzymes, or changed Fe(II) speciation through the mechanisms mentioned above, or both.

Experiments designed specifically to test these effects showed that bacterial reduction of Gt was sensitive to medium components that altered the distribution of Fe(II) between the aqueous and solid phase (adsorbed or surface precipitated) (Figure 7). Geochemical speciation modeling was performed to provide insights into how the chemical distribution of evolved Fe(II) was related to the extent of bacterial Fe(III) oxide reduction. The sorption behavior of Fe(II) in the reduction experiments was defined by using the experimentally determined isotherms for the mixed (Gt + BrY) system (Table 1). Although the model calculations did not accurately depict the amount of Fe(II) sorbed to MSA-Gt and cells under growth conditions (Figure 9), they did provide insights on the potential impact of chemically reactive medium components.

Effect of Phosphate

Phosphate had a significant impact on bacterial Fe(III) reduction (Figure 7), most likely because of the formation of Fe(II) phosphate precipitates (e.g., vivianite). Such precipitates may coat both cells and oxide and thereby physically interfere with cell–mineral interactions. Aqueous speciation and saturation index calculations indicated that conditions were favorable for vivianite formation (as a surface or discrete phase) soon after initiation of Fe(III) reduction in the 4.4 mM PO_4^{3-} medium (see the last section of *Results*). Model calculations estimated that cultures were saturated with respect to vivianite after ~30% of the Fe(II) sorption sites were occupied with Fe(II); they also accurately reproduced the observed data for sorbed Fe(II) in this medium (Figure 9, filled triangles). In agreement with these calculations, a greater proportion of solid-phase associated ("sorbed") Fe(II) was observed in 4.4 mM P (Figure 7F and G) than in 0.04 mM P medium (Figure 7D and E), and ratios of sorbed Fe(II) to "sorbed"-P (P lost from solution) in 4.4 mM P medium (1.3 to 1.8) were consistent with that in vivianite, 1.5. The presence of 4.4 mM P eliminated differences in the distribution of Fe(II) between the malate + H_2 and the lactate cultures that were observed at the lower P concentrations (discussed in the next section) (Figure 7F and G). These results suggest that Fe(II) phosphate precipitation may regulate Gt reduction in the 4.4 mM P medium typically used to cultivate FeRB (Caccavo et al. 1992; Lovley and Phillips 1988) and in Fe(III) reduction experiments using the full basal medium (Roden and Zachara 1996).

Effect of Malate

Soluble Fe(II) concentrations were higher in cultures that had malate as a C source than in those that had lactate as the C and energy source (Figure 7, C and E vs B and D). Geochemical speciation calculations estimated that malate complexation of Fe(II) could have accounted for as much as 90% of the soluble Fe(II) (see *Results*, last section). Our observation that less Fe(II) sorbed to MSA-Gt1 in 30 mM malate + 0.04 mM P medium than in Pipes buffer (Figure 3B) is consistent with this argument. Also, speciation calculations for the experiment with variable malate concentrations (Figure 8) showed that the computed fraction of Fe(II)-malate complexes [at a fixed Fe(II) concentration] grew at the expense of sorbed Fe(II) as the malate concentration was increased (data not shown). The lack of a $\log K$ value for complexation of Fe(II) by lactate prevented accurate modeling of Fe(II) speciation in the lactate system. However, $\log K$ values for lactate complexation of several divalent cations have been reported to vary between 1.9 and 2.4 (Martell and Smith 1974; Martell and Smith 1977; Martell and Smith 1978; Smith et al. 1993), in comparison to that of 3.48 for malate (Smith et al. 1993). Arnold et al. (1986) used a $\log K$ value of 1.82 for complexation of Fe(II) by lactate, estimated from the thermodynamic data available for glycolate. Thus, the potential ability of lactate to complex Fe(II) is <0.1 that of malate; therefore, lactate is unlikely to significantly complex Fe(II).

The extent of Fe(III) oxide reduction was also enhanced in cultures with malate as a C source (Figure 7B and D). The differences in total Fe(II) levels between malate and lactate media were greatest between 2 and 8 days of incubation. Cell numbers (Roden and Zachara 1996) and protein contents (Urrutia and Roden, in preparation) during growth conditions similar to these experiments indicated that protein production by *S. alga* increased rapidly between 1 and 10 days. We therefore speculate that malate prevented Fe(II) sorption to oxide and cell surfaces during the period in which the cell population was most active, thereby resulting in greater Fe(III) reduction overall.

Collectively, these results indicate that a medium composition that favors accumulation of soluble Fe(II) (malate, low PO_4^{3-}) may enhance oxide reduction by FeRB (Figure 7) in comparison with a medium in which Fe(II) sorption and surface precipitation predominate (lactate, high PO_4^{3-}). These effects are particularly important under nongrowth conditions,

when new cells cannot be synthesized. They also probably contributed to the effects observed in the second reinoculation experiment (Figure 2), in which Fe(III) reduction was further enhanced after reinoculation if medium containing malate was provided in addition to fresh cells and H_2. This difference probably resulted from complexation of Fe(II) by malate, which then allowed further Gt reduction by the fresh cells.

Other Influences on Bacterial Fe(III) Oxide Reduction and Reevaluation of the Oxide Fe(II) Surface Saturation Hypothesis

The total amount of Fe(II) generated in our experiments during MSA-Gt1 reduction by *S. alga* (Figures 5A and 6B) was threefold greater than the maximum Fe(II) adsorptive capacity of the mineral (determined to be ~0.25 mmol Fe(II) g^{-1}, Figure 4A). This quantity of Fe(II) (Figure 5A), 10–13% of the initial Fe(III) content of MSA-Gt1, was comparable with the amount of reduction obtained prior to reinoculation with fresh cells in the experiments shown in Figures 1 and 2, and with that observed in numerous transfers of the organism growing on MSA-Gt1 (data not shown). The only exception was the reduction experiment under nongrowth conditions in which cells were provided exclusively with H_2 in a suspension of Gt in Pipes buffer (Figure 7A). Therefore, Fe(III) reduction in excess of the Fe(II) sorption capacity was a consistent result in our experiments. Medium composition effects (e.g., the presence of malate) cannot account for the Fe(II) production in excess of the oxide Fe(II) sorption capacity in the cases mentioned above, because the experiments were conducted in the presence of 4.4 mM P, which, as previously discussed, overrode any enhancement of the extent of Fe(III) reduction by malate (Figure 7F and G). In the experiment with Fe(II)-coated Gt, the oxide was saturated with sorbed Fe(II) [in the samples with the higher levels of Fe(II) addition] prior to inoculation, and yet further reduction by *S. alga* was obtained. Medium composition effects cannot account for the observed amount of Fe(III) reduction in excess of the Fe(II) sorption capacity of the oxide.

The above findings suggest that the previously formulated hypothesis, that the capacity of the Fe(III) oxide surface to sorb Fe(II) quantitatively controls the long-term extent of oxide reduction in batch culture systems (Roden and Zachara 1996), must be reevaluated. As discussed above, the cells and (possibly) their biopolymers [e.g., EPS, lipopolysaccharides (LPS)] added to the medium at inoculation may represent a significant Fe(II) sink in addition to the oxide surface. Therefore, Fe(II) sorption by both the oxide surface and FeRB cells, and their synergistic interaction, must be considered in assessing how the long-term extent of oxide reduction may be quantitatively linked to the accumulation of sorbed Fe(II) in the system. The results of the Gt reduction experiment under nongrowth conditions in Pipes buffer with H_2 (Figure 7A) support a conceptual model in which the extent of reduction is determined by the Fe(II) sorption capacity of the combined system (Gt + cells) (Figure 9), thereby complying with a modified "surface saturation hypothesis," which includes the cell surfaces as a quantitatively significant sink for evolved Fe(II).

However, in all other conditions studied, the extent of Gt reduction was greater than this experimentally determined maximum adsorption capacity of the mixed system Gt + *S. alga* [~0.4 mmol Fe(II) g^{-1}]. There are several possible explanations for these observations. One is that the reducible sites on the surface of Gt are not equivalent to the adsorption sites for Fe(II). Surface-complexed Fe(II) may not completely interfere with microbial Fe(III) reduction in the long term, even though it causes a slow down of the initial rates of reduction (Figures 5 and 6). A possible explanation here is that FeRB can transfer electrons to the solid regardless of surface Fe(II) saturation, so long as some limit of Fe(II) surface layers is not exceeded. If this is the case, then our results indicate that only metabolically active

cells can carry out this process, since there was no indication of this effect in the nongrowth (H_2+ Pipes) experiment.

Another explanation may be that sinks for Fe(II)—other than those that we have accounted for—exist, such that Fe(III) reduction can exceed the measured cell + Gt Fe(II) sorption capacity. It is feasible that biosynthesis of EPS or other macromolecules such as LPS, or growth of the cell population, may take place. These Fe(II) "sinks" can increase with time, such that the extent of oxide reduction is enhanced, especially under growth conditions. This is supported by the results of experiments in which there was a potential for increases in EPS material, cell population, or both (Figure 7B and C). Although significant cell growth and biosynthesis in the Pipes + malate medium is unlikely since this medium lacks P, N, vitamins, and minerals, production of EPS may occur in the absence of these, given the presence of an assimilable C source. We have observed that *S. alga* produced greater amounts of EPS when incubated in presence of Fe(III) than when grown without Fe(III), both in rich or basal medium (Urrutia, unpublished data). A careful evaluation of EPS production and cell growth processes under these conditions is required to further evaluate this hypothesis.

Finally, it is possible that the total material balance of Fe(II)—sorbed, precipitated, surface-precipitated, and complexed—has simply not been appropriately resolved. The distinction between the formation of separate Fe(II) solid phases not directly associated with the Fe(III) oxide or cell surfaces and the formation of oxide/cell surface Fe(II) complexes/precipitates is probably key in this regard. More thorough understanding of Fe(II) speciation in dynamic systems must be achieved before we can fully evaluate the role of Fe(II) surface-complexation and precipitation on microbial reduction of Fe(III) oxides.

Summary and Significance

The rate and extent of microbial Fe(III) oxide reduction are controlled by complex interactions between the surface chemical properties of both bacterial cells and oxides, and the aqueous chemical composition effects on Fe(II) speciation. Oxide surface area is among the primary determinants of both the initial rate and final extent of reduction (Roden and Zachara 1996), but our results clearly show that other factors are also involved: sorption of Fe(II) to cell and oxide surfaces and the synergistic interaction between both, the aqueous concentration of Fe(II) in equilibrium with the adsorbed Fe(II), and the possibility of cell/population growth. Our data indicate that saturation of the sorption sites with Fe(II) does not alone define an upper limit on the ability of *S. alga* to reduce Fe(III) oxides.

We speculate that in open systems such as most natural sedimentary environments microbial Fe(III) reduction may proceed to a greater extent than in batch cultures because of the potential for continual removal of reaction products such as Fe(II). As a possible example of this phenomenon, ~70% of the crystalline Fe(III) oxide content of aquifer sediment has been reduced within the oldest (~15 years old) region of a landfill leachate contaminant plume in Denmark (Heron and Christensen 1995), an amount considerably in excess of the extent of crystalline Fe(III) oxide reduction observed in this and other experimental studies. Presumably, reduced sediments whose surfaces are nearly saturated with Fe(II) can be environments in which the activity of dissimilatory FeRB will be limited by the lack of Fe(III) availability. This seemed to be the case in the most Fe(II)-rich zone of a landfill leachate-contaminated aquifer in Denmark (Albrechtsen et al. 1995). Alternatively, in environments where Fe(III) oxides are abundant and many mineral and organic phases can function as sinks for Fe(II), the reduction of Fe oxides may proceed at a more rapid rate, controlled instead by the supply of respirable organic carbon or nutrients.

Note Added in Proof

While this article was in press, a relevant study was published by T. Krafft and J. M. Macy entitled "Purification and characterization of the respiratory arsenate reductase of Chrysiogenes arsenatis" in Eur. J. Biochem. 255:647–653(1998).

References

Albrechtsen HJ, Heron G, Christensen TH. 1995. Limiting factors for microbial Fe(III)-reduction in a landfill leachate polluted aquifer (Vejen, Denmark). FEMS Microbiol Ecol 16:233–247.

Allison JD, Brown DS, Novo-Gradac KJ. 1991. MINTEQA2/PRODEFA2, a geochemical assessment model for environmental systems: Version 3.0 user's manual. Washington, DC: US Environmental Protection Agency.

Arnold RG, DiChristina TJ, Hoffmann MR. 1988. Reductive dissolution of Fe(III) oxides by *Pseudomonas* sp. 200. Biotech Bioeng 32:1081–1096.

Arnold RG, Olson TM, Hoffmann MR. 1986. Kinetics and mechanism of dissimilative Fe(III) reduction by *Pseudomonas* sp. 200. Biotech Bioeng 28:1657–1671.

Atkinson RJ, Posner AM, Quirk JP. 1968. Crystal nucleation in Fe(III) solutions and hydroxide gels. J Inorg Nucl Chem 30:2371–2381.

Beveridge TJ. 1984. Mechanisms of the binding of metallic ions to bacterial walls and the possible impact on microbial ecology. In: CA Ready, MJ Klug, editors. Bioconversion of inorganic materials. Washington, DC: American Society for Microbiology, p 601–607.

Beveridge TJ. 1986. The immobilization of soluble metals by bacterial walls. Biotechnol Bioeng Symp 16:127–139.

Caccavo F Jr., Blakemore RP, Lovley DR. 1992. A hydrogen-oxidizing, Fe(III)-reducing microorganism from the Great Bay estuary, New Hampshire. Appl Environ Microbiol 58:3211–3216.

Chapelle FH. 1993. Groundwater microbiology and geochemistry. New York: John Wiley & Sons, Inc.

Corzo J, Leon-Barrios M, Hernando-Rico V, Gutierrez-Navarro AM. 1994. Precipitation of metallic cations by the acidic exopolysaccharides from *Bradyrhizobium japonicum* and *Bradyrhizobium* (*Chamaecytisus*) strain BGA-1. Appl Environ Microbiol 60:4531–4536.

Fendorf SE, Li G. 1996. Kinetics of chromate reduction by ferrous iron. Environ Sci Technol 30:1614–1617.

Ferris FG, Schultze S, Witten TC, Fyfe WS, Beveridge TJ. 1989. Metal interactions with microbial biofilms in acidic and neutral pH environments. Appl Environ Microbiol 55:1249–1257.

Fisher WR, Pfanneberg T. 1984. An improved method for testing the rate of iron(III)-oxide reduction by bacteria. Zentralbl Mikrobiol 139:163–166.

Goodman BA, Lewis DG. 1981. Mossbauer spectra of aluminous goethites (α-FeOOH). J Soil Sci 32:351–363.

Heron G, Christensen TH. 1995. Impact of sediment-bound iron on redox buffering in a landfill leachate polluted aquifer (Vejen, Denmark). Environ Sci Technol 29:187–192.

Ikeda F, Shuto H, Saito T, Fukui T, Tomita K. 1982. An extracellular polysaccharide produced by *Zooglea ramigera* 115. Eur J Biochem 123:437–445.

Jenne EA. 1977. Trace element sorption by sediments and soil-sites and processes. In: W Chappel, K Petersen, editors. Symposium on molybdenum in the environment. New York: Marcel Dekker, p 425–553.

Landa ER, Phillips EJP, Lovley DR. 1991. Release of 226Ra from uranium mill tailings by microbial Fe(III) reduction. Appl Geochem 6:647–652.

Lanstrom O, Tullborg E-L. 1995. Interactions of trace elements with fracture filling minerals from the Casp Hard Rock laboratory. Stockholm: Swedish Nuclear Fuel and Waste Management Co.

Lovley DR. 1991. Dissimilatory Fe(III) and Mn(IV) reduction. Microbiol Rev 55:259–287.

Lovley DR. 1995. Microbial reduction of iron, manganese, and other metals. Adv Agron 54:175–231.

Lovley DR, Baedecker MJ, Lonergan DJ, Cozzarelli IM, Phillips EJP, Siegel DI. 1989. Oxidation of aromatic contaminants coupled to microbial iron reduction. Nature 339:297–299.

Lovley DR, Coates JD, Woodward JC, Phillips EJP. 1995. Benzene oxidation coupled to sulfate reduction. Appl Environ Microbiol 61:953–958.

Lovley DR, Lonergan DJ. 1990. Anaerobic oxidation of toluene, phenol, and p-cresol by the dissimilatory iron-reducing organism, GS-15. Appl Environ Microbiol 56:1858–1864.

Lovley DR, Phillips EJP. 1986a. Availability of ferric iron for microbial reduction in bottom sediments of the freshwater tidal Potomac River. Appl Environ Microbiol 52:751–757.

Lovley DR, Phillips EJP. 1986b. Organic matter mineralization with reduction of ferric iron in anaerobic sediments. Appl Environ Microbiol 51:683–689.

Lovley DR, Phillips EJP. 1987. Rapid assay for microbially reducible ferric iron in aquatic sediments. Appl Environ Microbiol 53:1536–1540.

Lovley DR, Phillips EJP. 1988. Novel mode of microbial energy metabolism: Organic carbon oxidation coupled to dissimilatory reduction of iron or manganese. Appl Environ Microbiol 54:1472–1480.

Lovley DR, Phillips EJP, Lonergan DJ. 1991. Enzymatic versus nonenzymatic mechanisms for Fe(III) reduction in aquatic sediments. Environ Sci Technol 25:1062–1067.

Lovley DR, Woodward JC, Chapelle FH. 1994. Stimulated anoxic biodegradation of aromatic hydrocarbons using Fe(III) ligands. Nature 370:128–131.

Makos JD, Hrncir DC. 1995. Chemistry of Cr(VI) in a constructed wetland. Environ Sci Technol 29:2414–2419.

Martell AE, Smith RM. 1974. Critical stability constants. Vol. 1. Amino acids. New York: Plenum Press.

Martell AE, Smith RM. 1977. Critical stability constants. Vol. 3. Other organic ligands. New York: Plenum Press.

Martell AE, Smith RM. 1978. Critical stability constants. Vol. 6, 2nd suppl. New York: Plenum Press.

McLean RJC, Beauchemin D, Beveridge TJ. 1992. Influence of oxidation state on iron binding by *Bacillus licheniformis* capsule. Appl Environ Microbiol 58:405–408.

Murphy J, Riley JP. 1962. A modified single solution method for the determination of phosphate in natural waters. Anal Chim Acta 27:31–36.

Myers CR, Myers JM. 1994. Ferric iron reduction-linked growth yields of *Shewanella putrefaciens* MR-1. J Appl Bacteriol 76:253–258.

Nealson KH, Myers CR. 1992. Microbial reduction of manganese and iron—new approaches to carbon cycling. Appl Environ Microbiol 58:439–443.

Pedersen K, Karlsson F. 1995. Investigations of subterranean microorganisms: Their importance for performance assessment of radioactive waste disposal. Stockholm: Swedish Nuclear Fuel and Waste Management Co.

Roden EE, Wetzel R. 1996. Organic carbon oxidation and suppression of methane production by microbial Fe(III) oxide reduction in vegetated and unvegetated freshwater wetland sediments. Limnol Oceanogr 41:1733–1748.

Roden EE, Zachara JM. 1996. Microbial reduction of crystalline iron(III) oxides: influence of oxide surface area and potential for cell growth. Environ Sci Technol 30:1618–1628.

Rosselló-Mora RA, Caccavo F Jr., Osterlehner K, Springer N, Spring S, Schüler D, Ludwig W, Amann R, Vanncanneyt M, Schleifer KH. 1994. Isolation and taxonomic characterization of a halotolerant, facultatively iron-reducing bacterium. System Appl Microbiol 17:569–573.

Schwertmann U, Cornell RM. 1991. Iron oxides in the laboratory. Preparation and characterization. Weinheim: VCH Press.

Schwertmann U, Taylor RM. 1989. Iron oxides. Chapter 8. In: JB Dixon, SB Weed, editors. Minerals in soil environments. Madison, WI: Soil Science Society of America, p 379–438.

Smith RM, Martell AE, Motekaitis RJ, Smith RM. 1993. Critical stability constants of metal complexes database. Standard Reference Database 46. Gaithersburg, MD: National Institute of Standards and Technology.

Tugel JB, Hines ME, Jones GE. 1986. Microbial iron reduction by enrichment cultures isolated from estuarine sediments. Appl Environ Microbiol 52:1167–1172.

Urrutia MM. 1997. General bacterial sorption processes. In: JDA Wase, C Forster, editors. Biosorbents for metal ions. Philadelphia: Taylor and Francis, p 39–66.

Zachara JM, Gassman PL, Smith SC, Taylor D. 1995. Oxidation and adsorption of Co(II)EDTA^{2-} complexes in subsurface materials with iron and manganese oxide grain coatings. Geochim Cosmochim Acta 59:4449–4463.

Environ. Sci. Technol. **1999**, *33,* 1847−1853

Ferrous Iron Removal Promotes Microbial Reduction of Crystalline Iron(III) Oxides

ERIC E. RODEN* AND
MATILDE M. URRUTIA

Department of Biological Sciences, The University of Alabama, Tuscaloosa, Alabama 35487-0206

Semicontinuous cultures were used to assess the effect of aqueous Fe(II) removal on the dissimilatory reduction of crystalline Fe(III) oxides by *Shewanella alga* strain BrY. Aqueous phase replacement in semicontinuous cultures (average residence time of 9 or 18 days) resulted in a 2−3-fold increase in the cumulative amount of Fe(II) produced from synthetic goethite reduction over a 2-month incubation period, compared to parallel batch cultures. A more modest (maximum 30%) but significant stimulation of natural subsoil Fe(III) oxide reduction was observed. The extended Fe(III) reduction resulted from enhanced generation of aqueous Fe(II) which was periodically removed from the cultures. A concomitant stimulation of bacterial protein production was detected, which suggested that Fe(II) removal also promoted bacterial growth. A simulation model in which Fe(II) sorption to the solid-phase resulted in blockage of surface reduction sites captured the contrasting behavior of the batch vs semicontinuous Gt reduction systems. Our findings indicate that elimination of Fe(II) via advective transport could play a significant role in governing the rate and extent of microbial Fe(III) oxide reduction in sedimentary environments.

Introduction

Surface chemical reactions involving Fe(III) oxides play a central role in the geochemistry of soil and sedimentary environments (*1*). One such reaction with broad environmental significance is the reduction of Fe(III) oxides coupled to the oxidation of organic matter under anaerobic conditions (*2, 3*). In addition to contributing to the oxidation of sedimentary organic matter and generating soluble ferrous iron (a widespread groundwater contaminant), microbial Fe(III) oxide reduction can have an important influence on the persistence and mobility of various metal, radionuclide, and organic contaminants (*2, 4, 5*).

Microbial Fe(III) oxide reduction may also play an important role in facilitating the reductive immobilization of certain metal and radionuclide species (e.g. Cr, U), either by supporting the growth and maintenance of metal-reducing bacterial populations which can enzymatically reduce soluble, oxidized forms of these metals to insoluble reduced phases (*6*), or in the case of Cr by producing aqueous and/or solid-phase Fe(II) which can abiotically reduce Cr(VI) to insoluble Cr(III) oxides (*7*). Because perpetuation of such contaminant metal reduction processes will depend on the presence of active metal-reducing bacterial populations, the ongoing capacity for endogenous Fe(III) oxides to serve as the primary source of electron acceptor required for cell growth and maintenance becomes an important issue with regard to contaminant fate and transport. Oxidized contaminant metals may often not be present at concentrations sufficient to support continued cell growth, and in some cases bacterial growth with contaminant metals may not be possible for physiological reasons (*6*).

The above considerations suggest the need for information on how geochemical parameters influence the long-term potential for Fe(III) oxide reduction and maintenance of metal-reducing bacterial populations in anaerobic soils and sediments. Recent studies with the dissimilatory FeRB *Shewanella alga* suggest that adsorption and/or precipitation of Fe(II) compounds on Fe(III) oxide and FeRB cell surfaces (hereafter referred to collectively as Fe(II) sorption) is responsible for the cessation of Fe(III) oxide reduction activity in batch culture experiments (*8, 9*). Subsequent work has shown that aqueous Fe(II) ligands such as dissolved inorganic carbon or nitrilotriacetic acid as well as solid-phase components such as Al_2O_3 oxides or clay minerals can enhance the long-term extent of synthetic goethite reduction by *S. alga* by delaying or retarding the accumulation of Fe(II) on oxide and cell surfaces (*10*). These findings suggest the possibility that removal of Fe(II) by advective transport (e.g. via groundwater flow or recharge of shallow aquifers) could play an important role in governing the rate and extent of microbial Fe(III) oxide reduction in subsurface sedimentary environments. In the present study, we used semicontinuous cultures to test the hypothesis that advective Fe(II) removal can promote microbial reduction of natural and synthetic crystalline Fe(III) oxides by retarding the accumulation of sorbed Fe(II). We also tested whether aqueous Fe(II) complexants (synthetic chelators, humic acid) could further enhance the long-term extent of oxide reduction by accelerating removal of Fe(II).

Materials and Methods

Organism and Culturing Procedures. The dissimilatory Fe(III)-reducing bacterium *Shewanella alga* strain BrY (*11, 12*) was used as a test organism. Batch and semicontinuous cultures (SCs) were initiated in 60 mL serum bottles with 20−50 mmol Fe(III) L^{-1} in the form of synthetic goethite (Gt) or Fe(III) oxide-rich subsoil. The basal culture medium (30 mL/bottle) contained 10 mM Pipes buffer (pH 6.8), 18 mM NH_4Cl, and a low level of PO_4^{3-} (0.044 mM) compared to previous media used to cultivate Fe(III)-reducing bacteria (*8, 13*). Carbon and energy were provided by 8 mM malate and 30 mL of H_2 (10 mL overpressure) in the bottle headspace, respectively. Although malate has the capacity to complex Fe(II) and thereby influence the outcome of microbial Fe(III) oxide reduction experiments, previous studies have demonstrated that its presence at a concentration of 8 mM does not have a significant impact on the long-term extent of synthetic Gt reduction (*9*) or on Fe(II) sorption to Gt (Urrutia, M. unpublished). In one experiment, 30 mM lactate served as a combined carbon and energy source. All cultures were inoculated with washed (10 mM Pipes, pH 6.8) *S. alga* cells that had been grown to late exponential phase (16 h) in aerobic tryptic soy broth medium. The cells were added to a final cell density of ca. 10^8 mL^{-1}, equivalent to ca. 40 mg protein L^{-1}.

Fe(III) reduction was allowed to proceed for 6−7 days before medium replacement commenced in the SCs. After that, mean residence times of 18 or 9 days were established

* Corresponding author phone: (205)348-0556; fax: (205) 348-1403; e-mail: eroden@biology.as.ua.edu.

10.1021/es9809859 CCC: $18.00 © 1999 American Chemical Society
Published on Web 04/21/1999

TABLE 1. Characteristics of Fe(III) Oxide Materials

material	Fe(III) oxide content[a] (μmol/g dry wt)	surface area[b] (m^2/g)	Fe(II) sorption[c] sorption capacity[d] (μmol Fe^{II}/g dry wt)	Fe(II) sorption[c] sorption capacity[d] (μmol Fe^{II}/μmol Fe^{III})	Freundlich K[e]
synthetic Gt	1.79×10^4	55	0.25	0.020	0.62
CP subsoil	3.49×10^2	29	0.03	0.066	0.85
HC subsoil	6.73×10^2	41	>0.05	0.085	2.64

[a] Determined by citrate/dithionite extraction. [b] Determined by BET N_2 adsorption (Micromeritics Model Gemini). [c] Determined using $FeCl_2 \cdot 2H_2O$ in 10 mM Pipes buffer (pH 6.8) as described in ref *9*; the mass of solids per unit volume liquid in the sorption experiments was identical to that in the Fe(III) reduction cultures. [d] Assessed visually from isotherm plots. [e] Estimated by nonlinear least-squares fitting of sorption data in units of mmol Fe(II) L^{-1} (sorbed vs aqueous) to the Freundlich equation (*27*).

by replacing either 5 or 10 mL of the aqueous phase of the cultures with fresh anaerobic culture medium every 3−4 days. Medium was removed with a sterile 4″ 18G stainless steel needle without disturbing the solid-phase materials settled at the bottom of the bottle. An aliquot of the removed medium was acidified with 0.5 M HCl for subsequent analysis of aqueous Fe(II) concentration. A volume of fresh sterile medium identical to that removed was then added to the bottles, after which the bottles were thoroughly mixed and samples taken for determination of total (0.5 M HCl-extractable) Fe(II) and in some cases protein content as described below. An amount of H_2 gas equal to the amount of medium removed was then added to bottle headspace. Batch cultures which received no medium replacement were sampled for HCl-extractable Fe(II) and soluble Fe(II) in parallel with the SCs. Between samplings, the cultures were incubated statically at 30 °C in the dark. At 2-week intervals, the rubber stoppers in all bottles were replaced (working inside an anaerobic chamber) with new sterile stoppers, and 30 mL of H_2 was added to the bottle headspace.

Fe(III) Oxide Materials. A synthetic goethite (Gt), prepared and characterized as previously described (*9*), was employed for most of the experiments. Two Fe(III) oxide-rich subsoils (<106 μm fraction) were also used (see Table 1): a Holston/Cloudland, Typic Fragiudult from Tennessee (80−120 cm depth; designated HC) and a Cecil/Pacolet, Typic Hapludult from North Carolina (40−90 cm depth; designated CP). The soils differ in their clay mineralogy, with the HC being dominated by 2:1 layer silicates and CP by kaolinite (*14*). Previous studies (*8*) have shown that these two soils contain substantial quantities of microbially reducible Fe(III), the vast majority of which (>95%) is in the form of crystalline Fe(III) oxides (primarily goethite and hematite, respectively).

Fe(II) Complexants. The influence of three different potential aqueous Fe(II) complexants on Gt reduction in batch and SCs was evaluated: nitrilotriacetic acid (NTA), ethylenediamine tetraacetic acid (EDTA), 0.5 mM final concentration, and International Humic Substance Society Soil Humic Acid Standard (SHA), 100 mg L^{-1} final concentration. The NTA and EDTA were added to sterile culture medium from anaerobic filter-sterilized stock solutions, whereas the SHA was dissolved in culture medium prior to autoclaving.

The choice of 0.5 mM for the chelator additions represents a compromise between the relatively low levels present in subsurface contaminant plumes (<1 μM; *15*) and the mM levels used in previous experimental studies of the influence of chelators on bacterial Fe(III) oxide reduction (*10*, *16*, *17*). The choice of 100 mg L^{-1} for the humic acid addition, while high relative to most sedimentary environments, is substantially lower than levels used in recent studies of the influence of humics on Fe(III) oxide reduction (*18*, *19*).

Calculation of Cumulative Fe(II) and Protein Production. Cumulative Fe(II) production in the SCs was calculated at each sampling point from the sum of HCl-extractable Fe(II) plus the amount of Fe(II) eliminated with the aqueous phase during the current and previous medium replacements. Cumulative protein production was computed in a similar manner. However, protein measurements were only conducted every fourth sampling (every 2 weeks). Therefore, for those sampling times for which no protein data were available, protein content was estimated from the average of measurements made at the beginning and end of the corresponding 2-week interval.

Analytical Techniques. HCl-extractable Fe(II) (aqueous + solid-phase) was determined by extracting 0.5 mL culture samples in 5 mL of 0.5 M HCl for 2 h and then determining the Fe(II) content of the extracts with Ferrozine (*20*). Aqueous Fe(II) concentrations were determined by analyzing aliquots of 0.2 μm-filtered sample with Ferrozine. The total Fe(III) oxide content of the subsoils was determined by citrate/dithionite extraction followed by Ferrozine analysis as described previously (*8*).

The protein content of whole and aqueous phase culture samples was determined by the bicinchoninic acid (BCA) method after NaOH digestion. Because of the potential for Fe(III) oxides to adsorb proteins, standards (bovine serum albumin) were prepared in the same medium as the culture samples. Samples and standards were digested in 2.5 M NaOH for 15 min at 100 °C. Following cooling and neutralization with 2.5 M HCl, duplicate 1-mL aliquots of extract were mixed with an equal volume of freshly prepared BCA reagent (Pierce Chemical Co.) and incubated for 1 h in a 60 °C water bath. The colored extract was then passed through a 0.2-μm nylon filter, and the A_{562} was determined within 15 min. Protein contents are expressed in mg protein L^{-1} culture.

Results and Discussion

Synthetic Goethite Reduction. Medium replacement in the SCs resulted in a 2−3-fold increase in the extent of Gt reduction compared to parallel batch cultures (Figure 1). A clear trend toward continuously increasing cumulative Fe(II) production was evident in the SCs, whereas Fe(II) production approached an asymptote in the batch cultures. The higher volume of medium replacement led to a greater stimulation of Fe(III) oxide reduction.

Concentrations of aqueous Fe(II) ($Fe(II)_{aq}$) were slightly higher (0.1−0.2 mM) in the SC vs batch cultures. Although this may seem counterintuitive since $Fe(II)_{aq}$ was removed from the SCs during medium replacement, $Fe(II)_{aq}$ removal allowed for perpetuation of Fe(III) oxide reduction activity so that $Fe(II)_{aq}$ reaccumulated between dates of replacement. In contrast, concentrations of total (solid + aqueous) HCl-extractable Fe(II) were lower in the SC vs batch Gt cultures, by 50−100% toward the end of the experiments (see Table 2). This difference reflected primarily a decrease in solid-phase (sorbed) Fe(II). The extended Fe(III) reduction in the SCs was thus accounted for entirely by the $Fe(II)_{aq}$ removed during medium replacement. $Fe(II)_{aq}$ production accounted for 80−93% of cumulative Fe(II) production in the SCs, compared to ca. 25% in batch cultures (Table 2). The higher

TABLE 2. Fe(II) and Protein Production in Batch and Semicontinuous Cultures

medium	culture[a]	final HCl-Fe(II) (mmol L^{-1})[b,c]	cumulative Fe(II) (mmol L^{-1})[b]	% cumulative Fe(II) as Fe(II)aq[b]	cumulative protein (mg L^{-1})[b]
Gt, H_2/Mal	batch	1.27 ± 0.10	1.27 ± 0.10	23.48 ± 9.47	50.57 ± 2.56
	5 mL	0.84 ± 0.05	2.13 ± 0.04	81.57 ± 2.60	117.45 ± 4.38
	10 mL	0.57 ± 0.15	2.98 ± 0.09	89.76 ± 4.62	200.77 ± 5.27
Gt, lactate	batch	1.78 ± 0.23	1.78 ± 0.23	48.78 ± 3.48	ND[d]
	5 mL	1.11 ± 0.05	3.14 ± 0.12	85.01 ± 0.34	ND
	10 mL	1.02 ± 0.28	4.29 ± 0.18	93.25 ± 8.73	ND
Gt, H_2/Mal + NTA	batch	1.51 ± 0.03	1.52 ± 0.01	30.13 ± 1.33	62.80 ± 4.77
	5 mL	0.80 ± 0.05	2.24 ± 0.02	77.18 ± 1.56	98.69 ± 5.43
	10 mL	0.51 ± 0.02	2.86 ± 0.17	75.60 ±1.79	146.29 ± 5.62
Gt, H_2/Mal + EDTA	batch	1.65 ± 0.10	1.65 ± 0.10	36.70 ± 4.02	ND
	5 mL	0.82 ± 0.06	2.50 ± 0.08	64.28 ± 0.64	ND
	10 mL	0.91 ± 0.07	4.41 ± 0.21	73.94 ± 3.69	ND
Gt, H_2/Mal + SHA	batch	1.76 ± 0.17	1.76 ± 0.17	73.12 ± 2.00	225.79 ± 19.76
	5 mL	1.12 ± 0.04	2.20 ± 0.05	75.03 ± 2.47	425.70 ± 59.02
	10 mL	0.98 ± 0.16	2.93 ± 0.15	76.72 ± 4.23	708.03 ± 70.39
CP soil, H_2/Mal	batch	3.67 ± 0.20	3.67 ± 0.20	ND	ND
	5 mL	2.74 ± 0.19	4.39 ± 0.29	36.95 ± 3.23	ND
	10 mL	2.57 ± 0.03	5.11 ± 0.12	57.81 ± 6.92	ND
HC soil, H_2/Mal	batch	5.32 ± 0.38	5.32 ± 0.38	ND	ND
	5 mL	3.06 ± 0.35	4.74 ± 0.52	40.89 ± 1.94	ND
	10 mL	2.59 ± 0.18	5.27 ± 0.88	54.40 ± 4.14	ND

[a] Five milliliters and 10 mL refer to SCs receiving 5 and 10 mL medium replacements on each sampling date. [b] Mean ± SD of triplicate cultures. [c] HCl-extractable Fe(II) on the final sampling date; in batch systems, final HCl−Fe(II) equals cumulative Fe(II). [d] ND = not determined.

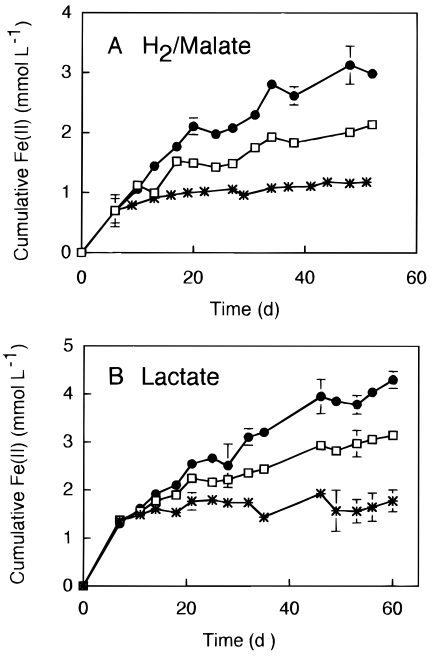


FIGURE 1. Cumulative Fe(II) (aqueous + solid-phase) production in batch (*) and semicontinuous synthetic Gt (50 mmol L^{-1}) cultures receiving 5 (□) or 10 (●) mL medium replacement every 3−4 days, with H_2/malate (A) or lactate (B) as the energy/carbon source. Medium replacement was carried out just prior to sampling the cultures for 0.5 M HCl-extractable Fe(II) content. Error bars show ± 1 SD of triplicate cultures; bars not visible are smaller than symbol.

proportion of aqueous to total Fe(II) production and lower concentration of sorbed Fe(II) in the SCs suggest that medium replacement enhanced Fe(III) reduction by altering the equilibrium between dissolved and "sorbed" Fe(II) such that the inhibitory effect of Fe(II) sorption on oxide reduction was reduced. This intepretation is consistent with previous studies which have demonstrated that Fe(II) sorption onto oxide and Fe(III)-reducing bacterial cell surfaces is the primary cause for cessation of Fe(III) oxide reduction in batch cultures (*9*). Recent experiments on soluble Fe(III)-citrate reduction by *S. alga* have verified that it is the association of Fe(II) with oxide and FeRB cell surfaces—rather than feedback inhibition of the reductase enzyme system by Fe(II)—that is primarily responsible for the cessation of Fe(III) reduction (*21*).

The possibility existed that periodic renewal of energy, carbon, or nutrients— as opposed to Fe(II) elimination— could have contributed to the enhanced Fe(III) reduction activity in the SCs. Of all the substrates that may have been limiting, phosphate (present at 0.044 mM in the culture medium) was the most logical possibility, given that both nitrogen, carbon, and energy were present in vast excess. However, a separate batch culture experiment in which phosphate was added (in an amount equivalent to that added during the 10-mL replacement in the SCs) every 3−4 days indicated that additional phosphate did not lead to an increase in synthetic Gt reduction (data not shown). This result supports the interpretation that removal of Fe(II), rather than nutrient renewal, was responsible for stimulation of Gt reduction in the SCs. To our knowledge these findings represent the first experimental demonstration that advective Fe(II) removal can promote microbial Fe(III) oxide reduction.

Subsoil Fe(III) Oxide Reduction. Medium replacement increased the extent of Fe(III) oxide reduction in the CP subsoil cultures (Figure 2), although not to the same degree observed in the synthetic Gt cultures. In contrast, no significant stimulation of reduction was detected in the HC subsoil cultures. The lesser stimulatory effect of medium replacement on subsoil Fe(III) oxide reduction vs synthetic Gt reduction may be related to the ability of clay minerals in the soils to bind Fe(II) and thereby function as Fe(II) sinks which "compete" with aqueous phase replacement as a mechanism for attenuating Fe(II) accumulation on Fe(III) oxide and FeRB cell surfaces. In other words, the effect of medium replacement was less because the clay minerals themselves acted as effective sinks for evolved Fe(II). This interpretation is consistent with (i) the Fe(II) sorption capacity of the subsoils, which when normalized to Fe(III) oxide content is 3−4 times higher than the synthetic Gt (Table 1), and (ii) our recent finding that layer silicates can act as Fe(II) sinks which enhance the long-term extent of synthetic Gt reduction (*10*). By the same line of reasoning, the fact that medium replacement stimulated reduction of CP more than

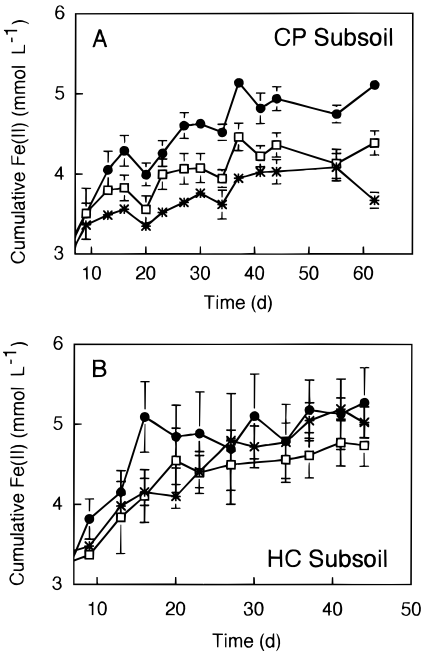


FIGURE 2. Cumulative Fe(II) (aqueous + solid-phase) production in batch and semicontinuous cultures containing CP (25 mmol Fe(III) L^{-1}) or HC (40 mmol Fe(III) L^{-1}) subsoils. Symbols as in Figure 1. Error bars show SD of triplicate cultures; bars not visible are smaller than symbol. *x* and *y* axes start at nonzero values in order to emphasize differences between treatments.

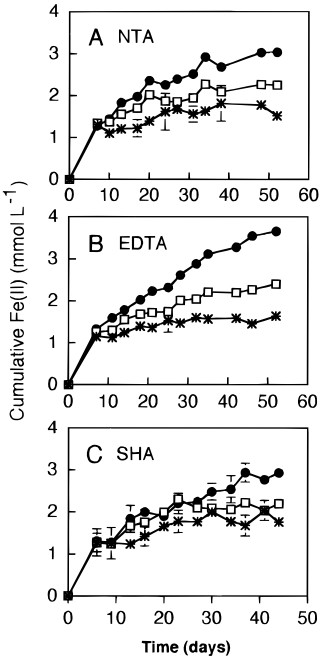


FIGURE 3. Cumulative Fe(II) (aqueous + solid-phase) production in batch and semicontinuous synthetic Gt (50 mmol L^{-1}) cultures amended with 0.5 mM NTA (A), 0.5 mM EDTA (B), or 100 mg L^{-1} IHSS Soil Humic Acid (C). Symbols as in Figure 1. Error bars show ± 1 SD of triplicate cultures; bars not visible are smaller than symbol.

HC subsoil can likely be attributed to HC's greater Fe(II) sorption capacity and higher affinity for Fe(II) (as indicated by Freundlich isotherm *K* values; see Table 1), since more effective Fe(II) binding would be expected to attenuate the influence of advective Fe(II) removal on oxide reduction. Our results do not necessarily mean that advective Fe(II) removal is not expected to promote the long-term extent of Fe(III) oxide in clay-rich sediments, but rather that the effect might take longer to manifest (e.g. after the onset of anaerobic conditions) than in clay-poor sediments due to the ability of the clay minerals to serve as alternative Fe(II) sinks.

Influence of Aqueous Fe(II) Complexants. Aqueous Fe ligands (e.g. NTA, EDTA) have been shown to stimulate microbial Fe(III) oxide reduction by (i) complexing and dissolving Fe(III) from the oxide surface (*10, 16, 17*), and (ii) complexing biogenic Fe(II), thereby retarding Fe(II) sorption to oxide and FeRB cell surfaces (*10*). An additional hypothesis of this study was that periodic renewal of fresh (i.e. non-Fe-complexed) chelator would enhance the stimulatory effect of medium replacement on Fe(III) oxide reduction in SCs by one or both of these mechanisms. In the case of humics, we anticipated that both Fe(II) complexation (*22*) as well as electron shuttling from quinone functional groups (*18, 19*) could enhance oxide reduction and that periodic influx of fresh humics would amplify these effects. In general, our results did not support these expectations. The presence of 0.5 mM NTA, 0.5 mM EDTA, or 100 mg L^{-1} SHA did not substantially increase the stimulatory effect of 5 or 10 mL medium replacements (Figures 1 and 3; Table 2), nor did they significantly increase the fraction of cumulative Fe(II) production accounted for by aqueous Fe(II) in the SCs (Table 2). These results suggest that the periodic removal of the Fe(II)-rich aqueous phase altered the equilibrium between sorbed (which inhibits reduction) and aqueous Fe(II) enough so that no major effect of the chelators was observed.

The presence of 0.5 mM NTA or EDTA did lead to a minor increase in the long-term extent of Gt reduction in batch cultures with H_2/malate as an energy/carbon source (Table 2). This result agrees with previous findings which demonstrated that NTA and (to a lesser extent) EDTA enhance the extent of Gt reduction by complexing evolved Fe(II) (*10*). Batch cultures containing soil humic acid produced ca. 50% more Fe(II) than their humic-free counterparts. Although this finding may indicate that the quinone electron shuttle mechanism stimulated Fe(III) reduction, it is not possible to assess whether the observed effect was due to electron shuttling or Fe(II) complexation by the humics. The latter explanation is favored by higher ratio of aqueous to total Fe(II) in the SHA cultures (Table 2). In any case, the stimulation of Gt reduction was not nearly so profound as that observed in experiments with much higher (20-fold) humic concentrations (*19*).

Bacterial Growth. Measurements of bacterial protein content suggested that FeRB cell growth was stimulated in the SCs (Figure 4). A substantial portion (40−50%) of bacterial biomass was present in the aqueous phase of the SCs, i.e., not attached to the Fe(III) oxide. Hence, removal of culture medium resulted in removal of bacterial biomass. This biomass was consistently replaced by bacterial growth in the SCs. In contrast, only minor increases in protein were observed in the batch cultures during the course of the experiments. While the lack of major protein production in the batch cultures does not necessarily mean that no net growth occurred (it is possible that some cells died while other cells underwent reproduction, leading to a constant level of protein, or that the protein content of dead cells was not completely degraded over the time scale of the experiments), the key result is that much greater cumulative protein production occurred in the SC vs batch cultures (Figure 4). Given that energy/nutrient renewal was not likely responsible for stimulation of Fe(III) oxide reduction in the SCs (see above), we conclude that Fe(II) removal led to a systematic stimulation of FeRB growth coupled to Gt reduction in the SCs. Because the standing stock of protein at any given time in the SCs was consistently lower than that in batch cultures, it is clear that the FeRB cells in SCs were considerably more active, in terms of Fe(III) reduction and growth, than those in the batch cultures.

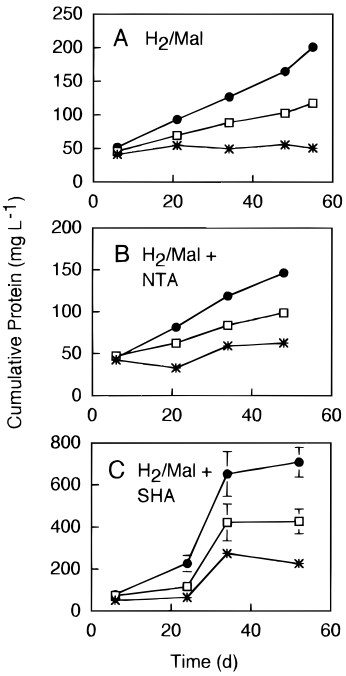


FIGURE 4. Cumulative protein production in batch and semicontinuous synthetic Gt cultures. Symbols as in Figure 1. Panels A−C show results of cultures with H_2/malate alone, H_2/malate + 0.5 mM NTA, and H_2/malate + 100 mg L^{-1} SHA, respectively. Error bars show ± 1 SD of triplicate cultures; bars not visible are smaller than symbol. Note difference in scale for panel C.

The presence of 0.5 mM NTA in the culture medium did not stimulate the production of bacterial cell protein in either batch cultures or SCs (Figure 4 and Table 2). However, the soil humic acids stimulated a 4-fold increase in protein in the batch cultures, and cumulative protein production in the soil humic SCs was 2−4-fold higher than in no-humic cultures (Figure 4). It is interesting that the humics stimulated protein production so much, given that the difference in total Fe(II) production was not nearly so dramatic (Table 2). As a result of this phenomenon, the ratio of protein to Fe(II) production was 3−4-fold higher in the humics-containing than in the no-humics cultures. The stimulation of cell growth by the humics was likely due to their use as an electron acceptor. This explanation is consistent with the previous demonstration that *S. alga* can grow with humic substances as the sole electron acceptor (*18*). While some of the electrons transferred to the humics were undoubtedly shuttled to the Gt (thereby regenerating oxidized humics available once again for enzymatic reduction), it appears that this humic recycling mechanism (*19*) was not a major factor in our experiments—given that cumulative Fe(II) production was not stimulated in proportion to the vastly increased cell growth in the humics-containing cultures.

Simulation Model. A simulation model was developed to illustrate how sorption of Fe(II) can limit the long-term extent of oxide reduction and how advective removal of aqueous Fe(II) could stimulate Fe(III) oxide reduction by retarding the accumulation of sorbed Fe(II). Our intention was to develop a simple model that could serve as a basis for future development of more sophisticated mechanistic models of bacterial Fe(III) oxide reduction.

(a) Model Design. The model depicts production and speciation of Fe(II) during microbial reduction of synthetic Gt in a batch vs "open" reactor system. A dilution rate constant of 0.1 d^{-1} was used to simulate advective Fe(II) removal in the open reactor system. Bulk Fe(II) production was governed by a first-order rate equation in which Fe(III) reduction is dependent on the concentration of free Fe(III)

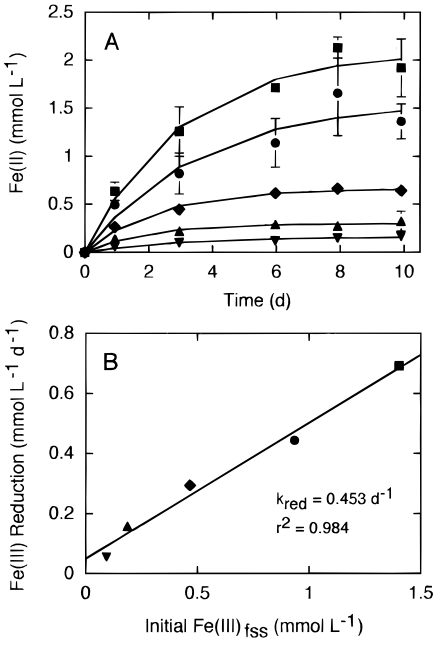


FIGURE 5. Kinetics of synthetic Gt reduction by *S. alga*. Panel A: time course of Gt reduction with a range of starting Fe(III) concentrations: ▼, 5 mmol L^{-1}; ▲, 10 mmol L^{-1}; ◆, 25 mmol L^{-1}; ●, 50 mmol L^{-1}; and ■, 75 mmol L^{-1}. Error bars show ± 1 SD of triplicate cultures; bars not visible are smaller than symbol. Solid lines are nonlinear least-squares regression fits of the data to the following equation which depicts Fe(II) accumulation from first-order consumption of a finite number of "free" surface Fe(III) reduction sites: $Fe(II) = Fe(III)_{fss}^0[1 - \exp(-k_{red}t)]$, where Fe(II) is the concentration of Fe(II) at time t, $Fe(III)_{fss}^0$ is the initial concentration of free surface sites, and k_{red} is a first-order rate constant. Both $Fe(III)_{fss}^0$ and k_{red} were allowed to vary in the curve-fitting procedure. Panel B: Initial Fe(III) reduction rate vs initial free Fe(III) surface site concentration (see text). Initial Fe(III) reduction rates were computed from the first-derivative of the nonlinear regression fits in panel A evaluated at $t = 0$.

oxide surface reduction sites ($Fe(III)_{fss}$):

$$\frac{dFe(II)}{dt} = k_{red}Fe(III)_{fss}$$

This formulation assumes that Fe(III) reduction was independent of electron donor and nutrient concentrations, in accordance with the excess of these substrates in our culture systems. The first-order reduction rate constant k_{red} was estimated from initial rates of synthetic Gt reduction as a function of oxide concentration in batch culture experiments identical to those run in parallel with the SCs (Figure 5). The estimated value of k_{red} (0.453 d^{-1}) was similar to the average (0.387 ± 0.099 d^{-1}; $n = 5$) of the first-order rate constants determined from curve fits of Fe(II) concentration vs time to an equation depicting the accumulation of end-product from a first-order reaction acting on a finite reservoir of surface reduction sites (Figure 5A). The fact that both these approaches as well as previous studies of Fe(III) oxide reduction kinetics (*8*) support a first-order rate model for Gt reduction suggests that use of this rate model is a reasonable way to depict the dependence of oxide reduction rate on oxide surface site concentration in our experimental systems. Although it may have been possible to base the model on growth of the FeRB population using recently determined growth rate and biomass yield parameters for *S. alga* in batch culture systems identical to those employed in this study (*23*), we do not yet know how FeRB growth rates vary as a function of Fe(III) oxide surface site concentration or the abundance of Fe(II) sorbed to oxide and/or cell surfaces.

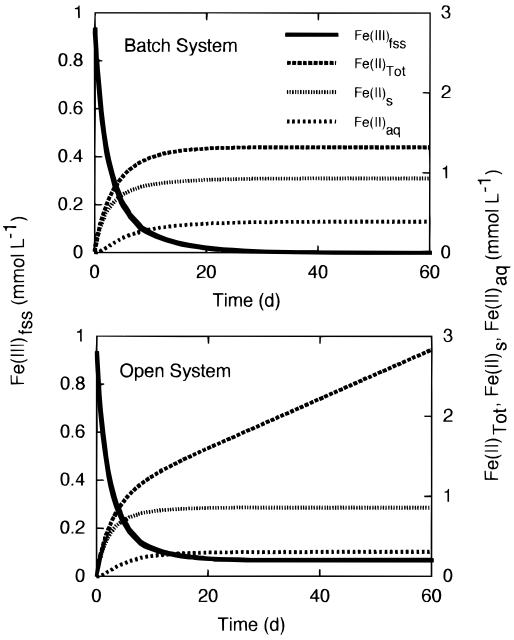


FIGURE 6. Simulation model results for batch and open (dilution rate of 0.1 d^{-1}) reactor systems. $Fe(III)_{fss}$ refers to "free" Fe(III) oxide surface sites (see text); $Fe(II)_{aq}$ and $Fe(II)_s$ refer to aqueous and sorbed Fe(II), respectively; $Fe(II)_{tot}$ refers to the cumulative amount of Fe(II) produced.

Thus inclusion of cell growth in the model is unwarranted at this time.

The initial abundance of Fe(III) oxide surface sites (0.93 mmol L^{-1}) was chosen in accordance with an assumed molar Fe(III) concentration of 50 mmol L^{-1}, the measured surface area of the oxide (55 m^2 g^{-1}), and the standard surface site density of 2.3 sites nm^{-2} recommended in ref *24*. Bulk Fe(II) was allowed to undergo equilibrium sorption to Fe(III) surface sites according to a Freundlich equation fit to Fe(II) sorption data for a mixture of 50 mmol L^{-1} Gt and a standard inoculum (same as that used in this study) of *S. alga* cells in Pipes-buffered growth medium (*9*).

To link the sorption of Fe(II) to the suppression of Fe(III) oxide reduction, Fe(III) surface sites occupied by sorbed Fe(II) were assumed to be unavailable for microbial reduction; in other words, a surface site with sorbed Fe(II) is no longer "free". This approach assumed that a sorbed Fe(II) occupies a single sorption site. It is important to note that because FeRB cells contribute significantly to the Fe(II) sorption capacity of our synthetic Gt culture systems (*9*), it may be appropriate to interpret the deactivation of Fe(III) reduction via Fe(II) sorption as the combined effect of sorption to binding sites on both FeRB cell and Fe(III) oxide surfaces—even though for the sake of simplicity the initial population of free reduction sites was defined only by those on the Gt surface.

The model was solved numerically over a 60-day simulation period using a stiff ODE solver algorithm described in ref *25*. Equilibrium sorption of Fe(II) onto Fe(III) surface sites was computed with a Newton–Raphson routine which operated within the ODE solver.

(b) Model Results. The model reproduced the basic trends observed in batch vs semicontinuous synthetic Gt reduction systems (Figure 6). Accumulation of sorbed Fe(II) ($Fe(II)_s$) in the batch system led to rapid blockage of free reduction sites, which in turn resulted in the cessation of Fe(III) reduction a few weeks into the simulation; this result is consistent with the batch culture data shown in Figures 1, 3, and 5. Advective removal of Fe(II) in the open system (residence time = 10 days) led to maintenance of a low but significant concentration of free reduction sites over time, which in turn allowed for continued Fe(III) reduction, resulting in a ca. 2-fold increase (relative to the batch system) in the total amount of Fe(II) produced during the 2-month simulation; this result is consistent with the SC data in Figures 1 and 3.

The basic agreement between the model and experimental results indicates that depicting inhibition of Fe(III) reduction through Fe(II) sorption is an appropriate first step toward modeling controls on the long-term extent of microbial Fe(III) oxide reduction. The success of this simple model suggests that pursuit of geochemically more sophisticated models (e.g. ones which include aqueous phase complexation, bulk-phase precipitation, surface precipitation, and Fe(II) sorption to non-oxide surface sites—including FeRB cells) will be justified when appropriate experimental data and modeling approaches become available. Other important steps will include incorporation of information on FeRB growth rate and biomass production as a function of Fe(III) oxide surface chemistry and incorporation of a mechanism for depletion of bulk Fe(III) oxide content in concert with the reductive dissolution of Fe(III) oxide surface sites.

Environmental Implications. Our results indicate that elimination of Fe(II) via aqueous phase transport could play a significant role in governing the rate and extent of microbial Fe(III) oxide reduction in sedimentary environments. These findings support the previous speculation (*8*, *9*) that advective Fe(II) removal was involved in facilitating the near-complete consumption of crystalline Fe(III) oxides within a shallow subsurface landfill leachate plume in Denmark (*26*). However, because the mean residence times in our SCs were probably considerably shorter than those in most subsurface environments and the rates of metabolic activity relatively high, quantitative extrapolation of our results to in situ subsurface conditions is difficult. Nevertheless, it is interesting to note that longer (600-day) model simulations using a 100-day residence time, and 10-fold lower k_{red} value, yielded total Fe(II) production values similar to those obtained in the 60-day simulation with a 10-day residence time and the k_{red} value for conditions of excess electron donor and nutrients. This agreement suggests that our 2-month experiments may give a reasonable impression of how crystalline Fe(III) oxide reduction might respond to advective Fe(II) removal over much longer periods of time in subsurface systems with slower rates of advective transport and metabolic activity. Experiments in reactor systems which more closely approximate in situ subsurface conditions will be required to evaluate this hypothesis.

In summary, the interaction between transport and Fe(II) sorption is likely to have a significant impact on the persistence of Fe(III) oxide reduction activity in subsurface environments. Of course, other geochemical interactions (in particular competitive sorption of Fe(II) and other cations and organics) may modify the influence of advection on oxide reduction. Such interactions may be a matter of significant concern in situations where the activity of FeRB is exploited for remediation of organic or metal/radionuclide contaminants.

Acknowledgments

This research was funded by Grant DE-FG07-96ER62321 from the U.S. Department of Energy, Office of Energy Research, Environmental Management Science Program. We thank Ginger Scott for technical assistance.

Literature Cited

(1) Stumm, W.; Sulzberger, B. *Geochim. Cosmochim. Acta* **1992**, *56*, 3233–3257.
(2) Lovley, D. R. *Microbiol. Rev.* **1991**, *55*, 259–287.
(3) Nealson, K. H.; Saffarini, D. *Annu. Rev. Microbiol.* **1994**, *48*, 311–343.

(4) Lovley, D. R. *J. Industrial Microbiol.* **1995**, *14*, 85−93.
(5) Fredrickson, J. K.; Gorby, Y. A. *Curr. Opin. Biotechnol.* **1996**, *7*, 287−294.
(6) Lovley, D. R. *Annu. Rev. Microbiol.* **1993**, *47*, 263−290.
(7) Fendorf, S. E. *Geoderma* **1995**, *67*, 55−71.
(8) Roden, E. E.; Zachara, J. M. *Environ. Sci. Technol.* **1996**, *30*, 1618−1628.
(9) Urrutia, M. M.; Roden, E. E.; Fredrickson, J. K.; Zachara, J. M. *Geomicrobiol. J.* **1998**, *15*, 269−291.
(10) Urrutia, M. M.; Roden, E. E.; Zachara, J. M. Submitted for publication.
(11) Caccavo, F.; Blakemore, R. P.; Lovley, D. R. *Appl. Environ. Microbiol.* **1992**, *58*, 3211−3216.
(12) Rossello-Mora, R. A.; Caccavo, F.; Osterlehner, K.; Springer, N.; Spring, S.; Schuler, D.; Ludwig, W.; Amann, R.; Vanncanneyt, M.; Schleifer, K. H. *Syst. Appl. Microbiol.* **1994**, *17*, 569−573.
(13) Lovley, D. R.; Phillips, E. J. P. *Appl. Environ. Microbiol.* **1988**, *54*, 1472−1480.
(14) Rai, D.; Zachara, J. M.; Ainsworth, C. C.; Eary, L. E.; Sass, B. M. *Physiochemical measurements of soils at solid waste disposal sites*; Electric Power Research Institute: Palo Alto, CA, 1986.
(15) Taylor, D. L.; Jardine, P. M. *J. Environ. Qual.* **1995**, *24*, 789−792.
(16) Arnold, R. G.; DiChristina, T. J.; Hoffman, M. R. *Biotechnol. Bioengin.* **1988**, *32*, 1081−1096.
(17) Lovley, D. R.; Woodward, J. C. *Chem. Geol.* **1996**, *132*, 19−24.
(18) Lovley, D. R.; Coates, J. D.; Blunt-Harris, E. L.; Phillips, E. J. P.; Woodward, J. C. *Nature* **1996**, *382*, 445−448.
(19) Lovley, D. R.; Fraga, J. L.; Blunt-Harris, E. L.; Hayes, L. A.; Phillips, E. J. P.; Coates, J. D. *Acta Hydrochim. Hydrobiol.* **1998**, *26*, 152−157.
(20) Stookey, L. L. *Anal. Chem.* **1970**, *42*, 779−781.
(21) Roden, E. E.; Urrutia, M. M. Unpublished data.
(22) Buffle, J. *Complexation reactions in aquatic systems. An analytical approach*; Ellis Horwood Ltd.: Chichester, England, 1990.
(23) Urrutia, M. M.; Roden, E. E. In *American Society for Microbiology 98th Annual Meeting Abstract Volume*; 1997; p 337.
(24) Davis, J. A.; Kent, D. B. In *Mineral-water interface geochemistry*; Hochella, M. F., White, A. F., Eds.; Mineralogical Society of America: Washington, DC, 1990; pp 177−260.
(25) Press, W. H.; Teukolsky, S. A.; Vetterling, W. T.; Flannery, B. P. *Numerical recipes in FORTRAN*; Cambridge University Press: Port Chester, NY, 1992, Vol. 1.
(26) Heron, G.; Crouzet, C.; Bourg, A. C. M.; Christensen, T. H. *Environ Sci Technol.* **1994**, *28*, 1698−1705.
(27) Stumm, W. *Chemistry of the solid-water interface*; John Wiley & Sons: New York, 1992.

Received for review September 23, 1998. Revised manuscript received February 23, 1999. Accepted March 9, 1999.

ES9809859

Additions and Corrections

1999, Volume 33, Pages 1847−1853

Eric E. Roden* and Matilde M. Urrutia: Ferrous Iron Removal Promotes Microbial Reduction of Crystalline Iron(III) Oxides

Corrections to Fe(II) sorption capacities listed in Table 1: (i) the sorption capacities per g dry wt of sorbent are in units of mmol Fe^{II}/g dry wt rather than μmol Fe^{II}/g dry wt.

(ii) the correct values for Fe(II) sorption capacities expressed in units of μmol Fe^{II}/μmol Fe^{III} are as follows:

synthetic Gt: 0.014
CP subsoil: 0.086
HC subsoil: 0.074

ES9920157

10.1021/es9920157 CCC: $18.00 © 1999 American Chemical Society
Published on Web 06/08/1999

Environ. Sci. Technol. **1999**, *33,* 4022−4028

Influence of Aqueous and Solid-Phase Fe(II) Complexants on Microbial Reduction of Crystalline Iron(III) Oxides†

MATILDE M. URRUTIA,*,‡
ERIC E. RODEN,‡ AND
JOHN M. ZACHARA§

Department of Biological Sciences, The University of Alabama, Box 870206, Tuscaloosa, Alabama 35487-0206, and Pacific Northwest National Laboratory, P.O. Box 999, Environmental Dynamics & Simulation Department, W. R. Wiley Environmental Molecular Sciences Lab, Mail Stop K8-96, Richland, Washington 99352

The influence of aqueous (NTA and EDTA) and solid-phase (aluminum oxide, layer silicates) Fe(II) complexants on the long-term microbial reduction of synthetic goethite by *Shewanella alga* strain BrY was studied. NTA enhanced goethite reduction by promoting aqueous Fe(II) accumulation, in direct proportion to its concentration in culture medium (0.01−5 mM). In contrast, EDTA failed to stimulate goethite reduction at concentrations ≤1 mM, and 5 mM EDTA enhanced the final extent of reduction by only 25% in relation to nonchelator controls. The minor effect of EDTA compared to NTA, despite the greater stability of the Fe(II)−EDTA complex, likely resulted from sorption of Fe(II)−EDTA complexes to goethite. Equilibrium Fe(II) speciation calculations showed that $Fe(II)_{aq}$ should increase with NTA at the expense of the solid-phase Fe(II) species, whereas the opposite trend was true for EDTA due to Fe(II)EDTA adsorption. The presence of aluminum oxide and layer silicates led to a variable but significant (1.5 to > 3-fold) increase in the extent of goethite reduction. Speciation of Fe(II) verified the binding of Fe(II) by these solid-phase materials. Our results support the hypothesis that iron(III) oxide reduction may be enhanced by aqueous or solid-phase compounds which prevent or delay Fe(II) sorption to oxide and FeRB cell surfaces.

Introduction

Microbial iron(III) oxide reduction strongly influences the geochemistry of anaerobic soil and sedimentary environments as well as the persistence and mobility of various types of organic and inorganic contaminants in such environments (*1, 2*). Recent studies indicate that the surface chemical properties of both the iron(III) oxide and the dissimilatory Fe(III)-reducing bacteria (FeRB) control the initial rate and long-term extent of microbial reduction of synthetic iron(III) oxides in defined growth medium (*3, 4*). Fe(II) coatings on the surface of iron(III) oxides and FeRB lead to deactivation of Fe(III) reduction as oxide and cell surface sites become saturated with sorbed Fe(II). However, reduction can proceed to greater levels than the measured Fe(II) sorption capacity if conditions favor bacterial growth (*3*). The importance of surface saturation as a passivation mechanism is supported by the observations that Fe(III) reduction can be reactivated if sorbed Fe(II) is removed from the oxide surface (*4*) or if fresh FeRB cells are added to Fe(II)-saturated materials (*3*). Our findings suggest that the extent of iron(III) oxide reduction in anaerobic environments may be influenced by reactions with associated solid phases and aqueous ligands that compete for and complex Fe(II) produced during oxide reduction.

Synthetic chelators such as EDTA and NTA have been shown to play an important role in metal/radionuclide speciation, solubility, and mobility in surface waters and groundwater (*5*−*11*). EDTA and NTA complex both Fe(III) and Fe(II) and may therefore influence the microbial reduction of iron(III) oxides by both dissolution (*12*) and Fe(II) sequestration (our untested hypothesis). Biogenic Fe(II) may exert a strong impact on the stability of mobile metal/radionuclide complexes by displacement reactions (*13*).

Fe(II)-sorbing mineral phases, such as aluminum oxides and layered silicates, may function as alternate sinks for Fe(II), thereby decreasing or delaying iron(III) oxide and bacterial surface saturation with Fe(II). Fe(II) binding by these phases could thus have a direct impact on the activity of FeRB in soil and sedimentary environments as well as the geochemical conditions influenced by their activity, including groundwater pH, alkalinity, and biomineralization. These geochemical effects may strongly influence the mobility of contaminant metals and radionuclides in anaerobic subsurface environments.

In this paper we investigate the influence of aqueous (NTA, EDTA) and solid-phase (aluminum oxide and layer silicates) complexants on the rate and extent of bacterial iron(III) oxide reduction. Our central hypothesis was that Fe(II) complexation would enhance the long-term reducibility of iron(III) oxides by delaying the formation of passivating oxide/cell surface Fe(II) coatings. Results indicate that all of these Fe(II) ligands have the potential to enhance microbial reduction of crystalline iron(III) oxides to some extent, but the biogeochemical interactions are complex and effects are nonlinear.

Material and Methods

Organism and Culture Conditions. The dissimilatory Fe(III)- and Mn(IV)-reducing bacterium *Shewanella alga* strain BrY(*14*) was used as a test organism. *S. alga* was grown anaerobically in basal culture medium with H_2 as electron donor, malate (30 or 8 mM as indicated) as carbon source, and synthetic goethite (50 mmol L^{-1}; 4.45 g L^{-1}) as electron acceptor in which the PO_4^{3-} concentration was reduced 100-fold (to 0.04 mM) relative to the original (*15*) basal salts composition. The medium was autoclaved prior to the addition of H_2 gas. *S. alga* was grown aerobically to late exponential phase in Tryptic Soy Broth (TSB). The TSB-grown cells were washed once with 10 mM Pipes buffer (piperazine-*N*,*N*′-bis{2-ethanesulfonic acid}, disodium salt, pH 6.8), resuspended in buffer to ∼10^8 cells mL^{-1} concentration, and made anaerobic by bubbling with O_2-free N_2 gas before being used as inoculum (0.5 mL of cell suspension to 10 mL culture tubes). Culture tubes were incubated on their side, without shaking and in the dark at 31 °C. Standard anaerobic techniques were used for all procedures as described in ref *16*.

* Corresponding author phone: (205)348-5191; fax: (205)348-1403; e-mail: murrutia@biology.as.ua.edu.
† This work is dedicated to the memory of Laureano Urrutia.
‡ The University of Alabama.
§ Pacific Northwest National Laboratory.

10.1021/es990447b CCC: $18.00 © 1999 American Chemical Society
Published on Web 09/29/1999

Synthesis of Fe(III) Goethite. Goethite (Gt) was synthesized and treated as explained previously (*3*). The mineral obtained had a surface area of 55 $m^2\ g^{-1}$ as determined by five-point BET N_2 adsorption.

Influence of EDTA and NTA Concentration on Gt Reduction. Chelators were added to culture tubes (30 mM malate, 0.04 mM P, pH 6.8) in triplicate from filter sterilized, anaerobic stock solutions (1, 5, 10, 50, 100, and 500 mM) to obtain final concentrations of 0.01, 0.05, 0.1, 0.5, 1.0, or 5.0 mM. The stocks were prepared with the tetrasodium salt of EDTA (Na_4EDTA) (Fisher Scientific) and the disodium salt of NTA (Na_2HNTA) (Sigma Chem. Co.). Tubes were inoculated with washed TSB-grown *S. alga* cells immediately following chelator addition. Duplicate sterile controls were included for each chelator concentration. Soluble Fe(II) and Fe(III), and HCl-extractable Fe(II), were determined at 1, 3, 7, 15, and 30 day intervals.

Effect of Chelators on Fe(II) Adsorption onto Gt. The influence of the chelators on Fe(II) sorption by Gt was evaluated by addition of soluble Fe^{2+} (added as $FeCl_2$) to 50 mmol L^{-1} suspensions of the mineral in the presence and absence of 0.5 mM EDTA or NTA under strictly anaerobic conditions. The Fe(II) sorption capacity of this mineral (in 10 mM Pipes buffer at pH 6.9 without chelators) had been characterized previously (*3*) as 0.25 mmol Fe(II) g^{-1}. EDTA or NTA (0.1 mL) was added to triplicate 10-mL portions of sterile Gt suspension in Pipes buffer (10 mM, pH 6.9) from filter sterilized anaerobic stocks. Immediately afterward, a 0.2-mL aliquot of an anaerobic, filter-sterilized $FeCl_2$ stock solution was added to each tube to obtain Fe(II) concentrations ranging from 0.032 to 5.12 mM. Samples were allowed to equilibrate for 18 h with gentle shaking (50 rpm on a rotary shaker), after which the concentration of aqueous Fe(II) [$Fe(II)_{aq}$] was determined as described below. The difference between total added Fe(II) and $Fe(II)_{aq}$ was taken to represent sorbed Fe(II).

Adsorption of Fe(II)−Chelator Complexes onto Gt. Equimolar volumes of anaerobic Fe(II) (as $FeCl_2$) and EDTA (as Na_4EDTA) or NTA (as Na_2HNTA) solutions (all prepared in 10 mM Pipes buffer at pH 6.9) were first mixed together in a 1:1 ratio, yielding final Fe(II) and chelator concentrations of 10 mM. After a period of 6 h, different amounts of this Fe(II)−EDTA or Fe(II)−NTA solution were added to 50 mmol L^{-1} suspensions of Gt (in 10 mM pipes buffer, pH 6.9), yielding final Fe(II)−chelator concentrations of 0.01, 0.05, 0.13, 0.33, 0.5, and 1 mM. After an 18-h equilibration period with shaking at 50 rpm, $Fe(II)_{aq}$ and 0.5 M HCl-extractable Fe(II) were analyzed. Adsorbed Fe(II) (as Fe(II)−EDTA or Fe(II)-NTA) was calculated from the difference between $Fe(II)_{aq}$ and total Fe(II) extracted in HCl (see below).

Fe(II) Speciation Calculations. The program MINTEQA2 (*17*) was used to model the adsorption of Fe(II) onto Gt in the presence of chelators (using the equilibrium constants for Fe(II)−chelator complexes formation included in Table 1, Supporting Information), and the adsorption of Fe(II)−chelators onto Gt. MINTEQA2 was also used to model results obtained at the end of the reduction experiments in the presence of NTA or EDTA. The modeling approach adopted here is explained in detail elsewhere (*3*).

Experiments with Solid-Phase Fe(II) Complexants. Two types of experiments were conducted (in 8 mM malate, 0.04 mM P media): some in which goethite, cells and the solid-phase Fe(II) sink (either aluminum oxide or layered silicates) were allowed to be in direct contact, and some in which the Fe(II) sink was separated from the goethite and cells by inclusion in a dialysis bag. The later approach allowed the exchange of solutes but avoided contact of the cells with the clay/Al mineral.

The minerals used were Al_2O_3 (adsorption grade alumina, 80−200 mesh particle size, Fisher Sci., surface area 113 $m^2\ g^{-1}$) and three phyllosilicate minerals, commercial kaolin (Ka) (external surface area 16 $m^2\ g^{-1}$), Aldrich KSF montmorillonite (KSF) (external surface area 7 $m^2\ g^{-1}$), and Aldrich K10 montmorillonite (K10) (external surface area 246 $m^2\ g^{-1}$) (all from Aldrich Chem. Co.). Surface areas were obtained by five-point BET N_2 adsorption in a Micromeritics Gemini 2360 surface area analyzer, after 2 h degassing under N_2 atmosphere at 200 °C in a Micromeritics Flowprep 060. HCl-extractable Fe in the layer silicates was determined with 12 M HCl, yielding values of 0.183 mmol Fe per gram of KSF, 0.064 mmol g^{-1} for K10, and only traces (0.0011 mmol g^{-1}) for Ka. Fe(II) and Fe(III) solubilized from the montmorillonites before and after autoclaving (as may occur in culture experiments) were also determined (Table 2, Supporting Information). The KSF montmorillonite produced significant amounts of HCl-extractable Fe(II) and Fe(III) upon resuspension in aqueous media as well as some aqueous Fe(II) and Fe(III). The K10 montmorillonite, on the other hand, contained practically no Fe(II), but some soluble and HCl-extractable Fe(III) (Table 2, Supporting Information). Because of the Fe content of the montmorillonite clays, total Fe in these reduction experiments was calculated as the sum of Fe(III) in Gt plus Fe(III/II) in the clay mineral (when present).

Direct Contact Experiments. The mineral solids were added to 50 mmol L^{-1} Gt suspensions (248 $m^2\ L^{-1}$) in the following concentrations: 1.0 or 5.0 g L^{-1} of Al_2O_3 (total surface area concentration of 113 or 565 $m^2\ L^{-1}$, respectively), 2.6 or 13.0 g L^{-1} of Ka (42 or 208 $m^2\ L^{-1}$, respectively), 3.7 or 18.5 g L^{-1} of KSF (26 or 130 $m^2\ L^{-1}$, respectively) or K10 (910 or 4551 $m^2\ L^{-1}$, respectively) (equivalent to solid in suspension concentrations of 10 and 50 mmol L^{-1}, respectively). Cultures were set up as explained above. Samples were collected aseptically and anaerobically at 1, 2, 7, 9, 15, 30, and 40 days after inoculation for Fe(II) determination as described below. Fe reduction was compared to controls with Gt only.

Dialysis Bag Experiments. Dialysis bags (Spectra/Por 1.1 Biotech sterile membranes, 8000 MWCO, 5 mL sample volume) were used to prevent bacterial attachment to the solid-phase complexants. In these experiments, 1 g L^{-1} aluminum oxide was sterilized in 1 mL of 10 mM Pipes buffer (pH 6.8) and aseptically transferred into a sterile dialysis bag. The same procedure was used with both concentrations of layer silicates. The bags were then aseptically introduced into anaerobic goethite in culture medium flasks inside an anaerobic chamber. Once resealed, H_2 gas was added, and samples were inoculated with *S. alga* cells as explained above. Fe reduction was compared to controls with the alternative Fe(II) sinks in direct contact with Gt. The aluminum oxide and layer silicates inside the dialysis bags were not sampled for Fe(II) until the last sampling date (30 days). For this analysis, cultures were taken into the anaerobic chamber, and the dialysis bags were collected and digested in 0.5 M HCl (see Analytical Techniques section). The total amount of Fe in the goethite suspensions was also determined at this time. In another repetition of this experiment, triplicate cultures were set up with 1 g L^{-1} aluminum oxide or 2.6 g L^{-1} Ka inside dialysis bags; empty dialysis membranes were introduced in triplicated Gt control cultures as well. Reduction of the Gt by *S. alga* was followed over time, and the Fe(II) content of dialysis membranes and the mineral complexants were analyzed at the completion of the experiment (30 days) as indicated above.

Adhesion Test. Adhesion of *S. alga* cells to goethite and aluminum oxide minerals was studied following the method of Caccavo et al. (*18*), modified for our experimental system. Pipes (10 mM, pH 6.9) was used as adhesion buffer as in all our reduction experiments. Total cell numbers determination was obtained from cell counts in control tubes to which no mineral was added (Pipes only), because neither goethite nor aluminum oxide were dissolved by the methodological

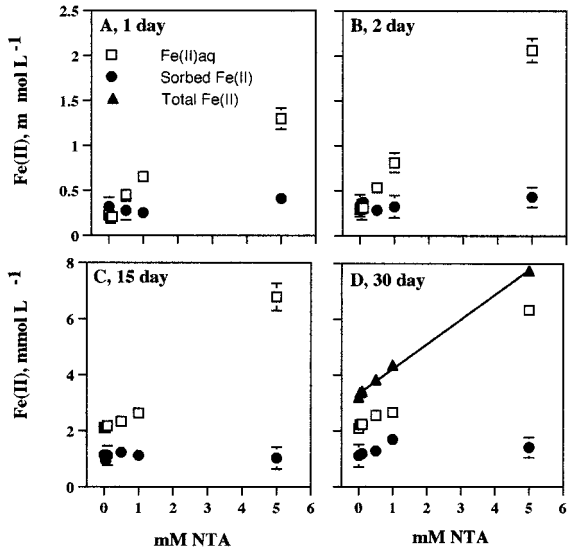


FIGURE 1. Reduction of Gt (50 mmol L^{-1}) by *S. alga* in the presence of different NTA concentrations after 1, 2, 15, and 30 days. Fe(II) was speciated into soluble Fe(II), ($Fe(II)_{aq}$), and sorbed Fe(II); total Fe(II) (soluble + sorbed) is included for the 30 d sample. Data represent the mean ± standard deviation of triplicate cultures; nonvisible error bars are smaller than the corresponding symbol. The solid line in panel D represents a linear regression analysis of total Fe(II) as a function of NTA concentration ($r^2 = 0.997$).

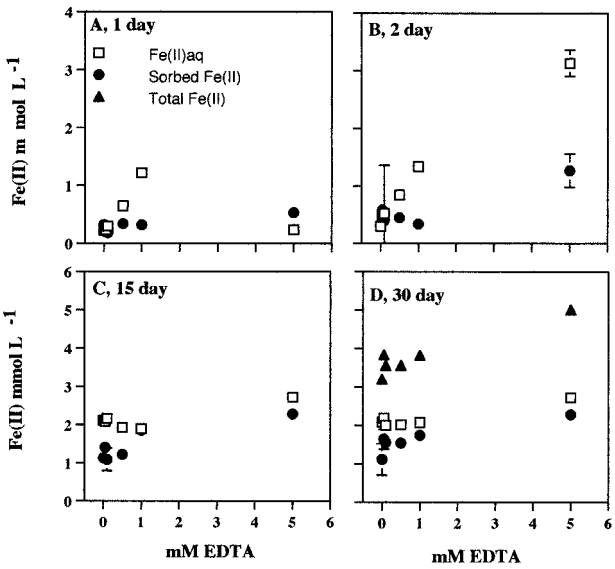


FIGURE 2. Reduction of Gt (50 mmol L^{-1}) by *S. alga* in the presence of several EDTA concentrations at 1, 2, 15, and 30 days. Fe(II) was speciated into soluble ($Fe(II)_{aq}$) and sorbed Fe(II); total Fe(II) (soluble + sorbed) is included for the 30 d sample. Data represent the mean ± standard deviation of triplicate cultures; nonvisible error bars are smaller than the corresponding symbol.

procedure used in Caccavo et al. (*18*). Adhesion of cells to aluminum oxide was compared to adhesion to Gt with triplicate tubes in which both minerals were present at equimolar concentrations (50 mM). A triplicate set of tubes with 50 mM Gt and 1 g L^{-1} aluminum oxide as in our reduction experiments was also included.

Analytical Techniques. Total Fe(II) in 0.2−0.5 mL culture samples was determined by extraction with 5 mL of 0.5 M HCl for 2 h, followed by colorimetric analysis of Fe(II) with ferrozine. $Fe(II)_{aq}$ was measured by filtering a 0.2−1.0 mL aliquot of sample through a 0.22 μm nylon syringe filter directly into ferrozine and reading the A_{562} immediately. Total Fe in aqueous phase samples and HCl extracts was obtained by reducing all Fe(III) with $NH_2OH{\cdot}HCl$ prior to colorimetric Fe determination. Fe(III) concentrations were calculated from the difference between total Fe and Fe(II).

Preliminary experiments showed a very slow color development during the Fe(II) ferrozine colorimetric assay in the presence of EDTA, most likely due to competition between EDTA and ferrozine for Fe(II). Therefore, standard curves were prepared with Fe(II) and Fe(III) standard solutions having EDTA concentrations equal to those used in the reduction experiments. Fe(II) (0.1, 0.2, 0.5, and 1 mM) was added as ferrous diammonium sulfate, and Fe(III) (0.1, 0.2, 0.5 and 1 mM) as $FeCl_3$. EDTA concentrations were 0.05, 0.1, 0.5, 1, and 5 mM for Fe(II) standard curves and 5 mM for Fe(III). Both Fe(II) and Fe(III) standard curves with 5 mM NTA were also prepared to test the effect of NTA on color development; the presence of NTA did not cause any interference with the assay. Regression equations obtained with each EDTA concentration were used to correct sample A_{562} readings in all subsequent experiments. Neither EDTA nor NTA caused any interference in the determination of Fe(III).

Results

Influence of EDTA or NTA on Gt Reduction. The presence of increasing NTA concentrations led to consistent enhancement of the initial (0−48 h) Gt reduction by *S. alga*, due to increases in $Fe(II)_{aq}$ (Figure 1A,B). A small amount of Fe(III) (maximum of 15 μmol Fe(III) L^{-1}) was dissolved from Gt by the highest NTA concentration (5 mM) in sterile controls (data not shown), whereas no $Fe(III)_{aq}$ was ever detectable in NTA-amended *S. alga* cultures. After a week to 1 month of incubation, Fe(III) reduction increased proportionally ($r^2 = 0.997$) to NTA concentration (Figure 1D). The increase in Fe(III) reduction was caused by solubilization of Fe(II) by NTA; there was no substantial effect of NTA on sorbed Fe(II) (closed circles).

The presence of increasing concentrations of EDTA noticeably enhanced initial Gt reduction by *S. alga* in relation to the nonchelator controls (Figure 2A,B). As with NTA, this effect was due to increases in the $Fe(II)_{aq}$ fraction (open squares in figure). The only exception was the samples to which 5 mM EDTA was added (Figure 2A). EDTA solubilized up to 25 μmol Fe(III) L^{-1} from goethite after 2 days and up to 100 μmol Fe(III) L^{-1} after 30 days in the sterile controls amended with 0.5 or 1 mM EDTA. $Fe(III)_{aq}$ was negligible in EDTA-amended *S. alga* cultures. The long-term extent of Gt reduction was not significantly increased by addition of EDTA at concentrations ≤1 mM ($p < 0.01$) (Figure 2D). The cultures that received 5 mM EDTA over time also showed increases in both $Fe(II)_{aq}$ and sorbed Fe(II) (Figure 2B,C). The final extent of goethite reduction was enhanced 25% by 5 mM EDTA in relation to the nonchelator controls (Figure 2D).

Influence of EDTA and NTA on Fe(II) Sorption by Goethite. Fe(II) adsorption isotherms were conducted in the presence of 0.5 mM NTA or EDTA under pH and ionic strength conditions identical to those in the Gt reduction experiments (Figure 3 A,B). The presence of 0.5 mM NTA reduced Fe(II) sorption at low Fe(II) loadings but did not significantly affect the amount of Fe(II) sorbed at near saturation levels (Figure 3A). The presence of 0.5 mM EDTA had a similar effect (Figure 3B). Fe(II) sorption at low Fe(II) loadings was slightly greater in the presence of EDTA than in the presence of NTA. The point on the isotherm below which the chelators influenced Fe(II) sorption is $10^{-3.3}$ mol L^{-1}, which is the added chelator concentration. This result was foreseen, since chelators would be expected to affect Fe(II) sorption only when the total chelator concentration is greater than the total Fe(II) concentration.

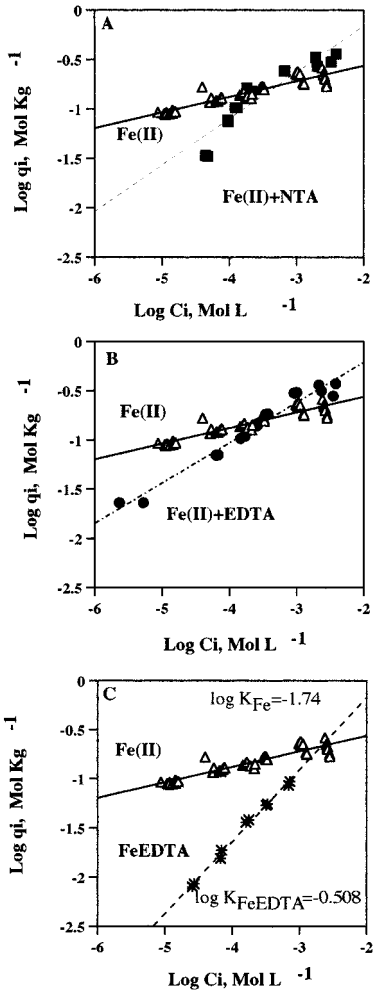


FIGURE 3. Fe(II) adsorption onto goethite (50 mmol L^{-1}) in the presence of NTA or EDTA. (A) Freundlich plot for Fe(II) adsorption onto Gt in the presence of 0.5 mM NTA (Fe(II) + NTA) (solid squares ■). (B) Freundlich plot for Fe(II) adsorption onto Gt in the presence of 0.5 mM EDTA (Fe(II) + EDTA) (solid circles ●). (C) Freundlich plot for adsorption of Fe(II)−EDTA complexes onto Gt (FeEDTA) (stars ∗). A previously determined (*3*) isotherm for uncomplexed Fe(II) adsorption to the same Gt mineral in the absence of chelators is included in each panel as a reference (open triangles △) (reproduced with permission from the publisher, Taylor & Francis, Ltd). Each point represents an individual sample. Ci = soluble Fe(II) at equilibrium; qi = adsorbed Fe(II) at equilibrium; Freundlich equations: Fe(II) adsorption in Pipes buffer, $y = 0.158x - 0.246$, $r^2 = 0.858$; Fe(II) adsorption in the presence of 0.5 mM NTA, $y = 0.469x + 0.777$, $r^2 = 0.860$; Fe(II) adsorption in the presence of 0.5 mM EDTA, $y = 0.409x + 0.609$, $r^2 = 0.965$; FeEDTA adsorption, $y = 0.733x + 1.287$, $r^2 = 0.993$. Log K_F values in (C) are derived from activity Freundlich transforms of the data using MINTEQA2.

Adsorption of Fe(II)−Chelator Complexes onto Goethite. Adsorption of Fe(II)−EDTA to Gt was low at low sorbate concentrations but at high loadings approached the levels of uncomplexed Fe(II) adsorption (Figure 3C). The adsorption data were fit to an activity Freundlich adsorption model using MINTEQA2 ($\log K_F = -0.508$). Fe(II)−NTA complexes sorbed much less strongly than Fe(II)−EDTA (data not shown).

Calculated Fe(II) Speciation. The equilibrium speciation of Fe(II) was computed as a function of chelator concentration (Table 3) to assess the potential solid and aqueous phase associations of biogenic Fe(II). The total Fe(II) concentration chosen for these calculations was 3.2 mmol L^{-1}, equal to the average amount of reduction obtained in the nonchelator controls at the end of the experiment (Figures 1D and 2D). Values for Fe(II)−chelator complexes equilibrium constants are compiled in Table 1, Supporting Information. Although the experimental Fe(II) speciation obtained in Fe reduction experiments is not always accurately described by these computations ((*3*)), they should nevertheless give an idea of the major speciation trends in the presence of the chelators. Fe(II) speciation calculations in the presence of EDTA (0.5−5 mM) were conducted to obtain equilibrium concentrations for all the Fe(II)−EDTA species. The most abundant Fe(II)-EDTA species under these conditions, $FeEDTA^{2-}$, was then considered to be the sorbing species. $FeEDTA^{2-}$ adsorption to Gt was then included with an activity Freundlich model (Figure 3C); for each EDTA concentration, the initial total $FeEDTA^{2-}$ was the equilibrium concentration for this species obtained previously. This approach allowed $FeEDTA^{2-}$ to distribute between $FeEDTA^{2-}_{aq}$ and $FeEDTA^{2-}_{sorbed}$ according to the measured isotherm (Figure 3C). These calculations revealed significant increases in $FeEDTA^{2-}_{sorbed}$ with increasing EDTA concentration that took place at the expense of the aqueous components (Table 3). These results agreed with the Fe(II) speciation observed in Gt reduction experiments in the presence of EDTA (Figure 2), in which there was an increase in the sorbed Fe(II) fraction in relation to nonchelator controls (note that solid-phase Fe(II) determinations do not differentiate what chemical species of Fe(II) is being measured).

Calculations for Fe(II) speciation in the presence of NTA (0.5−5 mM) indicated that $FeNTA^-$ was the predominant Fe(II)−NTA species for NTA concentrations ≤1 mM, whereas both $FeNTA^-$ and $FeNTA_2^{4-}$ were equally abundant at 5 mM NTA levels (Table 3). Increasing concentrations of NTA led to stepwise increases in $Fe(II)NTA_{aq}$ species at the expense of vivianite ($Fe_3(PO_4)_2 \cdot 8H_2O$), Fe(II)−malate complexes, and $Fe(II)_{sorbed}$ (from a total of 0.86 mmol L^{-1} in absence of NTA to 0.13 mmol L^{-1} with 5 mM NTA). Sorption of $FeNTA^-$ species ($FeNTA^-_{sorbed}$) was computed to be very low based on experimental data (Table 3). Consolidated budgets for $Fe(II)_{aq}$ and solid-phase Fe(II) for this exercise showed that $Fe(II)_{aq}$ would increase with increasing NTA concentrations through solubilization of the solid-phase Fe(II) fraction (Table 3). These results were conceptually consistent with experimental observation (Figure 1).

Solid-Phase Fe(II) Sinks. The reduction of goethite by *S. alga* was suppressed when Al_2O_3 particles were in direct contact with Gt and cells (Figure 4 A,B, filled diamonds). Cell adhesion assays showed that the cells adhered much strongly to Gt than to aluminum oxide, but there was measurable cell adhesion to the Al mineral. Overall a 70−75% cells were adhered in tubes with Gt (with or without aluminum oxide) versus around 20% in tubes with aluminum oxide only. When the aluminum oxide was enclosed inside a dialysis bag, which allowed exchange/diffusion of solutes but avoided contact between cells and the Al_2O_3, Gt was reduced more readily than in the absence of the Al mineral (Figure 4, open circles). At the end of the experiment, the alumina inside the dialysis bag had bound up to 12 mmol Fe L^{-1}, which represents 25% of the Fe(III) present initially in the goethite. Overall, the total amount of Fe(III) reduced in this system was approximately 35% of the total, in comparison to 7−10% reduced in absence of the aluminum oxide. A subsequent experiment (Figure 5) confirmed that Gt reduction was promoted by the presence of aluminum oxide due to sorption/binding of Fe(II) onto the Al mineral and the dialysis bag (Figure 5), since some Fe(II) was also bound by the dialysis bag itself.

Kaolinite in direct contact with the cells/goethite decreased Gt reduction (data not shown). When Ka was placed in a dialysis membrane, approximately 15% of the initial Fe(III) content was bound as Fe(II) by Ka at the end of the

TABLE 3. Calculated Fe(II) Speciation (MINTEQA2) in Presence of Different Concentrations of NTA or EDTA[b]

species	0 mM	0.1 mM	0.5 mM	1 mM	5 mM
			NTA		
Fe^{2+}	2.1×10^{-4}	2.0×10^{-4}	1.7×10^{-4}	1.4×10^{-4}	8.1×10^{-6}
$FeHPO_{4aq}$	1.3×10^{-7}	1.3×10^{-7}	1.4×10^{-7}	1.6×10^{-7}	7.2×10^{-8}
FeMalate	2.1×10^{-3}	2.0×10^{-3}	1.7×10^{-3}	1.4×10^{-3}	7.8×10^{-5}
$FeNTA^{1-}{}_{aq}$	0	9.8×10^{-5}	4.8×10^{-4}	9.2×10^{-4}	1.4×10^{-3}
$FeNTA_2^{4-}$	0	2.4×10^{-7}	6.8×10^{-6}	3.2×10^{-5}	1.6×10^{-3}
FeHNTA	0	1.3×10^{-9}	6.4×10^{-9}	1.2×10^{-8}	1.9×10^{-8}
$FeOHNTA^{2-}$	0	1.6×10^{-8}	7.9×10^{-8}	1.5×10^{-7}	2.4×10^{-7}
Fe_{sorbed}[a]	8.6×10^{-4}	8.4×10^{-4}	7.7×10^{-4}	6.8×10^{-4}	1.3×10^{-4}
Vivianite[a]	5.6×10^{-5}	5.5×10^{-5}	5.4×10^{-5}	5.2×10^{-5}	0
$FeNTA^{1-}{}_{sorbed}$[a]	0	4.1×10^{-7}	7.3×10^{-7}	9.3×10^{-7}	1.4×10^{-7}
Fe(II)aq total	2.3×10^{-3}	2.3×10^{-3}	2.4×10^{-3}	2.5×10^{-3}	3.1×10^{-3}
Solid-phase total	9.2×10^{-4}	9.0×10^{-4}	8.2×10^{-4}	7.3×10^{-4}	1.3×10^{-4}
			EDTA		
Fe^{2+}	2.1×10^{-4}	2.0×10^{-4}	1.7×10^{-4}	1.4×10^{-4}	3.5×10^{-11}
$FeHPO_{4aq}$	1.3×10^{-7}	1.3×10^{-7}	1.4×10^{-7}	1.6×10^{-7}	3.1×10^{-13}
FeMalate	2.1×10^{-3}	2.0×10^{-3}	1.7×10^{-3}	1.3×10^{-3}	3.4×10^{-10}
$FeEDTA^{2-}{}_{aq}$	0	3.0×10^{-5}	2.1×10^{-4}	4.7×10^{-4}	1.8×10^{-3}
$FeHEDTA^{-}$	0	7.6×10^{-9}	3.8×10^{-8}	7.6×10^{-8}	2.4×10^{-7}
$FeOHEDTA^{3-}$	0	5.8×10^{-7}	2.9×10^{-6}	5.8×10^{-6}	1.9×10^{-5}
$Fe(OH)_2EDTA^{4-}$	0	3.6×10^{-9}	1.8×10^{-8}	3.7×10^{-8}	1.3×10^{-7}
Fe_{sorbed}[a]	8.6×10^{-4}	8.4×10^{-4}	7.7×10^{-4}	6.7×10^{-4}	1.3×10^{-7}
Vivianite[a]	5.6×10^{-5}	5.6×10^{-5}	5.4×10^{-5}	5.2×10^{-5}	0
$FeEDTA^{-2a}{}_{sorbed}$	0	6.9×10^{-5}	2.9×10^{-4}	5.2×10^{-4}	1.4×10^{-3}
Fe(II)aq total	2.3×10^{-3}	2.2×10^{-3}	2.1×10^{-3}	1.9×10^{-3}	1.8×10^{-3}
Solid-phase total	9.1×10^{-4}	9.6×10^{-4}	1.1×10^{-3}	1.2×10^{-3}	1.4×10^{-3}

[a] Solid-phase Fe(II). [b] The total Fe(II) concentration in the modeled system (3.2×10^{-3} M) was equal to the amount generated during reduction experiments in the nonchelator cultures (see text). Only major species are presented. Concentrations are in units of mol L^{-1}.

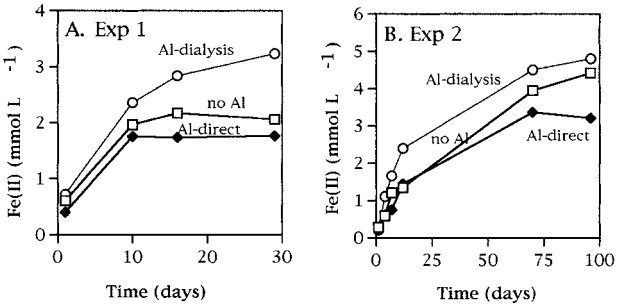


FIGURE 4. Reduction of Gt (50 mmol L^{-1}) by *S. alga* in the presence of Al_2O_3 (1 g L^{-1}) inside a dialysis bag (open circles) or in direct contact with the cells (filled diamonds) in comparison to a non-Al_2O_3 control (no Al, open squares). (A) Initial experiment. (B) Second experiment. Fe(II) concentrations reflect the Fe(II) content of the Gt suspension only (dialysis bag was not analyzed until the final sampling date). Data represent the mean ± standard deviation of triplicate cultures; nonvisible error bars are smaller than the corresponding symbol.

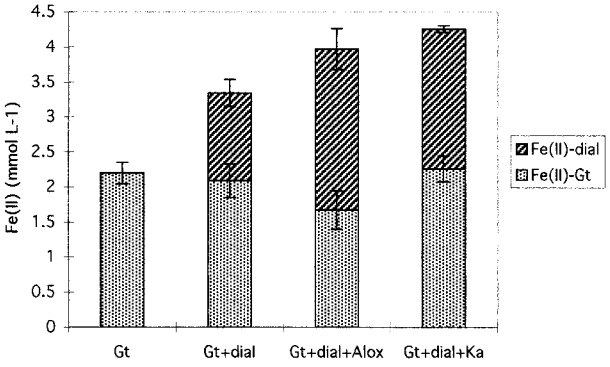


FIGURE 5. Reduction of Gt (50 mmol L^{-1}) by *S. alga* with or without Al_2O_3 (1 g L^{-1}) or kaolinite (2.6 g L^{-1}) within dialysis bags after 30 d incubation. Control cultures containing an empty dialysis bag were included. Fe-Dial: HCl-extractable Fe(II) contained in the dialysis bag and the enclosed solid. Fe-Gt: HCl-extractable Fe(II) from goethite at the end of the experiment. Data represent mean ± standard deviation of triplicate cultures.

experiment (Figures 5 and 6), enhancing Gt reduction by 2-fold.

The presence of K10 or KSF montmorillonites in direct contact with the cells either had no effect or slightly hindered Gt reduction (data not shown). When the montmorillonites were enclosed inside the dialysis bag, the total amounts of Fe(II) determined in the Gt suspension (outside the dialysis bag) were lower than in direct contact experiments. However, the K10 and KSF inside the dialysis bag bound significant quantities of Fe(II) at experiment termination, which led to a dramatic increase in total Fe(II) production (Figure 6).

Discussion

Effect of Synthetic Chelators. Previous studies suggested that NTA stimulated iron(III) oxide reduction in aquifer sediments due to solubilization of Fe(III), since laboratory tests (with ~2−4 mM NTA) demonstrated this chelator's ability to solubilize Fe(III) from amorphous iron oxides (*12*). Our results suggest that chelators can stimulate crystalline iron(III) oxide (goethite) reduction by this same mechanism, although the magnitude of the effect is much reduced due to the lower solubility of goethite. This solubilization effect was demonstrated by the enhanced initial rates of reduction with increasing chelator concentrations (Figures 1 and 2). The solubilization effect was more significant with EDTA (Figure 2) than NTA (Figure 1), because EDTA is a stronger Fe(III) ligand (log $K_{Fe(III)NTA}$= 17.83, log $K_{Fe(III)EDTA}$ = 27.57, (*19*)). EDTA solubilized more Fe(III) in sterile controls, with maximum values of 100 μmol L^{-1} after 1 week for 0.5 and 1 mM EDTA concentrations. Similar levels of goethite dissolution (between 40 and 60 μM Fe(III)) by >1 mM EDTA were reported by Davis and Upadhyaya (*20*).

Our results demonstrate that an even greater impact of chelators on iron(III) oxide reduction results from aqueous Fe(II) complexation. Formation of soluble Fe(II) complexes

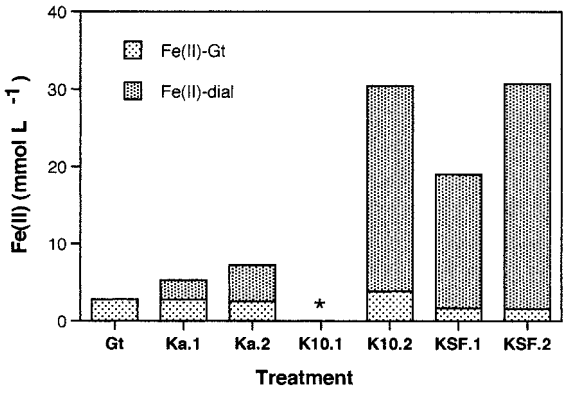


FIGURE 6. Reduction of Gt (50 mmol L^{-1}) by *S. alga* in the presence of layer silicates placed inside dialysis bags after a 30 d incubation. Data for montmorillonites (K10 and KSF) was corrected for (1) soluble Fe(III) released from the clays to the growth medium after autoclaving (see Table 2) and (2) HCl-extractable Fe(II) content of clays.* culture lost. Nomenclature: Ka.1 = 2.6 g clay L^{-1}; Ka.2 = 13 g clay L^{-1}; K10.1 = 3.7 g clay L^{-1}; K10.2 = 18.5 g clay L^{-1}; KSF.1 = 3.7 g clay L^{-1}; KSF.2 = 18.5 g clay L^{-1}.

in NTA amended cultures led to increases in $Fe(II)_{aq}$ concentration in direct proportion to the chelator concentration (Figure 1). These increases in $Fe(II)_{aq}$ were associated with a parallel increase in total Fe(III) reduction. In similar manner, complexation of evolved Fe(II) during iron(III) oxide reduction promoted reduction of goethite in the presence of the much weaker (compare log $K_{Fe(II)malate} = 3.48$ with values in Table 1, Supporting Information) organic chelator malate (*3*). Speciation calculations indicated that aqueous Fe(II)−NTA species formed mainly at the expense of the solid-phase Fe(II) pool (Table 3), particularly at NTA concentrations greater than 1 mM, and that sorption of Fe(II)−NTA species to Gt was insignificant. These calculations suggest that NTA enhanced bacterial reduction of goethite through formation of soluble Fe(II) complexes. The decrease in Fe(II) adsorption to Gt (Figure 3A) when NTA was in greater than equimolar concentration further support this conclusion.

In the case of EDTA, we observed that Fe(II)−EDTA complexes adsorbed to goethite (Figure 3C). Several metal−EDTA complexes are known to sorb to iron(III) oxides with increasing affinity at lower pH (*21*−*23*), including both Fe(III)−EDTA (*7*, *8*, *24*, *25*) and Fe(II)−EDTA (*13*). These later authors observed that $Fe(II)EDTA^{2-}$ complexes, which formed through dissociation of $Co(II)EDTA^{2-}$ in their system, exhibited comparable sorptivity to both the starting and bioreduced goethite mineral.

Sorption of $Fe(II)EDTA^{2-}$ may partly account for the increases in sorbed Fe(II) observed in samples amended with 5 mM EDTA (Figure 2D). Such sorption may also be reponsible for the smaller effect of EDTA, compared to NTA, on Gt reduction despite the higher stability of the Fe(II)-$EDTA^{2-}$ complex (log $K = 15.98$ for $Fe(II)EDTA^{2-}$ vs log $K = 9.85$ for $Fe(II)NTA^{-}$, Table 1, Supporting Information). The Fe(II) speciation calculations that included adsorption of $FeEDTA^{2-}$ to Gt (Table 3), which showed that there was no predicted increase in $Fe(II)_{aq}$ with increasing EDTA concentrations, support this conclusion.

Effect of Complexing Solids. Our initial experiments showed that aluminum oxide in direct contact with FeRB inhibited Gt reduction. Tests indicated that cells adhered to aluminum oxide, although to a lesser extent than to Gt (∼20% adhesion to Al_2O_3 vs 70−75% adhesion to Gt). A 20% reduction of the initial cell concentration added at inoculation (∼5 × 10^8 cells mL^{-1}) would leave an active population of approximately 4 × 10^8 cells mL^{-1}. Previous observations found significant decreases in Fe(III) reduction rates (of both HFO and Gt) with decreasing cell densities, particularly for cell densities lower than 6 × 10^8 cells mL^{-1} (*4*). Hence it is reasonable to expect an apparent decrease in Gt reduction in direct contact experiments due to adhesion of cells onto the accompanying aluminum oxide.

The argument and data above were further corroborated by the enhancement of Gt reduction observed when the aluminum oxide was enclosed in a dialysis bag that prevented adhesion of the cells to the aluminum oxide (Figures 4 and 5). In this case, approximately equal quantities of Fe(II) were found in the Gt suspension and aluminum oxide at completion of the experiment (Figure 5), overall doubling the total amount of Gt reduced in relation to the non-aluminum oxide control. Fe(II) sorption capacities for these minerals (normalized to surface area) are 6.4 μmol Fe(II) m^{-2} for the Gt and 4.4 μmol Fe(II) m^{-2} for the Al_2O_3. After 30 days incubation, around 25% of the total HCl-extractable Fe(II) in the growth medium (8 mM malate, 0.04 mM P) is present as $Fe(II)_{aq}$. Therefore, for the data presented in Figure 5, Gt was approximately 75% saturated with Fe(II) (5.05 μmol Fe(II) m^{-2}), and the aluminum oxide had about 1.5 times more Fe(II) (6.9 μmol Fe(II) m^{-2}) than the measured saturation level (4.4 μmol Fe(II) m^{-2}). These results suggest that the Fe(II) sorption by the aluminum oxide mineral and, possibly, surface precipitation mechanisms serve to partition Fe(II) away from active reduction surfaces on Gt and FeRB cells, thereby promoting the extent of Gt reduction.

The presence of the silicates in direct contact with cells and Gt generally did not enhance Fe(II) production (data not shown). Layer silicates and iron(III) oxides (*27*) or bacterial walls (*28*) have been shown to form aggregates when in contact. Therefore, blockage of surface sites involved in Fe(III) reduction via aggregation may have been responsible for the observed results. When this physical impediment was removed (dialysis bag experiments), the presence of kaolinite (Ka) (Figures 5 and 6) or montmorillonite (K10 and KSF) (Figure 6) greatly promoted the long-term extent of Gt reduction by *S. alga*.

Our results demonstrate that, under appropriate conditions, aluminum oxides and layer silicates enhance bacterial iron(III) oxide reduction by drawing biogenic Fe(II) away from the iron(III) oxide and cell surfaces. The solid-phase complexants compete for Fe(II) and delay surface passivation of the iron(III) oxide and cells. The inhibition of reduction which occurred in the direct contact experiments is not meaningful for natural environments, because established in situ populations of FeRBs would preferentially colonize the surfaces of the iron(III) oxides. In soils and sediments, layer silicates and aluminum/iron oxides are commonly found as discrete phases and, as such, could perpetuate the reduction of iron(III) oxides by the mechanisms mentioned above.

In conclusion, the long term extent of iron(III) oxide reduction may be enhanced by aqueous or solid-phase complexants which prevent Fe(II) sorption to the iron oxide and to the bacterial cells. NTA, aluminum oxide, and layer silicate minerals all enhance bacterial iron(III) oxide reduction. In the case of solid-phase Fe(II) complexants, however, physical effects such as adsorption of the cells to non-iron(III) oxide surfaces and/or aggregate formation hindered the positive effect on Fe(III) reduction. EDTA enhanced the long-term extent of reduction only at very high concentrations, probably as a result of $Fe(II)EDTA^{2-}$ complexes sorption to the iron(III) oxide surface. It is feasible that in an open system in which reaction products are eliminated, EDTA may also enhance the total extent of reduction by a continued solubilization of Fe(III). However, under nonflow conditions, concentrations of EDTA lower than 1 mM will not have a substantial effect on the amount of Fe reduced from crystalline iron(III) oxides by FeRB. In the case of NTA, our

results suggest that even low levels of chelator in an advective flow field could substantially enhance the degree of oxide reduction by complexing evolved Fe(II). Other Fe(II) ligands (natural humic or organic acids) could play a similar role. Collectively these findings emphasize the need for including the fate of biogenic Fe(II) in mechanistic models of the rate/extent of iron(III) oxide reduction in sedimentary environments.

Acknowledgments

We would like to thank Ginger Scott for conducting the laborious cell counts. This research was supported by the Subsurface Science Program, Office of Health and Environmental Research, U.S. Department of Energy (DOE), and by the DOE-EMSP Program through Grant No. DE-FG07-96ER62321. Pacific Northwest National Laboratory is operated for DOE by Battelle Memorial Institute under contract DE-AC06-76RLO 1830.

Supporting Information Available

Tables of equilibrium constants for formation of Fe(II)−chelator complexes used in equilibrium speciation calculations, and HCl-extractable and soluble Fe(II) and Fe(III) from the KSF and K10 montmorillonites before and after autoclaving suspensions in growth medium. This material is available free of charge via the Internet at http://pubs.acs.org.

Literature Cited

(1) Lovley, D. R. *Microbiol. Rev.* **1991**, *55*, 259−287.
(2) Lovley, D. R. *J Ind Microbiol* **1995**, *14*, 85−93.
(3) Urrutia, M. M.; Roden, E. E.; Fredrickson, J. K.; Zachara, J. M. *Geomicrobiol. J.* **1998**, *15*, 269−291.
(4) Roden, E. E.; Zachara, J. M. *Environ. Sci. Technol.* **1996**, *30*, 1618−1628.
(5) Girvin, D. C.; Gassman, P. L.; Bolton, J. H. *Soil Sci. Soc. Am. J.* **1993**, *57*, 47−57.
(6) Jardine, P. M.; Taylor, D. L. *Geoderma* **1995**, *67*, 125−140.
(7) Szecsody, J. E.; Zachara, J. M.; Bruckhart, P. L. *Environ. Sci. Technol.* **1994**, *28*, 1706−1716.
(8) Zachara, J. M.; Smith, S. C.; Kuzel, L. S. *Geochim. Cosmochim. Acta* **1995**, *59*, 4825−4844.
(9) Xue, H.; Sigg, L.; Kari, F. G. *Environ. Sci. Technol.* **1995**, *29*, 59−68.
(10) Bolton, H., Jr.; Li, S. W.; Workman, D. J.; Girvin, D. C. *J. Environ. Qual.* **1993**, *22*, 125−132.
(11) Gonsior, S. J.; Sorci, J. J.; Zoellner, M. J.; Landenberger, B. D. *J. Environ. Qual.* **1997**, *26*, 957−966.
(12) Lovley, D. R.; Woodward, J. C. *Chem. Geol.* **1996**, *132*, 19−24.
(13) Zachara, J. M.; Smith, S. C.; Fredrickson, J. K. *Geochim. Cosmochim. Acta* Submitted for publication.
(14) Rosselló-Mora, R. A.; Caccavo, F., Jr.; Osterlehner, K.; Springer, N.; Spring, S.; Schuler, D.; Ludwig, W.; Amann, R.; Vanncanneyt, M.; Schleifer, K. H. *System. Appl. Microbiol.* **1994**, *17*, 569−573.
(15) Lovley, D. R.; Phillips, E. J. P. *Appl. Environ. Microbiol.* **1988**, *54*, 1472−1480.
(16) Lovley, D. R.; Phillips, E. J. P. *Appl. Environ. Microbiol* **1987**, *53*, 1536−1540.
(17) Allison, J. D.; Brown, D. S.; Novo-Gradac, K. J. U.S. Environmental Protection Agency, Athens, GA, 1991.
(18) Caccavo, F. J.; Schamberger, P. C.; Keiding, K.; Nielsen, P. H. *Appl. Environ. Microbiol.* **1997**, *63*, 3837−3843.
(19) Smith, R. A.; Martell, A. E. *NIST Standard reference database 46;* U.S. Department Commerce: Gaithersburg, MD, 1997.
(20) Davis, A. P.; Upadhyaya, M. *Water Res.* **1996**, *30*, 1894−1904.
(21) Zachara, J. M.; Gassman, P. L.; Smith, S. C.; Taylor, D. *Geochim. Cosmochim. Acta* **1995**, *59*, 4449−4463.
(22) Bowers, A. R.; Huang, C. P. *J. Colloid Interface Sci.* **1986**, *110*, 575−590.
(23) Rueda, E. H.; Grassi, R. L.; Blesa, M. A. *J. Colloid Interface Sci.* **1985**, *106*, 243−246.
(24) Nowack, B.; Sigg, L. *J. Colloid Interface Sci.* **1996**, *177*, 106−121.
(25) Nowack, B.; Lutzenkirchen, J.; Behra, P.; Sigg, L. *Environ. Sci. Technol.* **1996**, *30*, 2397−2405.
(26) Grantham, M. C.; Dove, P. M.; DiChristina, T. J. *Geochim. Cosmochim. Acta* **1997**, *61*, 4467−4477.
(27) Swartz, C. H.; Ulery, A. L.; Gschwend, P. M. *Geochim. Cosmochim. Acta* **1997**, *61*, 707−718.
(28) Walker, S. G.; Flemming, C. A.; Ferris, F. G.; Beveridge, T. J.; Bailey, G. W. *Appl. Environ. Microbiol.* **1989**, *55*, 2976−2984.

Received for review April 21, 1999. Revised manuscript received August 24, 1999. Accepted August 30, 1999.

ES990447B

© 1999 American Chemical Society, Environ. Sci. Technol., Urrutia es990447b Supporting Info Page 1

Table 1. Equilibrium constants for formation of Fe(II)-chelator complexes used in equilibrium speciation calculations (I= 0; 25 °C) (Smith and Martell, 1997).

Species	Log K_a
$FeEDTA^{-2}$	15.98
$FeHEDTA^{-}$	19.11
$FeOHEDTA^{-3}$	6.27
$Fe(OH)_2EDTA^{-4}$	13.64
$FeNTA^{-}$	9.85
FeHNTA	12.00
$FeNTA_2^{-4}$	15.34
$FeOHNTA^{-2}$	-1.18

Supporting Information

Table 2. HCl-extractable and soluble Fe(II) and Fe(III) (μmol g^{-1}) from the KSF and K10 montmorillonites before and after autoclaving 3.7 (KSF.1, K10.1) or 18.5 g L^{-1} (KSF.2, K10.2) suspensions in growth medium (0.04 mM PO_4^{3-}, 8 mM malate, 10 mM Pipes buffer, pH 6.9).

Clay	Fe(II)-HCl	Fe(III)-HCl	FeT-HCl	$Fe(II)_{aq}$	$Fe(III)_{aq}$	FeT_{aq}
Before autoclaving						
KSF.1	11.65	115.38	127.03	0.00	74.79	74.79
KSF.2	7.59	97.29	104.88	0.42	54.52	54.84
K10.1	7.66	33.78	41.45	0.00	8.08	8.08
K10.2	3.01	27.37	30.37	0.00	4.42	4.42
After autoclaving						
KSF.1	19.19	63.13	82.31	4.88	48.47	53.35
KSF.2	16.97	62.49	79.46	5.10	43.11	48.21
K10.1	4.48	22.50	26.98	0.00	4.61	4.61
K10.2	3.29	23.52	26.81	0.00	1.20	1.20

Supporting Information

APPLIED AND ENVIRONMENTAL MICROBIOLOGY, Mar. 2000, p. 1062–1065 Vol. 66, No. 3
0099-2240/00/$04.00+0
Copyright © 2000, American Society for Microbiology. All Rights Reserved.

Bacterial Reductive Dissolution of Crystalline Fe(III) Oxide in Continuous-Flow Column Reactors

ERIC E. RODEN,* MATILDE M. URRUTIA, AND CARROLL J. MANN†

Department of Biological Sciences, The University of Alabama, Tuscaloosa, Alabama 35487-0206.

Received 15 October 1999/Accepted 4 January 2000

Bacterial reductive dissolution of synthetic crystalline Fe(III) oxide-coated sand was studied in continuous-flow column reactors in comparison with parallel batch cultures. The cumulative amount of aqueous Fe(II) exported from the columns over a 6-month incubation period corresponded to (95.0 ± 3.7)% ($n = 3$) of their original Fe(III) content. Wet-chemical analysis revealed that only (6.5 ± 3.2)% of the initial Fe(III) content remained in the columns at the end of the experiment. The near-quantitative removal of Fe was visibly evidenced by extensive bleaching of color from the sand in the columns. In contrast to the column reactors, Fe(II) production quickly reached an asymptote in batch cultures, and only (13.0 ± 2.2)% ($n = 3$) of the Fe(III) oxide content was reduced. Sustained bacterial-cell growth occurred in the column reactors, leading to the production and export of a quantity of cells 100-fold greater than that added during inoculation. Indirect estimates of cell growth, based on the quantity of Fe(III) reduced, suggest that only an approximate doubling of initial cell abundance was likely to have occurred in the batch cultures. Our results indicate that removal of biogenic Fe(II) via aqueous-phase transport in the column reactors decreased the passivating influence of surface-bound Fe(II) on oxide reduction activity, thereby allowing a dramatic increase in the extent of Fe(III) oxide reduction and associated bacterial growth. These findings have important implications for understanding the fate of organic and inorganic contaminants whose geochemical behavior is linked to Fe(III) oxide reduction.

Microbial Fe(III) oxide reduction is a key biogeochemical process in anaerobic sedimentary environments (10, 19). Although crystalline minerals such as goethite and hematite are typically the dominant Fe(III) oxide phases in soils and sediments (23), the apparent resistance of such minerals to enzymatic reduction (14, 16) has led to the view that amorphous Fe(III) oxide is the main form of Fe(III) oxide available for microbial reduction (10). Laboratory studies of bacterial crystalline Fe(III) oxide reduction typically reveal only minor degrees of reduction (14, 16, 21), and crystalline Fe(III) oxides have been shown to persist with depth in aquatic sediments (14, 18). However, extensive reduction of crystalline Fe(III) oxides has recently been observed in aquifer sediments contaminated with landfill leachate (5).

In a recent series of studies (21, 26, 27), we have shown that the low microbial reducibility of crystalline Fe(III) oxides is caused by sorption (adsorption and/or surface precipitation [25] of biogenic Fe(II) on oxide and Fe(III)-reducing bacterial (FeRB) surfaces. This process deactivates enzymatic Fe(III) reduction, possibly through an electrochemical passivation effect analogous to how buildup of Fe(III) oxide surface precipitates inhibits anodic corrosion of iron metal (28). The passivating influence of Fe(II) sorption can be relieved by chemical removal of sorbed Fe(II) from the mineral surface (21), as well as by the presence in culture medium of aqueous and solid-phase Fe(II) complexants which delay or retard the accumulation of surface-bound Fe(II) and thereby extend the degree of crystalline Fe(III) oxide reduction (27). In addition, removal of Fe(II) during aqueous-phase replacement in semicontinuous cultures stimulated crystalline Fe(III) oxide reduction, increasing the extent of oxide reduction two- to threefold relative to that observed in parallel batch cultures over a 2-month period (20). These results suggested the possibility that complete bacterial reductive dissolution of crystalline Fe(III) oxides could occur under conditions of sustained aqueous-phase flux. Such an effect would have important implications for the geochemistry of subsurface environments, in which Fe(III) oxides often constitute major phases for sorption of various organic and metal-radionuclide contaminants (9), as well as the dominant source of aquifer oxidation capacity (6). Complete microbial reduction of crystalline Fe(III) minerals has never been demonstrated experimentally; the observations of Heron and Christensen (5) in contaminated aquifer sediments provide the first indication of the possibility for quantitative removal of crystalline Fe(III) oxides through dissimilatory microbial activity.

In this study, we compared the long-term microbial reductive dissolution of a crystalline Fe(III) oxide in flow-through experimental columns to that occurring in closed-batch reactors. Our findings indicate that removal of biogenic Fe(II) via aqueous-phase transport in the column reactors decreased the passivating influence of surface-bound Fe(II) on oxide reduction activity, thereby allowing for virtually complete reductive dissolution of the oxide over a 6-month period.

MATERIALS AND METHODS

Goethite-coated sand preparation. Synthetic goethite-coated sand was prepared by air oxidation of $FeCl_2 \cdot 2H_2O$ (22) in a suspension of medium quartz sand (Sigma Chemicals). After Fe(II) oxidation was complete, the sand was washed repeatedly with distilled water and freeze-dried. The dried material had a Fe(III) content of 104 ± 8 μmol g^{-1} (0.58% dry weight) ($n = 6$). A sample of the oxide mineral associated with the quartz sand was obtained by vigorously dispersing a 50-g portion of sand in 100 ml of distilled water, followed by lyophilization of the resulting suspension of fine-grained material. The oxide was analyzed by X-ray diffraction. The diffraction peaks obtained matched with

* Corresponding author. Mailing address: The University of Alabama, Department of Biological Sciences, Box 870206, Tuscaloosa, AL 35487-0206. Phone: (205) 348-0556. Fax: (205) 348-1403. E-mail: eroden@biology.as.ua.edu.

† Present address: Southeast Environmental Research Center, Florida International University, Miami, FL 33199.

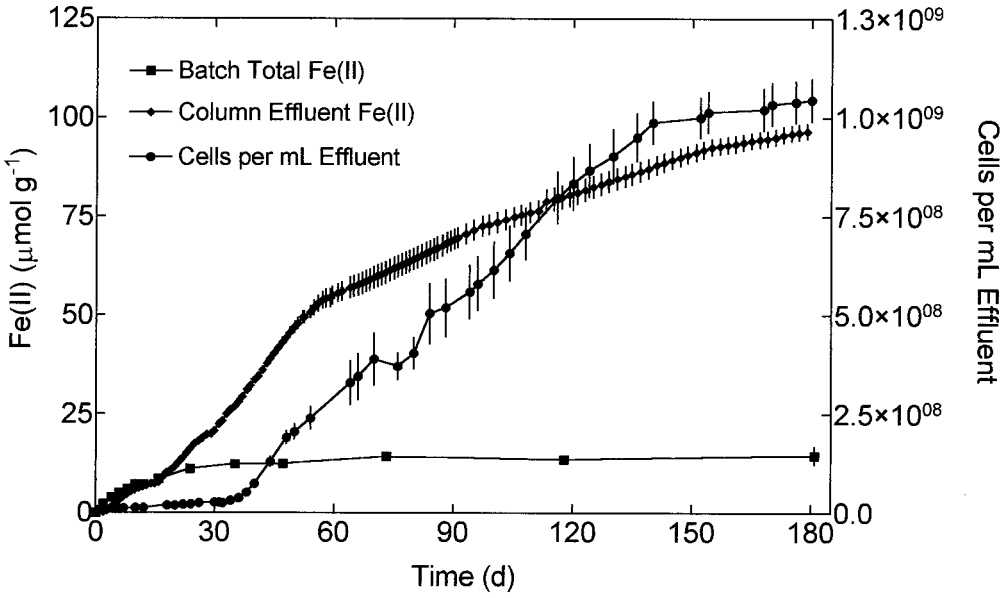


FIG. 1. Microbial reduction of synthetic goethite-coated sand in continuous-flow column reactors and batch cultures. Data for the column reactors (means of triplicate columns; error bars indicate standard deviations) are the cumulative amounts of aqueous Fe(II)- and Fe(III)-reducing bacteria collected in column effluent. Data for batch reactors are the means of duplicate cultures sacrificed for determination of aqueous and solid-phase Fe(II) at each sampling time; error bars indicate range of duplicates.

goethite and showed the broadening expected for the relatively small, high-surface-area particles formed during Fe(II) oxidation (22); no crystalline impurities were detected (data not shown).

Column and batch reactors. The flowthrough column reactors (Omnifit, Ltd.; 1.6 ml, total volume) were wet packed inside an anaerobic chamber with 2.2 g of synthetic goethite-coated sand and ca. 1-ml of culture medium containing ca. 5×10^7 cells ml^{-1} of the groundwater Fe(III)-reducing bacterium *Shewanella putrefaciens* strain CN32 (3). The final water content of the columns was ca. 40% (vol/vol). After an overnight equilibration period, the columns were flushed continuously (6-h residence time) in down-flow mode with a PIPES (piperazine-*N*, *N*′-bis(2-ethanesulfonic acid)-buffered (10 mM, pH 6.8) artificial groundwater medium (1) containing 10 mM sodium lactate as a carbon and energy source together with inorganic nutrients (50 μM KH_2PO_4, 500 μM NH_4Cl) and a mixture of vitamins and trace minerals (15). Effluent from the columns was collected in sterile, stoppered vials vented with a sterile 22-gauge needle to prevent pressure buildup. Direct microscopic counts of cells exported from the columns (see below) showed no evidence of bacterial strains other than *S. putrefaciens*. Parallel batch cultures (5-ml Wheaton serum vials) of similar total volume (2.2 g of goethite-coated sand plus 1.6 ml of culture medium) were established with artificial groundwater containing 30 mM lactate and inoculated with a quantity of FeRB cells comparable to that used in the column reactors.

Goethite-coated sand Fe(II) sorption experiment. Batch reactors containing 2.2 g of goethite-coated sand were amended with 2 ml of PIPES buffer containing ca. 10^9 cells ml^{-1} of *S. putrefaciens* strain CN32. Triplicate reactors were then amended with a 0.1-ml aliquot of $FeCl_2 \cdot 2H_2O$ stock solutions to achieve a range of final Fe(II) concentrations of 0.25 to 24 mmol $liter^{-1}$. The reactors were incubated overnight with gentle shaking, after which the concentration of Fe(II) remaining in solution was determined as described below.

Analytical procedures. Column effluent samples were analyzed for Fe(II) content using Ferrozine (24) and cell numbers by acridine orange direct count (7). Total Fe and Fe(II) concentrations in batch cultures were determined by citrate-dithionite and 0.5 M HCl extraction, respectively (21). The same methods were used to determine the total Fe and solid-phase Fe(II) content of the column reactors at the conclusion of the experiment. Concentrations of Fe(II) remaining in solution at the end of the Fe(II) sorption experiment were determined by Ferrozine analysis after filtering the suspension through a 0.2 μm syringe filter.

RESULTS AND DISCUSSION

A continuous efflux of aqueous Fe(II) from the column reactors occurred during the 6-month incubation period (Fig. 1). The cumulative amount of dissolved Fe(II) exported from the columns corresponded to (95.0 ± 3.7)% ($n = 3$) of their original Fe(III) content, and wet chemical analysis revealed that only (6.5 ± 3.2)% of the initial Fe(III) content remained in the columns at the end of the experiment. The near-quantitative removal of Fe was visibly evidenced by extensive bleaching of color from the sand in the columns. In contrast to these results, Fe(II) production quickly reached an asymptote in batch cultures (Fig. 1), and only (13.0 ± 2.2)% ($n = 3$) of the Fe(III) oxide content was reduced. No reduction of Fe(III) occurred in uninoculated batch cultures (data not shown). Previous work has shown that neither electron donor nor inorganic nutrient limitation are responsible for the minor degree of oxide reduction in closed (batch)-culture systems (20). Hence, the much greater degree of reduction observed in the flowthrough column reactors can be attributed to relief of Fe(II) inhibition of oxide reduction via advective Fe(II) removal.

In addition to its major impact on the degree of oxide reduction, aqueous-phase transport also promoted FeRB growth, as indicated by the sustained export of FeRB cells from the column reactors (Fig.1). The onset of cell export at ca. 15 days was associated with a sharp increase in the rate of Fe(II) output. The number of FeRB cells exported from the column reactors, normalized to reactor volume, was more than 100-fold greater than the initial abundance of cells added to the reactors (ca. 2.5×10^7 ml^{-1}). Although cell counts were not conducted on that batch cultures, the maximum number of cells likely to have been produced in them can be estimated from published information on the number of FeRB cells generated during Fe(III) oxide reduction. An analysis of several studies of FeRB growth coupled to Fe(III) oxide reduction revealed a maximum value of 6.4×10^6 cells produced per μmol of Fe(II) (21). This value is close to the cumulative number of cells exported from the column reactors divided by the cumulative amount of Fe(II) exported from the reactors (4.5×10^6 cells/μmol of Fe). Multiplying the volume-normalized amount of Fe(III) reduced in the batch reactors by the factor 6.4×10^6 yields a value of 7.3×10^7 cells ml^{-1}. This calculation suggests that cell growth in the batch reactors was

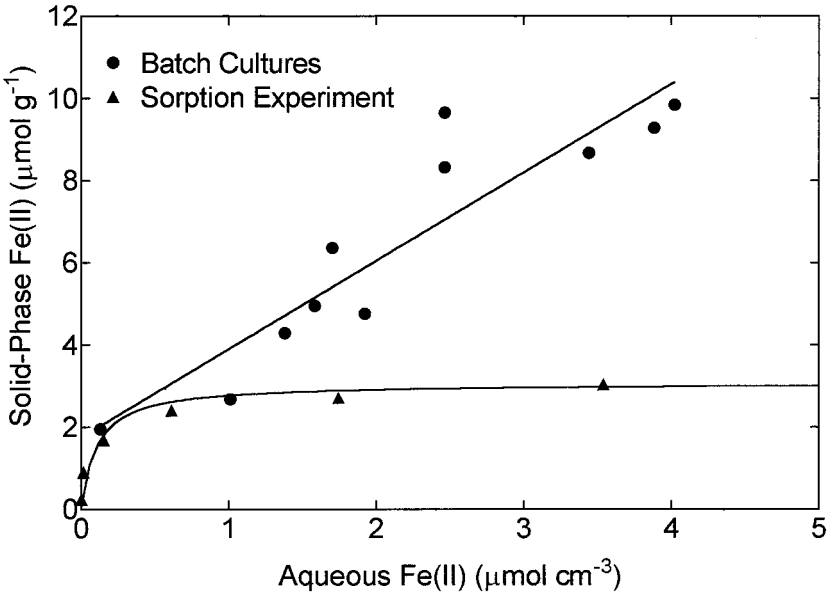


FIG. 2. Accumulation of solid-phase versus aqueous Fe(II) during synthetic goethite-coated sand reduction in the batch cultures, compared with solid- versus aqueous-phase Fe(II) partitioning during Fe(II) sorption experiments with the same goethite-coated sand. Data represent the means of duplicate (batch reactors) or triplicate (sorption experiment) samples. Solid lines represent curve fits of the batch culture and sorption experiment data to linear (r^2 = 0.84) and Langmuir (r^2 = 0.84) isotherms (25), respectively.

likely to have produced only an approximate doubling of the initial cell abundance, far less than the 100-fold increase which took place in the column reactors. The observed promotion of FeRB cell growth in the column reactors agrees with the recent finding that Fe(II) removal during medium replacement enhanced protein production by *Shewanella alga* (strain BrY) in semicontinuous culture systems (20).

The accumulation of solid-phase versus aqueous Fe(II) in the batch cultures was compared with independent data on Fe(II) sorption to a mixture of goethite-coated sand plus FeRB cells in order to assess the fate of Fe(II) in the batch system, an important consideration in relation to the mechanism of Fe(II) inhibition of oxide reduction (Fig. 2). Total solid-phase Fe(II) accumulation in the batch cultures far exceeded the measured Fe(II) sorption capacity of the mixed system, in agreement with previous experiments on synthetic goethite reduction (26). These findings suggest that bulk-phase mineral precipitation and/or surface Fe(II) precipitation were important sinks for Fe(II) in the batch cultures. Since the culture medium contained relatively low concentrations of phosphate (50 μM), vivianite [$Fe_2(PO_4)_3$] could not have been a major solid Fe(II) phase generated in these cultures. Hence, a combination of siderite ($FeCO_3$, formed with inorganic carbon generated during lactate oxidation) together with $Fe(OH)_2$ and/or mixed Fe(II)-Fe(III) phases (green rust, magnetite, or other spinel-like compounds [3]) were likely the main solid-phase end products of Fe(III) oxide reduction. Formation of such precipitates on or very near to oxide and FeRB cell surfaces can be viewed as a type of reductive corrosion which eventually impedes electron transfer from the cells to the oxide surface. When a small portion of the 6-month-old batch cultures was inoculated into fresh synthetic goethite-containing medium at the conclusion of the experiments, Fe(III) reduction activity resumed (data not shown), which suggests that the loss of reduction activity in the batch cultures could not be attributed to the death of the FeRB populations. Recent studies indicate that the simple presence of high concentrations of aqueous Fe(II) does not inhibit Fe(III) reductase activity of FeRB (unpublished data). These data support the idea that it is the formation of solid Fe(II) phases in the zone of FeRB-oxide contact that stops the reduction process.

If the observed relationship between solid and aqueous Fe(II) accumulation in the batch cultures (Fig. 2) is interpreted as a simple linear sorption isotherm (where sorption indicates both adsorption and surface Fe(II) precipitation reactions), then it is possible to view advective aqueous-phase flux as a mechanism which moves the reaction system down the sorption isotherm, thereby holding the abundance of surface-bound Fe(II) at a level low enough for oxide reduction to remain favorable. This conceptual model provides a mechanistic explanation for how near-complete reductive dissolution of crystalline Fe(III) oxide phases could be achieved in the landfill leachate-contaminated aquifer investigated by Heron and Christensen (5). Sustained aqueous-phase transport, together with the potentially accelerating influence of Fe(II)-complexing agents (27) in the leachate, is likely to have maintained a pool of microbially reducible Fe(III) which was eventually exhausted during the oxidation of organic carbon compounds in the leachate.

Bacterial cell growth is recognized as an important parameter which regulates the advective transport of bacteria in saturated porous medium (4, 17). Particularly relevant in this regard is the process in which an attached cell gives rise to a mobile daughter cell that is free to migrate some distance before becoming attached (8). Our results indicate that advective Fe(II) removal during aqueous-phase flow promoted FeRB growth (see above), which in turn led to major cell export from the column. This effect suggests a previously unrecognized mechanism whereby water flow could enhance FeRB movement in the subsurface beyond its obvious role in advective transport.

In summary, our findings document an interaction between aqueous phase transport and surface chemical reactions at the bacterium-mineral interface which has fundamental implica-

tions for control of the rate and extent of Fe(III) oxide reduction, as well as FeRB growth and transport, in subsurface sediments. Simulation model results (20) suggest that short-term laboratory experiments such as those presented here may provide a reasonable indication of how Fe(III) oxide reduction could respond to advective Fe(II) removal over much greater periods of time in natural aquifer environments, which typically have much longer residence times and slower rates of metabolic activity than those in our experimental reactors. Consideration of the impact of aqueous phase flux on FeRB metabolism will be important for predicting the influence of metal-reducing bacteria on the fate and transport of metal and radionuclide contaminants in the subsurface. Immediate examples include the efficacy with which the FeRB may serve as agents for liberation of sorbed or coprecipitated contaminant metals through reductive dissolution processes designed to complement pump-and-treat restoration (2), for reductive immobilization and/or retardation of redox-sensitive metals and radionuclides such as Cr(IV), ^{60}Co(III), and ^{238}U(IV) (11), or for hydrocarbon degradation in petroleum-contaminated aquifers (12, 13). In all cases, the coupling between stimulation of oxide reduction activity through advective Fe(II) removal and cell growth-promoted bacterial transport is likely to figure prominently in considerations of the spatial and temporal scales on which subsurface bioremediation strategies involving metal-reducing bacteria may be effectively implemented.

ACKNOWLEDGMENTS

This research was funded by the U.S. Department of Energy, Office of Energy Research, Environmental Management Science Program.

We thank D.C. Cooper for the XRD analysis and D.R. Lovley for review of a previous version of the manuscript.

REFERENCES

1. **DeFlaun, M. F., S. R. Oppenheimer, S. Streger, C. W. Condee, and M. Fletcher.** 1999. Alterations in adhesion, transport, and membrane characteristics in an adhesion-deficient pseudomonad. Appl. Environ. Microbiol. **65:**759–765.
2. **Deutsch, W. J.** 1997. Groundwater geochemistry: fundamentals and applications to contamination. Lewis, Boca Raton, Fla.
3. **Fredrickson, J. K., J. M. Zachara, D. W. Kennedy, H. Dong, T. C. Onstott, N. W. Hinman, and S. Li.** 1999. Biogenetic iron mineralization accompanying the dissimilatory reduction of hydrous ferric oxide by a groundwater bacterium. Geochim. Cosmochim. Acta **62:**3239–3257.
4. **Harvey, R. W.** 1991. Parameters involved in modeling movement of bacteria in groundwater, p. 89–114. *In* C. J. Hurst (ed.), Modeling the environmental fate of microorganisms. American Society for Microbiology, Washington, D.C.
5. **Heron, G., and T. H. Christensen.** 1995. Impact of sediment-bound iron on redox buffering in a landfill leachate polluted aquifer (Vejen, Denmark). Environ. Sci. Technol. **29:**187–192.
6. **Heron, G., T. H. Christensen, and J. C. Tjell.** 1994. Oxidation capacity of aquifer sediments. Environ. Sci. Technol. **28:**153–158.
7. **Hobbie, J. E., R. J. Daley, and S. Jasper.** 1977. Use of Nuclepore filters for counting bacteria by fluorescence microscopy. Appl. Environ. Microbiol. **33:**1225–1228.
8. **Kjelleberg, S., B. A. Humphrey, and K. C. Marshall.** 1982. Effect of interfaces on small, starved marine bacteria. Appl. Environ. Microbiol. **43:**1166–1172.
9. **Langmuir, D.** 1997. Aqueous environmental geochemistry. Prentice Hall, Upper Saddle River, N.J.
10. **Lovley, D. R.** 1991. Dissimilatory Fe(III) and Mn(IV) reduction. Microbiol. Rev. **55:**259–287.
11. **Lovley, D. R.** 1995. Microbial reduction of iron, manganese, and other metals, p. 175–231. *In* D. L. Sparks (ed.), Advances in agronomy, vol. 54. Academic Press, San Diego, Calif.
12. **Lovley, D. R.** 1997. Potential for anaerobic bioremediation of BTEX in petroleum-contaminated aquifers. J. Ind. Microbiol. Biotechnol. **18:**75–81.
13. **Lovley, D. R., M. J. Baedecker, D. J. Lonergan, I. M. Cozzarelli, E. J. P. Phillips, and D. I. Siegel.** 1989. Oxidation of aromatic contaminants coupled to microbial iron reduction. Nature **339:**297–299.
14. **Lovley, D. R., and E. J. P. Phillips.** 1986. Availability of ferric iron for microbial reduction in bottom sediments of the freshwater tidal Potomac River. Appl. Environ. Microbiol. **52:**751–757.
15. **Lovley, D. R., and E. J. P. Phillips.** 1988. Novel mode of microbial energy metabolism: organic carbon oxidation coupled to dissimilatory reduction of iron or manganese. Appl. Environ. Microbiol. **54:**1472–1480.
16. **Lovley, D. R., and E. J. P. Phillips.** 1987. Rapid assay for microbially reducible ferric iron in aquatic sediments. Appl. Environ. Microbiol. **53:**1536–1540.
17. **McInerney, M. J.** 1991. Use of models to predict bacterial penetration and movement within a subsurface matrix, p. 115–135. *In* C. J. Hurst (ed.), Modeling the environmental fate of microorganisms. American Society for Microbiology, Washington, D.C.
18. **Phillips, E. J. P., D. R. Lovley, and E. E. Roden.** 1993. Composition of nonmicrobially reducible Fe(III) in aquatic sediments. Appl. Environ. Microbiol. **59:**2727–2729.
19. **Ponnamperuma, F. N.** 1972. The chemistry of submerged soils. Adv. Agron. **24:**29–96.
20. **Roden, E. E., and M. M. Urrutia.** 1999. Ferrous iron removal promotes microbial reduction of crystalline iron (III) oxides. Environ. Sci. Technol. **33:**1847–1853.
21. **Roden, E. E., and J. M. Zachara.** 1996. Microbial reduction of crystalline Fe(III) oxides: role of oxide surface area and potential for cell growth. Environ. Sci. Technol. **30:**1618–1628.
22. **Schwertmann, U., and R. M. Cornell.** 1991. Iron oxxides in the laboratory. Weinheim, New York, N.Y.
23. **Schwertmann, U., and R. M. Taylor.** 1989. Iron oxides, p. 379–437. *In* Minerals in soil environments. Soil Science Society of America, Madison, Wis.
24. **Stookey, L. L.** 1970. Ferrozine—a new spectrophotometric reagent for iron. Anal. Chem. **42:**779–781.
25. **Stumm, W.** 1992. Chemistry of the solid-water interface. John Wiley & Sons, New York, N.Y.
26. **Urrutia, M. M., E. E. Roden, J. K. Fredrickson, and J. M. Zachara.** 1998. Microbial and geochemical controls on synthetic Fe(III) oxide reduction by *Schewanella alga* strain BrY. Geomicrobiol. J. **15:**269–291.
27. **Urrutia, M. M., E. E. Roden, and J. M. Zachara.** 1999. Influence of aqueous and solid-phase Fe(II) complexants on microbial reduction of crystalline Fe(III) oxides. Environ. Sci. Technol. **33:**4022–4028.
28. **West, J. M.** 1986. Basic corrosion and oxidation. Halsted Press, New York, N.Y.

APPLIED AND ENVIRONMENTAL MICROBIOLOGY, Mar. 2001, p. 1328–1334 Vol. 67, No. 3
0099-2240/01/$04.00+0 DOI: 10.1128/AEM.67.3.1328–1334.2001
Copyright © 2001, American Society for Microbiology. All Rights Reserved.

Suboxic Deposition of Ferric Iron by Bacteria in Opposing Gradients of Fe(II) and Oxygen at Circumneutral pH

DMITRI SOBOLEV AND ERIC E. RODEN*

Department of Biological Sciences, The University of Alabama, Tuscaloosa, Alabama

Received 10 August 2000/Accepted 11 December 2000

The influence of lithotrophic Fe(II)-oxidizing bacteria on patterns of ferric oxide deposition in opposing gradients of Fe(II) and O_2 was examined at submillimeter resolution by use of an O_2 microelectrode and diffusion microprobes for iron. In cultures inoculated with lithotrophic Fe(II)-oxidizing bacteria, the majority of Fe(III) deposition occurred below the depth of O_2 penetration. In contrast, Fe(III) deposition in abiotic control cultures occurred entirely within the aerobic zone. The diffusion microprobes revealed the formation of soluble or colloidal Fe(III) compounds during biological Fe(II) oxidation. The presence of mobile Fe(III) in diffusion probes from live cultures was verified by washing the probes in anoxic water, which removed ca. 70% of the Fe(III) content of probes from live cultures but did not alter the Fe(III) content of probes from abiotic controls. Measurements of the amount of Fe(III) oxide deposited in the medium versus the probes indicated that ca. 90% of the Fe(III) deposited in live cultures was formed biologically. Our findings show that bacterial Fe(II) oxidation is likely to generate reactive Fe(III) compounds that can be immediately available for use as electron acceptors for anaerobic respiration and that biological Fe(II) oxidation may thereby promote rapid microscale Fe redox cycling at aerobic-anaerobic interfaces.

Neutrophilic bacteria associated with Fe(III) oxide precipitation have been known for a long time (26). Some species were shown to precipitate Fe(III) oxides during heterotrophic metabolism (6, 7). However, neutrophilic autotrophic iron oxidation has only recently been reliably demonstrated (8, 10). The role of these bacteria in biogeochemical iron cycling, however, has not been extensively studied. Such lack of study can be attributed to the fact that Fe(II) is highly unstable in oxic environments at circumneutral pH, resulting in the widely held belief that Fe(II) will be rapidly oxidized regardless of the presence or absence of microbial catalysis (24). Furthermore, Emerson and Moyer (8) have convincingly demonstrated that Fe(II)-oxidizing bacteria do not alter the rate of Fe(III) oxide accumulation in diffusion-limited opposing-gradient systems.

Regardless of the possible influence of Fe(II)-oxidizing bacteria on rates of Fe(II) oxidation, these organisms have the potential to affect Fe(III) oxide precipitation processes by altering the spatial relationship between O_2 and Fe(II) gradients. Emerson and Moyer (8) suggested that bacterial Fe(II) oxidation might promote coupling between iron oxidation and reduction by producing amorphous (9) or poorly crystalline Fe(III) oxides which are readily available for Fe(III)-reducing bacteria. The potential for a tight, microbially mediated coupling between iron oxidation and reduction has important environmental implications, given the critical influence which iron cycling exerts on the behavior of various organic and inorganic compounds in aquatic systems (24).

In this study we examined O_2 and Fe(II) gradients together with bacterial numbers and patterns of Fe(III) oxide deposition at submillimeter resolution in Fe(II)-oxidizing gradient cultures, using organisms enriched from iron-rich freshwater wetland sediments. The goal was to determine the positioning of Fe(II)-oxidizing bacteria with respect to Fe(II) and O_2 gradients and to examine how these organisms influence patterns of Fe(III) oxide deposition within these gradients.

MATERIALS AND METHODS

Enrichment and isolation. A neutrophilic Fe(II)-oxidizing enrichment culture (TW1) was obtained from iron-rich surficial sediments of a freshwater wetland in the Talladega National Forest in north central Alabama by use of gradient cultures (15) with FeS as an Fe(II) source. After several passages on FeS (low iron) medium, the culture was transferred to medium with 50 mM PIPES [piperazine-*N*,*N*′-bis(2-ethenesulfonic acid)]-buffered $FeCl_2 \cdot 2H_2O$ as an iron source (high iron), the same medium used in the experiments reported here. The culture was shown to contain heterotrophic satellite bacteria capable of growth on rich medium (50% strength tryptic soy agar [TSA]). PCR-denaturing gradient gel electrophoresis (DGGE) analysis of ca. 200-bp 16S rRNA gene fragments was performed as described elsewhere (18) and revealed two strains, one presumably the lithotrophic Fe(II) oxidizer, and the other presumably a heterotrophic satellite. However, as described below, we found no evidence that the latter organism had a major impact on the results of our Fe(II) oxidation experiments. Another, apparently pure culture (TW2) used in this study was enriched and isolated by repeated passages on high-iron medium. This culture failed to grow on rich medium, and DGGE analysis revealed only a single genome. A BLAST search (2) on a 1,485-bp fragment of the 16S rRNA gene sequenced suggested that our organism is closely related (94% similarity) to *Dechlorisoma suilla*, a dissimilatory perchlorate-reducing bacterium (1, 4). Further molecular and physiological characterization of TW2 is under way.

Gradient cultures. The gradient culture system consisted of two layers in 250-ml beakers: a bottom layer containing the Fe(II) source (50 mM $FeCl_2$ in anaerobic 10 mM PIPES buffer with 2% [wt/vol] Noble agar [pH 7.0]), and a top layer consisting of mineral medium ($NaHCO_3$, 30 mM; NH_4Cl, 10 mM; KH_2PO_4, 1 mM) supplemented with vitamins and minerals (17) and stabilized with 0.25% Noble agar. Layer volumes were 25 ml (bottom) and 125 ml (top), resulting in layer depths of 12 and 60 mm, respectively. This concentration of Fe(II) was necessary to sustain Fe(II) flux over the course of the experiment. Although the Fe(II) concentration in the bottom layer was unrealistically high relative to natural systems, diffusion within the agar column resulted in environmentally relevant Fe(II) concentrations of 1 to 2 mM (22) close to the oxic-anoxic boundary. Prior to initiation of the experiment, beakers were covered with aluminum foil and autoclaved. The foil cover was kept on all the time except when components were added. After the bottom layer was poured, probes for Fe(II) and bacterial numbers (see below) were inserted, and the agar was al-

* Corresponding author. Mailing address: Department of Biological Sciences, University of Alabama, Tuscaloosa, AL 35487-0206. Phone: (205) 348-0556. Fax: (205) 348-1403. E-mail: eroden@bsc.as.ua.edu.

lowed to solidify under an anaerobic atmosphere (about an hour under approximately 95:5 [vol/vol] N_2-H_2). The top layer, which had been degassed with 80:20 (vol/vol) N_2-CO_2, autoclaved in crimp-sealed bottles, and cooled to approximately 30°C, was then added to the system. The beakers were incubated overnight in an anaerobic chamber in order to allow a supply of Fe(II) to diffuse into the top layer prior to inoculation. Inoculation was achieved by inserting a pipette into the top layer and ejecting about 0.1 ml of the microaerobic inoculum (surface layer of a high-iron culture of TW1 or TW2) as the pipette was withdrawn; this procedure was repeated four to six times per culture. Although this procedure could have enhanced O_2 penetration into the surface layer, our "time zero" O_2 measurements revealed no difference between O_2 profiles in inoculated and uninoculated cultures. Additionally, in later experiments with TW2, possible O_2 introduction was controlled for by stabbing uninoculated controls with a sterile pipette in the manner similar to the inoculation procedure.

Fe(II) measurements. We employed a diffusion microprobe technique modified from that of Davison et al. (5) to determine Fe(II) concentrations at submillimeter resolution in the gradient cultures. The probe consisted of a 0.1-mm-thick 5% (vol/vol) agar film attached to a glass microscope slide. The film was cast between hot (ca. 70°C) glass slides autoclaved in an aluminum foil boat, and the agar was allowed to solidify. Excess agar was trimmed from the sides of the slides, and the slides were separated, leaving the film attached to one slide. The probe was inserted into the culture beaker with the agar film facing the center. All of the above procedures were accomplished under aseptic conditions. Probes were retrieved immediately after the final O_2 measurements (see below), dipped into 1% (wt/vol) potassium ferricyanide [$K_3Fe(CN)_6$] solution [which forms an insoluble blue complex with Fe(II)] for about 1 s, retrieved, and allowed to react for ca. 3 min after being removed from the solution. This fixed the Fe(II) within the agar film and provided a colored substance whose abundance could be quantified. Probes were then soaked in distilled water for ca. 5 min to remove excess potassium ferricyanide. Images of the probes were collected under a dissecting microscope with an attached camera. The images were then digitized and converted to black and white by use of Adobe PhotoShop. The optical density of the images, presumably representing the density of $Fe_3[Fe(CN)_6]_2$, was measured by the NIH-Image software. For TW1 cultures and controls, three depth profiles from a single probe were collected and measured. For TW2, a single profile was recorded for each of the probes from triplicate cultures. Fe(II) concentrations in the probes were quantified against a calibration curve obtained by measuring the optical density of the agar strips of the same thickness incubated overnight in anoxic Fe(II)-EDTA solutions of known concentration. This yielded linear standard curves with an R^2 of 0.8 or greater within the range from 1 to 25 mM Fe(II).

In order to validate the diffusion probe technique, culture systems were cored with a detipped 1-ml plastic syringe immediately after O_2 measurements but before probe retrieval. The core was sectioned anoxically, and Fe(II) in several depth intervals was extracted with 0.5 M HCl and measured by the Ferrozine (23) method. To ensure complete extraction of Fe(II) from the agar, tightly closed vials containing 0.5 M HCl and sample were gently heated in a waterbath (ca. 80°C) until the agar dissolved.

To determine the abundance of Fe(III) in probes from control and live culture systems, high-iron cultures were set up as described above and incubated for 6 days at 20°C. Core samples of the medium which included the whole depth of the top layer were taken anaerobically and immediately placed into preweighed vials containing 0.5 M HCl. Probes were retrieved immediately after taking the core, and the agar film (exposed to the medium) was scraped off into preweighed vials containing 0.5 M HCl. The portion of the film exposed to the atmosphere above the medium dried out and was firmly attached to the slide, allowing collection of only the portion submerged in the medium. Acid extracts were analyzed using Ferrozine for Fe(II) and total Fe, from which Fe(III) content was calculated.

To estimate what percentage of the Fe(III) trapped in the probes comprised mobile (soluble and/or colloidal) compounds, triplicate sets of probes were retrieved from live and abiotic control cultures and washed three times in 100 ml of anoxic distilled water, transferring the probes each time into a fresh beaker of water. Results were compared to the Fe(III) content of triplicate unwashed probes retrieved from parallel cultures. The difference was assumed to represent the diffusionally mobile Fe(III) content.

Oxygen microelectrode measurements. A Clark-style O_2 microelectrode with guard cathode (21) (Diamond General Corp, Ann Arbor, Mich.), attached to an electronically controlled micromanipulator (National Aperture model MM33CR), was used to determine O_2 profiles in the gradient cultures. The microelectrode was calibrated to indicate percent air saturation of O_2, with a detection limit of approximately 0.1% saturation, which, under our conditions, was equivalent to 0.279 μM. Zero depth was set by manually lowering the electrode to the agar surface and identifying the moment of contact by the formation of a visible meniscus around the electrode tip. The electrode was raised until the tip separated from the surface and the meniscus disappeared, and slowly lowered until the meniscus formed again. At this point, the manipulator counter was set at zero. Oxygen was considered depleted when three consecutive measurements (covering a distance of 50 to 200 μm) below the detection limit (ca. 0.28 μM) were obtained.

In one experiment, O_2 microprofiles were measured repeatedly over a 7-day course. In this case, uninoculated culture systems were measured first to minimize contamination. Between sampling, the electrode was allowed to stand in distilled water. The electrode was occasionally soaked in dilute HCl to remove oxide precipitates.

In some experiments, pH gradients were measured using a microcombination pH electrode (Orion) according to the manufacturer's instructions. Since this electrode has a relatively large tip (ca. 1 mm diameter), pH was measured at 1-mm intervals.

Bacterial numbers. The Rossi-Cholodny buried slide technique (20) was employed to enumerate bacteria (in units of cells per unit area of slide) at submillimeter resolution in our cultures. This technique is based on colonization of glass slides inserted into stratified bacterial communities. After colonization, slides are retrieved, fixed, and stained, and the bacteria attached to them are enumerated. Although this technique enumerates only those bacteria which attach to the slide, it provides a better depth resolution (0.2 mm or better) than coring and slicing the culture (1 to 2.5 mm). A basic assumption of our application of this technique is that an equal percentage of bacteria attach to the slides at each depth, which is not unreasonable for a pure culture. Slides were inserted into the culture systems for the duration of the experiment, and bacterial growth was allowed to occur. Slides were then removed, fixed with 4% formaldehyde solution, and stained with acridine orange, and bacteria were counted under an epifluorescent microscope. Five fields were counted at each of the depth intervals spaced at 0.2 mm or greater. These area counts were used as a proxy for actual number of bacteria per unit volume.

RESULTS

Oxygen and Fe(III) oxide distributions. Oxygen gradients were much steeper in culture systems inoculated with Fe(II)-oxidizing bacteria than in sterile controls (Fig. 1). After 5 days of incubation, O_2 penetrated to 12 mm in the controls, versus 1.5 mm in the TW1 culture (average of three separate profiles in a single system for both control and live cultures). A distinct bacterial plate formed at the oxic-anoxic interface in the live cultures, whereas in the control system only low bacterial numbers (>10-fold lower) were detected, and only at the surface (Fig. 1A and B). A similar experiment conducted with the presumably pure TW2 culture produced nearly identical results (Fig. 1C and D).

Fe(III) oxides were deposited below the O_2 penetration zone in the bacterial cultures as opposed to the controls, in which the entire zone of oxide deposition was aerobic (Fig. 1).

Control experiments. Since TW1 was not pure, control experiments in iron-free cultures were conducted to account for possible heterotrophic growth of the satellite organisms on impurities in the agar, because such growth could influence O_2 gradients and thus confound interpretation of the oxide band data. TW1 formed a visible bacterial plate when inoculated into Fe-free gradient cultures and changed O_2 profiles compared to uninoculated controls (data not shown). However, this was not the case for TW2, which failed to grow or alter the O_2 profile in an identical Fe(II)-free system (data not shown).

The possible effect of the growth of heterotrophic bacteria in TW1 on the O_2/Fe(II) relationship in our experimental systems was tested by inoculating a culture of satellite organisms isolated and grown on 50% strength TSA into Fe(II)-containing gradient systems. After 10 days of incubation, no significant differences between O_2 profiles in inoculated and uninoculated control were detected (data not shown). These results suggest

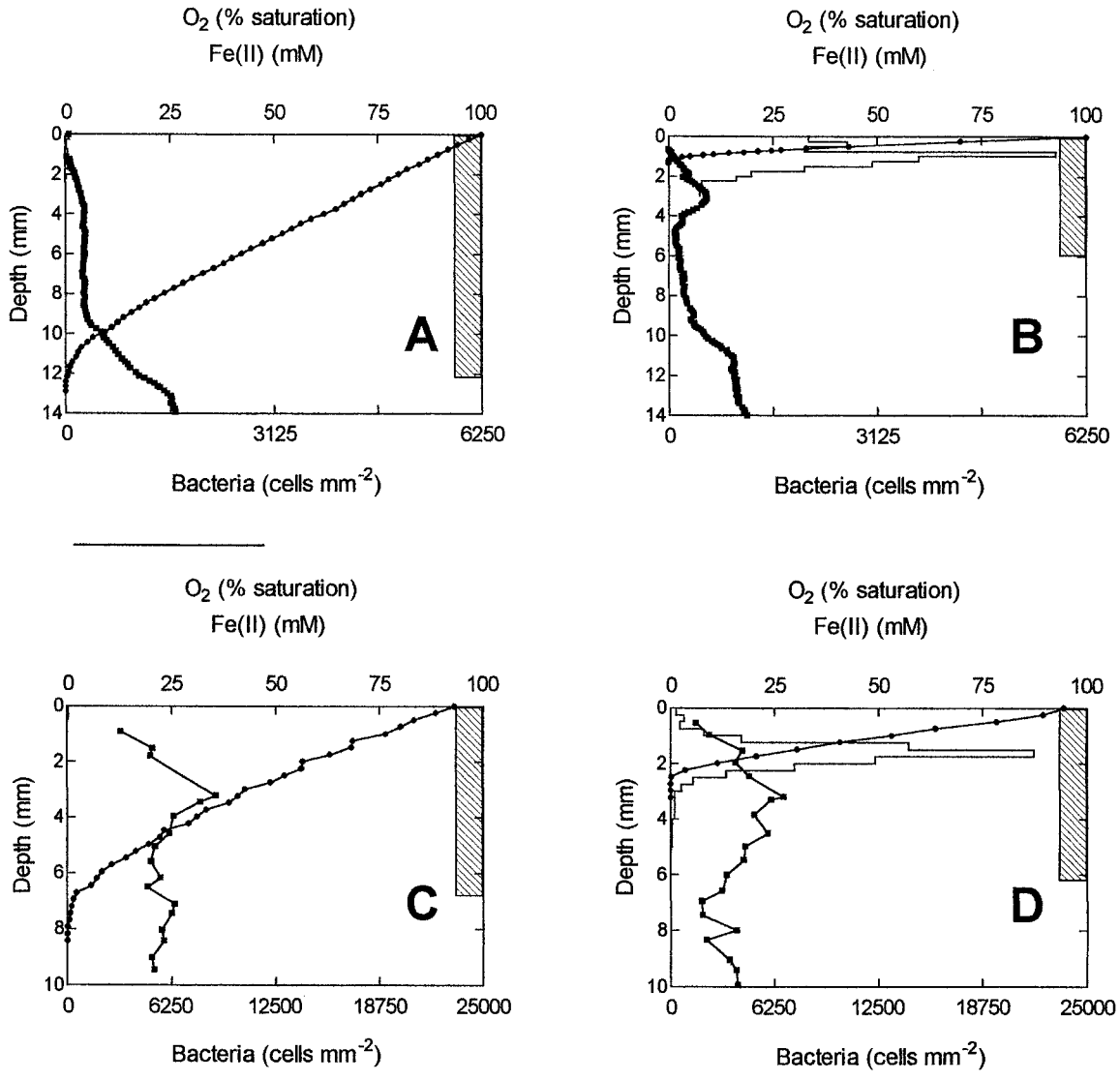


FIG. 1. Distribution of Fe(II), particulate Fe(III) oxides, O_2, and bacteria in two Fe(II)-oxidizing cultures. (B and D) TW1 and TW2 cultures, respectively. (A and C) Abiotic controls for the cultures shown in B and D, respectively. Note that Fe(II) profiles determined by densitometry in diffusion probes are confounded by the presence of Fe(III) compounds in the probe (see text). O_2 profiles are averages of triplicate measurements. (A and B) Representative Fe(II) profile from triplicate profiles obtained from a single probe. (C and D) Fe(II) profiles are averages of single measurements from probes in triplicate cultures. No error bars are shown. Bacterial numbers in A and B are averages of counts on triplicate slides from a single culture (A and B) or averages of counts from a single slide from each of triplicate cultures (C and D); error bars were omitted for clarity. In control cultures, bacterial numbers were never significantly different from zero.

that the effect of the heterotrophic bacteria on Fe(II) oxidation, independent of their possible synergistic interaction with Fe(II)-oxidizing bacteria, was minor.

We were concerned that deposition of oxide below the depth of O_2 penetration in the TW1 and TW2 cultures was an artifact caused by the existence of a deeper oxic-anoxic boundary early in the experiment. To test this possibility, measurements of O_2 and Fe(III) oxide band positions were obtained at daily intervals over 6 days in cultures inoculated with TW1. In the abiotic control systems, the bottom boundary of the oxide band was always observed above the oxic-anoxic boundary. This is illustrated in Fig. 2; where the depth of the oxide band lower boundary and the depth of O_2 penetration are plotted versus time; O_2 always penetrated to depths below the lower boundary of the oxide band (Fig 2A) in the controls. In contrast, in the TW1-inoculated cultures, the depth of O_2 penetration (as defined above) was above the bottom boundary of the oxide band at all times except for the first two measurements (Fig. 2B). In addition, the depth of O_2 penetration increased steadily during the experiment, which argues against the possibility that the oxides were deposited in association with an upward-retreating O_2 front.

Iron distributions. Fe(II) measurements obtained from the diffusion microprobes agreed well with Ferrozine analysis at depth in the cultures (Fig. 3). However, near the surface, the probes indicated Fe(II) concentrations several times higher than found by the Ferrozine analyses. This effect was likely due to (i) the presence of heavy oxide deposits in the probe from

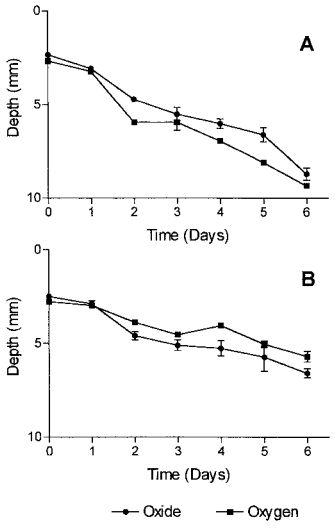


FIG. 2. Relationship between O_2 penetration depth and the base of the oxide band in control and TW1-inoculated cultures. Data represent averages of triplicate cultures, and error bars show 95% confidence intervals.

the control culture and to (ii) the presence of a dark green band in the probe from the live TW1 and TW2 cultures (Fig. 4). In both cases, the dark bands were detected by densitometric analysis of the images of the probes, leading to erroneously high Fe(II) concentration estimates. The green band observed in the probe from the live cultures was not observed in the untreated probes and was likely due to the presence of soluble or colloidal Fe(III) compounds which reacted with the potassium ferricyanide reagent. We infer this from the fact that potassium ferricyanide is known to form a green precipitate

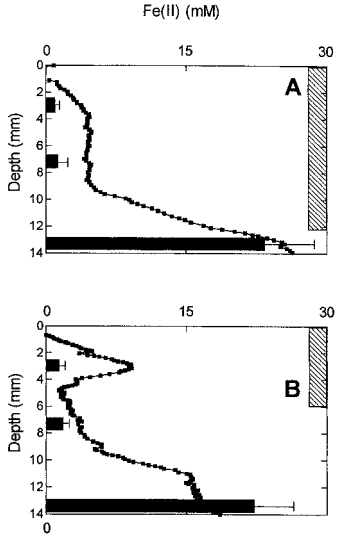


FIG. 3. Comparison of soluble Fe(II) concentration determined by microprobe technique and Ferrozine in control (A) and TW1-inoculated (B) cultures. Ferrozine data are averages of triplicate cores, and error bars represent the 95% confidence interval; they are omitted if smaller than the size of the symbol. For the microprobes, a single representative profile from three different measurements from a single probe is shown.

with Fe(III) at neutral pH (Fig. 4, standards) and that no other components in the medium were present in quantities sufficient to produce such a colored precipitate. Because no such bands were evident in the control cultures, the formation of soluble or colloidal Fe(III) can be attributed to bacterial activity.

Although copious amounts of Fe(III) oxide deposits, detected by their brownish color, were observed in probes from the sterile control cultures, much smaller quantities of such oxides were evident in the probes from the live cultures (Fig. 4). Similar observations were obtained consistently with both the mixed (TW1) and pure (TW2) cultures. As discussed further below, the lower abundance of particulate oxide deposits in live than in control cultures indicates that bacterial catalysis was the dominant mechanism for Fe(II) oxidation in the live cultures. In order to verify quantitatively the lower abundance of particulate oxides in probes from the live cultures, we measured the concentrations of Fe(III) in probes as well as in cores of whole medium in three replicate live and control cultures. We also examined how washing affected Fe(III) concentrations in probes from live cultures, which, as mentioned above, appeared to contain soluble and/or colloidal Fe(III). The concentration of Fe(II) was nearly identical in probes and whole medium in both culture systems (Fig. 5A). The same was true for Fe(III) concentrations in the control systems. In contrast, the concentration of Fe(III) was about threefold higher in whole medium than in probes from the live culture. Since oxides from the control culture did not dissolve completely in 0.5 M HCl (discussed below), the actual ratio is probably higher. These findings quantitatively confirm our consistent visual observation of lower Fe(III) oxide abundance in probes from live versus control cultures.

Washing of probes from the live culture resulted in removal of approximately 70% of their Fe(III) content (Fig. 5B, right). These results verified the presence of soluble Fe(III), as indicated by the green band in potassium ferricyanide-fixed diffusion probes. In contrast, identical washing of probes from the abiotic control cultures resulted in no change in Fe(III) content, whereas the amount of Fe(II) was significantly decreased (Fig. 5B, left). This observation is consistent with the potassium ferricyanide analysis and further indicates that the presence of mobile Fe(III) forms is a biologically mediated phenomenon. The concentration of Fe(III) in whole medium from live cultures was more than twice as high as in probes from the same cultures (Fig. 5A). In addition, we can attribute most of the Fe(III) present in the probe to soluble or colloidal Fe(III) compounds (detected visually with potassium ferricyanide) (Fig. 4), since washing with anoxic distilled water removed a large portion (ca. 70%) of the Fe(III) from these probes (Fig. 5B).

DISCUSSION

Oxygen distribution and locus of oxide deposition. One of the most important observations in this study is the inversion of the locus of oxide deposition in relation to the depth of O_2 penetration in biotic and abiotic opposing-gradient systems. In the abiotic systems, the whole oxide band resided within the oxic zone (Fig. 1A and C). However, when Fe(II)-oxidizing bacteria were present, a significant part of the band was lo-

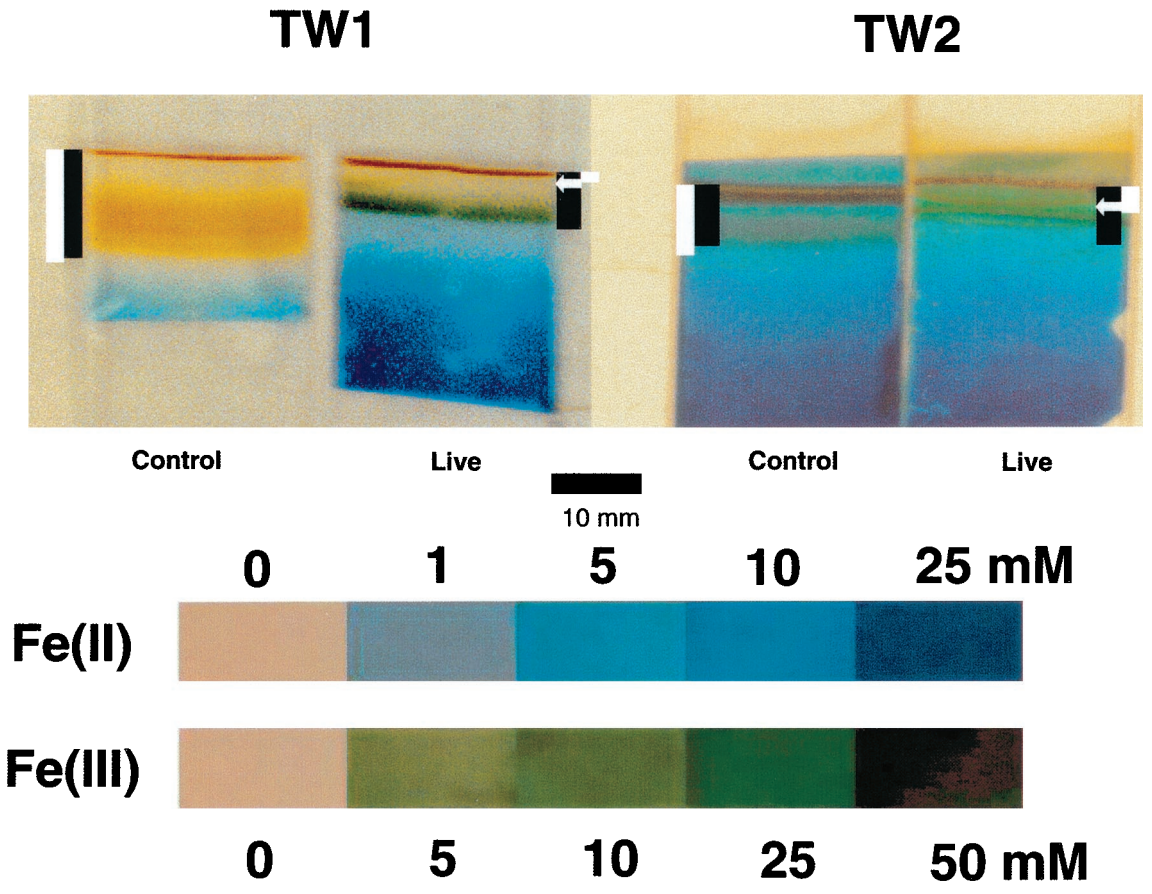


FIG. 4. Photo of $K_3Fe(CN)_6$-fixed microprobes from control and Fe(II)-oxidizing organism-inoculated cultures shown in Fig. 1. Superimposed black bars indicate the positioning of Fe(III) oxide bands, measured independently, in the cultures; white bars denote oxic zones. Arrows indicate the approximate position of the bacterial number peaks (live cultures only). Standards were photographed under different light conditions and may not be directly comparable with the microprobes.

cated below the depth of O_2 penetration, which was substantially shallower than in abiotic control cultures (Fig. 1B and D). This observation held true for both mixed and pure cultures. The control experiments demonstrated that the satellite bacteria present in TW1 did not alter O_2 gradients in the presence of Fe(II). Since TW2 failed to grow or alter O_2 gradients in the absence of Fe(II), we can safely assume that in all our experiments, O_2 gradients were controlled by bacterially mediated Fe(II) oxidation rather than heterotrophic metabolism.

A certain amount of Fe(III) oxide could have been deposited below the apparent O_2 penetration boundary by means of Fe(II) reacting with O_2 at concentrations below the detection limit of our electrode. However, several lines of evidence argue that this phenomenon had no significant confounding effect on our observations. First, the pronounced suboxic Fe(III) oxide deposition observed in the live cultures (up to 60% of the oxide band width, or up to approximately 4 mm, was found below the O_2 penetration boundary), together with our conservative estimate of the O_2 depletion depth (see Materials and Methods), suggests that even if O_2 was present at concentrations below the detection limit (<1 μM), it would have been depleted before reaching the bottom of the oxide band. In addition, no suboxic deposition was detected in abiotic cultures, in which gradients were not as sharp as in the live system, which suggests that interaction between Fe(II) and O_2 at subdetectable concentration did not play a significant role in suboxic deposition of Fe(III) compounds. Finally, the postulated presence of mobile forms of Fe(III) (discussed below) suggests a plausible mechanism responsible for the observed effects.

Previous studies in opposing-gradient systems similar to our low-iron system demonstrated decreased O_2 penetration depth in biotic versus abiotic cultures (8). However, no inversion of the oxide band relative to O_2 gradient position was reported. In the study of Emerson and Moyer (8), the use of FeS as an Fe(II) source provided a submillimolar equilibrium concentration of Fe^{2+} at circumneutral pH (24), far lower than the concentration of Fe(II) present in our culture systems. This low iron content resulted in lesser oxide deposition over the course of the experiment relative to that in the experiments presented here. Consequently, there was less material to be observed, so oxide deposition below the O_2 penetration zone (if any) would probably not have been as apparent as in our study. A recent study of bacterial Fe(II) oxidation by Benz et al. (3), in which millimolar concentrations of soluble Fe(II) were employed in an opposing-gradient system, failed to demonstrate suboxic deposition of Fe(III) alone or in the presence of microaerophilic nitrate-reducing, Fe(II)-oxidizing bacteria. The contrast between these findings and our own suggests that

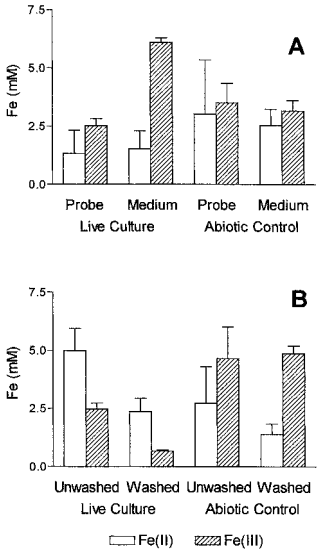


FIG. 5. Fe(II) and Fe(III) in whole medium samples and diffusion probes. (A) Comparison among probes and the medium in TW2 and control cultures; (B) comparison between washed and unwashed probes from TW2 and control cultures. Data represent averages of triplicate cultures, and error bars show 95% confidence intervals.

suboxic Fe(III) deposition may depend on the type of bacteria involved in Fe(II) oxidation—specifically, perhaps, on the organism's ability to produce a mobile form of Fe(III) as the initial end product of Fe(II) oxidation (see below).

Biotic and abiotic oxidation. Our original intent in deploying the diffusion probes was to try to detect the influence of bacterial activities on Fe(II) microgradients at the aerobic-anaerobic interface, in a manner analogous to the analysis of the influence of *Beggiatoa* spp. on H_2S oxidation done by Nelson et al. (19). Unfortunately, due to Fe(III) interference with the densitometric measurements, the diffusion probes did not provide satisfactory measurements of dissolved Fe(II) microgradients at the aerobic-anaerobic interface. However, they revealed several effects of biologically catalyzed Fe(II) oxidation which have not been described previously.

The relative scarcity of particulate oxides in the diffusion probes from the live cultures suggests that Fe(II) oxidation was dominated by biological processes. Since the 5% agar content of the probe would be expected to effectively exclude bacteria, only chemical oxidation would be expected to occur within the agar film. Equilibrium is achieved very rapidly in films as thin as our probes (h = 0.1 mm). Assuming a diffusion coefficient (D) of 10^{-5} cm^2 s^{-1} for Fe(II) (5), the characteristic diffusion time (h^2/D) is only 10 s, which is essentially instantaneous on the time scale of a week-long experiment. The low abundance of oxide deposits in probes from the live cultures therefore suggests that the Fe(II)-oxidizing bacteria scavenged Fe(II) rapidly enough to strongly depress Fe(II) diffusion into the probe and subsequent abiotic oxidation and oxide precipitation within the film.

The above findings suggest that the diffusion probes may provide a tool for distinguishing quantitatively between biological and abiotic oxidation of Fe(II) in opposing-gradient systems. Simply comparing total Fe(III) oxide deposition in biotic and abiotic systems will not be adequate, because the limiting step in Fe(II) oxidation is often diffusional transport of the reduced compounds rather then the reaction itself (8). However, by applying a diffusion probe to the system and quantifying the amount of ferric oxide deposited per unit volume of the probe [corrected for the presence of soluble Fe(III)], it should be possible to estimate the amount of oxide which was deposited abiotically. The difference between the concentration of oxide accumulated within the probe and that in the system as a whole will reflect the amount of oxide deposition that was biologically catalyzed. Applying this approach to our live cultures, we can estimate the percentage of Fe(III) oxide deposited abiotically as $(Fe(III)_{P\text{probe}})/Fe(III)_{T\text{medium}}$, where $Fe(III)_{P\text{probe}}$ is the Fe(III) remaining in the probe after anoxic wash and $Fe(III)_{T\text{medium}}$ is the total Fe(III) in the medium. Since Fig. 5B indicates that ca. 70% of the Fe(III) present in the probe from the live culture is lost during wash and Fig. 5A shows that there was ca. 2.5 times more total Fe(III) in the live culture medium than in the probe, we can estimate that ca. 90% of total Fe(III) in the live cultures was generated via biological processes. In fact, this fraction might be higher in steady-state systems, since in our situation some Fe(II) oxidation inevitably occurred abiotically before a plate of Fe(II)-oxidizing bacteria was established. The presence of similar Fe(III) oxide concentrations in the probes and the whole medium in control cultures suggested that Fe(II) oxidation and Fe(III) oxide deposition proceeded at similar rates and by the same mechanism in both the medium and the probes.

Soluble Fe(III) formation. The observation of a green band in the live system (Fig. 4) suggested the presence of soluble and/or colloidal forms of Fe(III). The presence of such compounds was verified by analysis of washed and unwashed probes (Fig. 5B). Although the pH decrease associated with Fe(II) oxidation at the O_2-Fe(II) boundary (8) might potentially account for the Fe(III) remaining in solution, in our experiments such a decrease was far less than would be required to stabilize any significant amount of Fe(III) (the lowest pH value observed was 6.6 in the zone of oxide deposition, compared to 7.2 at the surface; data not shown). It is possible that the Fe(III) was kept in solution by a chelator excreted by the bacteria specifically for the purpose of retarding or at least delaying cell surface encrustation with oxide precipitates. Encrustation of the bacterial cells with particulate oxides, leading to their eventual entombment, has been suggested as one of the possible environmental challenges which gradient-dwelling solid-phase oxide-producing organisms have to overcome (8). Formation of soluble Fe(III) compounds and eventual remote deposition of the oxides may reduce or delay such encrustation. We hypothesize that, as soluble ferric iron complexes diffuse away from the Fe(II)-oxidizing bacteria, they become destabilized, resulting in precipitation of Fe(III) oxides within as well as below the zone of O_2 penetration.

Davison et al. (5), using diffusion microprobe techniques in lake surface sediments, identified a soluble iron peak in their gels at a depth of approximately 8 mm beneath the sediment-water interface. The authors hypothesized that this peak represented accumulation of Fe(II) as a result of localized Fe(III) oxide reduction activity. However, their analysis could not distinguish between mobile forms of Fe(III) and Fe(II). Our results suggest a possible alternative explanation, i.e., that the activity of the iron-oxidizing bacteria caused a local accumu-

lation of soluble Fe(III). Interestingly, a green band was observed at a depth of ca. 2 mm when a diffusion probe was applied to a sediment core from the freshwater wetland from which the organisms used in this study were obtained (not shown). A recent study, employing voltammetric electrodes, demonstrated the presence of soluble organic complexes of Fe(III) in marine surface sediments (25). These observations suggest that the presence of bacterially generated dissolved or colloidal Fe(III) might be more widespread than has previously been recognized.

Biogeochemical implications. Measurements of Fe(III) abundance in the diffusion probes and the whole medium showed that the vast majority of Fe(II) was oxidized biologically in the presence of Fe(II)-oxidizing bacteria. These results suggest that bacteria can compete successfully with the abiotic oxidation process and that the biological oxidation of Fe(II) might be the predominant process leading to the formation of Fe(III) oxides in surficial aquatic sediments. Emerson and Revsbech (10) found that organisms from a natural Fe(III)-depositing bacterial mat accelerated Fe(II) oxidation in a reactor system designed to simulate the in situ conditions. Since their system was not diffusionally limited, acceleration of Fe(II) oxidation when bacteria were present suggested a significant involvement of those organisms in the process. Our experiments show that Fe(II)-oxidizing bacteria could be similarly involved in Fe(III) generation in a diffusion-limited system.

Our results indicate that Fe(II)-oxidizing bacterial activity can lead to suboxic deposition of reactive Fe(III) oxides. An important implication of these findings is that they suggest the possibility for a rapid coupling between Fe(II) oxidation and Fe(III) oxide reduction within millimeters of the oxic-anoxic interface. Furthermore, Emerson and Revsbech (9) found active Fe(III)-reducing bacteria in a natural Fe(II)-oxidizing mat in an iron seep, indicating tight coupling of Fe(II) oxidation and Fe(III) reduction.

Fe(III) produced by Fe(II)-oxidizing bacteria has traditionally been considered to be represented by immobile, solid-phase compounds. Our findings suggest, however, that, at least immediately after formation, Fe(III) compounds can be treated as soluble ions which are subject to diffusive transport. As mobile Fe(III) compounds diffuse away from the bacterial plate, they are likely to become destabilized, resulting in hydrolysis and precipitation of amorphous Fe(III) oxides. Formed in the anoxic zone, these oxides would be immediately available for reduction by Fe(III)-reducing bacteria, completing the microscale Fe redox cycle. In addition to sediment-water interface environments, other environments where microscale bacterial Fe redox coupling might occur include subsurface sediments, where Fe(II) and O_2 may coexist in "patchy" redox environments, forming a dynamic network of oxic-anoxic interfaces (14), and the rhizosphere of aquatic plants, in which rapid Fe cycling is known to occur (12, 13, 22) and in which the presence of both Fe(II)-oxidizing and Fe(III)-reducing bacteria in close association with plant roots has recently been demonstrated (11, 16).

ACKNOWLEDGMENTS

This research was supported by grants from the National Science Foundation (DEB 94-7233), the U.S. Department of Energy, Office of Energy Research, Environmental Management Science Program (DE-FG07-96ER62321), and the School of Mines and Energy Development, University of Alabama.

We thank D. Emerson, W. C. Ghiorse, and R. G. Wetzel for review of an earlier version of the manuscript.

REFERENCES

1. **Achenbach, L. A., U. Michaelidou, R. A. Bruce, J. Fryman, and J. D. Coates.** *Dechlorimonas agitata* n. n. gen., sp. nov., and *Dechlorosoma suillum* n. n. gen., sp. nov. Two novel environmentally dominant (per) chlorate-reducing bacteria and their phylogenetic position. Int. J. Syst. Evol. Microbiol., in press.
2. **Altschul, S. F., T. L. Madden, A. A. Schäffer, J. Zhang, Z. Zhang, W. Miller, and D. J. Lipman.** 1997. Gapped BLAST and PSI-BLAST: a new generation of protein database search programs. Nucleic Acids Res. **25:**3389–3402.
3. **Benz, M., A. Brune, and B. Schink.** 1998. Anaerobic and aerobic oxidation of ferrous iron at neutral pH by chemoheterotrophic nitrate-reducing bacteria. Arch. Microbiol. **169:**159–165.
4. **Coates, J. D., U. Michaelidou, R. A. Bruce, S. M. O'Connor, J. N. Crespi, and L. A. Achenbach.** 1999. Ubiquity and diversity of dissimilatory (per)chlorate-reducing bacteria. Appl. Environ. Microbiol. **65:**5234–5241.
5. **Davison, W., G. W. Grime, J. A. W. Morgan, and K. Clarke.** 1991. Distribution of dissolved iron in sediment pore waters at submillimeter resolution. Nature **352:**323–325.
6. **Dubinina, G. A.** 1978. Functional role of bivalent iron and manganese oxidation in *Leptothrix pseudoochracea*. Mikrobiologiya **47:**783–789.
7. **Dubinina, G. A.** 1978. Mechanism of the oxidation of the divalent iron and manganese by iron bacteria growing at a neutral pH of the medium. Mikrobiologiya **47:**591–599.
8. **Emerson, D., and C. Moyer.** 1997. Isolation and characterization of novel iron-oxidizing bacteria that grow at circumneutral pH. Appl. Environ. Microbiol. **63:**4784–4792.
9. **Emerson, D., and N. P. Revsbech.** 1994. Investigation of an iron-oxidizing microbial mat community located near Aarhus, Denmark: field studies. Appl. Environ. Microbiol. **60:**4022–4031.
10. **Emerson, D., and N. P. Revsbech.** 1994. Investigation of an iron-oxidizing microbial mat community located near Aarhus, Denmark: laboratory studies. Appl. Environ. Microbiol. **60:**4032–4038.
11. **Emerson, D., J. V. Weiss, and J. P. Megonigal.** 1999. Iron-oxidizing bacteria are associated with ferric hydroxide precipitate (Fe-plaque) on the roots of wetland plants. Appl. Environ. Microbiol. **65:**2758–2761.
12. **Frenzel, P., U. Bosse, and P. H. Janssen.** 1999. Rice roots and methanogenesis in a paddy soil: ferric iron as an alternative electron acceptor in the rooted soil. Soil Biol. Biochem. **31:**421–430.
13. **Giblin, A. E., and R. W. Howarth.** 1984. Porewater evidence for a dynamic sedimentary iron cycling in salt marshes. Limnol. Oceanogr. **29:**47–63.
14. **Hunter, K. S., Y. Wang, and P. Van Cappelen.** 1998. Kinetic modelling of microbially-driven redox chemistry of the subsurface environment: coupling transport, microbial metabolism and geochemistry. J. Hydrol. **209:**53–80.
15. **Jones, J. G.** 1983. A note on isolation and enumeration of bacteria which deposit and reduce ferric iron. J. Appl. Bacteriol. **54:**305–310.
16. **King, G. M., and M. A. Garey.** 1999. Ferric iron reduction by bacteria associated with the roots of freshwater and marine macrophytes. Appl. Environ. Microbiol. **65:**4393–4398.
17. **Lovley, D. R., and E. J. P. Phillips.** 1986. Availability of ferric iron for microbial reduction in bottom sediments of the freshwater tidal Potomac River. Appl. Environ. Microbiol. **52:**751–757.
18. **Muyzer, G., E. C. D. Waal, and A. G. Uitterlinden.** 1993. Profiling of complex microbial populations by denaturing gradient gel electrophoresis analysis of polymerase chain reaction-amplified genes coding for 16S rRNA. Appl. Environ. Microbiol. **59:**695–700.
19. **Nelson, D. C., N. P. Revsbech, and B. B. Jorgensen.** 1986. Microoxic-anoxic niche of *Beggiatoa* spp.: microelectrode survey of marine and freshwater strains. Appl. Environ. Microbiol. **52:**161–168.
20. **Perfil'ev, B. V., and D. R. Gabe.** 1969. Capillary methods of investigating micro-organisms. University of Toronto Press, Toronto, Canada.
21. **Revsbech, N. P.** 1989. An oxygen microelectrode with guard cathode. Limnol. Oceanogr. **34:**472–476.
22. **Roden, E. E., and R. G. Wetzel.** 1996. Organic carbon oxidation and suppression of methane production by microbial Fe(III) oxide reduction in vegetated and unvegetated freshwater wetland sediments. Limnol. Oceanogr. **4:**1733–1748.
23. **Stookey, L. L.** 1970. Ferrozine—a new spectrophotometric reagent for iron. Anal. Chem. **42:**779–781.
24. **Stumm, W., and J. J. Morgan.** 1996. Aquatic chemistry: chemical equilibria and rates in natural water, 2nd ed. Wiley-Interscience, New York, N.Y.
25. **Taillefert, M., B. A. B., and G. W. Luther III.** 2000. Reactivity of freshly formed Fe(III) in synthetic solutions and (pore) water: voltammetric evidence of an aging process. Environ. Sci. Technol. **34:**2169–2177.
26. **Winogradski, S.** 1888. Über Eisenbakterien. Bot. Ztg. **46:**263–270.

Appendix 2: Numerical simulation of U(VI) reductive immobilization in Fe(III) oxide-reducing subsurface sediments

Numerical simulation of U(VI) reductive immobilization in Fe(III) oxide-reducing subsurface sediments

1. Introduction

An underlying goal of our EMSP 96-10 research project was to generate experimental information which could be used as the basis for development of numerical simulations of the various microbiological and geochemical processes occurring in experimental Fe(III) oxide reduction systems, and ultimately subsurface sedimentary environments. As a provisional step toward this goal, we have developed simulations of hypothetical semicontinuous culture (SC) and column reactor systems which approximated the conditions in our experiments, using a nonsteady-state implementation of the STEADYQL algorithm developed by Westall and colleagues (Furrer et al., 1989; Westall et al., 1991). We previously used a simplified version of this model to simulate synthetic goethite reduction in batch vs. semicontinuous culture reactors (Roden and Urrutia, 1999). The purpose of presenting the results of these simulations in this proposal is two-fold: (i) to illustrate the basic operation of the simulation strategy; and (ii) to present some numerical predictions which illustrate the hypotheses to be tested in the research to be conducted in our renewal project.

2. STEADYQL (Nonsteady-state implementation)

The STEADYQL algorithm predicts the steady-state composition of a soil solution which is subject to a combination of kinetic and equilibrium reactions (homogeneous and/or heterogeneous). Aqueous speciation and surface complexation reactions are assumed to be *fast* processes which can be treated as reactions at equilibrium (Furrer et al., 1989). *Slow* processes are reactions described by explicit rate laws, for example transfer of materials between soil solution and solids. *Very slow* processes are ones which have a negligible effect during the period of interest, such as depletion of bulk mineral solids, and which are not explicitly included in the simulation.

We modified the STEADYQL algorithm to function in nonsteady-state mode within the Visual Basic for Applications (VBA) environment within Microsoft Excel. The model uses the MICROQL (Westall, 1979, 1986) algorithm to compute chemical equilibria, together with a fifth-order Runga-Kutta ODE solver adapted from the FORTRAN subroutines given in Press et al. (1992) to solve for time-dependent changes in a set of dependent variables, some of which are components in the system of equilibrium speciation reactions. An illustration of the operation of the simulation model as applied to a single-reservoir (REV) reactor system is given in Fig. 1. We verified our nonsteady-state implementation of the model by reproducing (over a long simulation interval) the steady-state solution to the example problem described in Furrer et al. (1989). We also verified the operation of the MICROQL algorithm by reproducing the solutions to a variety equilibrium problems obtained using the MINEQL+ software (Schecher and McAvoy, 1998). The MICROQL algorithm was modified to compute activity coefficients for charged species according to the Davies equation as described in Westall et al. (1986).

3. Semicontinuous Culture (REV) Simulation

In this section, we illustrate how the simulation model can be used to predict time-dependent changes in aqueous and solid-phase geochemistry and MeRB biomass during a SC experiment examining the simultaneous reduction of Fe(III) oxide and U(VI) in AGW. We use the model to assess the potential for sustained U(VI) scavenging, depending on whether or not U(VI) sorbed to Fe(III) oxide surfaces is assumed to be available for microbial (enzymatic) reduction.

Equilibrium Reactions

In keeping with the STEADYQL framework, aqueous speciation and surface complexation were assumed to be fast, equilibrium-controlled reactions. The composition of the aqueous phase was that listed in Table 1. The synthetic FeOOH-coated sand used by Roden et al. (2000)in column Fe(III) oxide reduction studies was assumed to represent the only solid-phase in the reactor system. Surface complexation by this material was modeled according to the diffuse layer model (DLM) as described in Dzombak and Morel (1990). The total abundance of oxide surface sites was defined by the bulk Fe(III) oxide concentration (assumed equal to 70 mmol L^{-1}, in keeping with concentrations to be used in the proposed SC experiments), the measured surface area of the oxide coating the sand grains (150 m^2 g^{-1}), and the standard mineral surface site density of 3.84 μmol m^{-2} recommended by Davis and Kent (1990). The oxide surface was assumed to possess both 'strong' and 'weak' binding sites, and the relative abundance of these sites was assumed to be equal to that used by Dzombak and Morel (1990) to model cation and anion surface complexation by hydrous ferric oxide (HFO). Values for first and second FeOOH surface acidity constants used in our simulations were those for HFO given in Dzombak and Morel (1990), which are in fact very similar to those determined for goethite by Goldberg and Sposito (1984). The same acidity constants were used for the two types of surface sites, as recommended in Dzombak and Morel (1990).

The aqueous speciation and surface complexation reactions considered in the model are summarized in the Tableau presented in Table 2. Sodium acetate was omitted from the speciation calculations, since neither Na^+ nor CH_3COO^- are expected to exert any major impact on the speciation of the other components in the AGW. However, the contribution of these ions to aqueous phase ionic strength was accounted for in the simulations by assuming a fixed ionic strength equal to that listed in Table 1. The surface complexation constants for Ca^{2+} adsorption are those listed for HFO in Dzombak and Morel (1990). Surface complexation of aqueous U(VI) species was modeled as described Waite et al. (Waite et al., 1994), using constants obtained by these authors for sorption of UO_2^{2+} and UO_2^{2+}+CO_3^{2-} to ferrihydrite. In contrast the simulations presented in Waite et al. (Waite et al., 1994), the total Fe(III) oxide surface site density and relative abundance of strong and weak sites was not modified relative to the values for HFO given in Dzombak and Morel (1990). Nevertheless, testing (using the MINEQL+ program) showed that our depiction of U(VI) sorption gave results similar to those presented in Waite et al. (Waite et al., 1994) in terms of pH edges with different levels total U (10^{-4}-10^{-6} M) and DIC (gas phase with atmospheric CO_2 levels vs. 1% CO_2). The ability of our implementation of the MICROQL algorithm to reproduce the sorption behavior of U(VI) species was checked against MINEQL+ simulations.

Depiction of the complexation of Fe(II) by Fe(III) oxide surfaces, particularly at the high levels of Fe(II) loading which typically arise during microbial Fe(III) oxide reduction, is not a

straightforward undertaking. Unique electrical interactions (promoted by Fe^{III}/Fe^{II} d-orbital overlap) may occur between Fe(II) and $Fe^{III}OH$ surface sites on the oxide (Sherman, 1987), leading sorption behavior which might better be described by surface reworking through formation of spinel-like compounds (Tronc et al., 1992; Coughlin and Stone, 1995). Alternatively, in some cases it may be appropriate to interpret Fe(II) complexation by Fe(III) oxide surfaces as a surface precipitation process which produces $Fe(OH)_2$ phases analogous to that which are known to occur with other divalent cations (Dzombak and Morel, 1990). However, no systematic evaluation of such phenomena as they may occur during bacterial Fe(III) oxide reduction has yet been performed, and thus for simplicity in our simulations we depict Fe(II) surface complexation through a standard divalent cation surface complexation framework. Unfortunately, there is very little experimental information available on binding constants for Fe(II) complexation by Fe(III) oxide surface, presumably because of the aforementioned complications. Hence, as a first approximation we computed Fe(II) binding constants for strong and weak sites according to the LFER relationships depicted in Figs. 10.1 and 10.2 in Dzombak and Morel (1990), obtaining log K values of approximately 1.0 and –2.0 for strong and weak sites, respectively. In order to evaluate the validity of these estimated constants, a preliminary Fe(II) sorption edge experiment (in 1 mM PIPES buffer) with the synthetic FeOOH-coated sand was conducted. MINEQL+ was then used to model Fe(II) adsorption, incorporating the appropriate bulk Fe(III) oxide concentration and using the measured surface area of the synthetic FeOOH to compute the abundance of strong and weak binding sites. The results (see Fig. 2A) indicated that a substantial adjustment (increase) in the value for the weak site binding constant was required in order to bring the sorption edge into approximate agreement the observed isotherm. A value of 0.5 for the weak binding site log K value gave a reasonable fit to the data. No adjustments were made to the binding constant for the strong sites, since the concentration of these sites is minor compared to the weak sites. To assess whether or not the set of constants for Fe(II) surface complexation by the synthetic FeOOH-coated sand could account for the observed sorption of Fe(II) as a function of Fe(II) concentration at a fixed pH of 6.9 in 10 mM PIPES buffer (data from Roden et al., 2000), a MINEQL+ simulation was conducted with a range (sweep) of Fe(II) values at constant pH. The results indicated reasonable agreement between the observed and predicted degree of Fe(II) sorption by the FeOOH-coated sand (Fig. 2B). Together, these provisional results lend a reasonable measure of confidence to the depiction of Fe(II) surface complexation included in the dynamic biogeochemical simulations described below.

In order to evaluate the potential impact of competitive Fe(II) sorption on U(VI) sorption by the synthetic FeOOH-coated sand in AGW, a MINEQL+ simulation was conducted in which the total Fe(II) concentration was varied from 0 to 10 mM, a range which is likely to include the values obtained in the proposed SC and column Fe(III) oxide reduction experiments. Total U(VI) concentrations of 10 or 100 μM were considered in separate simulations. The results (Fig. 3) indicate that even very high levels of Fe(II) would not be expected strongly suppress U(VI) complexation by strong binding sites on the oxide surface. While encouraging, these results must be interpreted with caution, since the strong site binding constant for Fe(II) was estimated based only the relative magnitude of first value hydrolysis constant for this cation. Hence, definitive evaluation of the impact of competitive Fe(II) sorption on U(VI) surface complexation will await the empirical studies proposed herein.

Kinetic Reactions

Three kinetic reactions were considered in the simulation: (1) production of Fe(II) via microbial reduction of "free" Fe(III) oxide surface sites (designated by $Fe(III)_{fss}$) according to a biomass-specific, quasi-first-order reduction rate constant (see "Kinetics of Fe(III) oxide reduction and MeRB growth" section in EMSP renewal proposal); (2) microbial reduction of U(VI) according to biomass-specific Monod-type expression; and (3) MeRB biomass production coupled to Fe(III) oxide and U(VI) reduction. A generalized cell death/senescence rate constant was included to prevent excessive biomass accumulation. At present, rate constants for MeRB death/senescence are unavailable; therefore the value used (0.024 d^{-1}) was set equal to the general literature value used by Tebes-Stevens et al. (Tebes-Stevens et al., 1998) for simulation of Co(III)-EDTA degradation in a subsurface multicomponent reactive transport model demonstration. The rate expressions used to model these kinetic reactions are given in Appendix 3. Microbial Fe(III) oxide reduction coupled to acetate oxidation was assumed to liberate stoichiometric amounts of Fe(II), dissolved inorganic carbon, and alkalinity (total H consumption + bicarbonate alkalinity production) according to the following reaction:

$$FeOOH + 0.125CH_3COO^- + 1.875H^+ \rightarrow Fe^{2+} + 0.25HCO_3^- + 1.5H_2O$$

The abundance of free Fe(III) oxide surface site available for microbial reduction at any given time during the simulation was equal to the total surface density (sum of the total concentrations of components 3 and 4 in the Tableau in Table 3) minus the concentration of Fe(II) sorbed to strong (species 25) and weak (species 32) oxide surface sites. Thus, rates of Fe(III) oxide reduction were dynamically controlled by the changing abundance of sorbed Fe(II). This same strategy was used successfully in a previous model of synthetic goethite reduction (Roden and Urrutia, 1999), with the exception that in the previous model, Fe(II) sorption to the oxide surface was depicted according to an empirical Freundlich isotherm fit to Fe(II) sorption data obtained for a reactor system identical to that used for the microbial Fe(III) oxide reduction experiments (Urrutia et al., 1998) – as opposed to the DLM used in the present model. At this time, using sorbed Fe(II) abundance as computed by some type of equilibrium speciation expression appears to be the most straightforward and tractable way to model the influence of surface-bound Fe(II) accumulation on Fe(III) oxide reduction activity.

The biomass-specific rate constant (k_{red}) for Fe(III) oxide reduction was obtained from a curve-fit of the time course of Fe(II) accumulation in the batch culture experiment conducted in parallel with the column FeOOH-coated sand experiment reported in Roden et al. (Roden et al., 2000) (Fig. 4). The rate constant obtained from this curve-fit was divided first by the estimated total Fe(III) oxide surface site abundance (3.8 mmol L^{-1}) to normalize the rate constant to site density, and then by the initial MeRB biomass added to the reactors (ca. 20 mg L^{-1}) to normalize the rate constant to MeRB biomass, resulting in a final value of 0.095 mg^{-1} d^{-1}. It is important to note that for the sake of simplicity, depletion of the bulk Fe(III) oxide pool was not considered explicitly in the simulations. Therefore, this process was by default assumed to represent a very slow process in the context of the STEADYQL framework. Future simulations will implement a shrinking-core model to depict loss of bulk Fe(III) oxide content and its control on the time-dependent abundance of total oxide surface site abundance, which in some experiments (e.g. the column experiments reported in Roden et al., 2000) may be a quite significant phenomenon.

Other DOE-funded research groups, notably that of J. Zachara at PNNL and W. Burgos at Penn State University, are also pursuing coupled experimental-modeling studies of the surface-chemical controls on bacterial Fe(III) oxide reduction

The biomass-specific V_{max} value for microbial U(VI) reduction was set equal the value of 2.4 μmol U(VI) mg dry weight biomass^{-1} hr^{-1} reported for *S. alga* in Truex et al. (Truex et al., 1997). A average half-saturation constant (K_m) for microbial U(VI) uptake/reduction of 100 μM was assumed, based on the value of 132 μM reported for *S. alga* in Truex et al. (1997) and the range of values obtained by Gorby et al. (Gorby et al., 2001) for several different MeRB.

The initial MeRB cell biomass in the reactor was set equal to the equivalent of ca. 10^5 cells mL^{-1} (0.2 mg L^{-1}). Subsequent production of MeRB biomass was computed based on calculated rates of Fe(III) and U(VI) reduction, using yield coefficients for MeRB growth coupled Fe(III)-citrate reduction determined in our own laboratory (Fig. 5), and yield coefficients for MeRB growth coupled to U(VI) reduction estimated from the growth experiments reported in Lovley et al. (Lovley et al., 1991). As mentioned above, the yield coefficients for growth coupled to Fe(III) and U(VI) so obtained were quite comparable on a per electron-transferred basis (ca. 4 mg cells per mmol electrons transferred).

Simulation Results

A standard simulation time of 120 d was adopted, corresponding to a hypothetical 4 month (120 d) SC incubation experiment. An aqueous phase residence time of 10 d was assumed. The input U(VI) concentration was 10 μM. Model output was collected at daily intervals. The simulations generally required a total 400-450 steps of the ODE solver algorithm, with an execution time of approximately 5 min on a 400 MHz Celeron processor. Truncation error for the ODE solver was set equal to max(RelTol*abs(y(i,t)), AbsTol), where RelTol is the *relative* accuracy tolerance, AbsTol is the *absolute* accuracy tolerance, and abs(y(i,t)) is the absolute value of dependent variable i at time t. For the simulations, RelTol was set equal to 0.001 (0.1% accuracy), and AbsTol was set equal to 1×10^{-12} (equivalent to 1×10^{12} mol L^{-1} or 0.001 nM).

The results of two simulations are shown in Fig. 6: one in which both aqueous and sorbed U(VI) were subject microbial reduction; and one in which only aqueous U(VI) was allowed to be reduced. In the presence of active U(VI) reduction, U(VI) was scavenged to concentrations less than 5% of the input concentration - in contrast to simulations without any FeOOH or U(VI) reduction activity, in which the aqueous U(VI) concentration approached the input value toward the end of the simulation period (data not shown). The efficiency of U(VI) scavenging was far greater in the simulation in which both aqueous and sorbed U(VI) reduction were permitted than the one in which only aqueous U(VI) was reduced. These results are consistent with the hypothesis that ability of MeRB to reduce sorbed U(VI) would lead to greatly enhanced U(VI) reductive immobilization in subsurface sediments, and emphasize the need for rigorous experimental evaluation of this question.

4. 1-D Column Transport-Reaction Simulation

The single-reservoir REV simulation model was expanded into a 1-dimensional transport-reaction model in order to conceptualize the results expected for a column reactive transport experiment involving U(VI) adsorption and microbial reduction under conditions of microbial Fe(III) oxide reduction. The VBA code developed solves the following general 1-dimensional advection/dispersion equation using a finite-difference approach:

$$\frac{\partial C_j}{\partial t} = D\frac{\partial^2 C_j}{\partial z^2} - v\frac{\partial C_j}{\partial z} - \frac{r(1-f)}{f}\frac{\partial s_i}{\partial t} - \Sigma R(c_{i,j})$$

Dispersion Advection Sorption (equil) Reaction (kinetic)

where: C_j = total aqueous concentration of component j
D = dispersion coefficient (L(length)^2 t(time)$^{-1}$)
X_j = concentration of component j (mol L^{-3})
v = linear flow velocity (L t^{-1})
z = distance in direction of flow (L)
s_i = concentration of sorbed species of component j (at equilibrium) (mol M(mass)$^{-1}$)
ρ = particle density (M L^{-3})
ϕ = porosity (L^3 H_2O L^{-3} wet sediment)
$\Sigma R(C_{i,j})$ = sum of kinetic reactions acting on species c_i of component j (mol L^{-3} t^{-1})

For simulations of the abiotic reactive transport experiments, the sorption term will not be accounted for by the typical linear isotherm (K_d value), but rather a diffuse double layer surface complexation or other surface complexation model, the equilibrium solution to which is computed dynamically throughout the simulation.

As with the REV simulations, the model was used to evaluate, among other things, the idea that reduction of U(VI) sorbed to Fe(III) oxide surfaces could promote the retardation of U(VI) transport. The function of the transport-reaction model is outlined in Fig. 7, and a Tableau summarizing the equilibrium reactions included in the simulation is given in Table 3. The same set of kinetic reactions which took place in the REV simulation model were allowed to occur in each cell of the 1-D spatial grid (10 cells, each 0.05 dm for total column length of 0.5 dm) used to simulate dispersive and advective transport by finite differences. The fluid flow rate was set at 0.05 dm hr^{-1}, and the dispersion coefficient at 0.005 dm^2 hr$^-$1, resulting in a column Peclet number of 5, which is similar to that observed in the abiotic U(VI) reactive transport experiments reported in Barnett et al. (Barnett et al., 2000). The coupled transport-equilibrium speciation-kinetic reaction equations were solved using a Numerical Method Of Lines (NUMOL) approach, as described in Schiesser (1991) and Boudreau (1997). As in the REV simulation, a fifth-order Runga-Kutta algorithm with truncation error control (Press et al., 1992) was used to integrate the system of ODEs generated by the NUMOL. Note that in the NUMOL approach, the time step is determined by the solver so as to conform to the specified truncation error tolerances, which were set at the same values used for the REV simulations. The performance of the transport-reaction model was verified by reproducing several of the test problems described in Steefel and

MacQuarrie (Steefel and MacQuarrie, 1996). Each simulation required approximately 30 min to execute on a 400 MHz Celeron processor.

Breakthrough curves for three different 1-month (720 hr) simulations, from which output was collected every 48 hr, are shown in Fig. 8 (upper panel). Also shown in Fig. 8 (lower panel) is the distribution of MeRB biomass vs. distance along the column at the end of the simulation. In the absence of both FeOOH and U(VI) reduction (abiotic conditions), $U(VI)_{aq}$ breakthrough began at 140 hours and was virtually complete after approximately 240 hrs. When both aqueous and sorbed U(VI) reduction were allowed to occur together with FeOOH reduction, $U(VI)_{aq}$ was very strongly retarded: $U(VI)_{aq}$ concentrations in the column effluent at the end of the simulation were well-below the 1×10^{-12} absolute error tolerance of the ODE solver. The ability of the MeRB to access the relatively high concentrations of sorbed U(VI) which accumulated at the influent end of the column led to the generation of a large MeRB biomass coupled to U(VI) reduction, which was undoubtedly responsible for the intense U(VI) scavenging. When only $U(VI)_{aq}$ together with FeOOH reduction were allowed to occur, the initial breakthrough of $U(VI)_{aq}$ was not retarded much relative to the abiotic simulation; however, as MeRB biomass began to accumulate as a result of FeOOH reduction, the concentration of $U(VI)_{aq}$ in the column effluent began to decline. An important experimental implication of these is that MeRB biomass production coupled to reduction of sorbed U(VI) reduction could play an important role in governing U(VI) retardation in column reactors with high flow rates and associate high rates of total U(VI) loading. The insight obtained from this relatively simple set of transport-reaction calculations illustrates the potential utility of simulation modeling for interpretation and prediction of coupled microbial-geochemical processes in experimental reactive transport systems.

References

Barnett, M.O., P.M. Jardine, S.C. Brooks, and H.M. Selim. 2000. Adsorption and transport of U(VI) in subsurface media. Soil Sci. Soc. Am. J. 64:1-43.

Boudreau, B.P. 1997. Diagenetic models and their implementation, Springer.

Coughlin, B.R., and A.T. Stone. 1995. Nonreversible adsorption of divalent metal ions (Mn-II, Co-II, Ni-II, Cu-II and Pb-II) onto goethite: Effects of acidification, Fe-II addition, and picolinic acid addition. Environ. Sci. Technol. 29:2445-2455.

Davis, J.A., and D.B. Kent. 1990. Surface complexation modeling in aqueous geochemistry, pp. 177-260. *In* Mineral-water interface geochemistry, Hochella, M.F., and A.F. White [eds], Mineralogical Society of America.

Dzombak, D.A., and F.M.M. Morel. 1990. Surface Complexation Modeling: Hydrous Ferric Oxide, John Wiley & Sons.

Furrer, G., J. Westall, and P. Sollins. 1989. The study of soil chemistry through quasi-steady-state models: I. Mathematical definition of model. Geochim. Cosmochim. Acta 53:595-601.

Goldberg, S., and G. Sposito. 1984. A chemical model of phosphate adsorption by soils. I. Reference oxide minerals. Soil Sci. Soc. Am. J. 48:772-778.

Gorby, Y.A., C. Brown, C. Liu, M. Gray, A. Plymale, S.W. Li et al. 2001. Kinetic analysis of multivalent metal reduction by metal-reducing bacteria. Manuscript in preparation.

Lovley, D.R., E.J.P. Phillips, Y.A. Gorby, and E.R. Landa. 1991. Microbial reduction of uranium. Nature 350:413-416.

Press, W.H., S.A. Teukolsky, W.T. Vetterling, and B.P. Flannery. 1992. Numerical Recipes in FORTRAN, Cambridge University Press.

Roden, E.E., and M.M. Urrutia. 1999. Ferrous iron removal promotes microbial reduction of crystalline iron(III) oxides. Environ. Sci. Technol. 33:1847-1853.

Roden, E.E., M.M. Urrutia, and C.J. Mann. 2000. Bacterial reductive dissolution of crystalline Fe(III) oxide in continuous-flow column reactors. Appl. Environ. Microbiol. 66:1062-1065.

Schecher, W.D., and D.C. McAvoy. 1998. MINEQL+ A chemical equilibrium modeling system. Version 4.0 for Winders User's Manual, Environmental Research Software.

Schiesser, W.E. 1991. The Numerical Method of Lines, Academic Press.

Sherman, D.M. 1987. Molecular orbital (SCF-Xα-SW) theory of metal-metal charge transfer processes in minerals I. Application to Fe2+ --> Fe3+ charge transfer and "electron delocalization" in mixed-valence iron oxides and silicates. Phys. Chem. Miner. 14:355-363.

Steefel, C.I., and K.T.B. MacQuarrie. 1996. Approaches to modeling of reactive transport in porous media, pp. 83-129. *In* Reactive transport in porous media, Lichtner, P.C., C.I. Steefel, and E.H. Oelkers [eds], The Mineralogical Society of America.

Tebes-Stevens, C., A.J. Valocchi, J.M. VanBriesen, and B.E. Rittman. 1998. Multicomponent transport with coupled geochemical and microbiological reactions: model description and example simulations. J. Hydrol. 209:8-26.

Tronc, E., P. Belleville, J.P. Jolivet, and J. Livage. 1992. Transformation of ferric hydroxide into spinel by Fe II adsorption. Langmuir 8:313-319.

Truex, M.J., B.M. Peyton, N.B. Valentine, and Y.A. Gorby. 1997. Kinetics of U(VI) reduction by a dissimilatory Fe(III)-reducing bacterium under non-growth conditions. Biotech. Bioengin. 55:490-496.

Urrutia, M.M., E.E. Roden, J.K. Fredrickson, and J.M. Zachara. 1998. Microbial and geochemical controls on synthetic Fe(III) oxide reduction by *Shewanella alga* strain BrY. Geomicrobiol. J. 15:269-291.

Waite, T.D., J.A. Davis, T.E. Payne, G.A. Waychunas, and N. Xu. 1994. Uranium(VI) adsorption to ferrihydrite: Application of a surface complexation model. Geochim. Cosmochim. Acta 58:5465-5478.

Westall, J.C. 1979. MICROQL II. Computation of adsorption equilibria in BASIC. Swiss Federal Institute of Technology, EAWAG, Duebendorf, Switzerland.

Westall, J.C. 1986. MICROQL I. A chemical equilibrium program in BASIC. Report 86-02, Department of Chemistry, Oregon State University, Corvalis, OR.

Westall, J.C., J.L. Zachary, and F.M.M. Morel. 1986. MINEQL. A computer program for the calculation of the chemical equilibrium composition of aqueous systems. Report 86-01, Department of Chemistry, Oregon State University, Corvalis, OR.

Westall, J.C., G. Furrer, P. Sollins, and P. Verburg. 1991. STEADYQL. A quasi-steady-state model for study of chemistry of soil solution. Report 91-01, Department of Chemistry, Oregon State University, Corvallis, OR.

Table 1. Artificial groundwater medium composition.

Component	Concentration (M)
$CaCl_2 \cdot 2H_2O$	1.0×10^{-3}
KCl	1.5×10^{-4}
$MgCl_2 \cdot 7H_2O$	5.0×10^{-4}
NaOH	1.0×10^{-3}
$SiO_2(aq)$	3.5×10^{-4}
NH_4Cl	1.0×10^{-4}
KH_2PO_4	1.0×10^{-5}
pH	6.5*
Ionic strength	5.7×10^{-3}

* after equilibration with 98:2 % N_2:CO_2 ($pCO_2 = 10^{-1.7}$ atm)

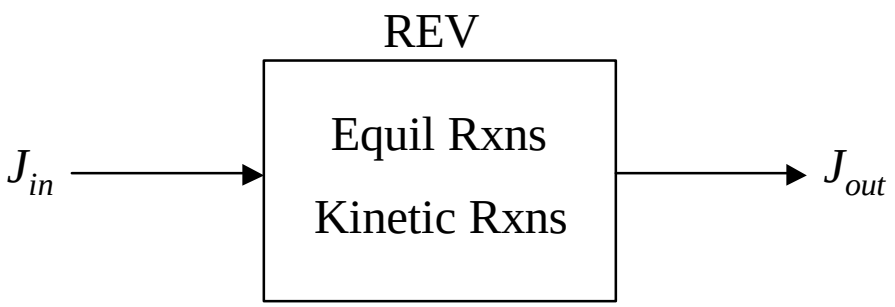
Table 2. Tableau of stoichiometric coefficients and stability constants (log K values) for semicontinuous culture (REV) simulation model.

		Components:	1 Ca^{2+}	2 Fe^{2+}	3 $Fe^{s}OH$	4 $Fe^{w}OH$	5 UO_2^{+}	6 f(Y)	7 H^{+}	8 CO2(g)	log K	f(out,i)
Species:	**1**	Ca^{2+}	1	0	0	0	0	0	0	0	0	1
	2	$CaOH^{+}$	1	0	0	0	0	0	-1	0	-12.78	1
	3	$CaHCO_3^{+}$	1	0	0	0	0	0	-1	1	11.44	1
	4	$CaCO_3$(aq)	1	0	0	0	0	0	-2	1	3.22	1
	5	H_2CO_3	0	0	0	0	0	0	0	1	16.68	1
	6	HCO_3^{-}	0	0	0	0	0	0	-1	1	10.33	1
	7	CO_3^{2-}	0	0	0	0	0	0	-2	1	0	1
	8	Fe^{2+}	0	1	0	0	0	0	0	0	0	1
	9	$FeOH^{+}$	0	1	0	0	0	0	-1	0	-9.5	1
	10	$FeHCO_3^{+}$	0	1	0	0	0	0	-1	1	12.33	1
	11	$FeCO_3$(aq)	0	1	0	0	0	0	-2	1	5.5	1
	12	$Fe(CO_3)_2^{2-}$	0	1	0	0	0	0	-4	2	7.1	1
	13	UO2+	0	0	0	0	1	0	0	0	0	1
	14	UO2OH+	0	0	0	0	1	0	-1	0	-5.09	1
	15	UO2(OH)2	0	0	0	0	1	0	-2	0	-12	1
	16	(UO2)2(OH)22+	0	0	0	0	2	0	-2	0	-5.645	1
	17	(UO2)3(OH)5+	0	0	0	0	3	0	-5	0	-15.93	1
	18	UO2CO3	0	0	0	0	1	0	-2	1	10.071	1
	19	UO2(CO3)22-	0	0	0	0	1	0	-4	2	17.008	1
	20	UO2(CO3)34-	0	0	0	0	1	0	-6	3	21.384	1
	21	$Fe^{s}OH$	0	0	1	0	0	0	0	0	0	0
	22	$Fe^{s}OH_2^{+}$	0	0	1	0	0	1	1	0	7.29	0
	23	$Fe^{s}O^{-}$	0	0	1	0	0	-1	-1	0	-8.93	0
	24	$Fe^{s}OHCa^{2+}$	1	0	1	0	0	2	0	0	4.97	0
	25	$Fe^{s}OFe^{+}$	0	1	1	0	0	1	-1	0	1	0
	26	$Fe^{s}O2UO2$	0	0	1	0	1	0	-2	0	-2.57	0
	27	$Fe^{s}O2UO2CO32-$	0	0	1	0	1	-2	-2	1	3.67	0
	28	$Fe^{w}OH$	0	0	0	1	0	0	0	0	0	0
	29	$Fe^{w}OH_2^{+}$	0	0	0	1	0	1	1	0	7.29	0
	30	$Fe^{w}O^{-}$	0	0	0	1	0	-1	-1	0	-8.93	0
	31	$Fe^{w}OCa^{+}$	1	0	0	1	0	1	-1	0	-5.85	0
	32	$Fe^{w}OFe^{+}$	0	1	0	1	0	1	-1	0	0.5	0
	33	$Fe^{w}O2UO2$	0	0	0	1	1	0	-2	0	-6.28	0
	34	$Fe^{w}O2UO2CO32-$	0	0	0	1	1	-2	-2	1	-0.42	0
	35	OH^{-}	0	0	0	0	0	0	-1	0	-14	1
	36	H^{+}	0	0	0	0	0	0	1	0	0	1
		IONZ:	2	2	0	0	2	0	1	0		

Table 3. Tableau of stoichiometric coefficients and stability constants (log K values) for 1-D transport-reaction model.

		Components:	1 Ca^{2+}	2 CO_3^{2-}	3 Fe^{2+}	4 $Fe^{s}OH$	5 $Fe^{w}OH$	6 UO_2^{+}	7 f(Y)	8 H^{+}	log K	f(out,i)
Species:	**1**	Ca^{2+}	1	0	0	0	0	0	0	0	0	1
	2	$CaOH^{+}$	1	0	0	0	0	0	0	-1	-12.78	1
	3	$CaHCO_3^{+}$	1	1	0	0	0	0	0	1	11.44	1
	4	$CaCO_3$(aq)	1	1	0	0	0	0	0	0	3.22	1
	5	H_2CO_3	0	1	0	0	0	0	0	2	16.68	1
	6	HCO_3^{-}	0	1	0	0	0	0	0	1	10.33	1
	7	CO_3^{2-}	0	1	0	0	0	0	0	0	0	1
	8	Fe^{2+}	0	0	1	0	0	0	0	0	0	1
	9	$FeOH^{+}$	0	0	1	0	0	0	0	-1	-9.5	1
	10	$FeHCO_3^{+}$	0	1	1	0	0	0	0	1	12.33	1
	11	$FeCO_3$(aq)	0	1	1	0	0	0	0	0	5.5	1
	12	$Fe(CO_3)_2^{2-}$	0	2	1	0	0	0	0	0	7.1	1
	13	UO2+	0	0	0	0	0	1	0	0	0	1
	14	UO2OH+	0	0	0	0	0	1	0	-1	-5.09	1
	15	UO2(OH)2	0	0	0	0	0	1	0	-2	-12	1
	16	(UO2)2(OH)22+	0	0	0	0	0	2	0	-2	-5.645	1
	17	(UO2)3(OH)5+	0	0	0	0	0	3	0	-5	-15.93	1
	18	UO2CO3	0	1	0	0	0	1	0	0	10.071	1
	19	UO2(CO3)22-	0	2	0	0	0	1	0	0	17.008	1
	20	UO2(CO3)34-	0	3	0	0	0	1	0	0	21.384	1
	21	$Fe^{s}OH$	0	0	0	1	0	0	0	0	0	0
	22	$Fe^{s}OH_2^{+}$	0	0	0	1	0	0	1	1	7.29	0
	23	$Fe^{s}O^{-}$	0	0	0	1	0	0	-1	-1	-8.93	0
	24	$Fe^{s}OHCa^{2+}$	1	0	0	1	0	0	2	0	4.97	0
	25	$Fe^{s}OFe^{+}$	0	0	1	1	0	0	1	-1	1	0
	26	$Fe^{s}O2UO2$	0	0	0	1	0	1	0	-2	-2.57	0
	27	$Fe^{s}O2UO2CO32-$	0	1	0	1	0	1	-2	0	3.67	0
	28	$Fe^{w}OH$	0	0	0	0	1	0	0	0	0	0
	29	$Fe^{w}OH_2^{+}$	0	0	0	0	1	0	1	1	7.29	0
	30	$Fe^{w}O^{-}$	0	0	0	0	1	0	-1	-1	-8.93	0
	31	$Fe^{w}OCa^{+}$	1	0	0	0	1	0	1	-1	-5.85	0
	32	$Fe^{w}OFe^{+}$	0	0	1	0	1	0	1	-1	0.5	0
	33	$Fe^{w}O2UO2$	0	0	0	0	1	1	0	-2	-6.28	0
	34	$Fe^{w}O2UO2CO32-$	0	1	0	0	1	1	-2	0	-0.42	0
	35	OH^{-}	0	0	0	0	0	0	0	-1	-14	1
	36	H^{+}	0	0	0	0	0	0	0	1	0	1
		IONZ:	2	-2	2	0	0	2	0	1		

$J \equiv Flux$



c_j = component j

x_i = species i of component j

$a_{i,j}$ = stoichiometric coefficienct of component j in species i

C_j = total aqueous conc of component j

τ = flushing rate constant

$fout$ = 1 for mobile (aqueous) species
0 for immobile (sorbed) species

$$Jin_j = tCin_j$$

$$Jout_j = t\sum_i a_{i,j} x_j \, fout_i$$

Cin_j = conc of C_j in inflow

$$\frac{dC_j}{dt} = Jin_j - Jout_j + \sum Rxns$$

Solution procedure for each time step:

1. Compute equilibrium speciation using MICROQL algorithm
2. Compute input/outplut fluxes (mobile components) and reaction rates
3. Transmit dC_j/dt's to ODE solver with specified truncation error limit (e_{max})
4. Take step and compute ε_j's
5. All ε_j's < e_{max}?
   Yes: update C_j's and go on to next time step
   No: don't update C_j's, reduce Δt, go back to step 1.

Fig. 1. Diagram of the operation of the semicontinuous (REV) simulation model

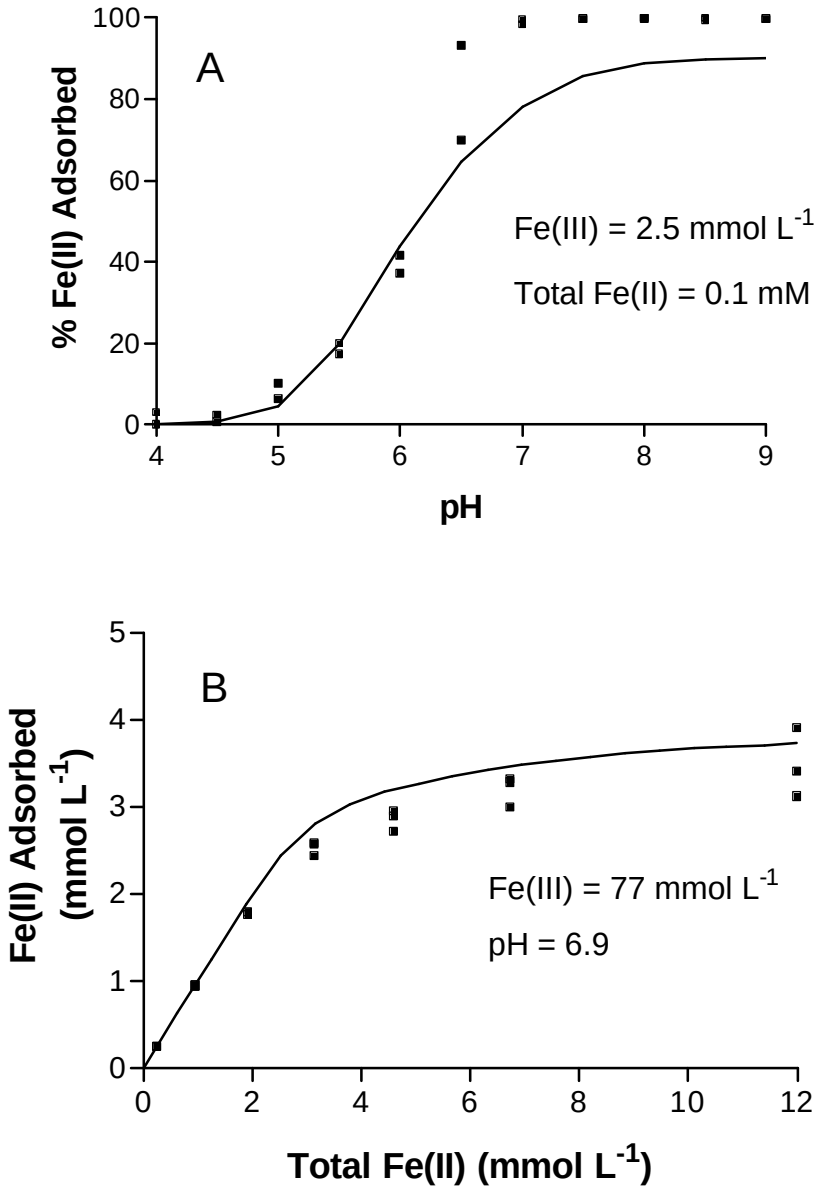


Fig. 2. Fe(II) sorption edge (upper) and isotherm (lower) for synthetic FeOOH-coated sand. Edge sorption data are unpublished data of E. Roden and M. Urrutia; isotherm sorption data are from Roden et al. (2000)

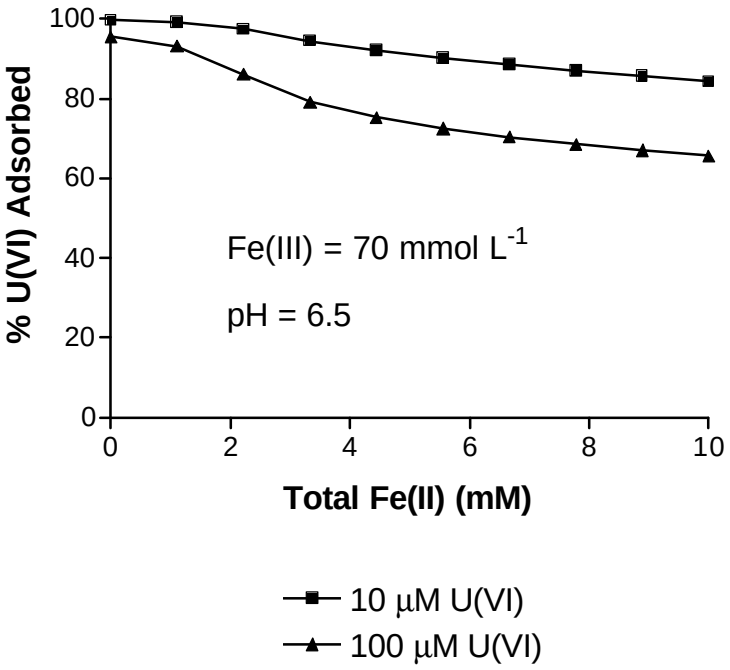


Fig. 3. Predicted (MINEQL+) influence of competitive Fe(II) sorption on U(VI) complexation by synthetic FeOOH-coated sand. See text for description of model parameters.

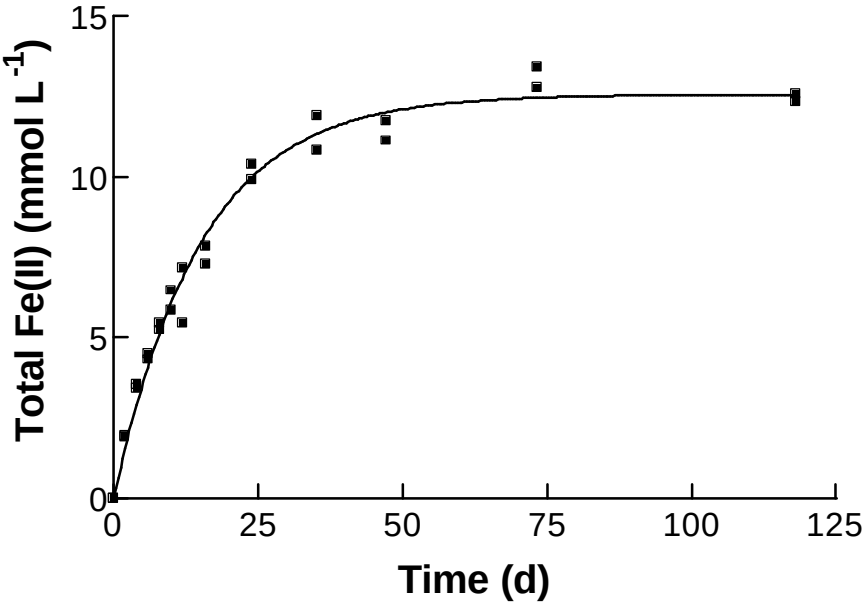


Fig. 4. Accumulation of total (aqueous+solid-phase) Fe(II) during synthetic FeOOH-coated sand reduction by *S. putrefaciens* in the batch culture experiment conducted in conjuction with the column Fe(III) oxide reduction experiment reported in Roden et al. (2000). The solid line represents a nonlinear least-squares fit (GraphPad Prism™) of the data to the following equation which depicts Fe(II) accumulation from first-order reduction of a finite number of "free" surface Fe(III) reduction sites, as described in Roden and Urrutia (1999).

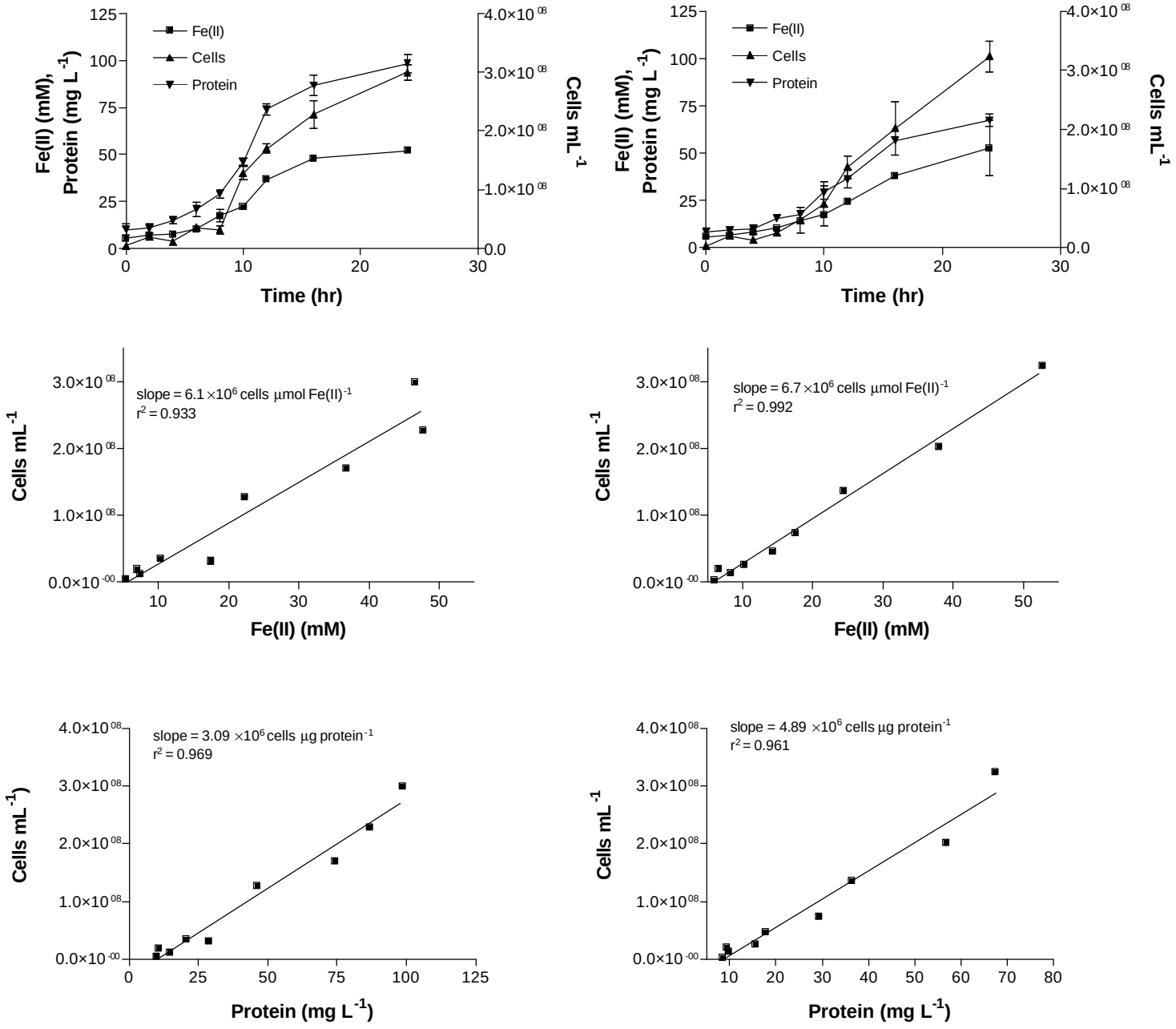


Fig. 5. Growth of *S. alga* (left panels) and *G. metallireducens* (right panels) with Fe(III)-citrate (50 mM) as an electron acceptor and lactate (*S. alga*) or acetate (*G. metallireducens*) as an electron donor. Cell numbers were determined by acridine orange direct count, and protein was determined by the bicinchoninic acid method after NaOH digestion. (Roden and Urrutia, manuscript in preparation).

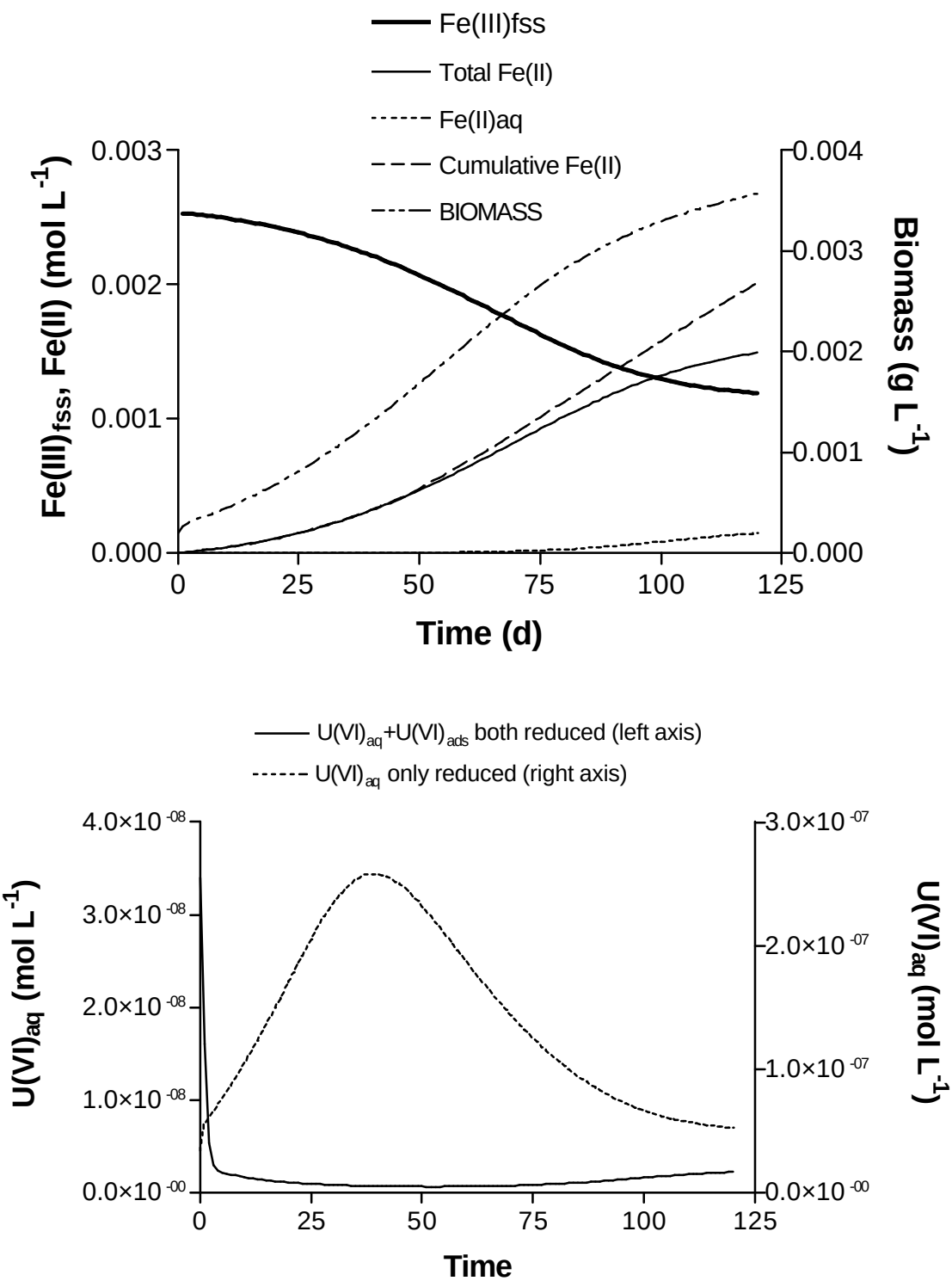
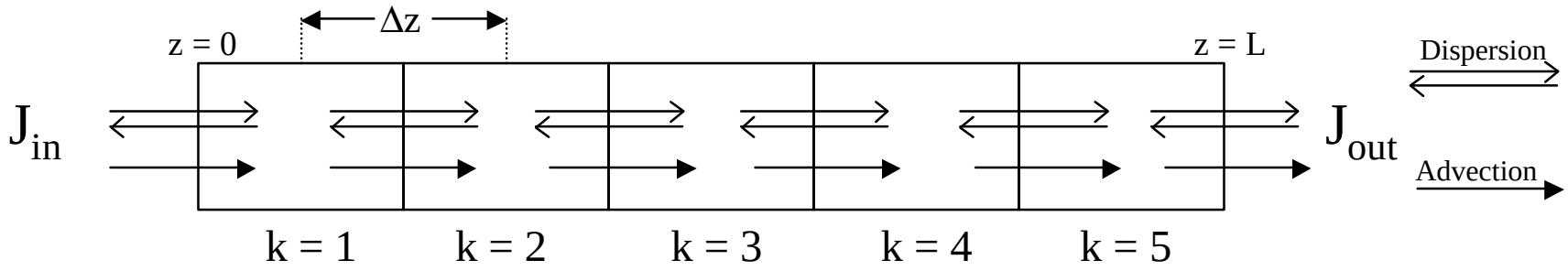


Fig. 6. Results of two runs of the SC (REV) Fe(III) oxide/U(VI) reduction simulation model, allowing either aqueous and adsorbed U(VI) to be reduced, or only aqueous U(VI) to be reduced. Fe(III) reduction and MeRB growth were similar in both cases; therefore data for the former case only are shown in the top panel.



Simulate dispersive and advective fluxes between boxes by finite differences, using central differencing for dispersion, and blended central/upwind differencing for advection. Transport acts only on mobile species of components C_j

$$\frac{dC_{j,k}}{dt} = Jin_{j,k}^{Disp} + Jin_{j,k}^{Adv} - Jout_{j,k}^{Disp} - Jout_{j,k}^{Adv} + \sum Rxns$$

$C_{j,k}$ = total aqueous conc of component j in box k

Boundary conditions:

$$z = 0, Jin_j = -D\frac{\partial C_{j,0}}{\partial z} + vC_{j,0}$$

Flux (third kind) boundary condition

$$z = L, \frac{\partial C_{j,k}}{\partial z} = 0$$

Zero gradient (Neumann) boundary condition

Solution procedure
For each time step:

1. Compute equil speciation in each box
2. Compute dispersive & advective flux rates of dissolved constituents among boxes
3. Compute reaction rates in each box
4. Transmit stack of $dC_{i,k}/dt$'s to ODE solver with specified truncation error limit (e_{max})
5. Take step and compute $\varepsilon_{j,k}$'s
6. All $\varepsilon_{j,k}$'s < e_{max})?
   Yes: update $X_{j,k}$'s and go onto next time step
   No: don't update $X_{j,k}$'s; reduce Δt, go back to 1

Fig. 7. Diagram of the 1-dimensional transport-reaction simulation model

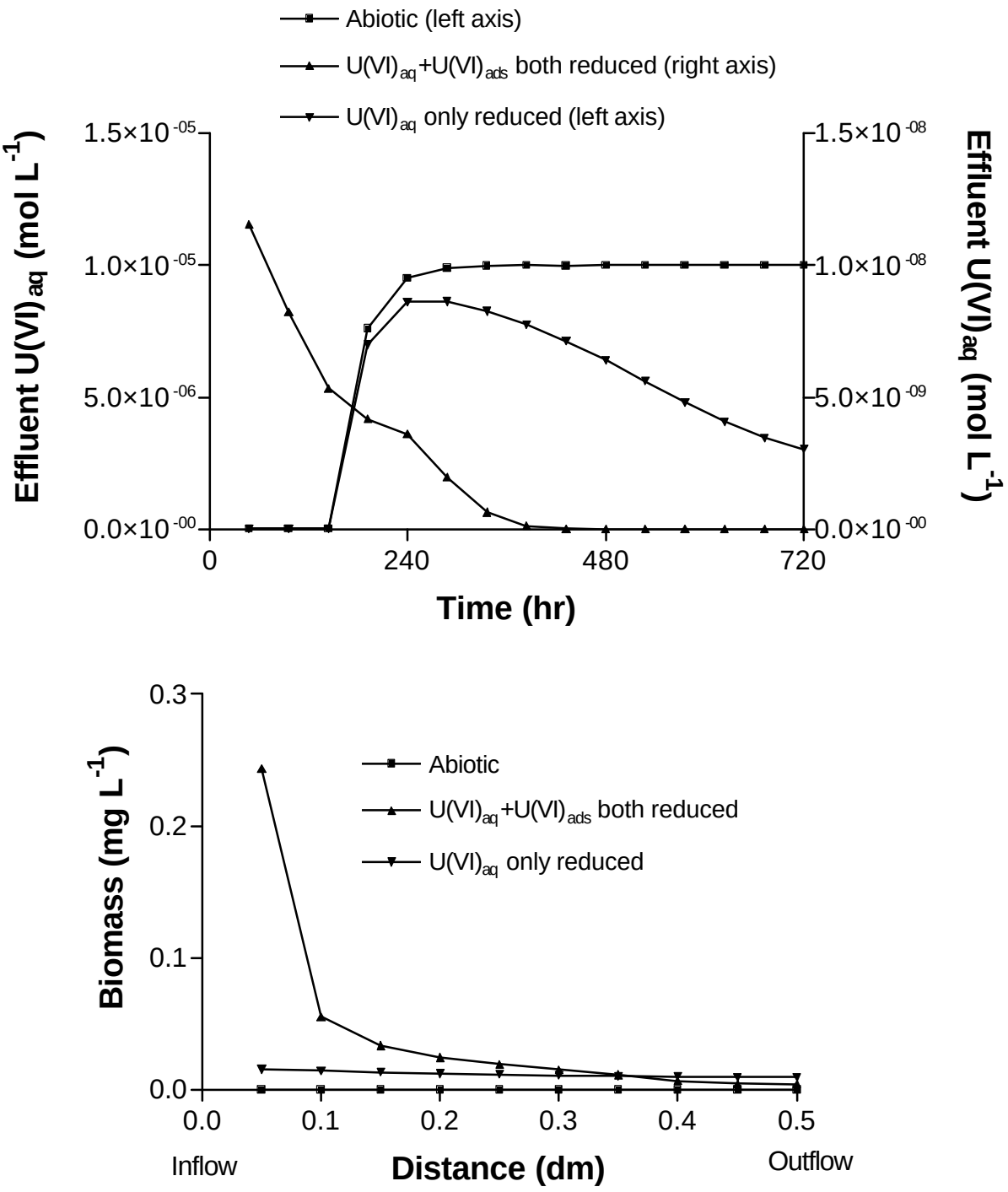


Fig. 8. Results of three runs of the 1-D transport-reaction simulation model, allowing either no reduction activity (Abiotic), FeOOH reduction and reduction of both aqueous and sorbed U(VI), or FeOOH reduction and only aqueous U(VI) reduction. Upper panel shows breakthrough curves for aqueous U(VI); lower panel shows distribution of MeRB biomass vs. distance along the column at the end of the simulation.

Appendix 2: Numerical simulation of U(VI) reductive immobilization in Fe(III) oxide-reducing subsurface sediments

One-dimensional simulation of U(VI) reactive transport in a hypothetical Fe(III) oxide-reducing column reactor

1. Background

Uranium (U) is an important radionuclide contaminant in soils and subsurface sediments at nuclear weapons manufacturing and uranium mining sites in the U.S. and abroad (BRADLEY et al., 1996; LANDA and GRAY, 1995). Uranium typically exists in the +6 oxidation state (U(VI)) in oxygenated aqueous solutions (LANGMUIR, 1997). In the absence of abundant complexing ligands, U(VI) exists in solution as the UO_2^+ ion at circumneutral pH. When dissolved inorganic carbon (DIC = CO_3^{2-} + HCO_3^- + H_2CO_3) is abundant, U(VI) forms stable aqueous carbonate complexes such as UO_2CO_3 and $UO_2(CO3)_2^{2-}$ (LANGMUIR, 1997).

Aqueous U(VI) species are subject to complexation by particle (mineral) surfaces in soils and sediments, in particular Fe(III) oxide surfaces (TICKNOR, 1994). Surface complexation ('sorption') of U(VI) can attenuate the migration of uranium in groundwater aquifer sediments. However, aqueous complexation of U(VI) by carbonate ions decreases the tendency of U(VI) to bind to particle surfaces (WAITE et al., 1994), leading to enhanced subsurface uranium migration. Since many subsurface environments contain substantial amounts of DIC, uranium can be relatively mobile in groundwater. As a result, there is substantial interest on the part of the U.S. Department of Energy in development of technologies for retarding uranium migration in subsurface sediments (NRC, 2000).

One possible approach for immobilization of uranium in the subsurface involves the activity of dissimilatory metal-reducing bacteria (MeRB) (GORBY and LOVLEY, 1992; LOVLEY and PHILLIPS, 1992; LOVLEY et al., 1991). Under anaerobic conditions, MeRB catalyze enzymatic reduction of U(VI) to U(IV) (2 electron transfer) via reactions such as:

$$2U(VI) + CH_2O \rightarrow 2U(IV) + HCO_3^-$$

where CH_2O represents a generic unit of organic carbon. The significance of this reaction in terms of uranium mobility stems from the fact that uranium in the +4 oxidation state tends to formation an insoluble mineral precipitate called *uraninite*, $UO_2(s)$ (LANGMUIR, 1978). As a result, microbial uranium reduction can provide a mechanism for immobilization of uranium in subsurface environments via reactions such as:

$$2U(VI) + CH_2O \rightarrow 2UO_2(s) + HCO_3^-$$

A prerequisite for this process to operate effectively is the existence of anaerobic conditions in aquifer sediments, because the MeRB which drive the above reaction are active only in the absence of molecular oxygen (O_2). Thus, unless a uranium-contaminated aquifer is *already* anaerobic, it would necessary to induce anaerobic conditions, e.g. through addition of large amounts of easily-degradable organic carbon, aerobic respiration of which would quickly utilize dissolved oxygen and render the system anaerobic. For the simulations to be conducted here, we

will assume that the subsurface environment is already anaerobic, such that MeRB have the potential to become active in U(VI) reduction when provided with organic substrates. More advanced subsurface reactive transport simulations would include molecular oxygen as a reactive species, whose distribution (controlled by a combination of chemical and microbial reactions together with physical transport) would have a major impact on the fate of uranium.

It is important to note that the MeRB which can reduce/precipitate uranium are the same organisms which can utilize Fe(III) oxides as electron acceptors for anaerobic respiration (LOVLEY, 1995). This is advantageous in relation to harnessing the activities of MeRB for uranium immobilization in the subsurface. Many subsurface sediments contain substantial quantities of Fe(III) oxides. In such environments, addition of electron donors and nutrients would stimulate utilization of the large supply of endogenous electron acceptor provided by the Fe(III) oxides to generate and maintain a relatively large biomass of MeRB. The MeRB biomass could then immobilize uranium moving through the treatment zone. This "*in situ* biogenic redox manipulation" concept is illustrated by the following simple reaction scheme:

Organic carbon + nutrients + Fe(III) oxides → Inorganic carbon + Fe(II) + MeRB

Organic carbon + U(VI) + MeRB → Inorganic carbon + UO_2(s)

If eventual removal of uranium is desirable, the treatment zone could be created immediately down-stream of the leading edge of the contaminant plume, so that as U(VI) moves into the zone and is reductively immobilized, the uranium becomes concentrated within a relatively narrow zone (or slowly advancing front) (Fig. 1). Conceptually, this set of interactions is analogous to processes involved in the formation of roll-front geological uranium ore deposits, in which U(VI) becomes reductively precipitated along an advancing front localized at the current interface between oxidized and reduced aquifer zones (LANGMUIR, 1997). In fact, the activity of dissimilatory MeRB is thought to be responsible for the formation of such deposits (LOVLEY, 1993; LOVLEY et al., 1991).

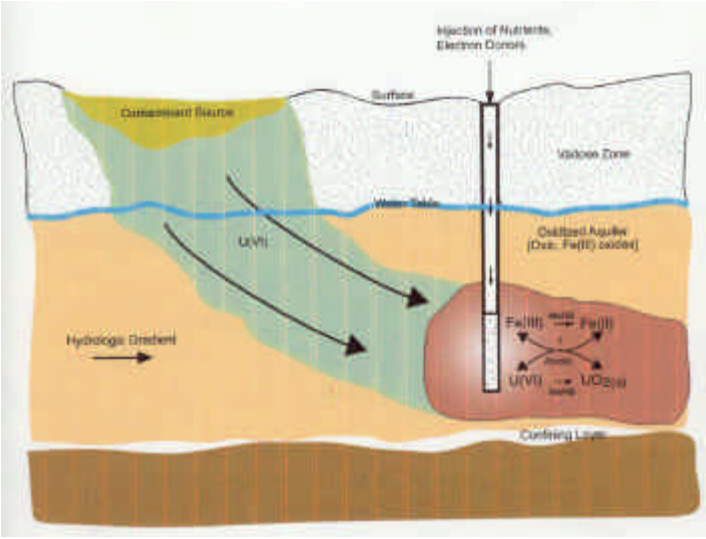


Fig. 1. Subsurface stabilization of uranium via reductive immobilization. Adapted from McCullough, J., T.C. Hazen, S.M. Benson, F.B. Metting, and A.C. Palmisano. 1999. Bioremediation of metals and radionuclides…What it is and how it works. U.S. Department of Energy, Natural and Accelerated Bioremediation Research

2. Preliminary simulation model

A preliminary 1-D simulation model of coupled Fe(III) oxide-U(VI) reduction in a hypothetical laboratory column reactor (Fig. 2) has been developed. The intent of the simulations

was to illustrate how reactive transport experiments to be conducted in our experimental research will be interpreted in a modeling context. In addition, a sensitivity analysis was performed to assess how variability in Fe(III) oxide abundance and key kinetic reaction parameters might influence the effectiveness of U(VI) reductive immobilization. As emphasized recently by Szecsody et al. (1998), combined experimental and modeling studies in laboratory reactors represents the initial step in transferring basic mechanistic information on geochemical (and biogeochemical) processes to larger-scale field systems.

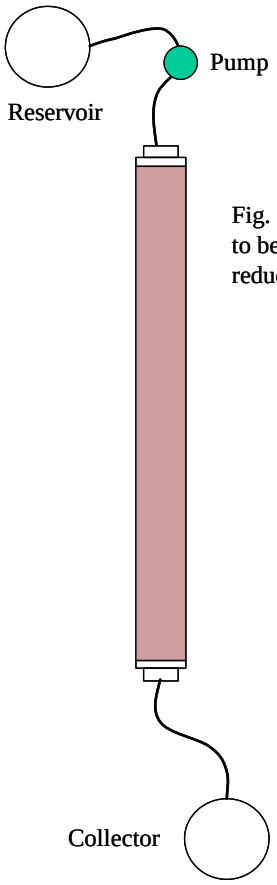


Fig. 2. Diagram of column reactors to be used in U(VI)/Fe(III) oxide reduction experiments.

A detailed summary of the reactive transport model, including description of equilibrium and kinetic parameter values and their origin, is given in Appendix 1. The size of the reactor considered in the simulations (1 dm) is typical of that used in laboratory reactive transport experiments and comparable in size to the reactors to be used in the proposed research. The fluid flow rate in the simulations was set at 0.5 dm d^{-1}, which assuming 50 % porosity corresponds to a 1-d residence time for pore fluid in the reactor. While this is a relatively short residence time compared to typical field conditions, such short residence times are required to obtain meaningful results in laboratory experiments with durations of weeks-to-months. As emphasized recently by Szecsody et al. (1998), combined experimental and modeling studies in laboratory reactors represents the initial step in transferring basic mechanistic information on geochemical (and biogeochemical) processes to larger-scale field systems.

The 1 dm spatial domain of the hypothetical laboratory column was discretized on an even grid with 0.1 dm node spacing. The transport-reaction simulations included 9 independent variables, and 8 chemical components involved in a total of 36 equilibrium speciation reactions. The equilibrium speciation system included competitive surface complexation of U(VI), Fe^{2+}, and Ca^{2+} according to the diffuse double layer model as described in Dzombak and Morel (1990). Inclusion of U(VI) surface complexation is critical to modeling the fate of U(VI) in Fe(III) oxide-bearing subsurface sediments, as such materials have a high affinity and capacity for U(VI) sorption (BARNETT et al., 2000). Hence, assessment of the potential impact of enzymatic U(VI) reduction on U(VI) immobilization must take abiotic sorption processes into account. Surface complexation of biogenic Fe(II) was included in the simulations in order to account for the inhibitory effect of surface-bound Fe(II) on bacterial reduction of Fe(III) oxides (RODEN and URRUTIA, 1999); see Appendix 1), as well as the influence of competitive Fe(II) sorption on U(VI) retardation. For simplicity, pH was fixed at 6.5 during all simulation runs.

Three kinetic reactions were considered in the model: (1) production of Fe(II) via microbial reduction of "free" Fe(III) oxide surface sites according to an electron donor-dependent, biomass-specific first-order reduction rate constant; (2) microbial reduction of aqueous U(VI) to insoluble UO_2(s) according to an electron donor-dependent, biomass-specific Monod-style rate expression (note: U(IV) produced via enzymatic U(VI) reduction was assumed to undergo instantaneous conversion to insoluble UO_2(s)); and (3) production of metal-reducing bacterial (MeRB) biomass coupled to Fe(III) oxide and U(VI) reduction. In addition, a generalized first-order cell death/maintenance rate constant was included to prevent unrealistic biomass accumulation. Parallel reduction of Fe(III) oxides and aqueous U(VI) was permitted to occur in the simulations, in accordance with recent experimental studies (FREDRICKSON et al., 2000; WIELINGA et al., 2000). Although the potential exists for abiotic reduction of U(VI) by surface-bound Fe(II) (FREDRICKSON et al., 2000; LIGER et al., 1999), the efficiency of this reaction has not yet been proven, and is likely to be strongly pH-dependent (LIGER et al., 1999). Available information suggests that direct microbial U(VI) reduction is likely to be much faster and more complete than abiotic reduction, assuming that potential kinetic limitations on enzymatic reduction (discussed above) are not prohibitive. Hence, such reactions were not included in the current simulations. Other researchers within the NABIR and other DOE research programs are addressing the potential for abiotic U(VI) reduction by surface-bound Fe(II) species. Should this process emerge as an important mechanism for U(VI) reduction in subsurface sediments, information provided by these researchers will be used to develop appropriate kinetic terms for inclusion of this process in reactive transport simulations of U(VI) reductive immobilization.

3. Results of preliminary simulations

A series of six-month (180 d) simulations were conducted using a range of bulk Fe(III) oxide concentrations (5-100 mmol dm^{-3}) in order to examine the potential influence of MeRB growth coupled to Fe(III) reduction on enzymatic reductive immobilization of U(VI), which was present (mainly in the form of UO_2CO_3 and $UO_2(CO_3)_2^{2-}$ complexes) at a concentration of 10 μM in the column influent. The results demonstrated that bacterial Fe(III) oxide reduction and MeRB growth had a dramatic influence on U(VI) scavenging. Breakthrough of U(VI) took place after ca. 20 days in abiotic simulations with 50 mmol Fe(III) dm^{-3} (Fig. 3A). U(VI)

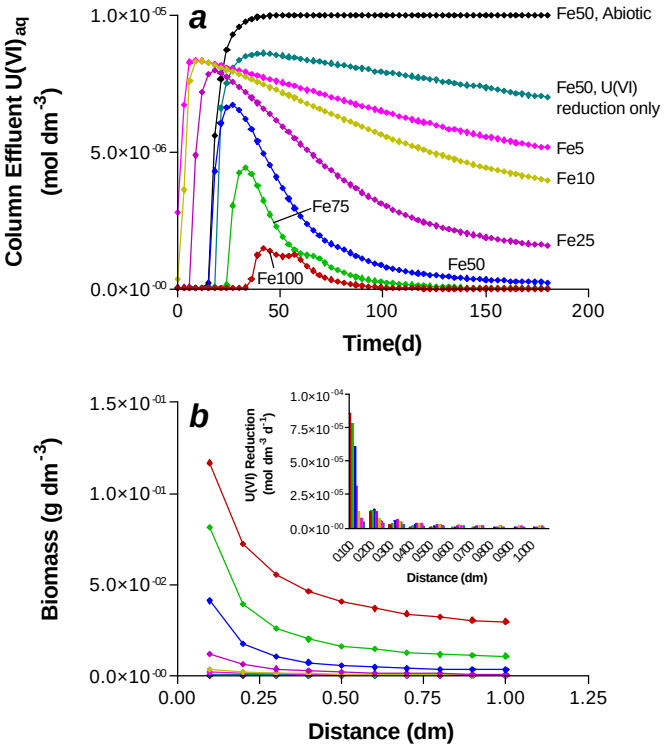


Fig. 3. Panel A: simulated breakthrough of U(VI) with different starting concentrations of Fe(III) oxide under conditions of both Fe(III) and U(VI) reduction, with U(VI)reduction only ,or with neither Fe(III) nor U(VI) reduction (abiotic). Panel B: biomass concentration profile at the end of the simulation period (t = 180d); inset shows rate of U(VI) reduction at the end of the simulation period.

was only poorly scavenged in simulations in which U(VI) reduction but not Fe(III) oxide reduction was active. In contrast, U(VI) was intensively scavenged in simulations of columns containing 50-100 mmol Fe(III) dm^{-3} in which both Fe(III) oxide reduction and U(VI) reduction were active. Less intensive (but still significantly greater than in the U(VI) reduction-only case) scavenging occurred in simulations with 5-25 mmol Fe(III) dm^{-3}. The increased effectiveness of U(VI) reductive immobilization in columns containing increasing amounts of Fe(III) oxide was associated with major increases in MeRB biomass and U(VI) reduction rate (Fig. 3B) along the length of the column reactor. These results strongly suggest that variations in Fe(III) oxide abundance on spatial scales ≥ 1 m (such as those observed at the Oyster site and in other DOE subsurface environments) are likely to have a major impact on the effectiveness of redox-sensitive metal-radionuclide bioremediation vis-à-vis their influence on the growth and activity of MeRB.

A series of simulations was conducted to examine the sensitivity of U(VI) scavenging in columns containing 50 mmol Fe(III) dm^{-3} to changes in key kinetic reaction parameters such as (i) the biomass-specific first-order reduction Fe(III) reduction rate constant; (ii) the maximum biomass-specific rate of U(VI) reduction; (iii) the half-saturation constant for U(VI) reduction; and (iv) the first-order MeRB death/maintenance coefficient. Halving or doubling the values of these coefficients led to 2 to 5-fold changes in the overall effectiveness of U(VI) fixation, as measured by the difference between total U(VI) input and total U immobilization (see Fig. 4). These results emphasize the critical importance of obtaining (e.g. by a combination of direct experimentation and simulation modeling) reasonably constrained values for kinetic parameters used in transport-reaction models of subsurface metal-radionuclide behavior.

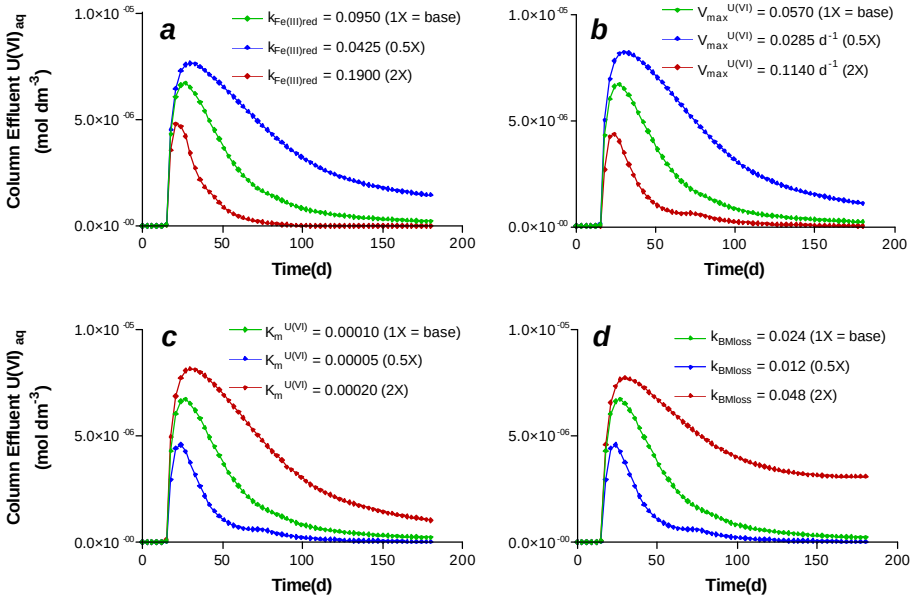


Fig. 4. Simulated breakthrough of U(VI) with different parameter values for (*a*) the biomass-specific first-order reduction Fe(III) reduction rate constant; (*b*) the maximum biomass-specific rate of U(VI) reduction; (*c*) the half-saturation constant for U(VI) reduction; and (*d*) the first-order MeRB death/maintenance coefficient.

References

Barnett M. O., Jardine P. M., Brooks S. C., and Selim H. M. (2000) Adsorption and transport of U(VI) in subsurface media. *Soil Sci. Soc. Am. J.* **64**, 1-43.

Bradley D. J., Frank C. W., and Mikerin Y. (1996) Nuclear contamination from weapon complexes in the former Soviet Union and the United States. *Phys. Today* **49**, 40-45.

Dzombak D. A. and Morel F. M. M. (1990) *Surface complexation modeling: hydrous ferric oxide*. John Wiley & Sons.

Fredrickson J. K., Zachara J. M., Kennedy D. W., Duff M. C., Gorby Y. A., Li S. W., and Krupka K. M. (2000) Reduction of U(VI) in goethite (α-FeOOH) suspensions by a dissimilatory metal-reducing bacterium. *Geochim. Cosmochim. Acta* **64**, 3085-3098.

Gorby Y. A. and Lovley D. R. (1992) Enzymatic uranium precipitation. *Environ. Sci. Technol.* **26**, 205-207.

Landa E. R. and Gray J. R. (1995) U.S. Geological Survey research on the environmental fate of uranium mining and milling wastes. *Environ. Geol.* **26**, 19-31.

Langmuir D. (1978) Uranium solution-mineral equilibria at low temperatures with applications to sedimentary ore deposits. *Geochim. Cosmochim. Acta* **42**, 547-569.

Langmuir D. (1997) *Aqueous Environmental Geochemistry*. Prentice Hall.

Liger E., Charlet L., and VanCapellen P. (1999) Surface catalysis of uranium(VI) reduction by Fe(II). *Geochim. Cosmochim. Acta* **63**, 2939-2955.

Lovley D. R. (1993) Dissimilatory metal reduction. *Annu. Rev. Microbiol.* **47**, 263-290.

Lovley D. R. (1995) Bioremediation of organic and metal contaminants with dissimilatory metal reduction. *Journal of Industrial Microbiology* **14**, 85-93.

Lovley D. R. and Phillips E. J. P. (1992) Bioremediation of uranium contamination with enzymatic uranium reduction. *Environ. Sci. Technol.* **26**, 2228-2234.

Lovley D. R., Phillips E. J. P., Gorby Y. A., and Landa E. R. (1991) Microbial reduction of uranium. *Nature* **350**, 413-416.

NRC. (2000) *Research needs in subsurface science*. National Academy Press.

Roden E. E. and Urrutia M. M. (1999) Ferrous iron removal promotes microbial reduction of crystalline iron(III) oxides. *Environ. Sci. Technol.* **33**, 1847-1853.

Szecsody J. E., Zachara J. M., Chilakapati A., Jardine P. M., and Ferrency A. S. (1998) Importance of flow and particle-scale heterogeneity on $Co^{II/III}$EDTA reactive transport. *J. Hydrol* **209**, 112-136.

Ticknor K. V. (1994) Uranium sorption on geological materials. *Radiochim. Acta* **64**, 229-236.

Waite T. D., Davis J. A., Payne T. E., Waychunas G. A., and Xu N. (1994) Uranium(VI) adsorption to ferrihydrite: Application of a surface complexation model. *Geochim. Cosmochim. Acta* **58**, 5465-5478.

Wielinga B., Bostick B., Hansel C. M., Rosenzweig R. F., and Fendorf S. (2000) Inhibition of bacterially promoted uranium reduction: ferric (hydr)oxides as competitive electron acceptors. *Environ. Sci. Technol.* **34**, 2190-2195.

Appendix – Description of one-dimensional reactive transport model of coupled bacterial Fe(III) -U(VI) reduction in a hypothetical laboratory column reactor

A. Components (basis species) in equilibrium speciation system:

1. Ca^{2+} (aqueous uncomplexed Ca)
2. CO_3^{2-} (aqueous uncomplexed carbonate ion)
3. Fe^{2+} (aqueous uncomplexed ferrous iron)
4. $Fe^{sr}OH$ (protonated "strong" binding site on Fe(III) oxide surface)
5. $Fe^{wk}OH$ (protonated "weak" binding site on Fe(III) oxide surface)
6. UO_2^{+} (aqueous uncomplexed uranyl ion)
7. f(Ψ) (electrostatic surface complexation interaction term)
8. H^{+} (aqueous uncomplexed hydrogen ion)

Following the notation of Kirkner and Reeves (1988), the vector of total component concentrations (equal to the sum of the concentration of the uncomplexed component plus all complexes which contain that component) is designated by $\mathbf{w} \equiv w_1, w_2, \ldots, w_{Nc}$, where N_c is the number of components in the equilibrium speciation system.

For the problem considered here, N_c=8 and

$\mathbf{w} = (Ca^{2+}{}_T, CO_3^{2-}{}_T, Fe^{2+}{}_T, Fe^{sr}OH_T, Fe^{wk}OH_T, UO_2^{+}{}_T, f(\Psi), TOTH)$

In formulating equilibrium speciation systems, each complex (species) is considered to be the product of a reaction among one or more of the components. Such reactions are depicted in general form as (Kirkner and Reeves, 1988):

$$\sum_{j=1}^{N_c} a_{ij} c_j^* \Leftrightarrow x_i^* \qquad (1)$$

where

c^*_j = chemical formula for component j
x^*_i = chemical formula for complex i
a_{ij} = stoichiometric coefficient
K_i = equilibrium constant for complex i

The mass action and mass balance equations listed below constitute the aqueous/solid-phase equilibrium system for the uranium reactive transport problem under consideration. *It should be noted that this equilibrium speciation system* ***does not include mineral precipitation/dissolution reactions***. Although such reactions may be relevant for simulation of subsurface uranium transport (e.g. for depicting the precipitation/dissolution of uraninite), *when/if such reactions are included they will be described by kinetic rather than equilibrium reactions,* for reasons which are explained in detail in Steefel and Lasaga (1994).

B. Mass action and mass balance equations for equilibrium speciation system

Mass-Action Equations

Reaction	log K
1. $Ca^{2+} \Leftrightarrow Ca^{2+}$	0.00
2. $Ca^{2+} + H_2O - H^+ \Leftrightarrow CaOH^+$	-12.78
3. $Ca^{2+} + CO_3^{2-} + H^+ \Leftrightarrow CaHCO_3^+$	11.44
4. $Ca^{2+} + CO_3^{2-} \Leftrightarrow CaCO_3(aq)$	3.22
5. $CO_3^{2-} + 2H^+ \Leftrightarrow H_2CO_3$	16.68
6. $CO_3^{2-} + H^+ \Leftrightarrow HCO_3^-$	10.33
7. $CO_3^{2-} \Leftrightarrow CO_3^{2-}$	0.00
8. $Fe^{2+} \Leftrightarrow Fe^{2+}$	0.00
9. $Fe^{2+} + H_2O - H^+ \Leftrightarrow FeOH^+$	-9.50
10. $Fe^{2+} + CO_3^{2-} + H^+ \Leftrightarrow FeHCO_3^+$	12.33
11. $Fe^{2+} + CO_3^{2-} \Leftrightarrow FeCO_3(aq)$	5.50
12. $Fe^{2+} + 2CO_3^{2-} \Leftrightarrow Fe(CO_3)_2^{2-}$	7.10
13. $UO_2^+ \Leftrightarrow UO_2^+$	0.00
14. $UO_2^+ + H_2O - H^+ \Leftrightarrow UO_2OH^+$	-5.09
15. $UO_2^+ + 2H_2O - 2H^+ \Leftrightarrow UO_2(OH)_2$	-12.0
16. $2UO_2^+ + 2H_2O - 2H^+ \Leftrightarrow (UO_2)_2(OH)_2^{2+}$	-5.65
17. $3UO_2^+ + 5H_2O - 5H^+ \Leftrightarrow (UO_2)_3(OH)_5^+$	-15.93
18. $UO_2^+ + CO_3^{2-} \Leftrightarrow UO_2CO_3$	10.07
19. $UO_2^+ + 2CO_3^{2-} \Leftrightarrow UO_2(CO_3)_2^{2-}$	17.01
20. $UO_2^+ + 3CO_3^{2-} \Leftrightarrow UO2(CO_3)_3^{4-}$	21.38
21. $Fe^{sr}OH \Leftrightarrow Fe^{sr}OH$	0.00
22. $Fe^{sr}OH + H^+ + f(\Psi) \Leftrightarrow Fe^{sr}OH_2^+$	7.29
23. $Fe^{sr}OH - H^+ - f(\Psi) \Leftrightarrow Fe^{sr}O^-$	-8.93
24. $Fe^{sr}OH + Ca^{2+} + 2f(\Psi) \Leftrightarrow Fe^{sr}OHCa^{2+}$	4.97
25. $Fe^{sr}OH + Fe^{2+} - H^+ + f(\Psi) \Leftrightarrow Fe^{sr}OFe^+$	1.00
26. $Fe^{sr}OH + UO_2^+ + H_2O - 2H^+ \Leftrightarrow Fe^{sr}O_2UO_2$	-2.57
27. $Fe^{sr}OH + UO_2^+ + CO_3^{2-} - 2f(\Psi) \Leftrightarrow Fe^{sr}OHUO_2CO_3^{2-}$	3.67
28. $Fe^{wk}OH \Leftrightarrow Fe^{wk}OH$	0.00
29. $Fe^{wk}OH + H^+ + f(\Psi) \Leftrightarrow Fe^{wk}OH_2^+$	7.29
30. $Fe^{wk}OH - H^+ - f(\Psi) \Leftrightarrow Fe^{wk}O^-$	-8.93
31. $Fe^{wk}OH + Ca^{2+} - H^+ + f(\Psi) \Leftrightarrow Fe^{wk}OCa^+$	-5.85
32. $Fe^{wk}OH + Fe^{2+} - H^+ + f(\Psi) \Leftrightarrow Fe^{wk}OFe^+$	0.50
33. $Fe^{wk}OH + UO_2^+ + H_2O - 2H^+ \Leftrightarrow Fe^{wk}O_2UO_2$	-6.28
34. $Fe^{wk}OH + UO_2^+ + CO_3^{2-} - 2f(\Psi) \Leftrightarrow Fe^{wk}OHUO_2CO_3^{2-}$	-0.42
35. $H_2O - H^+ \Leftrightarrow OH^-$	-14.00

36. $H^+ \Leftrightarrow H^+$ 0.00

Mass balance equations

$$Ca^{2+}_T = [Ca^{2+}] + [CaOH^+] + [CaHCO_3^+] + [CaCO_3(aq)] + [Fe^{sr}OHCa^{2+}] + [Fe^{wk}OCa^+]$$

$$CO_3^{2-}_T = [CO_3^{2-}] + [HCO_3^-] + [H_2CO_3] + [CaHCO_3^+] + [CaCO_3(aq)] + [FeHCO_3^+] + [FeCO_3(aq)] + 2[Fe(CO_3)_2^{2-}] + [UO_2CO_3] + 2[UO_2CO_3] + 3[UO2(CO_3)_3^{4-}] + [Fe^{sr}OHUO_2CO_3^{2-}] + [Fe^{wk}OHUO_2CO_3^{2-}]$$

$$Fe^{2+}_T = [Fe^{2+}] + [FeOH^+] + [FeHCO_3^+] + [FeCO_3(aq)] + [Fe(CO_3)_2^{2-}] + [Fe^{sr}OFe^+] + [Fe^{wk}OFe^+]$$

$$Fe^{sr}OH_T = [Fe^{sr}OH] + [Fe^{sr}OH_2^+] + [Fe^{sr}O^-] + [Fe^{sr}OHCa^{2+}] + [Fe^{sr}OFe^+] + [Fe^{sr}O_2UO_2] + [Fe^{sr}OHUO_2CO_3^{2-}]$$

$$Fe^{wk}OH_T = [Fe^{wk}OH] + [Fe^{wk}OH_2^+] + [Fe^{wk}O^-] + [Fe^{wk}OCa^+] + [Fe^{wk}OFe^+] + [Fe^{wk}O_2UO_2] + [Fe^{wk}OHUO_2CO_3^{2-}]$$

$$UO_2^{+}_T = [UO_2^+] + [UO_2OH^+] + [UO_2(OH)_2] + 2[(UO_2)_2(OH)_2^{2+}] + 3[(UO_2)_3(OH)_5^+] + [UO_2CO_3] + [UO_2(CO_3)_2^{2-}] + [UO_2(CO_3)_3^{4-}] + [Fe^{sr}O_2UO_2] + [Fe^{sr}OHUO_2CO_3^{2-}] + [Fe^{wk}O_2UO_2] + [Fe^{wk}OHUO_2CO_3^{2-}]$$

$$f(\Psi)_T = 0.1174 * I^{0.5} * \sinh(19.46 * PSI) * SA * SC / 96487$$

where:
I = ionic strength
$PSI = -0.05916 * \log(\Psi)$

$$TOTH = -[CaOH^+] + [CaHCO_3^+] + 2[H_2CO_3] + [HCO_3^-] - [FeOH^+] + [FeHCO_3^+] - [UO_2OH^+] - 2[UO_2(OH)_2] - 2[(UO_2)_2(OH)_2^{2+}] - 5[(UO_2)_3(OH)_5^+] + [Fe^{sr}OH_2^+] - [Fe^{sr}O^-] - [Fe^{sr}OFe^+] - 2[Fe^{sr}O_2UO_2] + [Fe^{wk}OH_2^+] - [Fe^{wk}O^-] - [Fe^{wk}OCa^+] - [Fe^{wk}OFe^+] - 2[Fe^{wk}OHUO_2CO_3^{2-}] - [OH^-] + [H^+]$$

C. Notation for total aqueous and sorbed component concentrations

For the purpose of constructing the mass conservation equations, the following notation (based on that developed in Kirkner and Reeves, 1988) is used to represent the total aqueous or sorbed concentration of components in the chemical equilibrium system:

$f^{uw}_j(\mathbf{w})$ = total aqueous concentration of component j (2)

$f^{sw}_j(\mathbf{w})$ = total sorbed concentration of component j (3)

The total aqueous or sorbed concentration of a component is a nonlinear function of equilibrium speciation reactions among the components (i.e. it is a nonlinear function of $w_1, w_2, \ldots, w_{Nc}$). The

superscript notation “u” is used to denote the total aqueous concentration, whereas “s” indicates total sorbed concentration of U(VI).

D. Primary dependent variables (PDVs) for mass conservation equations

1. Fe(III) = solid-phase (immobile) ferric oxide mineral (mol dm_{ws}^{-3})*,†
2. CH_2O = aqueous organic carbon (mol dm^{-3}) (0.001)§
3. $Ca^{2+}{}_T$ = total (aqueous+sorbed) calcium* (mol dm^{-3}) (0.001)
4. $CO_3^{2-}{}_T$ = total (aqueous+sorbed) carbonate* (mol dm^{-3}) (0.0017)
5. $Fe^{2+}{}_T$ = total (aqueous+sorbed Fe(II))* (mol dm^{-3}) (1×10^{-15})
6. UO_2^{+} = total (aqueous+sorbed) U(VI) in form of uranyl ion* (mol dm^{-3}) (1×10^{-5})
7. TOTH = total acidic hydrogen, equal to the negative of alkalinity* (mol dm^{-3}) (0.0025)
8. UO_2(s) = solid-phase (immobile) uraninite (mol dm_{ws}^{-3})
9. BM = biomass (immobile) of MeRB (g dm_{ws}^{-3})

Subscript “ws” indicates “whole sediment”

* Dependent variable involved in equilibrium speciation reactions

† The concentration of Fe(III) oxide is connected to the equilibrium speciation system by virtue of the fact that the abundance of this mineral phase defines the abundance of strong and weak surface binding sites (see above) according to the following relationships:

$$[Fe^{sr}OH] = \frac{[Fe(III)]\times MW\times SA\times DNS1}{NA} \qquad (4)$$

$$[Fe^{wk}OH] = \frac{[Fe(III)]\times MW\times SA\times DNS2}{NA} \qquad (5)$$

where

MW= molecular weight of oxide mineral (g mol^{-1})
SA = specific surface area of oxide mineral (m^2g^{-1})
DNS1 = density of strong surface sites per unit oxide surface area (sites m^{-2})
DNS2 = density of weak surface sites per unit oxide surface area (sites m^{-2})
NA = Avagadro’s number

§ Numbers in parentheses indicate solute concentrations in the fluid entering the column reactor

E. Stoichiometric equations for Fe(III) oxide reduction and U(VI) reduction coupled to CH_2O oxidation:

$$4FeOOH + CH_2O + H_2O \rightarrow 4Fe^{2+} + HCO_3^- + 7OH^- \quad (6)$$

$$2U(VI) + CH_2O \rightarrow UO_2(s) + HCO_3^- \quad (7)$$

F. Mass conservation equations:

A generalized one-dimensional transport-reaction equation using notation appropriate for the problem considered here is as follows:

$$\frac{\partial(\phi w_j)}{\partial t} = L\left(f_j^{uw}(w)\right) + R_j^{f_j^{sw}(w)} + R_j^{kinetic} \quad (8)$$

where

$$L\left(f_j^{uw}(w)\right) = \frac{\partial}{\partial x}\left(-D\frac{\partial f_j^{uw}(w)}{\partial x} + v f_j^{uw}(w)\right) \quad \text{(advection-dispersion operator)}$$

with

ϕ = porosity, volume of fluid per unit bulk volume

v = steady-state fluid flow velocity in the column

D = coefficient of hydrodynamic dispersion, including molecular diffusion

$R_j^{f_j^{sw}(w)}$ = rate of accumulation of component j due to equilibrium sorption reactions

$R_j^{kinetic}$ = rate of accumulation of component j due to kinetic reactions

Notes:

(i) the above expressions assume that the PDV under consideration participates in equilibrium speciation reactions, which is not always the case (e.g. CH_2O, $UO_2(s)$, and BM in the equations below);

(ii) for PDVs which represent immobile precipitates or biomass, the advection-dispersion term is equal to zero (e.g. Fe(III) oxide, $UO_2(s)$, and BM in the equations below);

(iii) the term $R_j^{f_3^{sw}(\mathbf{w})}$ is omitted from the mass conservation expressions given below, since this term is accounted for implicitly when equilibrium speciation reactions are solved simultaneously with the transport-kinetic reaction equations.

1. Fe(III) (immobile)

$$\frac{\partial \mathrm{Fe(III)}}{\partial t} = -R_{\mathrm{Fe(III)}}$$

where

$$R_{\mathrm{Fe(III)}} = -k_{red} \frac{[CH_2O]}{} \frac{BM}{BM_{scal}} \left[Fe^{sr}OH_T + Fe^{wk}OH_T - f_3^{sw}(\mathbf{w}) \right]$$

with

$k_{Fe(III)red}$ = electron donor- and biomass-dependent first-order rate constant

K_m^{CH2O} = half-saturation CH_2O concentration for microbial Fe(III) oxide reduction

BM_{scal} = scaling factor used to make the Fe(III) reduction rate constant dependent the biomass of MeRB (BM).

$[Fe^{sr}OH_T + Fe^{wk}OH_T - f_3^{sw}(\mathbf{w})]$ = total number of strong and weak Fe(III) oxide sites minus the total sorbed Fe(II) concentration. This formulation implies that binding sites on the Fe(III) oxide surface occupied by sorbed Fe(II) are not available for microbial reduction – a phenomenon consistent with experimental studies of the geochemical/microbiological controls on this process (RODEN and URRUTIA, 1999; RODEN and ZACHARA, 1996; URRUTIA et al., 1998).

2. CH_2O

$$\frac{\partial(\phi CH_2O)}{\partial t} = L(CH_2O) - 0.25R_{\mathrm{Fe(III)}}$$

3. $Ca^{2+}{}_T$

$$\frac{\partial(\phi Ca^{2+}{}_T)}{\partial t} = L\left(f_1^{uw}(\mathbf{w}) \right)$$

4. $CO_3^{2-}{}_T$

$$\frac{\partial(\phi CO_{3\,T}^{2-})}{\partial t} = L\left(f_2^{uw}(w)\right) + 0.25R_{Fe(III)} + 0.5R_{U(VI)}$$

5. $Fe^{2+}{}_T$

$$\frac{\partial(\phi Fe^{2+}{}_T)}{\partial t} = L\left(f_3^{uw}(w)\right) + R_{Fe(III)}$$

6. $UO_2^{+}{}_T$

$$\frac{\partial(\phi UO_{2\,T}^{+})}{\partial t} = L\left(f_6^{uw}(w)\right) - R_{U(VI)}$$

where

$$R_{U(VI)} = -V\max\frac{[CH_2O]}{\left(K_m^{CH2O} + [CH_2O]\right)}\frac{f_6^{uw}(w)}{\left(K_m^{U(VI)} + f_6^{uw}(w)\right)}BM$$

with

$V_{max}{}^{U(VI)}$ = maximum electron donor and biomass-dependent rate of U(VI) reduction

$K_m{}^{CH2O}$ = half-saturation CH_2O concentration for microbial U(VI) reduction

$K_m{}^{U(VI)}$ = half-saturation U(VI) concentration for microbial U(VI) reduction

Note that all aqueous U(VI) species are subject to reduction at the same rate’

7. TOTH

$$\frac{\partial(\phi TOTH)}{\partial t} = L\left(f_8^{uw}(w)\right) - 2R_{Fe(III)} - 0.5R_{U(VI)}$$

8. UO_2*(s) (immobile)*

$$\frac{\partial UO_2(s)}{\partial t} = R_{U(VI)}$$

9. BM (immobile)

$$\frac{\partial BM}{\partial t} = Y_{Fe(III)} R_{Fe(III)} + Y_{U(VI)} R_{U(VI)} - k_d BM$$

where

$Y_{Fe(III)}$ = yield coefficient (g cells mol^{-1}) for growth coupled to Fe(III) oxide reduction
$Y_{U(VI)}$ = yield coefficient (g cells mol^{-1}) for growth coupled to U(VI) reduction
k_d = first-order death/maintenance constant

G. Boundary conditions

x = 0 (column inlet)

$$vw_{j,in} = -D \frac{\partial w_j}{\partial x} + vw_j$$ Flux (third kind) boundary condition

where

$w_{j,in}$ = total aqueous concentration of component j in the influent stream

x = L (column outlet)

$$\frac{\partial w_j}{\partial x} = 0$$ Zero gradient (Neumann) boundary condition

H. Solution procedure

The mass conservation equations with coupled kinetic and equilibrium chemical reactions were solved simultaneously (without operator splitting) by the numerical method-of-lines (SCHIESSER, 1991) using the stiff ODE solver VODE (BROWN et al., 1989). The advection and dispersion terms in equation 8 were discretized by finite differences on an even grid (Δx = 0.1 dm). Dispersion was modeled by central differences (STEEFEL and MACQUARRIE, 1996), whereas advection was modeled with a blend of backward (upwind) and central differences (FIADEIRO and VERONIS, 1977). The algorithm used for computation of equilibrium speciation reactions (MICROQL) was that described in Westall (1986) and Westall (1979), modified to compute activity coefficients for charged species according to the Davies equation as described in Westall et al. (WESTALL et al., 1986). The performance of the method-of-lines code was verified by reproducing the one-dimensional Co-NTA test problem described in Steefel and MacQuarrie (1996), as well as a one-dimensional version of the Co-EDTA reactive transport problem described in Tebes-Stevens et al. (1998).

I. Parameter values

Equilibrium speciation reactions

Stability constants (log K values) for the aqueous equilibrium speciation reactions listed above were obtained from Nordstrom et al. (1990), with the exception of those for the Fe^{2+}-CO_3^{2-}-H_2O system, which were obtained from Bruno et al. (1992). Surface complexation by Fe(III) oxides was modeled according to the diffuse layer model as described in Dzombak and Morel (DZOMBAK and MOREL, 1990). The total abundance of oxide surface sites was defined by the specified bulk Fe(III) oxide concentration (mol Fe dm^{-3}), an assumed Fe(III) oxide surface area of 150 m^2 g^{-1} (chosen to be representative of poorly crystalline goethite, a common Fe(III) oxide component of soils and sediments; (CORNELL and SCHWERTMANN, 1996)), and the standard mineral surface site density of 3.84 μmol m^{-2} recommended by Davis and Kent (DAVIS and KENT, 1990). The oxide surface was assumed to possess both 'strong' and 'weak' binding sites, and the relative abundance of these sites was assumed to be equal to that used by Dzombak and Morel (1990) to model cation and anion surface complexation by hydrous ferric oxide. Values for first and second FeOOH surface acidity constants used in our simulations were those for HFO given in Dzombak and Morel (1990), which are similar to those determined for goethite by Goldberg and Sposito (1984). The same acidity constants were used for the two types of surface sites, as recommended in Dzombak and Morel (1990). Stability constants for complexation of various aqueous U(VI) species by Fe(III) oxide surfaces were obtained from Waite et al. (1994). The ability of our implementation of the MICROQL algorithm to reproduce the sorption behavior of U(VI) species was checked against MINEQL+ simulations. Stability constants for complexation of Fe^{2+} by Fe(III) oxide surfaces were derived from sorption isotherms conducted with goethite-coated sand (RODEN et al., 2000) together with unpublished pH sorption edge measurements conducted on the same material.

Kinetic reactions

A summary of the kinetic reaction parameters used in the simulations is provided in Table 1 below. The biomass-specific rate constant for Fe(III) oxide reduction ($k_{Fe(III)ed}$) was obtained from a curve-fit of the time course of Fe(II) accumulation in the batch culture experiment conducted in parallel with the column FeOOH-coated sand experiment reported in Roden et al. (2000). The rate constant obtained from this curve-fit was divided first by the estimated total Fe(III) oxide surface site abundance to normalize the rate constant to site density, and then by the initial MeRB biomass added to the reactors to normalize the rate constant to MeRB biomass. The abundance of free Fe(III) oxide surface site available for microbial reduction at any given time during the simulation was equal to the total surface density (sum of the total concentrations of components 4 and 5 in the equilibrium speciation system) minus the concentration of Fe(II) sorbed to strong (species 25) and weak (species 32) oxide surface sites. Thus, rates of Fe(III) oxide reduction were dynamically controlled by the changing abundance of sorbed Fe(II). This same strategy was used successfully in a previous model of synthetic goethite reduction (RODEN and URRUTIA, 1999), with the exception that in the previous model, Fe(II) sorption to the oxide surface was depicted according to an empirical Freundlich isotherm fit to Fe(II) sorption data

obtained for a reactor system identical to that used for the microbial Fe(III) oxide reduction experiments (URRUTIA et al., 1998) – as opposed to the diffuse layer model used in the present model. At this time, use of sorbed Fe(II) abundance as computed by some type of equilibrium speciation expression appears to be the most straightforward and tractable way to model the influence of surface-bound Fe(II) accumulation on Fe(III) oxide reduction activity.

The biomass-specific V_{max} value for microbial U(VI) reduction was set equal the value reported for *S. alga* in Truex et al. (1997). An average half-saturation constant (K_m) for microbial U(VI) uptake/reduction of 100 μM was assigned, based on the value reported for *S. alga* in Truex et al. (1997) and the range of values obtained by Gorby et al. (2000) for several different MeRB. The half-saturation constant for utilization of organic carbon was set at 100 μM based on recent studies with *Shewanella putrefaciens* strain CN32 (LIU et al., 2001). The initial MeRB cell biomass in the column reactor was set equal to the equivalent of ca. 10^5 cells mL^{-1} based on cell number-dry weight relationships determined for *S. alga* (Roden and Urrutia, unpubl data). Subsequent production of MeRB biomass was computed based on calculated rates of Fe(III) and U(VI) reduction, using yield coefficients for MeRB growth coupled Fe(III)-citrate reduction determined in our own laboratory (Roden and Urrutia, unpubl data), and yield coefficients for MeRB growth coupled to U(VI) reduction estimated from the growth experiments reported in Lovley et al. (1991).

Table 1. Kinetic parameters used in reactive transport simulations

Parameter	Units	Value	Reference
$k_{Fe(III)red}$	(mol CH_2O dm^{-3})$^{-1}$ (g BM dm^{-3})$^{-1}$ d^{-1}	0.0950	(RODEN and URRUTIA, 1999)
BM_{ref}	g BM dm^{-3}	0.0200	(RODEN and URRUTIA, 1999)
K_m^{CH2O}	mol CH_2O dm^{-3}	0.0001	(LIU et al., 2001)
$V_{max}^{U(VI)}$	(mol U(VI) dm^{-3} d^{-1}) (mol CH_2O dm^{-3})$^{-1}$ (g BM dm^{-3})$^{-1}$	0.0570	(RODEN and URRUTIA, 1999)
$K_m^{U(VI)}$	mol U(VI) dm^{-3}	0.0001	(TRUEX et al., 1997)
$Y_{Fe(III)}$	g BM mol Fe(III)$^{-1}$	4.4	Roden, unpubl
$Y_{U(VI)}$	g BM mol U(VI)$^{-1}$	7.5	(LOVLEY et al., 1991)
k_d	d^{-1}	0.024	(TEBES-STEVENS et al., 1998)

References

Brown P. N., Byrne G. D., and Hindmarsh A. C. (1989) VODE: A variable-coefficient ODE solver. *SIAM J. Sci. Stat. Comput.* **10**, 1038-1051.

Bruno J., Wersin P., and Stumm W. (1992) On the influence of carbonate in mineral dissolution: II. The solubility of $FeCO_3$ (s) at 25 degrees C and 1 atm pressure. *Geochim. Cosmochim. Acta* **56**, 1149 - 1155.

Cornell R. M. and Schwertmann U. (1996) *The Iron Oixides*. VCH.

Davis J. A. and Kent D. B. (1990) Surface complexation modeling in aqueous geochemistry. In *Mineral-water interface geochemistry* (ed. M. F. Hochella and A. F. White), pp. 177-260. Mineralogical Society of America.

Dzombak D. A. and Morel F. M. M. (1990) *Surface complexation modeling: hydrous ferric oxide*. John Wiley & Sons.

Fiadeiro M. E. and Veronis G. (1977) On weighted-mean schemes for the finite-difference approximation to the advection-diffusion equation. *Tellus* **29**, 512-522.

Goldberg S. and Sposito G. (1984) A chemical model of phosphate adsorption by soils. I. Reference oxide minerals. *Soil Sci. Soc. Am. J.* **48**, 772-778.

Gorby Y. A., Brown C., Liu C., Gray M., Plymale A., Li S. W., Fredrickson J. K., and Wildung R. (2000) Kinetic analysis of multivalent metal reduction by metal-reducing bacteria. *Manuscript in preparation*.

Kirkner D. J. and Reeves H. (1988) Multicomponent mass transport with homogeneous and heterogenous chemical reactions: effect of the chemistry on the choice of numerical algorithm 1. Theory. *Wat. Resour. Res.* **24**, 1719-1729.

Liu C., Kota S., Zachara J. M., Fredrickson J. K., and Brinkman C. (2001) Kinetic analysis of the bacterial reduction of goethite. *Environ. Sci. Technol.* **Submitted for publication**.

Lovley D. R., Phillips E. J. P., Gorby Y. A., and Landa E. R. (1991) Microbial reduction of uranium. *Nature* **350**, 413-416.

Nordstrom D. K., Plummer L. N., Langmuir D., Busenberg E., and May H. M. (1990) Revised chemical equilibrium data for major water-mineral reactions and their limitations. In *Chemical modeling of aqueous systems II* (ed. D. C. Melchior and R. L. Bassett), pp. 398-413. Am. Chem. Soc.

Roden E. E. and Urrutia M. M. (1999) Ferrous iron removal promotes microbial reduction of crystalline iron(III) oxides. *Environ. Sci. Technol.* **33**, 1847-1853.

Roden E. E., Urrutia M. M., and Mann C. J. (2000) Bacterial reductive dissolution of crystalline Fe(III) oxide in continuous-flow column reactors. *Appl. Environ. Microbiol.* **66**, 1062-1065.

Roden E. E. and Zachara J. M. (1996) Microbial reduction of crystalline iron(III) oxides: Influence of oxide surface area and potential for cell growth. *Environ. Sci. Technol.* **30**, 1618-1628.

Schiesser W. E. (1991) *The numerical method of lines*. Academic Press.

Steefel C. I. and Lasaga A. C. (1994) A coupled model for transport of multiple chemical species and kinetic precipitation/dissolution reactions with application to reactive flow in single phase hydrothermal systems. *Am. J. Sci.* **294**, 529-592.

Steefel C. I. and MacQuarrie K. T. B. (1996) Approaches to modeling of reactive transport in porous media. In *Reactive transport in porous media*, Vol. 34 (ed. P. C. Lichtner, C. I. Steefel, and E. H. Oelkers), pp. 83-129. The Mineralogical Society of America.

Tebes-Stevens C., Valocchi A. J., VanBriesen J. M., and Rittman B. E. (1998) Multicomponent transport with coupled geochemical and microbiological reactions: model description and example simulations. *J. Hydrol.* **209**, 8-26.

Truex M. J., Peyton B. M., Valentine N. B., and Gorby Y. A. (1997) Kinetics of U(VI) reduction by a dissimilatory Fe(III)-reducing bacterium under non-growth conditions. *Biotech. Bioengin.* **55**, 490-496.

Urrutia M. M., Roden E. E., Fredrickson J. K., and Zachara J. M. (1998) Microbial and geochemical controls on synthetic Fe(III) oxide reduction by *Shewanella alga* strain BrY. *Geomicrobiol. J.* **15**, 269-291.

Waite T. D., Davis J. A., Payne T. E., Waychunas G. A., and Xu N. (1994) Uranium(VI) adsorption to ferrihydrite: Application of a surface complexation model. *Geochim. Cosmochim. Acta* **58**, 5465-5478.

Westall J. C. (1979) MICROQL II. Computation of adsorption equilibria in BASIC. Swiss Federal Institute of Technology, EAWAG.

Westall J. C. (1986) MICROQL I. A chemical equilibrium program in BASIC. Department of Chemistry, Oregon State University.

Westall J. C., Zachary J. L., and Morel F. M. M. (1986) MINEQL. A computer program for the calculation of the chemical equilibrium composition of aqueous systems. Department of Chemistry, Oregon State University.